Models of radiative neutrino mass and lepton-flavour non-universality

John Gargalionis

Submitted in total fulfilment
of the requirements of the degree of

Doctor of Philosophy

School of Physics
The University of Melbourne

September 2020

Abstract

This is a summary of what we did. We did x and y.

Publications

Refs. [1–5] below are the journal publications, and preprints authored or co-authored during my PhD candidature. The authors are listed alphabetically in all of the titles.

Journal papers and preprints

[1] R. Foot and J. Gargalionis, *Explaining the 750 GeV diphoton excess with a colored scalar charged under a new confining gauge interaction*, *Phys. Rev. D* **94** (2016), no. 1 011703, [arXiv:1604.06180].

[2] Y. Cai, J. Gargalionis, M. A. Schmidt, and R. R. Volkas, *Reconsidering the One Leptoquark solution: flavor anomalies and neutrino mass*, *JHEP* **10** (2017) 047, [arXiv:1704.05849].

[3] I. Bigaran, J. Gargalionis, and R. R. Volkas, *A near-minimal leptoquark model for reconciling flavour anomalies and generating radiative neutrino masses*, *JHEP* **10** (2019) 106, [arXiv:1906.01870].

[4] J. Gargalionis, I. Popa-Mateiu, and R. R. Volkas, *Radiative neutrino mass model from a mass dimension-11 $\Delta L = 2$ effective operator*, *JHEP* **03** (2020) 150, [arXiv:1912.12386].

[5] J. Gargalionis and R. R. Volkas, *Exploding operators for Majorana neutrino masses and beyond*, [arXiv:2009.13537].

Declaration

This is to certify that

1. the thesis comprises only my original work towards the PhD except where indicated clearly,

2. due acknowledgement has been made in the text to all other material used,

3. the thesis is less than 100,000 words in length, exclusive of tables, maps, bibliographies and appendices.

John Gargalionis, September 2020

Statement of contribution

I did x and someone else did y.

Preface

Particle physics currently finds itself in a strange or exciting place, depending on who you ask. The discovery of a Higgs-like boson at close to 125 GeV has meant both the completion of the Standard Model (SM), and the end of clear signs of new particles at the electroweak scale. Although the Large Hadron Collider (LHC) will continue to collect data well into the next few decades, the mass reach will not increase significantly. The community waits for a new machine, for which there are many candidates and promises, that will continue to push the energy frontier and test theories addressing the many shortcomings of the SM. Time frames for many of these see data taking beginning at the end of my career. If progress is driven by experiment, where do we go from here?

Thankfully, there are already clear signs of new physics in the neutrino sector. The observation of neutrino oscillations, and therefore neutrino masses, is by far the strongest terrestrial evidence demanding an extension of the SM. It is no surprise that a full understanding of the neutrinos has alluded us so far; they are, with the possible exception of the Higgs boson, the most elusive particles currently under laboratory scrutiny. As we move into an era of precision neutrino measurements, now is the right time to take stock of the phenomenologically viable and economic models that explain the pattern of neutrino masses and mixings observed. Armed with the list of possible mechanisms, we can make progress in probing those that are testable and, given that these models are falsified, build circumstantial evidence in favour of those that are not.

Even on the collider front, it is unclear yet that the LHC has left us with the so-called 'nightmare scenario' of a lonely Higgs. Perhaps unexpectedly, the most interesting signs of new physics from CERN have come from the LHC*b* experiment. The now famous 'flavour anomalies' are a collection of theoretically consistent anomalous measurements indicating a departure from the lepton-flavour universality present in the SM. Are these related to the growing evidence for deviations in leptonic anomalous magnetic moments? Might they be clues to a deeper theory of flavour and mass? The Belle II experiment has only just begun taking data, and we wait eagerly for what it has to say on these matters. LHC*b* too will continue to improve its measurements with more collisions; if the anomalies persist, these will be undeniable evidence of physics beyond the SM accessible to the next generation of hadron colliders.

These measurements are tantalising because of their consistency and breadth, but it would not be the first time that physicists have been lead astray, should they disappear with more statistics. Even so, what is perhaps the central result of my doctoral work will remain unchanged: that deviations from lepton-flavour universality in four-fermion operators may be intimately connected to mass generation in the neutrino sector.

Acknowledgements

I would like to thank x and y.

For x and y.

Contents

List of Figures

List of Tables

1 Introduction

The following is a general introduction to the background topics referred to and assumed in subsequent chapters. This includes a review of popular theories of neutrino mass, the current status of neutrino-oscillation parameters, a general introduction to Effective Field Theory (EFT), the experimental situation relevant to the flavour anomalies, and topics peripheral to all of these.

1.1 The Standard Model and neutrinos

Laboratory experiments to date have firmly established the predictive power of the Standard Model (SM) of particle physics, a combined theory of the electroweak and strong interactions described by the gauge group $G_{\mathrm{SM}} = \mathrm{SU}(3)_c \otimes \mathrm{SU}(2)_L \otimes \mathrm{U}(1)_Y$. It is a model whose probes and predictions span at least 33 orders of magnitude[1] with varying degrees of precision, and these are consistent with almost all known experiments. Although it displays a number of arbitrary features, the dynamics of the theory are mostly fixed by the fundamental principles of gauge theory and Lorentz invariance. Most of this arbitrariness resides in the matter sector of the theory, whose properties (masses, coupling constants, quantum numbers, *etc.*) are not predicted, but are instead motivated on phenomenological grounds. We show the fields of the SM and their defining properties in Table 1.1, according to the mathematical conventions of Appendix A.

[1]The interval given is from the distance scales probed at the LHC (roughly 10^{-17} cm) to the size of the solar system (roughly 10^{16} cm).

Field	$\mathrm{SU}(3)_c \otimes \mathrm{SU}(2)_L \otimes \mathrm{U}(1)_Y$	$\mathrm{SU}(2)_+ \otimes \mathrm{SU}(2)_-$
$Q^{\alpha a i}$	$(\mathbf{3}, \mathbf{2}, \frac{1}{6})$	$(\mathbf{2}, \mathbf{1})$
$L^{\alpha i}$	$(\mathbf{1}, \mathbf{2}, -\frac{1}{2})$	$(\mathbf{2}, \mathbf{1})$
$\bar{u}_a^{\alpha}$	$(\bar{\mathbf{3}}, \mathbf{1}, -\frac{2}{3})$	$(\mathbf{2}, \mathbf{1})$
$\bar{d}_a^{\alpha}$	$(\bar{\mathbf{3}}, \mathbf{1}, \frac{1}{3})$	$(\mathbf{2}, \mathbf{1})$
$\bar{e}^{\alpha}$	$(\mathbf{1}, \mathbf{1}, 1)$	$(\mathbf{2}, \mathbf{1})$
$(G_{\alpha\beta})^a{}_b$	$(\mathbf{8}, \mathbf{1}, 0)$	$(\mathbf{3}, \mathbf{1})$
$(W_{\alpha\beta})^i{}_j$	$(\mathbf{1}, \mathbf{3}, 0)$	$(\mathbf{3}, \mathbf{1})$
$B_{\alpha\beta}$	$(\mathbf{1}, \mathbf{1}, 0)$	$(\mathbf{3}, \mathbf{1})$
H^i	$(\mathbf{1}, \mathbf{2}, \frac{1}{2})$	$(\mathbf{1}, \mathbf{1})$

Table 1.1: The SM fields and their transformation properties under the SM gauge group G_{SM} and the Lorentz group written as $\mathrm{SU}(2)_+ \otimes \mathrm{SU}(2)_-$. The final unbolded number in the 3-tuples of the G_{SM} column represents the $\mathrm{U}(1)_Y$ charge of the field, normalised such that $Q = I_3 + Y$. For the fermions a generational index has been suppressed. See Appendix A for details about the mathematical notation used here and throughout this work.

The SM inherits the experimental success of the $\mathrm{SU}(2) \otimes \mathrm{U}(1)$ theory of the weak interactions, first proposed by Glashow [30] in 1961 as a possible underlying structure for Fermi's theory of beta decay. Before the end of the same decade, Weinberg [31] and Salam [32] had constructed the modern theory of leptons based on the spontaneous breaking of $\mathrm{SU}(2)_L \otimes \mathrm{U}(1)_Y$ to the electromagnetic symmetry. Interestingly, it seems that these seminal papers went mostly unnoticed (see Fig. 1.1) until the early 1970s, when 't Hooft proved the renormalisability of spontaneously broken gauge theories [33] as a graduate student working under the supervision of Veltman. By the mid 1970s the framework had been extended to include the quarks [34] and the unbroken chromodynamic group, which was successfully shown to reproduce the Bjorken scaling seen in deep-inelastic-scattering experiments through asymptotic freedom [35].

Despite its successes, the SM cannot be the complete theory of fundamental particles and their interactions. It does not explain phenomena such as the baryon asymmetry present, and the particle spectrum contains no viable candidate for dark matter. The SM cannot explain why the electric dipole moment of the neutron is so small, why there are three generations of matter or, notably in our case, the origin of neutrino oscillations and the implied small but non-zero neutrino masses.

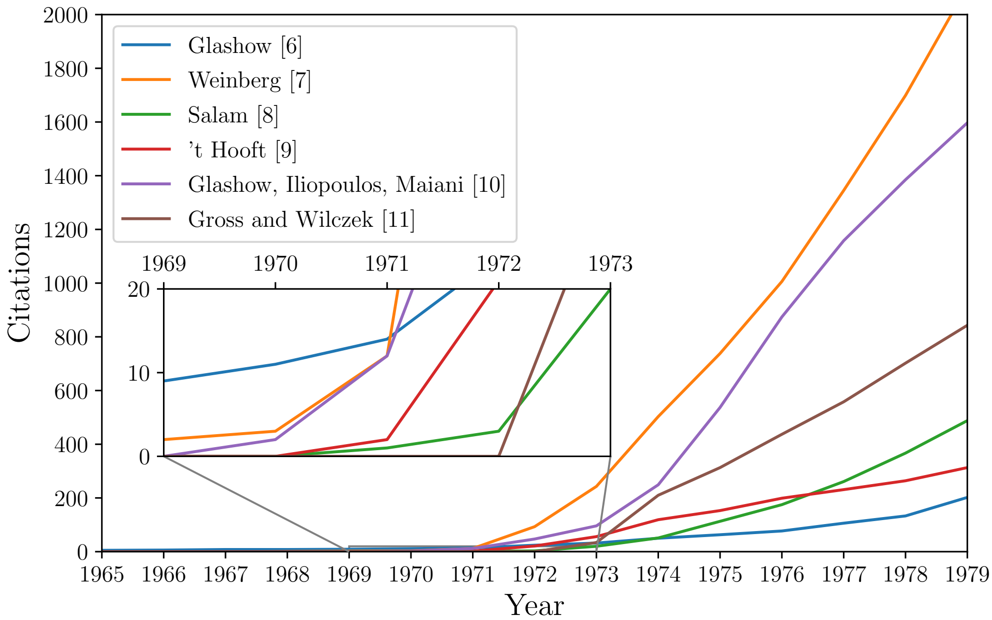

Figure 1.1: The cumulative citation graph for a selection of papers presenting foundational results relevant to the SM. Weinberg's seminal paper 'A model of leptons' (1967) saw an explosion of citations following 't Hooft's work on the renormalisability of gauge theories (1971).

1.2 Massive neutrinos in experiment and theory

The minimal SM predicts massless neutrinos, a prediction that today sits in contradiction to a wealth of empirical evidence. This evidence could in principle have come from many kinds of experiments, but currently only neutrino oscillations provide strong signs that the masses are non-zero. Below we discuss the phenomenon of neutrino oscillations in the context of the outstandingly successful three-flavour mixing paradigm. We then move on to other probes of neutrino masses, which currently only provide limits on the mass scale. On the theory side, we summarise some popular and motivated extensions of the SM that accommodate massive neutrinos, placing particular emphasis on the direction we have followed in the novel work presented in this thesis. This includes an overview of tree- and loop-level models of Majorana neutrino mass.

1.2.1 Neutrino oscillations

The neutrino flavour eigenstates $\check{\nu}_i = (\nu_e, \nu_\mu, \nu_\tau)$ are defined as the states that couple at charged-current interaction vertices with the corresponding charged lepton. These are the states in which the neutrinos are almost always produced in experiments, and certainly always measured. If neutrinos are massive there is no reason to expect these to coincide with the mass eigenstates $\nu_i = (\nu_1, \nu_2, \nu_3)$. In general, the flavour eigenstates will be an admixture of the propagating fields

$$\check{\nu}_i = U_i^{\ j} \nu_j \, , \tag{1.1}$$

where the $U_i^{\ j}$ are elements of the unitary Pontecorvo–Maki–Nakagawa–Sakata (PMNS) neutrino mixing matrix [36, 37]. The PMNS matrix is defined such that it diagonalises the neutrino mass matrix:

$$\mathbf{U}^\dagger \mathbf{m}_\nu \mathbf{U}^* = \mathrm{diag}(m_1, m_2, m_3), \tag{1.2}$$

where the m_i are the neutrino masses. Being a 3×3 unitary matrix, $\mathbf{U}$ is in general parametrised by three mixing angles and six phases. Not all of the phases are physical, since the neutrino and charged-lepton fields can be redefined in such a way that five of the phases are removed in the case of Dirac neutrinos. In the presence of a Majorana mass term, only the charged leptons can be rephased. This leaves three physical phases with the two additional ones termed *Majorana phases.* In general

$$\mathbf{U} = \begin{bmatrix} c_{12}c_{13} & s_{12}c_{13} & s_{13}e^{-i\delta_{\mathrm{CP}}} \\ -s_{12}c_{23} - c_{12}s_{23}s_{13}e^{i\delta_{\mathrm{CP}}} & c_{12}c_{23} - s_{12}s_{23}s_{13}e^{i\delta_{\mathrm{CP}}} & s_{23}c_{13} \\ s_{12}s_{23} - c_{12}c_{23}s_{13}e^{i\delta_{\mathrm{CP}}} & -c_{12}s_{23} - s_{12}c_{23}s_{13}e^{i\delta_{\mathrm{CP}}} & c_{23}c_{13} \end{bmatrix} \mathbf{P} \, , \tag{1.3}$$

where $c_{ij} = \cos\theta_{ij}$, $s_{ij} = \sin\theta_{ij}$ and

$$\mathbf{P} = \begin{cases} \mathrm{diag}(e^{i\alpha_1}, e^{i\alpha_2}, 1) & \text{for Majorana neutrinos} \\ \mathbf{1}_{3\times 3} & \text{for Dirac neutrinos} \end{cases} . \tag{1.4}$$

The phase δ_{CP} is often called the *Dirac phase*, while $\alpha_{1,2}$ are the Majorana phases discussed above.

Neutrino oscillation experiments typically involve the production of neutrino flavour states from charged-current processes, *e.g.* leptonic pion decays. Each mass eigenstate evolves in time independently according to the Schrödinger equation: *i.e.* $|\nu_i(t)\rangle = \exp(-iE_i t)|\nu_i(0)\rangle$, for evolution *in vacuo.* This alters the initial superposition away from being a pure flavour eigenstate:

$$|\check{\nu}_i(t)\rangle = \sum_j U_i^{*j} e^{-iE_j t} |\nu_j\rangle \tag{1.5}$$

$$= \sum_{j,k} U_i^{*j} e^{-iE_j t} U_j^{\ k} |\check{\nu}_k\rangle \, . \tag{1.6}$$

The probability of measuring a specific flavour through the charged-current interaction then oscillates with time:

$$\mathrm{P}(\check{\nu}_m \to \check{\nu}_n) = |\langle \check{\nu}_n | \check{\nu}_m(t) \rangle|^2 = \left| \sum_i U^{*i}_{m} U_i{}^{n} e^{-iE_i t} \right|^2 . \tag{1.7}$$

The expression can be expanded and the kinematic factors simplified from the fact that the neutrinos are ultra-relativistic. We follow the usual convention and take $E_i = \sqrt{\mathbf{p}^2 + m_i^2} \approx |\mathbf{p}| + m_i^2/(2E)$ with $E = |\mathbf{p}|$. This gives

$$\begin{aligned} \mathrm{P}(\check{\nu}_m \to \check{\nu}_n) = \delta_{mn} &- 4 \sum_{i<j} \mathrm{Re}\left(U_m^i U_m^{*j} U_n^{*i} U_n{}^j \right) \sin^2 \frac{\Delta m^2_{ij} L}{4E} \\ &+ 2 \sum_{i<j} \mathrm{Im}\left(U_m^i U_m^{*j} U_n^{*i} U_n{}^j \right) \sin \frac{\Delta m^2_{ji} L}{2E} , \end{aligned} \tag{1.8}$$

where $\Delta m^2_{ij} \equiv m_j^2 - m_i^2$ are the squared neutrino mass differences and $L = ct$, sometimes called the baseline, is the approximate distance travelled by the particles. To interpret the results of many experiments, it is often sufficient to consider an effective two-flavour oscillation paradigm. In this case, the neutrino-oscillation probabilities are governed by by a single squared mass difference Δm^2 and a single angle θ. Interestingly, the CP-violating phase is completely absent from the two flavour formula:

$$\mathrm{P}(\check{\nu}_m \to \check{\nu}_n)_{n_f=2} = \sin^2(2\theta) \sin^2 \frac{\Delta m^2 L}{4E} . \tag{1.9}$$

From the expressions in Eqs. (1.8) and (1.9) a number of properties of the vacuum neutrino oscillations become clear.

1. The neutrino oscillation probabilities depend on the neutrino mass differences, and not on the absolute mass scale. For three flavours, there are only two independent squared mass differences. Typically chosen to be Δm^2_{21} and Δm^2_{31}, although often they are refereed to with the historical names $\Delta m^2_{\mathrm{sol}}$ and $\Delta m^2_{\mathrm{atm}}$, discussed in detail below.

2. From Eq. (1.8) it is clear that the oscillations only occur if the neutrinos are non-degenerate and the neutrino mixing is non-trivial, *i.e.* if $\Delta m_{ij} \neq 0$ and $\mathbf{U} \neq \mathbf{1}$.

3. The PMNS matrix elements only appear in the combination $U_m^i U_m^{*j}$, to which the Majorana phases contained within the matrix $\mathbf{P}$ do not contribute. This implies that oscillation experiments cannot comment on the Dirac or Majorana nature[2] of the neutrinos. Oscillations can however probe δ_{CP}.

[2] Of course, this is already clear from the fact that neutrino oscillations conserve total lepton number, despite breaking the individual familial lepton-number symmetries $L_{e,\mu,\tau}$.

4. In the effective two-flavour mixing paradigm, both θ and Δm^2 appear in such a way that neither the sign of Δm^2 nor the octant of θ can be uniquely determined.

Thus, neutrino oscillations imply that the neutrino masses of at least two of the mass eigenstates are non-degenerate, and therefore only one neutrino could potentially be massless. The largest squared mass difference can therefore be translated into an lower bound on the mass of the heaviest neutrino, which we present later with modern data.

Historically, the effective two-flavour mixing paradigm has provided a good framework for interpreting early indications of neutrino oscillations. Specifically, the solar and atmospheric neutrino puzzles have approximate descriptions in terms of a two-flavour picture. Oscillations $\nu_e \to \nu_{\text{active}}$, where ν_{active} is a coherent superposition of ν_μ and ν_τ, in both matter and vacuum account for the deficit of electron neutrinos measured from the sun, and $\nu_\mu \to \nu_\tau$ oscillations *in vacuo* explain the shortage of muon neutrinos from cosmic-ray-induced production in the upper atmosphere.

The measurement and resolution of these puzzles is an interesting and exciting chapter in the recent history of physics. Experiments as early as the 1960s had noticed a shortage of electron neutrinos coming from the sun relative to the predictions of solar models [38–41], which themselves were subject to much uncertainty [42]. For detection there were three main approaches: Raymond Davis and collaborators [43] pioneered experiments that measured the solar electron-neutrino flux using Chlorine, the Kamiokande and later Super-Kamiokande collaborations [44, 45] used water Cherenkov detectors, and the experiments GALLEX [46] and SAGE [47] had Gallium as the detecting material. All of these experiments showed a deficit of solar electron neutrinos, although they were sensitive to neutrinos of different energies. The Sudbury Neutrino Observatory gave the final word on the oscillation solution to the solar neutrino puzzle with accurate confirmation of the electron-neutrino deficit, along with a measurement of the *total* neutrino flux which was found to be in agreement with the solar models [48, 49].

Atmospheric neutrinos were known to come about from helicity-suppressed kaon and pion decays to muons and muon neutrinos. A zenith-angle and energy-dependent suppression in the flux of atmospheric muon neutrinos was measured by the Kamiokande and Irvine–Michigan–Brookhaven experiments [50, 51] in the early 1990s, and after the upgrade to Super-Kamiokande the deficit was confirmed to high precision with results presented at the 'Neutrino 1998' conference [52–55].

The pairs of mixing parameters associated with these two classes of measurements are usually dubbed $\theta_{\text{sol}}, \Delta m^2_{\text{sol}}$ and $\theta_{\text{atm}}, \Delta m^2_{\text{atm}}$. Experimental results find $\Delta m^2_{\text{sol}} \ll \Delta m^2_{\text{atm}}$ and that both θ_{sol} and θ_{atm} are large compared to any angles found in the CKM matrix, the quark mixing matrix. Interpreted in terms of three-flavour mixing, common convention identifies Δm^2_{sol} with the squared mass difference between ν_2 and ν_1, which is known to be positive[3] (*i.e.* $\Delta m^2_{21} > 0$). The solar mixing angle θ_{sol} is then

[3]We note that the sign of Δm^2_{21} can be known since oscillations in matter are also relevant for the

associated with θ_{12}. The atmospheric mixing parameters are identified with $|\Delta m^2_{31}|$ or $|\Delta m^2_{32}|$ and θ_{23}. Of course, three-flavour effects alter the simplistic picture presented here and must be included to interpret measurements of θ_{13} and δ_{CP}, see *e.g.* Ref. [56] and references therein for a more detailed discussion. The picture that emerges from these experiments is then

$$\Delta m^2_{\mathrm{sol}} \approx \Delta m^2_{21} \ll |\Delta m^2_{31}| \approx |\Delta m^2_{32}| \approx |\Delta m^2_{\mathrm{atm}}| \,, \tag{1.10}$$

with which both the *normal mass ordering* $m_1 < m_2 < m_3$ and the *inverted mass ordering* $m_3 < m_1 < m_2$ are consistent.

Neutrino oscillation experiments have continued to probe the squared mass differences and mixing parameters with impressively high precision, see *e.g.* Refs. [6, 57]. Reactor neutrino experiments like KamLAND [58] and long-baseline accelerators, *e.g.* T2K [59] and NOνA [60], are sensitive to all of these parameters, although $\Delta m^2_{\mathrm{atm}}$ and θ_{13} are best measured at short-baseline reactors like Double Chooz [61], RENO [62] and Daya Bay [63]. Today the octant of θ_{12} is certainly known, while θ_{13} is constrained to be close to 0.15. The sign of the atmospheric squared mass difference is still unknown, and therefore so is the mass ordering for the neutrinos. The value of the CP-violating Dirac phase δ_{CP} is less clear, although there is a preference for a value somewhere between π and $3\pi/2$. The extent of CP-violation in the neutrino sector can be represented in a rephasing-invariant way with the leptonic Jarlskog invariant

$$J_{CP} = \frac{1}{8} \cos\theta_{13} \sin 2\theta_{12} \sin 2\theta_{13} \sin 2\theta_{23} \sin\delta_{\mathrm{CP}} \,, \tag{1.11}$$

so a value of π would imply no CP-violating effects, while $\delta_{\mathrm{CP}} = 3\pi/2$ would make these maximal. For this work we take the results of the most recent fit to neutrino oscillation data by the NuFit collaboration [6, 7] in the context of the three-flavour paradigm. These results are summarised in Fig. 1.2 separately for the cases of normal and inverted mass ordering. Results including atmospheric neutrino oscillation data from Super-Kamiokande and those not are also distinguished. Two-dimensional projections of the χ^2 fit for the same parameters are shown in Fig. 1.3. These data suggest a leptonic mixing matrix that has a very different form to the CKM matrix, which we call $\mathbf{V}$. We represent this qualitatively by using boxes whose side lengths are scaled to the magnitude of the best-fit values of the parameters in the matrices, the textures are

$\mathbf{U} \sim$ 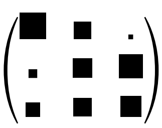 , $\mathbf{V} \sim$ 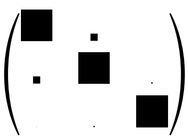 . (1.12)

For the PMNS matrix we take the best fit values for the normal mass ordering including the Super-Kamiokande results, *i.e.* the numbers in the top-left quadrant of Fig. 1.2. The

solar squared mass difference, which depart from the simple formula of Eq. (1.9).

same numbers also imply an upper bound on the mass of the heaviest neutrino at

$$m_{\text{heaviest}} \leq \sqrt{|\Delta m^2_{\text{atm}}|} \approx 0.05\,\text{eV} \,. \tag{1.13}$$

1.2.2 Other experimental probes

Although neutrino oscillations provide a wealth of evidence for non-zero masses for at least two of the neutrino fields, they do not probe the absolute mass scale. There are however kinematic and cosmological probes which bound the neutrino masses, and some of these are mentioned here.

Beta decay

A study of the kinematics of beta-decay experiments shows that differences in the energy distribution of the emitted electron are expected for different values of the neutrino mass. Currently these experiments only provide upper bounds on the effective neutrino mass [64]

$$m_\beta \equiv \sqrt{\sum_i |U_1{}^i|^2 m_i^2} \,. \tag{1.14}$$

The best results come from tritium experiments which probe ${}^3\text{H} \to {}^3\text{He} + e + \bar{\nu}_e$. The KATRIN experiment recently presented the most stringent upper bound [65, 66]

$$m_\beta < 1.1\,\text{eV} \,, \tag{1.15}$$

at 90% confidence, with a projected limit of $m_\beta < 0.2\,\text{eV}$ with the full dataset.

Another process with the potential to probe the absolute scale of the neutrino masses, as well as the Majorana phases, is neutrinoless double beta decay ($0\nu\beta\beta$). The process requires the violation of lepton-number by two units, and is therefore intimately tied to the neutrinos' possible Majorana nature. If double-beta decay is seen, the *black box theorem* [67–69] guarantees that the neutrinos pick up a radiative Majorana mass, even if the neutrino masses vanish at tree level. Graphically this is easy to understand: a $0\nu\beta\beta$ operator can always be turned into a neutrino self-energy graph with four loops. The amplitude for the process is proportional to

$$\langle m_\nu \rangle_{\beta\beta} = \sum_i (U_1{}^i)^2 m_i \,, \tag{1.16}$$

which features both the neutrino masses and the Majorana phases. (Of course it may be that the four-loop contribution to the neutrino mass implied by the double-beta-decay operator represents only a small correction to the neutrino masses, which could

NuFIT 5.0 (2020)

		Normal Ordering (best fit)		Inverted Ordering ($\Delta\chi^2 = 2.7$)	
		bfp $\pm 1\sigma$	3σ range	bfp $\pm 1\sigma$	3σ range
without SK atmospheric data	$\sin^2\theta_{12}$	$0.304^{+0.013}_{-0.012}$	$0.269 \to 0.343$	$0.304^{+0.013}_{-0.012}$	$0.269 \to 0.343$
	$\theta_{12}/^\circ$	$33.44^{+0.78}_{-0.75}$	$31.27 \to 35.86$	$33.45^{+0.78}_{-0.75}$	$31.27 \to 35.87$
	$\sin^2\theta_{23}$	$0.570^{+0.018}_{-0.024}$	$0.407 \to 0.618$	$0.575^{+0.017}_{-0.021}$	$0.411 \to 0.621$
	$\theta_{23}/^\circ$	$49.0^{+1.1}_{-1.4}$	$39.6 \to 51.8$	$49.3^{+1.0}_{-1.2}$	$39.9 \to 52.0$
	$\sin^2\theta_{13}$	$0.02221^{+0.00068}_{-0.00062}$	$0.02034 \to 0.02430$	$0.02240^{+0.00062}_{-0.00062}$	$0.02053 \to 0.02436$
	$\theta_{13}/^\circ$	$8.57^{+0.13}_{-0.12}$	$8.20 \to 8.97$	$8.61^{+0.12}_{-0.12}$	$8.24 \to 8.98$
	$\delta_{\mathrm{CP}}/^\circ$	195^{+51}_{-25}	$107 \to 403$	286^{+27}_{-32}	$192 \to 360$
	$\frac{\Delta m^2_{21}}{10^{-5}\ \mathrm{eV}^2}$	$7.42^{+0.21}_{-0.20}$	$6.82 \to 8.04$	$7.42^{+0.21}_{-0.20}$	$6.82 \to 8.04$
	$\frac{\Delta m^2_{3\ell}}{10^{-3}\ \mathrm{eV}^2}$	$+2.514^{+0.028}_{-0.027}$	$+2.431 \to +2.598$	$-2.497^{+0.028}_{-0.028}$	$-2.583 \to -2.412$
		Normal Ordering (best fit)		Inverted Ordering ($\Delta\chi^2 = 7.1$)	
		bfp $\pm 1\sigma$	3σ range	bfp $\pm 1\sigma$	3σ range
with SK atmospheric data	$\sin^2\theta_{12}$	$0.304^{+0.012}_{-0.012}$	$0.269 \to 0.343$	$0.304^{+0.013}_{-0.012}$	$0.269 \to 0.343$
	$\theta_{12}/^\circ$	$33.44^{+0.77}_{-0.74}$	$31.27 \to 35.86$	$33.45^{+0.78}_{-0.75}$	$31.27 \to 35.87$
	$\sin^2\theta_{23}$	$0.573^{+0.016}_{-0.020}$	$0.415 \to 0.616$	$0.575^{+0.016}_{-0.019}$	$0.419 \to 0.617$
	$\theta_{23}/^\circ$	$49.2^{+0.9}_{-1.2}$	$40.1 \to 51.7$	$49.3^{+0.9}_{-1.1}$	$40.3 \to 51.8$
	$\sin^2\theta_{13}$	$0.02219^{+0.00062}_{-0.00063}$	$0.02032 \to 0.02410$	$0.02238^{+0.00063}_{-0.00062}$	$0.02052 \to 0.02428$
	$\theta_{13}/^\circ$	$8.57^{+0.12}_{-0.12}$	$8.20 \to 8.93$	$8.60^{+0.12}_{-0.12}$	$8.24 \to 8.96$
	$\delta_{\mathrm{CP}}/^\circ$	197^{+27}_{-24}	$120 \to 369$	282^{+26}_{-30}	$193 \to 352$
	$\frac{\Delta m^2_{21}}{10^{-5}\ \mathrm{eV}^2}$	$7.42^{+0.21}_{-0.20}$	$6.82 \to 8.04$	$7.42^{+0.21}_{-0.20}$	$6.82 \to 8.04$
	$\frac{\Delta m^2_{3\ell}}{10^{-3}\ \mathrm{eV}^2}$	$+2.517^{+0.026}_{-0.028}$	$+2.435 \to +2.598$	$-2.498^{+0.028}_{-0.028}$	$-2.581 \to -2.414$

Figure 1.2: The figure shows a table taken from the latest global fit to neutrino mass and mixing parameters by the NuFit collaboration [6, 7] in the three-flavour picture. The results presented in the upper (lower) panel are obtained by excluding (including) the χ^2 data on atmospheric neutrinos provided by the Super-Kamiokande collaboration (SK). The numbers in the 1st (2nd) column are obtained assuming normal (inverted) neutrino mass ordering. See Ref. [7] for more information.

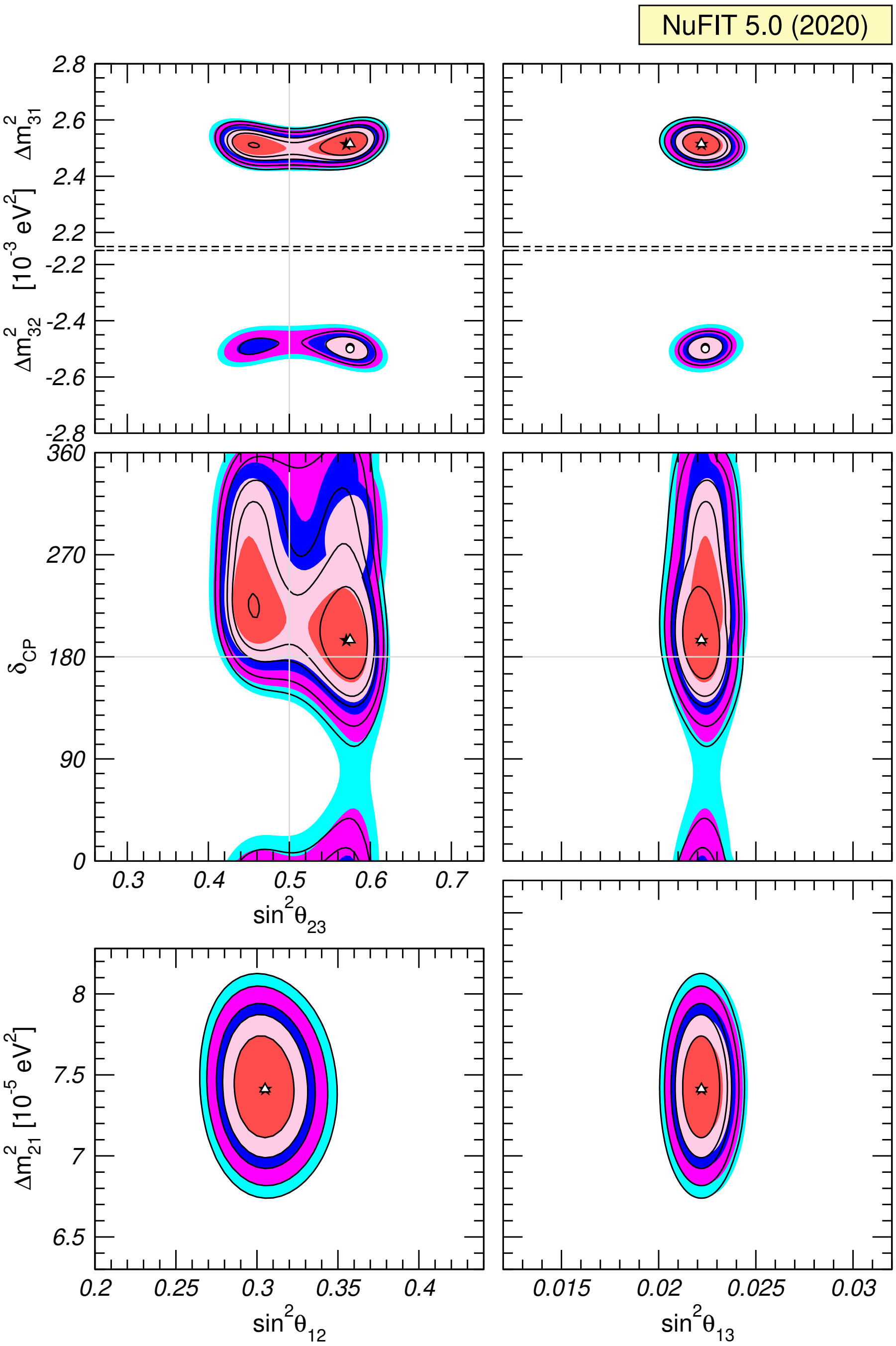

Figure 1.3: The figure shows the two-dimensional allowed regions obtained by the latest fit to the neutrino mass and mixing parameters by the NuFit collaboration [6, 7]. Each plot shows the two-dimensional projection of the allowed region after marginalising with respect to the other parameters. The coloured regions (black contour curves) are obtained by excluding (including) the Super-Kamiomande χ^2 data. The different contours correspond to the two-dimensional allowed regions at 1σ, 90%, 2σ, 99%, 3σ confidence. See Ref. [7] for more information.

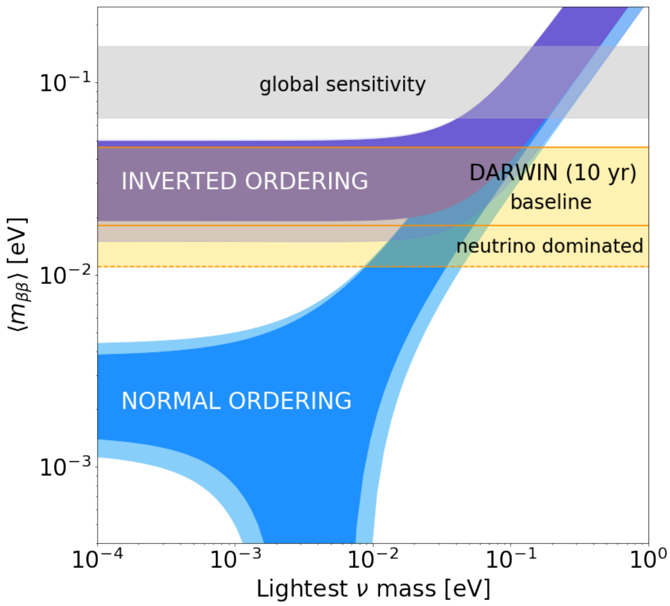

Figure 1.4: The figure shows limits on the effective neutrino mass for different values of m_{lightest} for both normal and inverted mass ordering. The grey region represents the combined sensitivity from a number of leading experiments [8]. The yellow regions are projections for the DARWIN experiment under different background hypotheses. The figure is taken from Ref. [9], and we point the reader there for more information.

arise at lower order.) Current limits on $\langle m_\nu \rangle_{\beta\beta}$ are around 0.2 eV, see *e.g.* Ref. [70] for a recent review of the experimental status and prospects. Constraints on $\langle m_\nu \rangle_{\beta\beta}$ are usually presented against the mass of the lightest neutrino mass eigenstate. The behaviour of $\langle m_\nu \rangle_{\beta\beta}$ is very sensitive to the neutrino mass ordering, in such a way that the inverted scenario implies a minimum allowed value of $\langle m_\nu \rangle_{\beta\beta}$, which will begin to be probed by the next generation of experiments. A combined global limit and the projected sensitivity of the DARWIN experiment [9] are shown in Fig. 1.4, which also illustrates the different behaviour of the inverted and normal neutrino mass orderings in the $\langle m_\nu \rangle_{\beta\beta}$ vs. m_{lightest} plane.

Cosmological limits

The most stringent limits on the sum of the neutrino masses come from cosmology, although they are model-dependent. In the minimal ΛCDM model adjusted for massive neutrinos, the limit implied by the most recent Planck data release [71] is

$$\sum_i m_i < 0.12\,\mathrm{eV}\,, \tag{1.17}$$

at 95% confidence. This is impressively small, and puts pressure on the inverted-ordering scenario, for which $\sum_i m_i \gtrsim 0.1\,\mathrm{eV}$. Excitingly, future cosmological probes will likely make a measurement of the sum of the neutrino masses.

1.2.3 Models of neutrino masses

In the SM the neutrino fields appear only within the lepton doublet L, and one cannot write down—in analogy to the up-type Yukawa—a renormalisable operator that leads to neutrino masses because of the absence of the right-handed fields. A simple model of neutrino mass then involves introducing right-handed neutrino fields $\bar{\nu} \sim (\mathbf{1}, \mathbf{1}, 0)_{(1,2)}$, extending the Yukawa sector of the SM accordingly to

$$-\mathscr{L}_Y \supset y_e \bar{e} L H^\dagger + y_d \bar{d} Q H^\dagger + y_u \bar{u} Q H + y_\nu \bar{\nu} L H\,, \tag{1.18}$$

in a simplified one-flavour picture. This implies Dirac neutrinos with a mass $m_\nu \approx y_\nu v$, and makes mass generation symmetric between the quarks and leptons.

There are a number of problems with this simplistic scenario. First, it is perhaps uncomfortable to suppose that the neutrinos are many orders of magnitude lighter than the charged fermions only because y_ν is a very small number. Indeed, the posited large hierarchy between y_ν and y_u seems to spoil any aesthetic arguments for quark–lepton symmetry in favour of this hypothesis. Although the Yukawa couplings for the other SM fermions span six orders of magnitude, couplings within any one generation are all of similar order. We illustrate this in Fig. 1.5, where the fermion masses are plotted by generation. Whereas one could consider that some underlying theory of flavour may explain, for example, the disparity in scale between the masses of the electron and the top quark, the large mass difference between the electron and the lightest neutrino, although technically natural, seems to cry out for its own explanation.

A second point of criticism with the simple scenario presented above is that it ignores the Majorana mass term for $\bar{\nu}$

$$\mathscr{L} \supset -\tfrac{1}{2}\mu\bar{\nu}\bar{\nu} + \mathrm{h.c.} \tag{1.19}$$

In order to maintain the Dirac neutrino mass with the relation $m_\nu \approx y_\nu v$, the Majorana mass must be forbidden or else chosen to be negligibly small, assumptions adding additional layers of contrivance to the theory. A sensible choice for the scale μ is some high scale Λ associated with the breaking of $\mathrm{U}(1)_{B-L}$. Taking $\mu \gg y_\nu v$, the neutrino-mass matrix takes on the form

$$\mathbf{m}_\nu = \begin{pmatrix} 0 & y_\nu v \\ y_\nu v & \mu \end{pmatrix}\,, \tag{1.20}$$

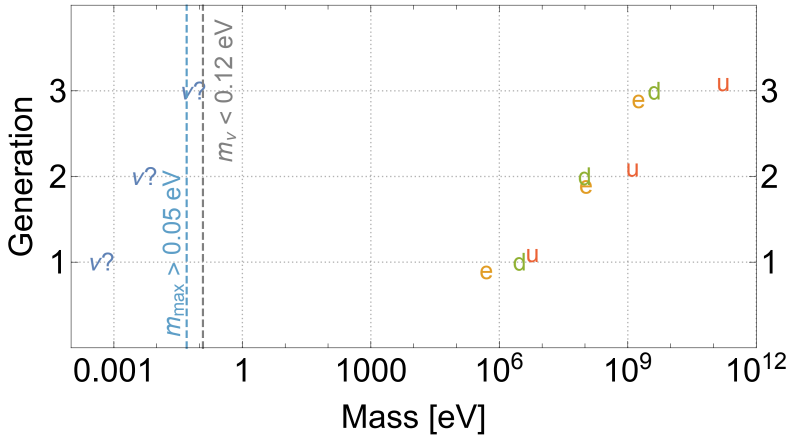

Figure 1.5: The masses of the SM fermions grouped by generation. While the SM Yukawa couplings span a wide range of values, within any specific generation they are all of similar order. The tiny masses of the neutrinos seem to suggest an alternate mass-generation mechanism.

with eigenvalues

$$m_l \approx \frac{y_\nu^2 v^2}{\mu}, \quad m_h \approx \mu \,. \tag{1.21}$$

The assumption $\mu \gg y_\nu v$ implies that $m_l \ll y_\nu v$, and the neutrino is successfully arranged to be much lighter than $y_\nu v$, which can now be taken to be on the order of the charged fermion masses. The theory also leaves us with a neutrino whose mass must be significantly larger than the electroweak scale: $m_h \gtrsim 10^{14}$ GeV, assuming $m_l = 0.05$ eV and $y_\nu = 1$. After transforming into the mass-diagonal basis, the physical fields ν_l and ν_h correspond to Majorana particles. Thus, in the most motivated region of parameter space, the phenomenology of the light neutrinos in even the SM + $\bar{\nu}$ scenario is Majorana. This toy scenario illustrates the mechanism commonly called the *seesaw mechanism*: making the neutrinos very light at the expense of making other fields very heavy. This is discussed more broadly below.

Tree-level models of neutrino mass

The toy seesaw scenario discussed above can be understood more generally by studying the effective theory valid below the scale μ, which does not contain the field $\bar{\nu}$. The leading-order lepton-number-violating (LNV) effects appear at dimension five in the operator

$$\mathscr{L} \supset \frac{\kappa}{\Lambda}(L^i L^j) H^k H^l \cdot \epsilon_{ik}\epsilon_{jl} \,, \tag{1.22}$$

with κ a dimensionless coefficient. This operator is commonly called the *Weinberg operator*. In the broken phase it gives rise to a Majorana mass for the neutrinos consistent with the seesaw formula:

$$\mathscr{L} \supset \frac{v^2\kappa}{\Lambda}\nu\nu \, . \tag{1.23}$$

The SM + $\bar{\nu}$ scenario is not the only simplified model that generates the Weinberg operator at tree-level. A simple diagram-topology analysis suggests there are another two seesaw mechanisms in the UV: a model with a scalar isotriplet field $\Xi_1 \sim (\mathbf{1}, \mathbf{3}, 1)_S$, called the type-II mechanism, and another with an isotriplet Majorana fermion $\Sigma \sim (\mathbf{1}, \mathbf{3}, 0)_F$, called type-III. Along with the type-I heavy $\bar{\nu}$ model, these are collectively referred to as the canonical seesaw mechanisms [72–82] and have been studied at length in the literature. They are simple models in that they introduce only very few exotic degrees of freedom and free parameters. However, the high seesaw scale makes these models practically untestable at current and future collider experiments.

Models of Majorana neutrino mass can be made more testable if, instead of the suppression of the neutrino masses coming from a large Λ in Eq. (1.23), the coefficient κ were somehow arranged to be small. Although there are a number of mechanisms to achieve this, we concentrate below on radiative models of Majorana neutrino mass, in which κ is made small through loop and coupling suppression.

Radiative models and their classification

It may be the case that the field content of whatever high-energy theory describes the neutrino masses is such that no neutrino self-energy diagram can be drawn at the tree level. Indeed, this will be the case if there is lepton-number violation by two units ($\Delta L = 2$) from interactions other than those present in the canonical seesaw models. Such models are called radiative, since the neutrino masses arise through loop graphs. The historically important Zee [83] and Zee–Babu [84, 85] models have come to be archetypal radiative scenarios in which the neutrinos gain masses through $\Delta L = 2$ the interactions of exotic scalars at one and two loops respectively. In the Zee model, an additional Higgs doublet $\varphi \sim (\mathbf{1}, \mathbf{2}, \frac{1}{2})$ and a charged scalar $\mathcal{S}_1 \sim (\mathbf{1}, \mathbf{1}, 1)$ are introduced, while the Zee–Babu model contains $\mathcal{S}_1$ and the doubly-charged scalar $\mathcal{S}_2 \sim (\mathbf{1}, \mathbf{1}, 2)$. The neutrino self-energy diagrams for these models are shown in Fig. 1.6 as examples. The corresponding neutrino-mass matrices are

$$[\mathbf{m}_\nu^{\text{Zee}}]_{rs} = \frac{\mu v^2}{16\pi^2} \sum_t x_{[rt]} I_t [\mathbf{m}_e]_t y_{ts} + (r \leftrightarrow s) \, , \tag{1.24}$$

$$[\mathbf{m}_\nu^{\text{Zee–Babu}}]_{rs} = \frac{\mu' v^2}{(16\pi^2)^2} \sum_{t,u} x_{[rt]} [\mathbf{m}_e]_t z_{\{tu\}} [\mathbf{m}_e]_u x_{[us]} I'_{tu} + (r \leftrightarrow s) \, , \tag{1.25}$$

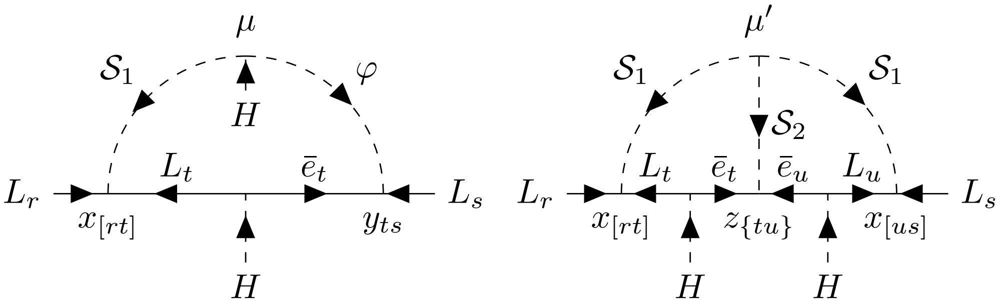

Figure 1.6: The neutrino self-energy diagrams relevant to the Zee (left) and Zee–Babu (right) models.

written in terms of the couplings $x, y, z \in \mathbb{C}$ as shown in Fig. 1.6, and the associated loop functions I and I'. One can see that in these models, the coefficient of the Weinberg operator κ is naturally suppressed with respect to the seesaw formula by SM-fermion masses (charged-lepton masses in this case), exotic couplings, and loop factors.

Such models are economic, since they do not require the imposition of *ad hoc* symmetries, and in many cases make a connection to other unsolved problems of the SM such as the nature of dark matter or the matter–antimatter asymmetry of the Universe. They are also elegant, since the smallness of the neutrino masses emerges as a natural consequence, rather than through the imposed requirement of exceedingly small coupling constants. Radiative models are easier to probe experimentally since the additional loop suppression and products of couplings bring down the allowed scale of the new physics, in some cases to LHC-accessible energy ranges [86]. The Zee–Babu model, for example, is non-trivially constrained by same-sign dilepton searches performed by ATLAS [87–89] and CMS [90–92]. Additionally, the predicted dependence of the neutrino-mass matrix on SM parameters, as is clear from Eqs. (1.24) and (1.25), can make these models very predictive as far as neutrino phenomenology is concerned. For example, the minimal version of the Zee model has the charged-lepton masses arising from couplings to φ, allowing for a simplification of the expression Eq. (1.24) such that the leptonic flavour index t is identified with s. The antisymmetry in the leptonic flavour indices implied by $x_{[rs]}$ must be accounted for by an antisymmetry in the loop integral such that $I \sim I_r - I_s$. The flavour structure then becomes [93]

$$[\mathbf{m}_\nu^{\text{Min. Zee}}]_{rs} \propto x_{[rs]}([\mathbf{m}_e]_r^2 - [\mathbf{m}_e]_s^2)\,, \tag{1.26}$$

which makes clear predictions relevant to neutrino oscillations that in this case rule out the model. For recent reviews of radiative models see Refs. [94, 95].

The Zee and Zee–Babu scenarios are only two of a very large number of radiative models, none of which are *a priori* more likely to be true than any other. In the context of such a large theory-space, it is useful to have an organising principle to aid in the study and classification of these models, and beginning with $\Delta L = 2$ effective operators has been shown to be an effective strategy.

One approach to this model taxonomy involves studying loop-level completions of the Weinberg operator, and its dimension-$(5 + 2n)$ generalisations

$$\mathcal{O}_1^{\prime \cdots \prime} = (LL)HH(H^\dagger H)^n \,.$$

Here, models can be systematically written down by studying the various topologies able to be accommodated by the operator with increasing number of loops. This is done in such a way that models implying lower-order contributions to the neutrino mass can be discarded [96]. Such an approach has been applied to the Weinberg operator up to three loops [24, 26, 97] and to its dimension-seven generalisation at one loop [98]. An alternative and complementary method begins by considering all of the gauge-invariant $\Delta L = 2$ operators in the SM effective field theory (SMEFT), first listed in this context by Babu and Leung [99] and extended by de Gouvêa and Jenkins [86]. Supposing that the tree-level coefficient of one of these is non-zero at the high scale, neutrino masses will be generated from loop graphs contributing to the mixing of this operator and the Weinberg-like operators $\mathcal{O}_1^{\prime \cdots \prime}$. The process of expanding the operator into a series of UV-complete, renormalisable models that generate the parent operator at tree-level is called *opening up* or *exploding* the operator. The remaining external fields must be looped-off, with additional loops of SM gauge bosons or Higgs fields added as necessary in order to obtain a neutrino self-energy diagram. A model-building formula along these lines has been formulated in Ref. [100], and it has been used to write down all of the minimal, tree-level UV-completions of $\Delta L = 2$ operators at dimension seven [101] corresponding to tree-level and radiative neutrino-mass models. The tree-level completions of the Weinberg-like operators have been written down up to dimension eleven [101–103]. The $\Delta L = 2$ operators in the SM EFT are discussed in more detail in Sec. 1.3.2.

We note that an economic classification scheme, separate from an EFT framework, was presented in Ref. [104] based on the number of exotic degrees of freedom by which the SM is extended. There, the method is applied to the case of radiative models with two exotics[4], and has also been used to study minimal neutrino-mass models compatible with SU(5) unification [105].

1.3 Effective field theory

In the following we introduce EFT in general, and then specialise to those built out of SM fields: the Standard Model EFT (SMEFT) and the Weak Effective Theory (WET). We place particular emphasis on the operators appearing at dimension-six, since these play

[4]Including models with one scalar and one Dirac fermion.

an important role in phenomenological analyses. Much of the focus of this work is the operators of odd mass-dimension up to dimension eleven, which organise the building of neutrino-mass models in the tradition of Refs. [86, 99–101]. Many of the principles introduced here for the dimension-six SMEFT will be directly relevant there. We begin with prefatory comments on the process of tree-level matching, then move on to discuss the SMEFT and some of the intricacies associated with redundancies among operators.

1.3.1 Tree-level matching

Suppose one has a theory with light particle states described by fields π_i and heavy states described by Π_i with a Lagrangian of the form

$$\begin{aligned} \mathscr{L}_{\text{UV}}[\pi, \Pi] &= \mathscr{L}_{\text{kin}}[\pi, \Pi] + \mathscr{L}_{\text{int}}[\pi, \Pi], \text{ with} \\ \mathscr{L}_{\text{int}}[\pi, \Pi] &= \mathscr{L}^{l}[\pi] + \mathscr{L}^{h}[\Pi] + \mathscr{L}^{lh}[\pi, \Pi]. \end{aligned} \tag{1.27}$$

Below the threshold for Π_i production, an effective description of the theory can be used that involves interactions only between the light fields. This effective theory is described by a Lagrangian $\mathscr{L}_{\text{eff}}[\pi]$ involving interactions between the π_i that correspond to diagrams in the full theory containing only heavy internal propagators and light external states. At the classical level, $\mathscr{L}_{\text{eff}}$ can be written down by integrating out the Π_i. Perturbatively this corresponds to expanding the heavy propagators Δ in powers of momenta on the heavy mass scale[5] Λ, such that

$$\Delta = \begin{cases} -\dfrac{1}{\Lambda^2}\left(1 + \dfrac{p^2}{\Lambda^2} + \cdots\right) & \text{for} \quad \text{- - - - - - - - - - -} \\ -\dfrac{\delta_\alpha^{\ \beta}}{\Lambda}\left(1 + \dfrac{p^2}{\Lambda^2} + \cdots\right) & \text{for} \quad \beta \longleftarrow\!\!\!\!\longrightarrow \alpha \\ -\dfrac{ip \cdot \bar{\sigma}^{\dot{\alpha}\beta}}{\Lambda^2}\left(1 + \dfrac{p^2}{\Lambda^2} + \cdots\right) & \text{for} \quad \beta \longleftarrow \dot{\alpha} \end{cases} . \tag{1.28}$$

In this notation, the arrow-preserving propagator corresponds to the part of the regular four-component fermion propagator proportional to momentum, while the arrow-violating one is the part proportional to the fermion mass. Expressions for the fermion propagators with reversed arrows follow from $\bar{\sigma}^\mu \to \sigma^\mu$ and interchanging dotted and undotted indices (see Ref. [22] Sec. 4.2 for the Lorentz structure).

Equivalently, the integration can be performed using the classical EOM of the Π_i. For some heavy field Π, the linearised solution to its classical EOM can be used to remove it from the Lagrangian completely. This procedure is mildly different for scalars

[5]We note that some UV scenarios may have more than one characteristic scale. In this case Λ can be understood as an effective scale which may not necessarily correspond to the mass of a specific particle.

and fermions, and we briefly outline these separately below. In both cases, we begin with a Lagrangian $\mathscr{L}_{\rm UV}$ for which we imagine that kinetic and mass mixing terms between heavy and light fields have been removed.

There are tree-level contributions to $\mathscr{L}^{\rm eff}$ as long as there are interaction terms linear in Π. For scalar Π, the UV Lagrangian contains the terms

$$\mathscr{L}_{\rm UV}[\Pi,\pi] \supset \Pi^\dagger(-D^2 - m_\Pi^2)\Pi + \left(\Pi\frac{\partial\mathscr{L}^{lh}}{\partial\Pi} + \text{h.c.}\right)\,, \tag{1.29}$$

where $\partial\mathscr{L}^{lh}/\partial\Pi$ is a function only of light fields, and we are neglecting interactions of the form $\Pi^\dagger\Pi f(\pi)$ for the sake of conciseness. The EOM are

$$(-D^2 - m_\Pi^2)\Pi = -\frac{\partial\mathscr{L}^{lh}}{\partial\Pi^\dagger} + \mathcal{O}(\Pi^2)\,, \tag{1.30}$$

which can be solved for $\Pi^{\rm cl}$, the classical field configuration, by inverting the differential operator on the LHS of Eq. (1.30) and expanding in D^2/m_Π^2:

$$\Pi^{\rm cl} = -\frac{1}{m_\Pi^2}\left(1 - \frac{D^2}{m_\Pi^2} + \cdots\right)\frac{\partial\mathscr{L}^{lh}}{\partial\Pi^\dagger}\,. \tag{1.31}$$

This solution can be substituted back into Eq. (1.29) to give interactions between light fields in the tree-level effective Lagrangian:

$$\mathscr{L}_{\rm eff}[\pi] \supset -\frac{\partial\mathscr{L}^{lh}}{\partial\Pi}\frac{1}{m_\Pi^2}\left(1 - \frac{D^2}{m_\Pi^2} + \cdots\right)\frac{\partial\mathscr{L}^{lh}}{\partial\Pi^\dagger}\,. \tag{1.32}$$

Many concrete examples of this procedure can be found in the literature, see *e.g.* Ref. [106]. The expansion in D^2/m_Π^2 corresponds to the expansion in p^2/Λ^2 in the first case of Eq. (1.28), showing the expansion of the scalar propagator.

Next we sketch out the procedure for a Dirac fermion $\Pi + \bar{\Pi}^\dagger$, where Π and $\bar{\Pi}$ are separate two-component spin-$\frac{1}{2}$ fields transforming oppositely under $G_{\rm SM}$. In this case, the UV theory is described by a Lagrangian like

$$\mathscr{L}_{\rm UV}[\Pi,\pi] \supset i\Pi^\dagger\bar{\sigma}^\mu D_\mu\Pi + i\bar{\Pi}^\dagger\bar{\sigma}^\mu D_\mu\bar{\Pi} + \left(\Pi\frac{\partial\mathscr{L}^{lh}}{\partial\Pi} + \bar{\Pi}\frac{\partial\mathscr{L}^{lh}}{\partial\bar{\Pi}} - m_\Pi\bar{\Pi}\Pi + \text{h.c.}\right) \tag{1.33}$$

Varying the action with respect to the heavy fields gives two coupled EOM:

$$i\bar{\sigma}^\mu D_\mu\Pi - m\bar{\Pi}^\dagger + \frac{\partial\mathscr{L}^{lh}}{\partial\Pi^\dagger} = 0\,, \tag{1.34}$$

$$i\bar{\sigma}^\mu D_\mu\bar{\Pi} - m\Pi^\dagger + \frac{\partial\mathscr{L}^{lh}}{\partial\bar{\Pi}^\dagger} = 0\,. \tag{1.35}$$

Substituting Eq. (1.34) into Eq. (1.35) gives a second-order partial differential equation in Π, analogous to Eq. (1.30). Inverting the differential operator in a similar way gives

$$\Pi^{\mathrm{cl}}_{\beta} = \frac{1}{m_\Pi^2}\left(\epsilon_{\alpha\beta} + \frac{\frac{1}{2}X_{\alpha\beta} - D^2\epsilon_{\alpha\beta}}{m_\Pi^2} + \cdots\right)\left(iD^{\alpha\dot\alpha}\frac{\partial \mathscr{L}^{lh}}{\partial \Pi^\dagger_{\dot\beta}}\epsilon_{\dot\alpha\dot\beta} + m_\Pi \frac{\partial \mathscr{L}^{lh}}{\partial \bar\Pi_\alpha}\right), \tag{1.36}$$

where the field-strength tensor comes about from a structure like

$$[\sigma^\mu\bar\sigma^\nu]_\alpha^{\ \beta} D_\mu D_\nu = \eta^{\mu\nu} D_\mu D_\nu \delta_\alpha^{\ \beta} - 2i[\sigma^{\mu\nu}]_\alpha^{\ \beta} D_\mu D_\nu \tag{1.37}$$
$$= D^2\delta_\alpha^{\ \beta} - \tfrac{1}{2}X_\alpha^{\ \beta}\,. \tag{1.38}$$

Here, and later in this section, the replacement $\bar\Pi \to \Pi$ should be understood for Majorana Π. Each contribution corresponds to a particular kind of propagator in the perturbative picture. The first term in the last parenthesis of Eq. (1.36) results from the fermion propagator proportional to momentum: the arrow-preserving fermion propagator shown as the last case of Eq. (1.28). The second term in the same parentheses stems from the fermion propagator proportional to the mass, corresponding to the arrow-violating propagator shown in the middle case of Eq. (1.28). Replacing Π in Eq. (1.33) gives the tree-level effective Lagrangian with the heavy fermion integrated out:

$$\begin{aligned}\mathscr{L}_{\mathrm{eff}}[\pi] \supset{}& \frac{\partial \mathscr{L}^{lh}}{\partial \Pi_\beta}\frac{1}{m_\Pi^2}\left(\epsilon_{\alpha\beta} + \frac{\frac{1}{2}X_{\alpha\beta} - D^2\epsilon_{\alpha\beta}}{m_\Pi^2} + \cdots\right) iD^{\alpha\dot\alpha}\frac{\partial \mathscr{L}^{lh}}{\partial \Pi^\dagger_{\dot\beta}}\epsilon_{\dot\alpha\dot\beta} \\ &+ \frac{\partial \mathscr{L}^{lh}}{\partial \Pi_\beta}\frac{1}{m_\Pi^2}\left(\epsilon_{\alpha\beta} + \frac{\frac{1}{2}X_{\alpha\beta} - D^2\epsilon_{\alpha\beta}}{m_\Pi^2} + \cdots\right)\frac{\partial \mathscr{L}^{lh}}{\partial \bar\Pi_\alpha}\,.\end{aligned} \tag{1.39}$$

As shown in Eqs. (1.32) and (1.39), expanding in powers of derivatives on heavy masses leads to a tower of local operators of increasing mass dimension d_i organised as a power series in the inverse heavy scale:

$$\mathscr{L}_{\mathrm{eff}}[\pi] = \mathscr{L}^{l}[\pi] + \sum_i \frac{C_i}{\Lambda^{d_i-4}}\mathscr{O}_i[\pi]. \tag{1.40}$$

The C_i are dimensionless coefficients which are in general calculable if one knows the high-energy theory.

1.3.2 Effective field theories of the SM

Below we discuss EFTs constructed from SM fields and invariant under SM symmetries. The main theory of study is the SMEFT: the gauge- and Lorentz-invariant EFT built from the fields listed in Table 1.1. We also mention the WET, also known as the LEFT (Low-energy Effective Field Theory), for which invariance under $SU(2)_+ \otimes SU(2)_- \otimes SU(3)_c \otimes U(1)_{EM}$ is required.

The SMEFT at dimension six

Given the broad experimental success of the SM, it is perhaps a sensible assumption that there should be a sizeable mass gap between the electroweak scale and the mass-scale characterising any new physics. In this context, the SMEFT can be a powerful tool for constraining how this new physics might look in a model-independent way. Indeed, the SMEFT operators at dimension six are already coming to play an increasingly important role in particle phenomenology, and they have become the *de facto* framework for interpreting low-energy constraints on theoretical models and experimental deviations from SM predictions. For an extensive review, we point the reader to Ref. [107].

It has not been easy to write down a complete basis of operators in the SMEFT [27, 28], although this is now a mostly solved problem [108–112]. The lowest-dimensional operator appearing in the EFT is also the only dimension-five operator:

$$\mathscr{L}^{(5)} = [C_5]_{\{rs\}}(L_r^i L_s^j) H^k H^l \epsilon_{ik}\epsilon_{jl} + \text{h.c.} \,, \tag{1.41}$$

already discussed briefly in Sec. ??. The matrix of operator coefficients is necessarily symmetric by Fermi–Dirac statistics. The operator violates lepton-number by two units, and usually gives the dominant contribution to the neutrino mass in Majorana models. Ref. [113] shows that operators in the SMEFT of mass-dimension d satisfy

$$\frac{1}{2}(\Delta B - \Delta L) = d \mod 2 \,, \tag{1.42}$$

and thus odd mass-dimension operators must violate $B-L$ by two units, while operators of even mass-dimension cannot violate $B-L$. So, aside from lepton-number-violating effects, the leading-order deviations from the SM appear at dimension six, where there are many more operators.

The dimension-six operators come in eight general classes: X^3, H^6, H^4D^2, X^2H^2, ψ^2H^3, ψ^2XH, ψ^2H^2D and ψ^4. (Here, X represents a general field-strength tensor, D is a covariant derivative and ψ is a fermion field.) The ψ^4-type operators illustrate some of the difficulties encountered when writing down a complete basis of operators, since they can be simplified by Fierz and Schouten identities relating to the spinor, isospin and colour structure. The most common basis found in the literature is the Warsaw basis [27, 28], which tends to prefer vector currents for fermions. Thus, for example, the four-fermion operators with field content L^4 written in this way are

$$[\mathcal{O}_{ll}]_{rstu} = (L_r^\dagger \bar{\sigma}_\mu L_s)(L_t^\dagger \bar{\sigma}_\mu L_u) \,, \tag{1.43}$$

$$[\mathcal{O}_{ll}^{(3)}]_{rstu} = (L_r^\dagger \bar{\sigma}_\mu \tau^I L_s)(L_t^\dagger \bar{\sigma}_\mu \tau^I L_u) \,. \tag{1.44}$$

Here $\mathcal{O}_{ll}^{(3)}$ contracts the $\bar{\mathbf{2}} \otimes \mathbf{2}$ of the $L^\dagger$ and L into the triplet representation. Naively there seem to be two operators, however $\mathcal{O}_{ll}^{(3)}$ can be rewritten using the SU(2) Fierz identity

$$[\tau^I]^i{}_j[\tau^I]^k{}_l = 2\delta^i{}_m\delta^k_j - \delta^i{}_j\delta^k_l \tag{1.45}$$

and the related identity acting on the spinor structure

$$(\psi_1^\dagger\bar{\sigma}^\mu\psi_2)(\psi_3^\dagger\bar{\sigma}^\mu\psi_4) = (\psi_1^\dagger\bar{\sigma}^\mu\psi_4)(\psi_3^\dagger\bar{\sigma}^\mu\psi_2) \tag{1.46}$$

such that

$$[\mathcal{O}_{ll}^{(3)}]_{rstu} = 2[\mathcal{O}_{ll}]_{ruts} - [\mathcal{O}_{ll}]_{rstu} \,. \tag{1.47}$$

Thus, the operators $[\mathcal{O}_{ll}^{(3)}]_{rstu}$ can be expressed as linear combinations of the $[\mathcal{O}_{ll}]_{rstu}$, and both operators should not be included in a genuine basis. The situation is slightly more complicated for the four-quark operators, since there is an additional space of indices to handle. In the case of operators with field content Q^4, there seem to naively be four invariants, which can be written as vector currents

$$(Q^\dagger\bar{\sigma}_\mu\Gamma Q)(Q^\dagger\bar{\sigma}_\mu\Gamma Q) \,, \tag{1.48}$$

where the possible structures $\Gamma \otimes \Gamma$ can be expressed schematically as

$$1 \otimes 1, \quad \tau^I \otimes \tau^I, \quad \lambda^A \otimes \lambda^A, \quad \tau^I\lambda^A \otimes \tau^I\lambda^A \,. \tag{1.49}$$

The $SU(2)_L$ and $SU(3)_c$ index contraction can either be internal to the fermion current, or it may connect fermions in adjacent currents. For example, the $SU(2)_L$ contraction is internal for the structures $1 \otimes 1$ and $\lambda^A \otimes \lambda^A$, but external for $\tau^I \otimes \tau^I$ and $\tau^I\lambda^A \otimes \tau^I\lambda^A$. The spinor identity Eq. (1.46) exchanges the Q fields, so it interchanges the isospin and colour indices so that

$$\text{both internal} \leftrightarrow \text{both external}, \quad SU(2)_L \text{ external} \leftrightarrow SU(3)_c \text{ external} \,. \tag{1.50}$$

This means only two of the four invariants are independent. These are chosen to be $1 \otimes 1$ and $\tau^I \otimes \tau^I$ in the Warsaw basis.

The operators in the Warsaw basis are listed in Tables 1.2 and 1.3. This is the form in which we use the operators throughout the rest of this work. Each operator is given in four-component spinor notation, as is usual in the literature. We refer the reader to Appendix A for the correspondence to the two-component notation we use elsewhere, along with other relevant mathematical notation used in the tables. Our conventions are chosen to comply with those of Ref. [114].

	Operator	Label	Operator	Label
$(\bar{L}L)(\bar{L}L)$	$(\bar{L}\gamma_\mu L)(\bar{L}\gamma^\mu L)$	$\mathcal{O}_{ll}$		
	$(\bar{Q}\gamma_\mu Q)(\bar{Q}\gamma^\mu Q)$	$\mathcal{O}_{qq}^{(1)}$	$(\bar{Q}\gamma_\mu \tau^I Q)(\bar{Q}\gamma^\mu \sigma^I Q)$	$\mathcal{O}_{qq}^{(3)}$
	$(\bar{L}\gamma_\mu L)(\bar{Q}\gamma^\mu Q)$	$\mathcal{O}_{lq}^{(1)}$	$(\bar{L}\gamma_\mu \sigma^I L)(\bar{Q}\gamma^\mu \sigma^I Q)$	$\mathcal{O}_{lq}^{(3)}$
$(\bar{R}R)(\bar{R}R)$	$(\bar{e}_R\gamma_\mu e_R)(\bar{e}_R\gamma^\mu e_R)$	$\mathcal{O}_{ee}$		
	$(\bar{u}_R\gamma_\mu u_R)(\bar{u}_R\gamma^\mu u_R)$	$\mathcal{O}_{uu}$	$(\bar{d}_R\gamma_\mu d_R)(\bar{d}_R\gamma^\mu d_R)$	$\mathcal{O}_{dd}$
	$(\bar{u}_R\gamma_\mu u_R)(\bar{d}_R\gamma^\mu d_R)$	$\mathcal{O}_{ud}^{(1)}$	$(\bar{u}_R\gamma_\mu \lambda^A u_R)(\bar{d}_R\gamma^\mu \lambda^A d_R)$	$\mathcal{O}_{ud}^{(8)}$
	$(\bar{e}_R\gamma_\mu e_R)(\bar{u}_R\gamma^\mu u_R)$	$\mathcal{O}_{eu}$	$(\bar{e}_R\gamma_\mu e_R)(\bar{d}_R\gamma^\mu d_R)$	$\mathcal{O}_{ed}$
$(\bar{L}L)(\bar{R}R)$	$(\bar{L}\gamma_\mu L)(\bar{e}_R\gamma^\mu e_R)$	$\mathcal{O}_{le}$	$(\bar{Q}\gamma_\mu Q)(\bar{e}_R\gamma^\mu e_R)$	$\mathcal{O}_{qe}$
	$(\bar{L}\gamma_\mu L)(\bar{u}_R\gamma^\mu u_R)$	$\mathcal{O}_{lu}$	$(\bar{L}\gamma_\mu L)(\bar{d}_R\gamma^\mu d_R)$	$\mathcal{O}_{ld}$
	$(\bar{Q}\gamma_\mu Q)(\bar{u}_R\gamma^\mu u_R)$	$\mathcal{O}_{qu}^{(1)}$	$(\bar{Q}\gamma_\mu \lambda^A Q_L)(\bar{u}_R\gamma^\mu \lambda^A u_R)$	$\mathcal{O}_{qu}^{(8)}$
	$(\bar{Q}\gamma_\mu Q)(\bar{d}_R\gamma^\mu d_R)$	$\mathcal{O}_{qd}^{(1)}$	$(\bar{Q}\gamma_\mu \lambda^A Q_L)(\bar{d}_R\gamma^\mu \lambda^A d_R)$	$\mathcal{O}_{qd}^{(8)}$
$(\bar{L}R)(\bar{R}L)$	$(\bar{L}e_R)(\bar{d}_R Q)$	$\mathcal{O}_{ledq}$		
$(\bar{L}R)(\bar{L}R)$	$(\bar{Q}_i u_R)(\bar{Q}_j d_R)\epsilon^{ij}$	$\mathcal{O}_{quqd}^{(1)}$	$(\bar{Q}_i \lambda^A u_R)(\bar{Q}_j \lambda^A d_R)\epsilon^{ij}$	$\mathcal{O}_{quqd}^{(8)}$
	$(\bar{L}_i e_R)(\bar{Q}_j u_R)\epsilon^{ij}$	$\mathcal{O}_{lequ}^{(1)}$	$(\bar{L}_i \sigma_{\mu\nu} e_R)(\bar{Q}_j \sigma^{\mu\nu} u_R)\epsilon^{ij}$	$\mathcal{O}_{lequ}^{(3)}$
$\Delta B = 1$			$(d_R^a u_R^b)(Q^{ci} L^j)\epsilon_{abc}\epsilon_{ij}$	$\mathcal{O}_{duq}$
			$(Q^{ai} Q^{bj})(u_R^c e_R)\epsilon_{abc}\epsilon_{ij}$	$\mathcal{O}_{qqu}$
			$(d_R^a u_R^b)(u_R^c e_R)\epsilon_{abc}$	$\mathcal{O}_{duu}$
			$(Q^{ai} Q^{bk})(Q^{cl} L^j)\epsilon_{abc}\epsilon_{ij}\epsilon_{kl}$	$\mathcal{O}_{qqq}$

Table 1.2: The table shows the four-fermion operators in the dimension-six SMEFT in the Warsaw basis [27, 28]. The operators are listed in four-component spinor notation, and a full correspondence to the two-component notation we use elsewhere can be found in Appendix A. We remind the reader that combinations like (QQ) stand for $(\bar{Q}^C Q)$, where Q^C is the charge-conjugated spinor. Flavor indices are omitted, and should be understood to label the fermions in the order $\{r, s, t, u\}$ as they appear.

	Operator	Notation	Operator	Notation
X^3	$W_\mu^{I\nu} W_\nu^{J\rho} W_\rho^{K\mu} \epsilon_{IJK}$	$\mathcal{O}_W$	$\tilde{W}_\mu^{I\nu} W_\nu^{J\rho} W_\rho^{K\mu} \epsilon_{IJK}$	$\mathcal{O}_{\tilde{W}}$
	$G_\mu^{A\nu} G_\nu^{B\rho} G_\rho^{C\mu} f_{ABC}$	$\mathcal{O}_G$	$\tilde{G}_\mu^{A\nu} G_\nu^{B\rho} G_\rho^{C\mu} f_{ABC}$	$\mathcal{O}_{\tilde{G}}$
H^6	$(H^\dagger H)^3$	$\mathcal{O}_H$		
$H^4 D^2$	$(H^\dagger H)\Box(H^\dagger H)$	$\mathcal{O}_{H\Box}$	$H_i^\dagger (D_\mu H)^i \cdot (D^\mu H)_j^\dagger H^j$	$\mathcal{O}_{HD}$
$\psi^2 H^2$	$(H^\dagger H)(\bar{L} H e_R)$	$\mathcal{O}_{eH}$		
	$(H^\dagger H)(\bar{Q} H d_R)$	$\mathcal{O}_{dH}$	$(H^\dagger H)(\bar{Q} \tilde{H} u_R)$	$\mathcal{O}_{uH}$
$X^2 H^2$	$(H^\dagger H) B_{\mu\nu} B^{\mu\nu}$	$\mathcal{O}_{HB}$	$(H^\dagger H) \tilde{B}_{\mu\nu} B^{\mu\nu}$	$\mathcal{O}_{H\tilde{B}}$
	$(H^\dagger H) W^I_{\mu\nu} W^{I\mu\nu}$	$\mathcal{O}_{HW}$	$(H^\dagger H) \tilde{W}^I_{\mu\nu} W^{I\mu\nu}$	$\mathcal{O}_{H\tilde{W}}$
	$(H^\dagger \tau^I H) W^I_{\mu\nu} B^{\mu\nu}$	$\mathcal{O}_{HWB}$	$(H^\dagger \tau^I H) \tilde{W}^I_{\mu\nu} B^{\mu\nu}$	$\mathcal{O}_{H\tilde{W}B}$
	$(H^\dagger H) G^A_{\mu\nu} G^{A\mu\nu}$	$\mathcal{O}_{HG}$	$(H^\dagger H) \tilde{G}^A_{\mu\nu} G^{A\mu\nu}$	$\mathcal{O}_{H\tilde{G}}$
$\psi^2 X H$	$(\bar{L} \sigma^{\mu\nu} e_R) H B_{\mu\nu}$	$\mathcal{O}_{eB}$	$(\bar{L} \sigma^{\mu\nu} e_R) \tau^I H W^I_{\mu\nu}$	$\mathcal{O}_{eW}$
	$(\bar{Q} \sigma^{\mu\nu} u_R) \tilde{H} B_{\mu\nu}$	$\mathcal{O}_{uB}$	$(\bar{Q} \sigma^{\mu\nu} u_R) \tau^I \tilde{H} W^I_{\mu\nu}$	$\mathcal{O}_{uW}$
	$(\bar{Q} \sigma^{\mu\nu} d_R) H B_{\mu\nu}$	$\mathcal{O}_{dB}$	$(\bar{Q} \sigma^{\mu\nu} d_R) \tau^I H W^I_{\mu\nu}$	$\mathcal{O}_{dW}$
	$(\bar{Q} \sigma^{\mu\nu} \lambda^A u_R) \tilde{H} G^A_{\mu\nu}$	$\mathcal{O}_{uG}$	$(\bar{Q} \sigma^{\mu\nu} \lambda^A d_R) H G^A_{\mu\nu}$	$\mathcal{O}_{dG}$
$\psi^2 H^2 D$	$(H^\dagger i\bar{D}_\mu H)(\bar{L} \gamma^\mu L)$	$\mathcal{O}_{Hl}^{(1)}$	$(H^\dagger i\bar{D}^I_\mu H)(\bar{L} \gamma^\mu \tau^I L)$	$\mathcal{O}_{Hl}^{(3)}$
	$(H^\dagger i\bar{D}_\mu H)(\bar{e}_R \gamma^\mu e_R)$	$\mathcal{O}_{He}$		
	$(H^\dagger i\bar{D}_\mu H)(\bar{Q} \gamma^\mu Q)$	$\mathcal{O}_{Hq}^{(1)}$	$(H^\dagger i\bar{D}^I_\mu H)(\bar{Q} \gamma^\mu \tau^I Q)$	$\mathcal{O}_{Hq}^{(3)}$
	$(H^\dagger i\bar{D}_\mu H)(\bar{u}_R \gamma^\mu u_R)$	$\mathcal{O}_{Hu}$	$(H^\dagger i\bar{D}_\mu H)(\bar{d}_R \gamma^\mu d_R)$	$\mathcal{O}_{Hd}$
	$H^i (iD_\mu H)^j \epsilon_{ij} \cdot (\bar{u}_R \gamma^\mu d_R)$	$\mathcal{O}_{Hud}$		

Table 1.3: The table shows the operators featuring in the Warsaw basis [27, 28] of the dimension-six SMEFT that are not four-fermion operators. We point the reader to Appendix A for the correspondence between the four-component notation used here and the two-component notation used elsewhere in this work for spinors, along with the definition of $\bar{D}^\mu$. Flavor indices are omitted and should be understood to act on fermions in the order $\{r, s\}$ as they appear in each operator.

The Low-energy or Weak Effective Theory

Many experimental constraints on the SM and its extensions come from low-energy flavour-changing process involving four fermions. These can be accurately described using an effective theory, similar to the Fermi theory of the Weak interactions, in which the electroweak gauge bosons, the physical higgs and the top quark have been integrated out. The dimension six operators in this low-energy EFT [115–118] have been extensively applied to B, K and D meson decays, meson–anti-meson oscillations and leptonic decays, *e.g.* [119]. They are also an invaluable tool for studying deviations from the SM in a way independent from many of the assumptions underlying SMEFT. The symmetries of the theory are only those of QCD and electromagnetism, and the fermions are the usual quarks and leptons with the top quark excluded from the theory. At dimension six there are 3,631 $\Delta B = \Delta L = 0$ operators [115], and we do not list them all here. Rather, we introduce the pertinent operators within the discussion of each specific phenomenological process we study in this work.

1.3.3 Operator redundancy and the Hilbert series

The previous section introduced some of the difficulties involved with writing down a basis of four-fermion operators for a complex EFT like the SMEFT. Additional redundancy can occur once operators with (covariant) derivatives are included. These include operator relations through integration by parts (IBP) and field redefinitions involving the classical equations of motion (EOM) [27, 120, 121]. At mass-dimensions larger than six, these come to be a large source of the difficulty in writing down a complete operator basis, but the problem can be addressed through Hilbert-series methods [108–112]. Below, we motivate how the EOM can be used to simplify effective operator bases, and explain how these redundancies can be accounted for through Hilbert series techniques.

Field redefinitions and the equations of motion

It is clear that operators can be simplified using the EOM at lowest order [27, 122–124], since the external legs are put on-shell in the Feynman rules. That is, an operator like

$$(H^\dagger H)(\bar{e}_R i\not{D} e_R) \tag{1.51}$$

can be simplified when it appears in calculations with all legs external. So, any leading-order amplitude involving the operator can be reduced through

$$i\not{D} e_R = y_e H^\dagger L\,, \tag{1.52}$$

(or equivalently $\mathcal{M} \sim \not{p} u_e = m_e u_e$ by the momentum-space Dirac equation) to $\mathcal{O}_{eH}$. Surprisingly, this useful result can be extended even to cases involving propagators and loops by performing field redefinitions. Specifically, field redefinitions that preserve the symmetries of the theory and contain a term linear in the original field allow the EOM to simplify a local effective Lagrangian without affecting the S-matrix [125–131]. We illustrate this with a toy ϕ^4 theory:

$$\mathscr{L} = \frac{1}{2}(\partial_\mu\phi)(\partial^\mu\phi) - \frac{1}{2}m^2\phi^2 - \frac{\lambda}{4!}\phi^4 + \frac{c_1}{\Lambda^2}\phi^6 + \frac{c_2}{\Lambda^2}\phi^3\Box\phi + \mathcal{O}(\Lambda^{-4})\,. \tag{1.53}$$

Under the field redefinition

$$\phi \to \phi + \frac{c_2}{\Lambda^2}\phi^3\,, \tag{1.54}$$

the kinetic term becomes

$$\frac{1}{2}(\partial_\mu\phi)(\partial^\mu\phi) \to \frac{1}{2}(\partial_\mu\phi)(\partial^\mu\phi) - \frac{c_2}{\Lambda^2}\phi^3\Box\phi + \mathcal{O}(\Lambda^{-4})\,, \tag{1.55}$$

where the second term comes from integrating $c_2\Lambda^{-2}(\partial_\mu\phi)(\partial^\mu\phi^3)$ by parts. This term cancels the last term in Eq. (1.53), for which the additional operators induced by the field redefinition are all $\mathcal{O}(\Lambda^{-4})$ terms. Performing the field redefinition on the other interaction terms in the Lagrangian leads to an effective redefinition of λ and c_1, with all other induced operators suppressed by four powers of Λ. Concretely,

$$\begin{aligned}\mathscr{L} \to\ & \frac{1}{2}(\partial_\mu\phi)(\partial^\mu\phi) - \frac{1}{2}m^2\phi^2 - \frac{\lambda}{4!}\phi^4 + \frac{c_1}{\Lambda^2}\phi^6 + \frac{c_2}{\Lambda^2}\phi^3\Box\phi \\ & + \frac{c_2}{\Lambda^2}\phi^3\underbrace{\left(-\Box\phi - m^2\phi - \frac{\lambda}{3!}\phi^3\right)}_{\equiv E[\phi]} + \cdots \\ = & \frac{1}{2}(\partial_\mu\phi)(\partial^\mu\phi) - \frac{1}{2}m^2\phi^2 - \underbrace{\left(\frac{\lambda}{4!} + \frac{c_2}{\Lambda^2}m^2\right)}_{\equiv\lambda'/4!}\phi^4 + \underbrace{\left(\frac{c_1}{\Lambda^2} - \frac{c_2}{\Lambda^2}\frac{\lambda}{3!}\right)}_{\equiv c_1'/\Lambda^2}\phi^6 + \mathcal{O}(\Lambda^{-4})\,.\end{aligned} \tag{1.56}$$

This is guaranteed since in the effective theory all of the operators consistent with the symmetries are already present, so the effects of the additional terms are exclusively to shift the coefficients of the theory around. The appearance of the EOM operator $E[\phi]$ above can be understood on the basis of the nature of the field redefinition Eq. (1.54). The additional terms induced by the field redefinition up to $\mathcal{O}(\Lambda^{-2})$ will be those in which a ϕ or its derivative has been replaced with $c_2\Lambda^{-2}\phi^3$. That is,

$$\begin{aligned}\Delta\mathscr{L} &= \frac{c_2}{\Lambda^2}\phi^3\frac{\partial\mathscr{L}}{\partial\phi} + \frac{c_2}{\Lambda^2}(\partial_\mu\phi^3)\frac{\partial\mathscr{L}}{\partial(\partial_\mu\phi)} + \mathcal{O}(\Lambda^{-4}) \\ &= \frac{c_2}{\Lambda^2}\phi^3\left[\frac{\partial\mathscr{L}}{\partial\phi} - \partial_\mu\frac{\partial\mathscr{L}}{\partial(\partial_\mu\phi)}\right] + \mathcal{O}(\Lambda^{-4})\,,\end{aligned} \tag{1.57}$$

where we have integrated the second term by parts in the last step. In order to show that the S-matrix is unaffected, it is not sufficient to show only that the Lagrangian has not changed form (up to order Λ^{-2}). In the path integral picture, the field redefinition Eq. (1.54) will also change the measure of the path integral and the sources $\mathcal{J}_i$ for each of the fields, whose effects we have not considered. These additional changes can be dealt with generically [120]. In short, the Jacobian can be written as a Lagrangian involving ghost fields, similar to the Fadeev–Popov approach taken in Gauge Theory. In this case the ghost fields acquire a mass of order Λ, and are therefore not relevant to the effective theory. The change to the source $\mathcal{J}_\phi$ does lead to a change in the Green's functions of the theory, although the S-matrix remains unchanged. We can see this easily in our toy theory. The LSZ reduction formula [132]

$$\begin{aligned} &G^{(n+m)}(q_1, \dots, q_m; p_1, \dots, p_n) \\ &\underset{\substack{p_j^2 \to m^2 \\ q_k^2 \to m^2}}{\sim} \left(\prod_{j=1}^{m} \frac{i\sqrt{Z_j}}{p_j^2 - m^2 + i\epsilon} \right) \left(\prod_{k=1}^{n} \frac{i\sqrt{Z_k}}{q_k^2 - m^2 + i\epsilon} \right) \langle q_1, \dots, q_m | S | p_1, \dots, p_n \rangle , \end{aligned} \tag{1.58}$$

relates the poles in the $(m+n)$-point Green's function to the S-matrix, up to wavefunction renormalisation factors Z_i. Here momenta p_i label the m incoming particles and q_i label the n outgoing particles. Consider, for example, the four-point Green's function with all particles taken to be incoming for simplicity:

$$G^{(4)}(p_1, p_2, p_3, p_4) = \left(\prod_{i=1}^{4} \int d^4 x_i \cdot e^{-ip_i \cdot x_i} \right) \langle 0 | T\{ \phi(x_1) \phi(x_2) \phi(x_3) \phi(x_4) \} | 0 \rangle . \tag{1.59}$$

The effect of the term $c_1 \Lambda^{-2} \mathcal{J}_\phi \phi^3$ is to alter the momentum-space Green's function to

$$\begin{aligned} &\langle 0 | T\{ [\phi(x_1) + c_1 \Lambda^{-2} \phi(x_1)^3] \cdots [\phi(x_4) + c_1 \Lambda^{-2} \phi(x_4)^3] \} | 0 \rangle \\ &\quad = \langle 0 | T\{ \phi(x_1)\phi(x_2)\phi(x_3)\phi(x_4) \} | 0 \rangle + \langle 0 | T\{ c_1 \Lambda^{-2} \phi(x_1)^3 \phi(x_2)\phi(x_3)\phi(x_4) \} | 0 \rangle \\ &\qquad + \sum_{i=2}^{4} (1 \leftrightarrow i) + \mathcal{O}(\Lambda^{-4}) , \end{aligned} \tag{1.60}$$

which differs only by the terms like $\langle 0 | T\{ c_1 \Lambda^{-2} \phi(x_1)^3 \phi(x_2)\phi(x_3)\phi(x_4) \} | 0 \rangle$ to order Λ^{-2}. These matrix elements do not affect the S-matrix, since the singularity structure is different. In this case, there is no single-particle pole at x_1, and so there is no contribution to scattering.

In the context of this toy ϕ^4 theory we have motivated that terms in the effective Lagrangian $\mathscr{L}$ that are connected by the EOM are redundant when working to a fixed order in Λ. Such field redefinitions are a powerful tool for simplifying operator bases, and they are often used to eliminate as many operators with derivatives as possible. We proceed to illustrate how such redundancies, along with those from IBP, can be accounted for systematically with the Hilbert series.

The Hilbert series

In the following we discuss the Hilbert series (HS), also known as the Molien or Poincaré function, as a tool for writing down Lagrangian invariants in a conceptually clean and efficient way. The Hilbert series is a generating function that contains information about the number and structure of the invariants that can be constructed from a set of multiplets. The approach has been used in more formal contexts *e.g.* [133–135], although it has also been used to count lepton and quark flavour invariants [136, 137] as well as operators in the SMEFT [111]. Our aim here is to illustrate the essential components of the HS approach with examples.

The HS $\mathfrak{H}$ is a generating function that counts the number of operators with a certain field content, *i.e.*

$$\mathfrak{H}(\{\chi_j\}) = \sum_i c_i \mathcal{O}_i(\{\chi_j\}) , \tag{1.61}$$

where $c_i \in \mathbb{N}$ is the number of independent invariants with field content $\mathcal{O}_i$, a polynomial in the fields of the theory $\{\chi_j\}$. The c_i and $\mathcal{O}_i$ in the simplified case of a theory with a single field χ transforming under the compact Lie group G can be computed from the general formula for the HS:

$$\mathfrak{H}(\chi) = \int_G d\mu_G \exp\left[\sum_{r=1}^{\infty} \frac{\Delta(r)\chi^r \chi_R(z_j^r)}{r}\right] , \tag{1.62}$$

where $d\mu_G$ is Haar measure of the group, the invariant measure one can use to integrate over the manifold of G, and $\chi_R(z_j^r)$ is the character function associated with the representation R in which χ transforms under G. The character functions can be found using character generating functions [138] in general, but the functions relevant to the SM representations are listed in Appendix A.1 of Ref. [108]. The function

$$\Delta(r) = \begin{cases} 1 & \chi \text{ bosonic} \\ (-1)^{r+1} & \chi \text{ fermionic} \end{cases} , \tag{1.63}$$

accounts for the fact that χ is anticommuting in the fermionic case [138].

Even redundancies due to IBP and EOM relations can be incorporated into the HS technique. The space of invariants modulo EOM can be organised into representations of the conformal group [111, 112]. Irreducible representations of the conformal group involve a 'primary operator' $\mathcal{O}$ and its derivatives, called 'descendant operators': $(\mathcal{O}, \partial_\mu \mathcal{O}, \partial_\mu \partial_\nu \mathcal{O}, \ldots)$. The invariants can be constructed by decomposing tensor products of these irreps, which accounts for EOM redundancy, and then projecting out the primary operator, which deals with IBP relations. This alters the formula Eq. (1.62) slightly:

$$\mathfrak{H}(D, \chi) = d\mu_G \frac{1}{P(D, x_+, x_-)} \exp\left[\sum_{r=1}^{\infty} \frac{\Delta(r)\chi^r \chi_R(z_j^r)}{r D^{d_r}}\right] + \Delta\mathfrak{H}(D, \chi) , \tag{1.64}$$

where D is a spurion field representing the (covariant) derivative, d_r is the mass-dimension of the field χ_r and

$$P(D, x_+, x_-) = \frac{1}{(1 - D x_+ x_-)\left(1 - \frac{D}{x_+ x_-}\right)\left(1 - \frac{D x_+}{x_-}\right)\left(1 - \frac{D x_-}{x_+}\right)} , \tag{1.65}$$

with $x_\pm$ the $\mathrm{SU}(2)_\pm$ integration variables. The function $\Delta\mathfrak{H}$ can be obtained from a general formula presented in Ref. [112]. It's role is to cancel unwanted terms (of mass-dimension $d \leq 4$) from the HS that come about because the character functions of the conformal group are not orthonormal [112].

We illustrate the use of Eq. (1.64) with a simple example: the independent invariants built out of the SM Higgs doublet H. The Higgs doublet transforms in the fundamental representation of $\mathrm{SU}(2)_L$ and carries hypercharge $Y = \frac{1}{2}$, for which the relevant Haar measures are [139]

$$\int_{\mathrm{SU}(2)} d\mu_{\mathrm{SU}(2)} = \frac{1}{2\pi i} \oint_{|x|=1} \frac{dx}{x}(1 - x^2) , \qquad \int_{\mathrm{U}(1)} d\mu_{\mathrm{U}(1)} = \frac{1}{2\pi i} \oint_{|y|=1} \frac{dy}{y} , \tag{1.66}$$

and the character functions are [108, 140]

$$\chi_{I=\frac{1}{2}}(x) = \frac{1}{x} + x , \quad \chi_{Y=\frac{1}{2}}(y) = y^{1/2} , \tag{1.67}$$

for $x, y \in \mathbb{C}$. This gives [112]

$$\begin{aligned} \mathfrak{H}(H, \tilde{H}) = &\frac{1}{(2\pi i)^4} \oint_{|x_+|=1} dx_+ \oint_{|x_-|=1} dx_- \cdot \oint_{|x|=1} \frac{dx}{x}(1 - x^2) \cdot \oint_{|y|=1} \frac{dy}{y} \\ &\cdot \exp\left[n_f \sum_{r=1}^{\infty} \frac{H^r}{rD} \left(\frac{1}{x^r} + x^r \right) y^{r/2} \chi^r_{(0,0)} \right] \cdot \exp\left[n_f \sum_{r=1}^{\infty} \frac{\tilde{H}^r}{rD} \left(\frac{1}{x^r} + x^r \right) y^{-r/2} \chi^r_{(0,0)} \right] \\ &\cdot \frac{1}{P(D, x_+, x_-)} + (H^\dagger H D^2 - D^4) \end{aligned} \tag{1.68}$$

for the Hilbert series, where we have accounted for H and it's conjugate $\tilde{H}$ separately, and included the possibility of n_f flavours. The last term in parentheses is the relevant part of $\Delta\mathfrak{H}$ in this case, and $\chi_{(0,0)}$ is the scalar character function:

$$\chi_{(0,0)} = D P(D, x_+, x_-)(1 - D^2) . \tag{1.69}$$

The contour integrals can be done by expanding the integrand in H and $\tilde{H}$, and integrating up to the required order [133]. For this example, the first few terms in the HS are

$$\mathfrak{H}(H, \tilde{H}) = \text{Fill this in} . \tag{1.70}$$

The HS approach has an attractive module structure. For example, if one wanted to count the number of invariants while not accounting for IBP and EOM redundancies, one need only remove the Lorentz integrals, character functions and $\Delta\mathfrak{H}$. Something that is perhaps less clear is that the HS can also be used to construct operators that are not invariants of the symmetry groups in G, but rather violate those symmetries in specific ways.

We work through this point with an even simpler example than the previous one: a scalar ϕ charged only under a U(1) symmetry, motivated by Ref. [108]. In this case, the HS is

$$\mathfrak{H}(\phi,\phi^*) = \sum_{n=0}^{\infty}(\phi^*\phi)^n \tag{1.71}$$

$$= \frac{1}{1-\phi^*\phi}\,, \tag{1.72}$$

where we treat $\phi^*\phi$ as a c-number less than one. This sum can be written as a contour integral, making a more clear connection[6] to Eq. (1.62):

$$\mathfrak{H}(\phi,\phi^*) = \frac{1}{2\pi i}\oint_{|z|=1}\frac{dz}{z}\frac{1}{(1-\phi z)(1-\phi^*/z)}\,. \tag{1.73}$$

This connection is made more clear by expanding:

$$\begin{aligned}\frac{1}{(1-\phi z)(1-\phi^* z)} = {} & [1+\phi^*\phi+(\phi^*\phi)^2+\cdots]+z[\phi+\phi(\phi^*\phi)+\phi(\phi^*\phi)^2+\cdots]\\ & +z^2[\phi^2+\phi^2(\phi\phi^*)+\cdots]+\cdots\end{aligned} \tag{1.74}$$

The invariants sit in the first term, and so are picked out by the contour integral after dividing through by z in Eq. (1.73). Importantly, the terms proportional to z in Eq. (1.74) violate the symmetry by one unit, and so these can be picked out by the contour integral if we divide by z^2 in Eq. (1.73), and similarly for any desired value of charge violation.

The HS provides information about the field content of the invariants and the number of independent operators, but does not tell us exactly how to construct the singlets. This is an important drawback of the approach, although even here there has been much recent progress using on-shell methods, *e.g.* [141–144].

[6] The integrand can also be written as an exponential like in Eq. (1.62) containing ϕ and ϕ^*:

$$\frac{1}{(1-\phi z)(1-\phi^*/z)} = \exp\left[\sum_{r=1}^{\infty}\frac{(\phi z)^r}{r}+\sum_{r=1}^{\infty}\left(\frac{\phi^*}{z}\right)^r\frac{1}{r}\right]\,.$$

1.4 The flavour anomalies and their explanation

In recent years, measurements of a number of processes involving leptons have established a large set of significant and unresolved deviations from SM prediction. Many of these measurements involve semileptonic B-meson decays, and these can be placed into two broad classes:

Neutral-current These involve flavour-changing neutral-current (FCNC) $b \to s$ transitions and include branching-ratio measurements in final states with muons, anomalous angular observables in $B \to K^* \mu\mu$, and violations of μ–e LFU in $B \to K^{(*)}\ell\ell$ processes. This class corresponds to hundreds of discrepant measurements in total, and single-operator fits suggest a preference for new-physics at roughly 6σ, *e.g.* [14].

Charged-current These involve $b \to c\ell\nu$ transitions and shown apparent deviations from τ–μ and τ–e LFU. The main observables measured in this case are LFU ratios in $B \to D^{(*)}\ell\nu$, for which the combined deviation from the SM expectation is just over 3σ [21].

Excitingly there is a high-degree of self-consistency between the measurements, both within and across these two classes. That is, the measurements imply coherent and theoretically well-motivated patterns when interpreted in terms of deviations in four-fermion operator coefficients.

In addition to these classes, the most precise measurement of the anomalous magnetic moment of the muon $(g-2)_\mu$ [145], is in tension with the SM expectation [146] at roughly 3.5σ. More recently, a smaller discrepancy has also been measured in $(g-2)_e$ [147]. Taken together, these anomalies paint a picture of new-physics coupling to leptons in way that violates the LFU present in the SM. In the following we discuss the experimental situation relevant to each of these classes, and the extent to which new contributions to dimension-six operator coefficients can reconcile the discrepancies.

1.4.1 Neutral-current anomalies

The neutral-current anomalies represent a large family of measurements in tension with SM prediction with a common underlying $b \to s$ transition at the quark level and usually a $\mu^+\mu^-$ pair. The measurements come in three main categories: branching ratios, LFU ratios, and angular observables.

There are many discrepancies seen in branching ratio data at dimuon invariant masses below the charmonium threshold. Examples include the branching ratios for the semileptonic decays $B \to K^{(*)}\mu\mu$ [148] and $B_s \to \phi\mu\mu$ [149], the leptonic decay $B_s \to \mu\mu$ [150–153], and the hyperon channels $\Lambda_b \to \Lambda\mu\mu$ [154]. In all cases, the measured values tend to fall short of the respective SM expectations.

Semileptonic B decays like $B \to K^{(*)}\mu\mu$ had already been recognised as good probes of new physics even before the start of the LHC, *e.g.* [155]. This is because, being FCNC processes, they are additionally suppressed in the SM by off-diagonal CKM matrix elements, weak couplings, and a loop factor. The differential decay rate for $B^+ \to K^+\ell\ell$ is [156]

$$\begin{aligned}\frac{d\Gamma}{dq^2} = \frac{G_F^2\alpha^2|V_{tb}V_{ts}^*|^2}{128\pi^5}|k|\beta\Bigg[\frac{2}{3}|k|^2\beta^2|C_{10}f_+(q^2)|^2 + \frac{4m_\ell^2(m_B^2-m_K^2)^2}{q^2m_B^2}|C_{10}f_0(q^2)|^2 \\ + |k^2|\left(1-\frac{1}{3}\beta^2\right)\left|C_9f_+(q^2)+2C_7\frac{m_b+m_s}{m_B+m_K}f_T(q^2)\right|^2\Bigg],\end{aligned} \tag{1.75}$$

where k is the kaon momentum, $\beta = (1-4m_\ell^2q^{-2})^{1/2}$, and $f_{0,+,T}$ are the $B \to K$ scalar, vector and tensor form factors. The expression is representative of the structure of the whole class of relevant semileptonic decays. The strongest dependence is on the operator coefficients C_9 and C_{10} in the WET, defined as

$$\mathcal{O}_9 = (\bar{s}\gamma^\mu P_L b)(\bar{\mu}\gamma_\mu\mu)\,, \tag{1.76}$$

$$\mathcal{O}_{10} = (\bar{s}\gamma^\mu P_L b)(\bar{\mu}\gamma_\mu\gamma_5\mu)\,, \tag{1.77}$$

with the coefficients usually normalised such that

$$\mathscr{L} = \frac{4G_F}{\sqrt{2}}V_{tb}V_{ts}^*\frac{e^2}{16\pi^2}\sum_i C_i\mathcal{O}_i\,. \tag{1.78}$$

Experimentally, semileptonic process like $B \to K\mu\mu$ are difficult to separate from the corresponding background processes like $B \to K\psi(\to \mu\mu)$, where ψ represents any of the vector charmonium resonances. For this reason, kinematic regions close to the narrow charmonium resonances are excluded from experimental analyses. The most significant single deviation is in the semileptonic decay $B_s \to \phi\mu\mu$, for which the data depart from the SM prediction by more than 3σ in the $q^2 \in [1,5]$ GeV^2 bin [149]. A problematic feature of this and many of these channels is that the SM prediction is plagued by hadronic uncertainties, which can be difficult to calculate. We show the differential branching ratio for $B_s \to \phi\mu\mu$ measured by LHC*b* in Fig. 1.7, taken from Ref. [13], along with the SM predictions using different methods to deal with the form factors [10–12]. Both the large uncertainties on the theory side and the apparent suppression of the measured values are clear. The discrepancy with the SM is largest in the aforementioned q^2 bin.

The decay $B_s \to \mu\mu$ is cleaner than the semileptonic decays on the theory side: the final state is leptonic and the only non-perturbative physics needed is the B_s decay constant, which can be calculated to high precision on the lattice [157]. The measurements performed by ATLAS [153], LHC*b* [151, 152] and CMS [150] are shown in Fig. 1.8,

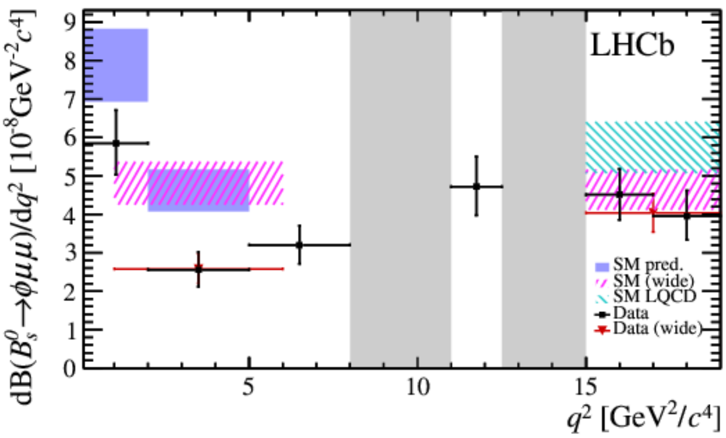

Figure 1.7: The figure shows the measured and predicted values for the differential branching ratio for $B_s \to \phi\mu\mu$ by bins of q^2. The data points are the LHCb measurements, while the coloured rectangles are the SM predictions with form factors calculated using light-cone sum rules [10, 11] and lattice QCD [12]. The greyed out regions correspond to charmonium resonances, exluded from the analysis as discussed in the main text. The LHCb data points are generally lower than the SM expectation, especially in the $q^2 \in [1, 5]$ GeV^2 bin where the discrepancy is larger than 3σ. The plot is taken from Ref. [13].

along with correlated limits on $B^0 \to \mu\mu$. The combination of the measurements shown is taken from Ref. [14], and suggests a compatibility with the SM at close to 2σ. Currently, measurements of $B_s \to \mu\mu$ are statistically limited; the branching ratio in the SM is very small because it is chirality suppressed, but this also makes it a promising mode for measuring new-physics effects.

The large theoretical uncertainties featuring in the expressions for the decay rates $\Gamma[B \to K^{(*)}\mu\mu]$ can be tamed in a more direct way by constructing a ratio with the electronic mode $B \to K^{(*)}ee$, in which many sources of uncertainty cancel in the regime where new-physics effects are small [158–160]. Interestingly, the LHCb collaboration has measured a suppression in the ratios

$$R_{K^{(*)}} = \frac{\Gamma[B \to K^{(*)}\mu\mu]}{\Gamma[B \to K^{(*)}ee]} \tag{1.79}$$

in the $q^2 \in [1, 6]$ GeV^2 bin. In the SM the prediction of the observables outside of the low-q^2 region is determined by physics which is wholly independent of the flavor of the lepton pair in the final state, making R_K and R_{K^*} finely sensitive to violations of LFU. LHCb finds [15]

$$R_K = 0.846\,^{+0.060+0.016}_{-0.054-0.014}\,, \tag{1.80}$$

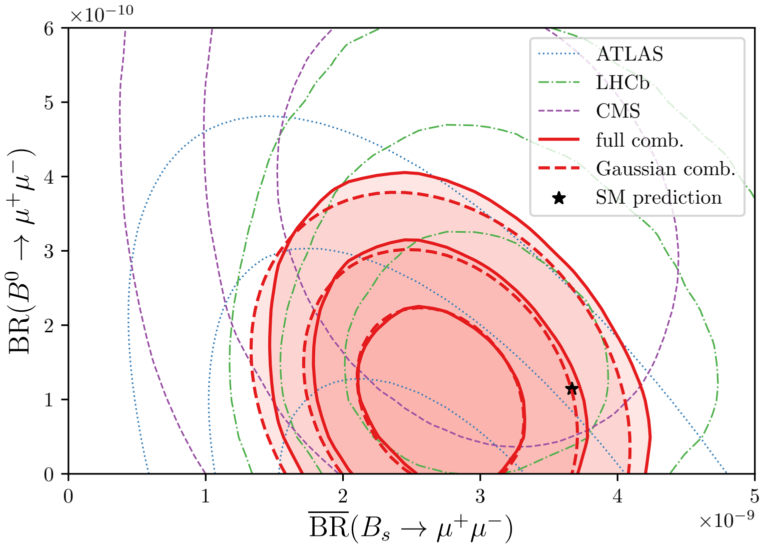

Figure 1.8: The figure shows the two-dimensional likelihood contours in Br($B^0 \to \mu\mu$) and Br($B_s \to \mu\mu$). The thin contours are individual measurements, while the thick contours are the combination. A Gaussian approximation to the combined fit is shown with thick dashed contours. For more details see Ref. [14], from where the figure is taken. The SM prediction (shown with a star) is compatible with the combined fit at 2σ.

for dilepton invariant mass squared range $q^2 \in [1.1, 6]$ GeV^2, while the SM demands $R_K^{\rm SM} = 1.0003 \pm 0.0001$ [161]. The analysis accounts for systematic differences in the reconstruction of muons and electrons by LHC*b* by first normalising the decay rates to the $B^+ \to K^+ J/\psi(\to \mu\mu/ee)$ rates. The measurement is then a double ratio in which many theoretical and experimental uncertainties cancel. The ratio R_K has also been measured by Belle [16] and BaBar [17] to be suppressed, although with larger uncertainties.

The K^* ratio has also been measured by LHC*b* [19] to show an approximately 2.5σ discrepancy in the central q^2 bin:

$$R_{K^*} = \begin{cases} 0.660\,^{+0.110}_{-0.070} \pm 0.024 & \text{for } 0.045\,\text{GeV}^2 < q^2 < 1.1\,\text{GeV}^2 \\ 0.685\,^{+0.113}_{-0.069} \pm 0.047 & \text{for } 1.1\,\text{GeV}^2 < q^2 < 6\,\text{GeV}^2 \end{cases} . \tag{1.81}$$

The Belle measurement [18] is consistent with the SM prediction at $\lesssim 2\sigma$:

$$R_{K^*} = \begin{cases} 0.90\,^{+0.27}_{-0.21} \pm 0.10 & \text{for } 0.1\,\text{GeV}^2 < q^2 < 8\,\text{GeV}^2 \\ 1.18\,^{+0.52}_{-0.32} \pm 0.10 & \text{for } 15\,\text{GeV}^2 < q^2 < 19\,\text{GeV}^2 \end{cases} . \tag{1.82}$$

Although the error bars are large, the central value is still suppressed with respect to the SM prediction in the low-q^2 region. A summary of the experimental situation relevant to R_K and R_{K^*} is presented in Fig. 1.9.

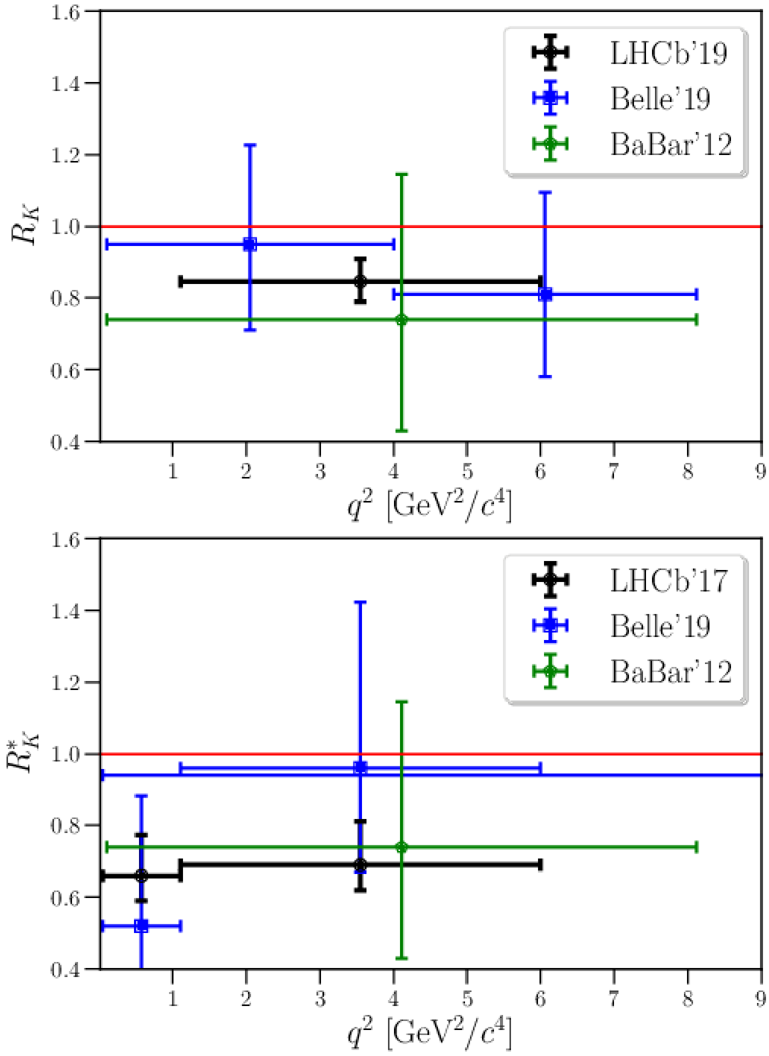

Figure 1.9: (top) The measurements of the LFU R_K by LHC*b* [15], Belle [16] and BaBar [17]. All measurements are suppressed relative to the SM prediction, shown in red. (bottom) The figure shows the experimental situation for R_{K^*} [17–19]. Like R_K, the measured values are found to be smaller than the SM value, shown in red. Both figures are taken from Ref. [20].

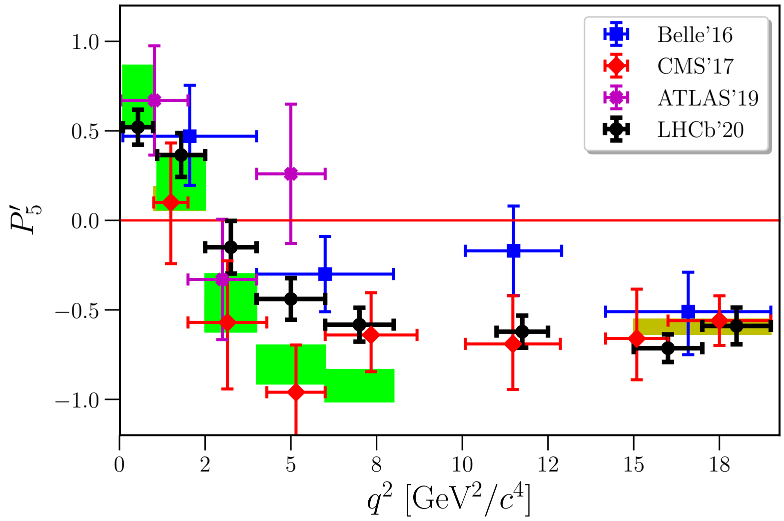

Figure 1.10: The figure shows the measured values of the P_5' angular observable in the decays $B \to K^*\mu\mu$ binned by q^2. With the exception of the CMS measurements, there is an enhancement with respect to the SM prediction (green) around $q^2 \sim 5\,\text{GeV}^2$. The plot is taken from Ref. [20].

The distribution of final-state particles in the semileptonic decays $B \to K^*\mu\mu$ define a number of angular observables, some of which have also been measured to be in disagreement with SM predictions. The P_5' asymmetry [162–164] is constructed as a ratio of angular observables to minimise from-factor uncertainties. Measurements show a significant deviation from the SM at around $q^2 \sim 5\,\text{GeV}^2$ [165–168] as shown in Fig. 1.10, although the CMS measurement [169] is consistent with the SM prediction [10, 11, 170, 171] in this region. The hadronic uncertainties are still sizeable in this case.

Fits

The picture of the neutral-current anomalies given above is still only a small cross-section of the several hundred observables that are in tension with the SM predictions. A large number of global-fit analyses have been conducted in which these anomalies are interpreted in terms of deviations in the operators C_9 and C_{10}, introduced above in Eq. (1.76). These analyses are all in mutual agreement, and generally find that a sizeable negative value for C_9 is preferred over the SM value at between 4 and 7σ [14, 172–174]. (This was first pointed out in Ref. [175], which analysed the 2013 data.) This wide range is largely due to differences in dealing with uncertainties in the semileptonic decays. Importantly, no large deviation in the electronic modes is necessary for a good fit. An example of one of the recent global fits [14] to C_9 and C_{10} is shown in Fig. 1.11. The

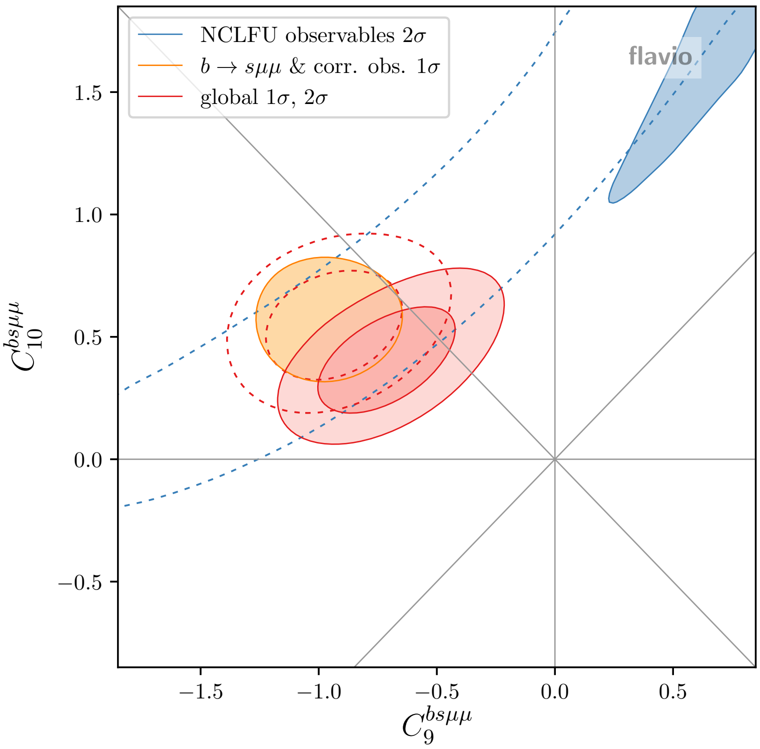

Figure 1.11: The figure shows the results of the global fit conducted in Ref. [14] in the C_9–C_{10} plane. The fit to just the LFU ratios is shown in blue, while that for the other $b \to s$ data is shown in yellow, with the combined fit shown in red. The $\mathrm{SU}(2)_L$-invariant direction $C_9 = -C_{10}$ gives a good fit to the data, and any acceptible fit requires a sizeable negative value for C_9. The plot is taken from Ref. [14].

authors find the single-operator best-fit scenario to be in the $\mathrm{SU}_L(2)$-invariant direction $C_9 = -C_{10}$, with $C_9 = -C_{10} = -0.53$ giving a pull from the SM of 6.6σ. We note that following the updated measurements of R_K [15] and R_{K^*} [18] presented at the 2019 Moriond conference, there is a slight tension between explaining the LFU ratios and the rest of the $b \to s$ data. We point the reader to Ref. [14] for a more detailed discussion on this point.

That much of the tension is driven by a deviation in C_9 also allows for an explanation of many of the anomalies in a way that does not require the introduction of new physics. The deviation in C_9 necessary to explain much of the anomalous $b \to s$ data can be mimicked by non-perturbative effects associated with loops of charm quarks, *e.g.* [13], and the data seem to be currently consistent with both hypotheses [176, 177]. Such effects cannot account for the violation of LFU seen in the ratios $R_{K^{(*)}}$, again highlighting their importance in understanding the potential role of new physics in explaining the neutral-current anomalies.

1.4.2 Charged-current anomalies

The class of charged-current anomalies in the $b \to c$ transition consists of a smaller number of measurements and processes. The primary observables of interest are the LFU ratios

$$R_{D^{(*)}} = \frac{\mathrm{Br}[B \to D^{(*)}\tau\nu]}{\mathrm{Br}[B \to D^{(*)}\ell\nu]} , \tag{1.83}$$

where ℓ denotes one of the light leptons: $\ell \in \{e, \mu\}$. The ratio has been measured by BaBar [178, 179], Belle [180–183] and LHC*b* [184–186], with combined values from HFLAV given by [21]

$$R_D = 0.340 \pm 0.027 \pm 0.013 \quad \text{and} \quad R_{D^*} = 0.295 \pm 0.011 \pm 0.008 . \tag{1.84}$$

These combinations are in tension with the SM predictions [187–190] as averaged by HFLAV:

$$R_D^{\mathrm{SM}} = 0.299 \pm 0.003 \quad \text{and} \quad R_{D^*}^{\mathrm{SM}} = 0.258 \pm 0.005 \tag{1.85}$$

at approximately 3σ. We note that BaBar and Belle use the average of the electronic and muonic modes in the denominator, while LHC*b* uses only the muonic mode. The tension was significantly decreased following the most recent Belle measurement presented at the Moriond 2019 conference [183]; this combined measurement is consistent with the SM prediction at 1.2σ. A summary of the measurements of $R_{D^{(*)}}$ is shown in Fig. 1.12. BaBar [179] and Belle [180] have measured the q^2 distributions of the tau-mode decay rate, which has proved to be a powerful model discriminator, *e.g.* [191].

Although the ratios $R_{D^{(*)}}$ are our primary concern in this work, we also introduce a number of other observables relevant to the charged current process. The first of these is the LFU ratio $R_{J/\psi}$:

$$R_{J/\psi} = \frac{\mathrm{Br}(B_c \to J/\psi\tau\nu)}{\mathrm{Br}(B_c \to J/\psi\mu\nu)} , \tag{1.86}$$

has recently been measured by LHC*b* to be $R_{J/\psi} = 0.71 \pm 0.17 \pm 0.18$ [192]. Although the ratio is also measured to be enhanced with respect to the SM prediction $R_{J/\psi}^{\mathrm{SM}} \approx 0.25$–$0.29$ [193? –204], the central value of the measurement shows a very large effect that cannot be well-accommodated with BSM contributions [205], although the error bars are very large. The observable $f_L^{D^*}$, the longitudinal polarisation of the D^* in $B \to D^*\tau\nu$, also differs from the SM expectation by $\sim 1.6\sigma$:

$$f_L^{D^*} = 0.60 \pm 0.08 \pm 0.04, \tag{1.87}$$

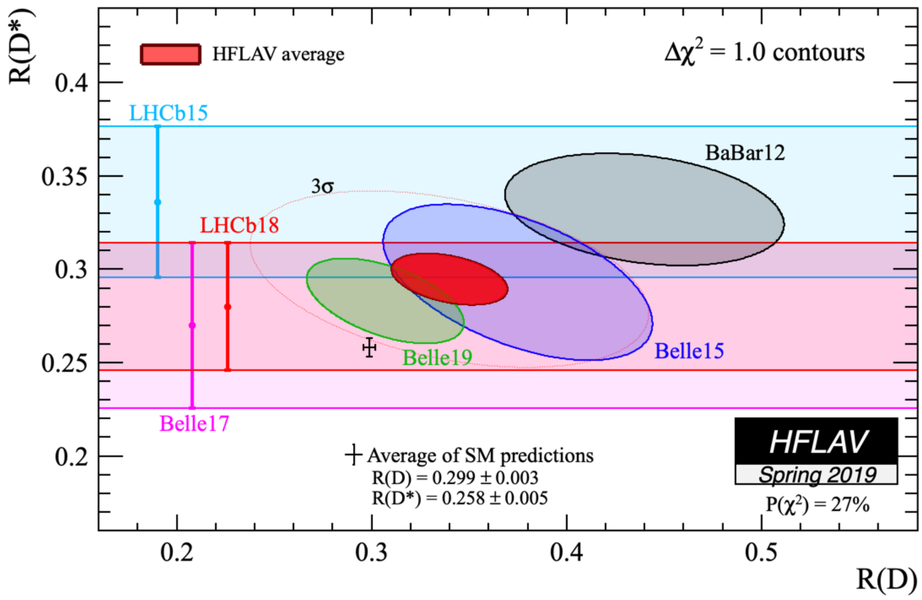

Figure 1.12: The figure shows the combined fit to the available R_D and R_{D^*} data from HFLAV [21]. The combination is shown in red, just over 3σ away from the SM prediction (black data point). Both ratios are measured to be enhanced compared to the SM value.

as measured by the Belle collaboration [206], and has been shown to have good discriminating power for BSM explanations of $R_{D^{(*)}}$. The third class of observables we consider are tau polarisation asymmetries [see Ref. [207] for a detailed discussion in the context of explaining $R_{D^{(*)}}$]. The polarisation asymmetry in the longitudinal direction of the τ in the D^* mode has also recently been measured by Belle [181]:

$$\mathscr{P}_\tau^* = -0.38 \pm 0.51^{+0.21}_{-0.16}. \tag{1.88}$$

Although the errors are large, the projected Belle II sensitivity at 50 ab^{-1} for the same observable in the D mode is estimated at about 3% [208], and we expect the $\mathscr{P}_\tau^*$ to be measured even more precisely at Belle II.

The leptonic decays of the charmed B meson have not been measured yet, although measurements of its lifetime may imply serious constraints on models attempting to explain the discrepancies in R_D and R_{D^*} with new physics. A number of groups have inferred a wide variety of limits

$$\mathrm{Br}(B_c \to \tau\nu) < [0.1, 0.6] \tag{1.89}$$

using differing theoretical arguments [209–213]. The range of limits is so wide because it is sensitive to the ratio of hadronisation probabilities of the charm and up quarks:

f_c/f_u. The range of values given for the limit in Eq. (1.89) corresponds only to a change in f_c/f_u of a factor of five [213].

John, When you put in chapter 3, move discussion of agreement in LFU between light-lepton modes and absence of lattice results for $B \to D^*$ form factors here.

Fits

The charged-current $b \to c$ anomalies can be interpreted in terms of deviations from dimension-six operator coefficients in the WET. The pertinent Hamiltonian for $b \to c\ell_r\nu_s$ is

$$H_{\text{eff}}^{b\to c} = \frac{4G_F}{\sqrt{2}} V_{cb} \sum_{rs} [(\delta^{rs} + C_{V_L}^{rs})\mathcal{O}_{V_L}^{rs} + C_{V_R}^{rs}\mathcal{O}_{V_R}^{rs} + C_{S_L}^{rs}\mathcal{O}_{S_L}^{rs} + C_{S_R}^{rs}\mathcal{O}_{S_R}^{rs} + C_T^{rs}\mathcal{O}_T^{rs}] + \text{h.c.} \quad (1.90)$$

where

$$\mathcal{O}_{V_X}^{rs} = (\bar{c}\gamma^\mu P_X b)(\bar{e}_r\gamma_\mu P_L \nu_s)\,, \; \mathcal{O}_{S_X}^{rs} = (\bar{c}P_X b)(\bar{e}_r P_L \nu_s)\,, \; \mathcal{O}_T^{rs} = (\bar{c}\sigma^{\mu\nu} P_X b)(\bar{e}_r \sigma_{\mu\nu} P_L \nu_s)\,, \quad (1.91)$$

and $X \in \{L, R\}$. The left-handed vector operator is the same one generated in the SM, while the scalar and tensor operators can provide large enhancements to the decay rate, since they lift the helicity-suppression.

A number of analyses have considered interpreting the measurements of R_D and R_{D^*} in the context of these operators, usually restricting to single-operator fits, *e.g.* [191, 202, 205, 214–217]. In Fig. 1.13 we present a plot taken from Ref. [205] in which the effects of each of the operators on the observables of interest are explored. The plot indicates that a number of single-operator solutions exist that reconcile the predicted and measured values for both R_D and R_{D^*}, although single-operator resolutions of the mild tension in $f_L^{D^*}$ are disfavoured by the limits on the B_c lifetime, discussed above.

1.4.3 Anomalous magnetic moment of the muon

The most precise measurement of the anomalous magnetic moment of the muon

$$a_\mu \equiv \frac{(g-2)_\mu}{2} \quad (1.92)$$

shows a sizeable tension with the SM prediction. The difference between the measured value [146, 218] and the SM prediction [] is

$$\Delta a_\mu = a_\mu^{\text{exp}} - a_\mu^{\text{SM}} = (286 \pm 63 \pm 43) \cdot 10^{-11}\,, \quad (1.93)$$

corresponding to a 3.6σ discrepancy. More recently, the measured value a_e, the anomalous magnetic moment of the electron, has also been found to disagree with the SM value at 2.5σ [219].

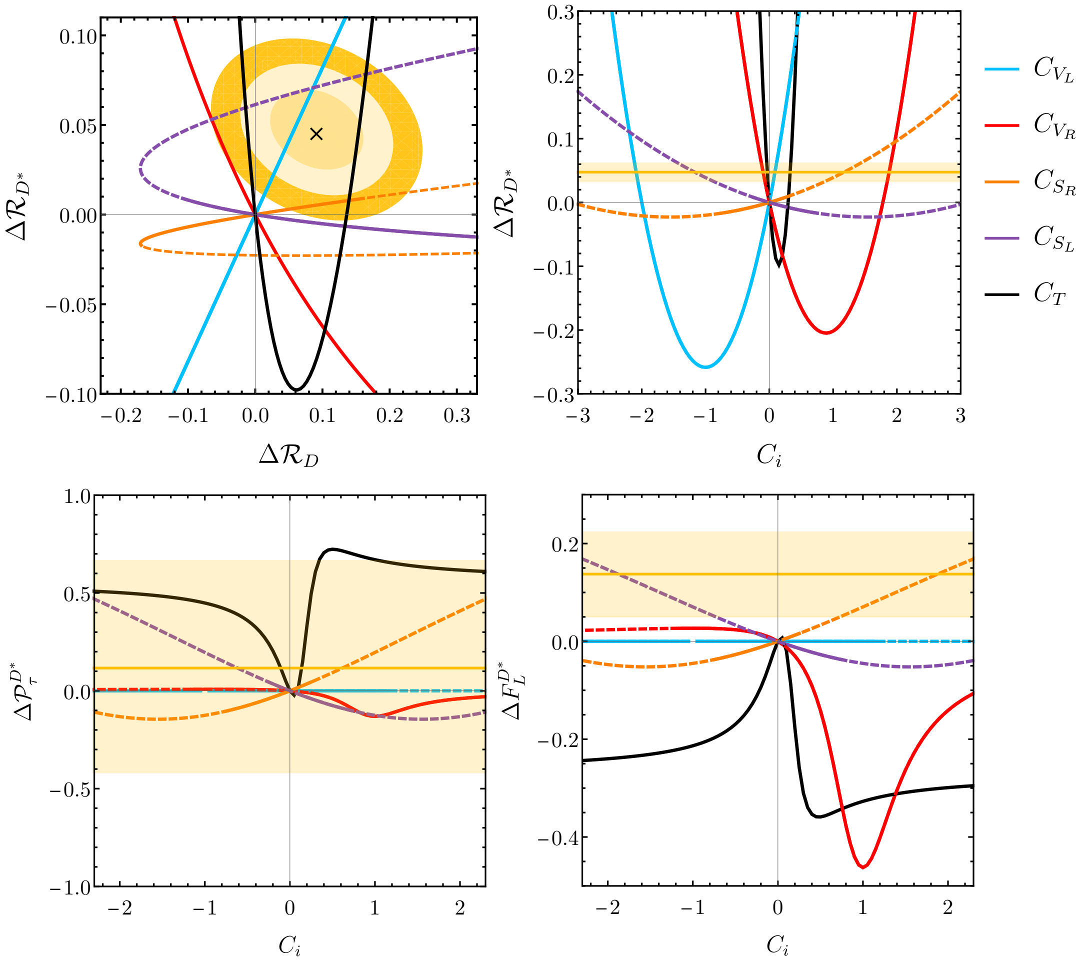

Figure 1.13: Individual contributions of the Wilson coefficients of the WET Hamiltonian in different observables ($\Delta X \equiv X - X_{\text{SM}}$): correlation between ΔR_D and ΔR_{D^*}, and $\Delta\mathscr{R}_{D^*}$, $\Delta\mathscr{P}_\tau^{D^*}$ and $\Delta F_L^{D^*}$ as a function of the Wilson coefficients. Left-top panel: the experimental central value is denoted by a black cross and the $1\sigma, 2\sigma$ and 3σ uncertainties by yellow rings. Right-top and bottom panels: experimental central values are displayed by a solid yellow line and their 1σ uncertainty by a yellow band. Dashed lines indicate regions excluded by the constraint $\text{Br}(B_c \to \tau\nu) < 0.1$.

2

Neutrino mass *ex machina*

This chapter is based on the publication 'Exploding operators for Majorana neutrino masses and beyond,' written in collaboration with Raymond R. Volkas [5]. We describe and implement an algorithm for 'exploding' operators: taking an effective operator and deriving from it renormalisable models that generate the operator at the low scale. We systematise this model-building procedure in a way that is easy to automate, and our methods are implemented in our publicly available example code [220]. We use the algorithm to generate computational representations of all of the tree-level completions of the $\Delta L = 2$ operators in the SMEFT up to and including mass-dimension eleven. Almost all of these correspond to models of radiative neutrino mass. Our work includes operators involving derivatives, updated estimates for the bounds on the new-physics scale associated with each operator, an analysis of various features of the models, and a look at some examples. We also make available a searchable database containing all of our results [221].

2.1 Introduction

We saw in Sec. 1.2.3 that the space of neutrino-mass models can be organised in various ways. One way we call the loop-level-matching paradigm, in which graphs of various loop orders are matched onto the Weinberg operator. Thorough analyses have been conducted in this framework, studying the Weinberg operator and its dimension-seven generalisation [24, 26, 97, 98] up to three and one loop, respectively. An alternative approach to neutrino-mass model taxonomy is to start with the $\Delta L = 2$ operators in the SMEFT and consider what field content generates these operators at tree-level in the UV [86, 99–101]. As discussed briefly in Sec. 1.2.3, this approach has been applied up to dimension-seven [101] to systematically write down a large class of simple models of neutrino mass.

Our analysis continues in the tradition of the latter methodology, but where appropriate we make a connection to the results from loop-level matching for completeness. We consider that there is complementary insight to be gained from thorough and complete analyses involving both approaches. Building models from tree-level completions of the $\Delta L = 2$ operators allows for a direct connection to be made between the neutrino-mass mechanism and other lepton-number-violating phenomena. The models derived in this way are also minimal in the sense that they involve the fewest number of exotic fields required to furnish a given loop-level topology, since the neutrino self-energy graphs always involve some SM fields. This has a number of important implications. First, the neutrino masses depend on SM parameters, and their rough scale can therefore be readily estimated from the effective operator alone. Second, neutrino-mass mechanisms containing SM gauge bosons are included automatically, and these constitute a large fraction of the models. Finally, it also means that our approach never produces models that contain loops of only exotic fields, although these can be added easily (see, for example, section IV.C of Ref. [100]). The appeal of these models notwithstanding, a benefit of giving up heavy loops is that the transformation properties of the beyond-the-standard-model particle content of each model are now uniquely determined, and therefore the total number of minimal models is finite. Minimal exotic particle content, in the aforementioned sense, is an attractive feature of this approach. Indeed, there are many examples of operators whose insertion and closure lead to neutrino masses at dimension nine and higher, but for which the number of exotic degrees of freedom introduced are not more than those of a garden-variety model generating the Weinberg operator at the low scale. The consideration of such equally simple models in the loop-level matching paradigm would require a detailed analysis of the dimension-seven and dimension-nine analogues of the Weinberg operator[1] up to a large number of loops.

Here, we sharpen the model building prescription developed in Ref. [100] and extend it to the case of operators involving field-strength tensors and derivatives. This procedure is automated and applied to all $\Delta L = 2$ operators in the SMEFT up to dimension eleven. We classify the neutrino-mass topologies, completions and their exotic fields. We also make available a database containing our main results and example code used to generate the operators along with their completions and Lagrangians [220]. We emphasise that the usefulness of these methods and tools extends beyond the study of neutrino mass and lepton-number-violating phenomena. To illustrate this point we reproduce some recent results of work listing completions of SMEFT operators [23].

The remainder of the paper is structured as follows. Section 2.2 sets out some conventions. Section 2.3 contains a review of tree-level matching and a description of the

[1] One can always generate the dimension-five Weinberg operator from its analogues at dimensions seven, nine and eleven with additional Higgs loops, but these models usually contain more than three loops.

methods we use to find the tree-level completions of the operators. Neutrino mass model building is described in section 2.4, while section 2.5 presents a preliminary analysis of the models along with some examples.

2.2 Conventions

In this section we establish the conventions we employ throughout the rest of the paper: our operational semantics and the classification of the lepton-number-violating operators on which our analysis is based. We highlight that this classification differs mildly from that found in earlier work, since our list includes additional structures as well as operators containing derivatives. We find the operators containing field-strength tensors to be uninteresting from the perspective of model building — a point justified in detail in Sec. 2.3.1 — and choose not to include them in our classification in this section. We remind the reader that our mathematical and notational conventions can be found in Appendix A, and these are drawn on heavily in this chapter.

2.2.1 On operators and tree-level completions

Below we discuss our use of the terms operator and completion. We establish naming conventions of types of operators that we use throughout the paper, and illustrate the sense in which we talk about models as completions of operators with the use of a simple example from the dimension-six SMEFT.

The term operator is used in the literature to loosely denote one of three[2] things:

1. A gauge- and Lorentz-invariant product of fields of specified flavour and their derivatives. Understood in this sense, the Weinberg 'operator'

$$\mathcal{O}_1^{\{rs\}} = (L_r^i L_s^j) H^k H^l \epsilon_{ik}\epsilon_{jl} \tag{2.1}$$

is really $n_f(n_f+1)/2$ complex operators for n_f SM-fermion generations.

2. A gauge- and Lorentz-invariant product of fields of unspecified flavour and their derivatives. According to this definition, $\mathcal{O}_1^{\{rs\}}$ is counted as a single operator.

3. A collection of fields and their derivatives whose product contains a Lorentz- and gauge-singlet part. In this sense, the string of fields $LLHH$ could be called an operator. In this category we also include operators of an intermediate type for which some gauge or Lorentz structure is specified but the rest is implied.

[2]These correspond to *operators*, *terms* and (roughly) *types of operators* in the convention of Ref. [222].

For example, a term like[3] $\mathcal{O}_{3a} = L^i L^j Q^k \bar{d} H^l \epsilon_{ij}\epsilon_{kl}$, for which colour and Lorentz structure are implicit.

The catalogues of $\Delta L = 2$ operators are lists of operators of type 3 in the above sense, since they are only distinguished on the basis of field content and $\mathrm{SU}(2)_L$ structure. Thus, the operators $\mathcal{O}_{3a}$ and $\mathcal{O}_{3b} = L^i L^j Q^k \bar{d} H^l \epsilon_{ik}\epsilon_{jl}$, for example, are understood to stand in for a large family of operators of types 1 and 2. In this case these differ in Lorentz structure (since the colour contraction is unique), and almost all of them are linearly dependent. They are related to each other by Fierz and SU(2)-Schouten identities, and can in general be related to other dimension-seven operators such as $(\bar{d}L)(LD\bar{u}^\dagger)$ and $(LL)H\Box H$ through field redefinitions involving the classical equations of motion (EOM) of SM-fermion and Higgs fields. (Operators related by these kinds of field redefinitions lead to identical S-matrix elements [120].) The total number of independent operators of type 1 can be found using Hilbert-series techniques [108–112], which give $2n_f^4$ independent operators with field content $L^2 Q\bar{d}H$ with the methods of Ref. [111]. These can be arranged into two terms with the Lorentz structure of the operators chosen such that the flavour indices don't have any permutation symmetries [223]:

$$\mathcal{O}^{(LQ)(Ld)}_{\substack{3a\\ rstu}} = (L^i_r Q^k_t)(L^j_s \bar{d}_u) H^l \epsilon_{ij}\epsilon_{kl}, \tag{2.2a}$$

$$\mathcal{O}^{(LQ)(Ld)}_{\substack{3b\\ rstu}} = (L^i_r Q^k_t)(L^j_s \bar{d}_u) H^l \epsilon_{ik}\epsilon_{jl}. \tag{2.2b}$$

From the perspective of $\Delta L = 2$ phenomenology, the $\mathrm{SU}(2)_L$ structure of the operators is most important. This can be seen in the following way: given a non-zero value for the coefficient of such an operator, the $\mathrm{SU}(2)_L$ structure is sufficient to tell at how many loops the neutrino self-energy or neutrinoless-double-beta-decay diagrams will arise, and what they will look like. Considering the example of operators $\mathcal{O}_{3a}$ and $\mathcal{O}_{3b}$ introduced above, it is clear that no component of $\mathcal{O}_{3a}$ contains two neutrino fields. Therefore, the Weinberg operator will be generated by one-loop graphs involving W bosons, which are additionally suppressed by powers of the weak coupling g. This coupling and loop suppression leads to inferred values of the new-physics scale characterising the operators $\mathcal{O}_{3a}$ and $\mathcal{O}_{3b}$ that differ by three orders of magnitude. On the other hand, predictions for the neutrino-mass scale from operators with different Lorentz structures differ only by $\mathcal{O}(1)$ factors [86].

Thus, our main goal is to find particle content in the UV that generates particular $\mathrm{SU}(2)_L$ structures of $\Delta L = 2$ operators at the low scale through tree graphs. In this way, we organise the catalogue of radiative neutrino-mass models by the number of loops in the neutrino self-energy diagram, or equivalently, by the implied scale of the new physics. In this sense, exploding the operator $\mathcal{O}_{3a}$, for instance, means finding the combinations of heavy field content that generate an operator of type 2 with $\mathrm{SU}(2)_L$

[3] Although the colour structure is unique here, this is not true of the Lorentz structure.

structure $3a$. This generated operator will not in general be $\mathcal{O}_{3a}^{(LQ)(Ld)}$ of Eq. (2.2), but will be expressible as a linear combination of $\mathcal{O}_{3a}^{(LQ)(Ld)}$ and $\mathcal{O}_{3b}^{(LQ)(Ld)}$, or any other chosen spanning set of operators.

This last point highlights the importance of the operator basis in talking about the completions of operators. A completion of an operator $\mathcal{O}$ is a model generating a non-zero value for the operator coefficient $C_{\mathcal{O}}$ at the high scale. Even a change of basis that leaves $\mathcal{O}$ unchanged will in general change $C_{\mathcal{O}}$, so one cannot talk about the completions of $\mathcal{O}$ *in vacuo*, apart from the other operators which together constitute the EFT. Restricting to the case of tree-level matching, after eliminating the heavy fields through their EOM, a UV model will generate some structure organically, which we call the *organic* operator, and this must then be matched onto the operator basis to extract coefficients. Our goal here is not to perform this matching onto a complete set of operators. Instead, we work with an implicitly overcomplete set of operators and define a convention that allows us to speak unambiguously about the UV models that might give rise to an operator in the set.

The existing catalogues of $\Delta L = 2$ operators enumerate operators of type 3 with definite $\mathrm{SU}(2)_L$-structure. The different isospin contractions are constructed by contracting indices in all possible ways with the invariant ϵ tensor. Operators with symmetric combinations of indices [which come about from non-trivial exotic irreps of $\mathrm{SU}(2)_L$] generate organic operators in general expressible as many linear combinations of different operators in the spanning set. One such combination is sufficient for our purposes, and we choose the one implied by the convention that non-trivial irreps never give rise to fields contracted with an ϵ symbol. We now illustrate this with an example from the dimension-six SMEFT below.

An overcomplete spanning set of two-Higgs–two-derivative operators is

$$\mathcal{O}_{H^2D^2}^{(1)} = \tilde{H}^i \tilde{H}^j \Box H^k H^l \epsilon_{ik}\epsilon_{jl}, \tag{2.3a}$$

$$\mathcal{O}_{H^2D^2}^{(2)} = \tilde{H}^i H^j \Box \tilde{H}^k H^l \epsilon_{ij}\epsilon_{kl}, \tag{2.3b}$$

$$\mathcal{O}_{H^2D^2}^{(3)} = \tilde{H}^i H^j \Box \tilde{H}^k H^l \epsilon_{ik}\epsilon_{jl}, \tag{2.3c}$$

$$\mathcal{O}_{H^2D^2}^{(4)} = \tilde{H}^i H^j \Box \tilde{H}^k H^l \epsilon_{il}\epsilon_{jk}. \tag{2.3d}$$

The renormalisable UV models of interest are a scalar $\mathrm{SU}(2)_L$ triplet with unit hypercharge $\Xi_1 \sim (\mathbf{1}, \mathbf{3}, 1)_S$, as well as a triplet and a singlet with vanishing hypercharge: $\Xi \sim (\mathbf{1}, \mathbf{3}, 0)_S$ and $\mathcal{S} \sim (\mathbf{1}, \mathbf{1}, 0)_S$. We envisage integrating these out from an interaction Lagrangian like

$$-\mathcal{L} \supset \tilde{H}^i H^j (x\mathcal{S}\epsilon_{ij} + y\Xi^{\{kl\}}\epsilon_{ik}\epsilon_{jl}) + (zH^i H^j \tilde{\Xi}_1^{\{kl\}}\epsilon_{ik}\epsilon_{jl} + \text{h.c.}), \tag{2.4}$$

with couplings $x, y, z \in \mathbb{C}$. They will generate organic operators that can be written as linear combinations of the operators listed above

$$\mathcal{S} \;:\quad \frac{x^2}{M_{\mathcal{S}}^2}\mathcal{O}^{(2)}_{H^2D^2}, \tag{2.5a}$$

$$\Xi \;:\quad \frac{y^2}{M_{\Xi}^2}\left[\mathcal{O}^{(3)}_{H^2D^2} + \mathcal{O}^{(4)}_{H^2D^2}\right], \tag{2.5b}$$

$$\Xi_1 \;:\quad \frac{|z|^2}{M_{\Xi_1}^2}\mathcal{O}^{(1)}_{H^2D^2}, \tag{2.5c}$$

up to $\mathcal{O}(1)$ factors. Of course, these can then be matched onto a genuine basis of operators like

$$\mathcal{O}_{\phi\Box} = \mathcal{O}^{(2)}_{H^2D^2} = \tilde{H}^i H^j \Box \tilde{H}^k H^l \epsilon_{ij}\epsilon_{kl}, \tag{2.6a}$$

$$\mathcal{O}_{\phi D} \overset{\text{IBP}}{\sim} \mathcal{O}^{(3)}_{H^2D^2} = \tilde{H}^i H^j \Box \tilde{H}^k H^l \epsilon_{ik}\epsilon_{jl}, \tag{2.6b}$$

but this is unnecessary for our purposes. (Note here that IBP stands for integration by parts.) The construction of the organic operator is in general not unique, since we work with an overcomplete set of operators. Here, for example, $\mathcal{O}^{(3)}_{H^2D^2} + \mathcal{O}^{(4)}_{H^2D^2} = 2\mathcal{O}^{(3)}_{H^2D^2} - \mathcal{O}^{(2)}_{H^2D^2}$, indicating clearly the redundancy of one of the operators. The convention that non-trivial representations never give rise to fields contracted with an ϵ symbol implies $\mathcal{O}^{(2)}_{H^2D^2}$ should not be chosen to feature in Eq. (2.5b). Thus, we call Ξ a completion of operators $\mathcal{O}^{(3)}_{H^2D^2}$ and $\mathcal{O}^{(4)}_{H^2D^2}$, even though the operator it generates can also be expressed as a linear combination of $\mathcal{O}^{(2)}_{H^2D^2}$ and $\mathcal{O}^{(3)}_{H^2D^2}$. This convention allows us to talk unambiguously about completions of the $\Delta L = 2$ operators in a way that makes their implications for neutrino mass most clear, while avoiding constructing a complete basis all the way up to dimension eleven.

We remark that this discussion can be extended to operators of type 3 with explicit $SU(3)_c$-structure with minor modifications. Here, irreducible representations are furnished by traceless tensors with raised and lowered symmetrised indices, which can be written as sums of operators in which contractions between raised and lowered indices are written with the δ symbol. The tracelessness condition can be enforced by additionally allowing contractions with the three-index ϵ symbol, and choosing that non-trivial representations never give rise to fields contracted with a δ, *i.e.* always choosing $[\lambda^A]^a_c[\lambda^A]^b_d = \frac{4}{3}\delta^a_d\delta^b_c - \frac{2}{3}\epsilon_{cde}\epsilon^{abe}$ over $[\lambda^A]^a_c[\lambda^A]^b_d = 2\delta^a_d\delta^b_c - \frac{2}{3}\delta^a_c\delta^b_d$. Explicit examples involving non-trivial colour contractions are presented in Sec. 2.3 and in the publicly available notebook we introduce in Sec. 2.3.2, which contains complete matching calculations for some of the dimension-six operators in the SMEFT.

2.2.2 Operator taxonomy

The list of gauge-invariant, $\Delta L = 2$ operators first provided by BL runs from $\mathcal{O}_1$ to $\mathcal{O}_{60}$ [99]. Each numbered operator is distinguished on the basis of field content, although each in general corresponds to a family of operators differing in $\mathrm{SU}(2)_L$-, Lorentz-, and flavour-structure. The operators are constructed from SM fermion fields and Higgs fields only and no internal global symmetries are imposed on the operators aside from baryon number. To violate lepton number by two units, each operator must contain at least one $\Delta L = 2$ fermion bilinear: one of $\{LL, L\bar{e}^\dagger, \bar{e}^\dagger\bar{e}^\dagger\}$. The operators enter the list at odd mass dimension [113] and only up to dimension eleven, since it was thought that higher dimensional operators generally imply neutrinos insufficiently heavy to meet the atmospheric lower bound. (It seems that a truly exhaustive treatment requires operators of higher mass-dimension [4], and this is discussed in detail in Sec. 2.4.1.) An additional 15 operators (acknowledged by BL, but left implicit) of mass dimension nine and eleven were added to the list by dGJ, increasing the total number to 75. These are constructed as products of lower-dimensional operators with the dimension-four Yukawa operators of the SM. Thus, they have the same field content as other operators in the list but carry different numerical labels. Latin subscripts were introduced by the same authors to distinguish different $\mathrm{SU}(2)_L$ contractions. The number of type-3 operators counted in this way is 129. Inclusion of the *all-singlets* operator $\bar{e}^\dagger\bar{e}^\dagger\bar{u}^\dagger\bar{u}^\dagger\bar{d}\bar{d}$, whose tree-level completions were recently written down [224], brings the tally to 130. Even in the extended dGJ scheme, product operators of the form $\mathcal{O} \cdot H_i^\dagger H^i$ are left implicit.

Here we work with a modified classification scheme which differs mildly from those used in the previous analyses. We list all operators explicitly, including product operators built from lower-dimensional ones and SM Yukawas or $H^\dagger H$, and enforce that operators with the same field content carry the same numerical labels. We adopt the convention of labelling $\mathrm{SU}(2)_L$-structures with an additional Latin subscript[4]. We have a greater number of such structures for each numbered operator than the other catalogues because we include product-type operators and new structures which may have been missed previously. We attempt to ensure that these new operators have labels that do not break compatibility with these and other previous works using lepton-number violating operators. A small exception is the case where only one structure is listed by BL and dGJ. In such situations this corresponds to operator a in our classification.

We find some new non-product operators not appearing in previous classifications even implicitly. These include new $\mathrm{SU}(2)_L$-structures but also new numbered operators. Dimension-eleven product-type operators built from a lower-dimensional operator and factors of $H^\dagger H$ that are not given numerical labels in the previous catalogues are given primed labels here, a common convention in the literature. In cases where a number of such operators carry the same field content, we prefer to use a new numerical label.

[4]We note that this introduces a notational ambiguity with colour indices, the resolution of which must be based on context.

For example, operators $\mathcal{O}'_{5a} = \mathcal{O}_{5a}(H^\dagger H)$ and $\mathcal{O}''_{3a} = \mathcal{O}_{3a}(H^\dagger H)^2$ have the same field content. They appear in our list as different $\mathrm{SU}(2)_L$-structures of the new numbered operator $\mathcal{O}_{80}$.

This means that the 75 numbered type-3 operator classes presented by dGJ now correspond to 82 classes and additional $\mathrm{SU}(2)_L$-structures $\{a, b, c, \ldots\}$. We present our list of $\Delta L = 2$ operators containing SM fermion and Higgs fields in Table B.1, located in Appendix B. Product operators as presented in our tables must be read with care. This is just a convenient shorthand to represent the field-content of an operator and illustrate that isospin indices are internally contracted. For example, by writing $\mathcal{O}_{5b} = \mathcal{O}_1 Q^i \bar{d} \tilde{H}^j \epsilon_{ij}$, we do not mean to suggest that Lorentz indices must be contracted internally to $\mathcal{O}_1$ and the down-type Yukawa. We discuss the additional information presented in Table B.1 as it is introduced throughout the paper.

The table also includes a list of $\Delta L = 2$ operators involving derivatives up to dimension nine. The pertinent operators at dimension seven were mentioned in Ref. [99] and listed in the context of a complete basis of operators for the dimension-seven SMEFT in Ref. [223]. The operators of higher dimension were excluded from the earlier catalogues of $\Delta L = 2$ operators on the basis that they may be less important for neutrino-mass model building, although they have appeared recently [144]. We find that opening up these operators does yield novel neutrino-mass models, although this is not clear at dimension seven. The derivative operators are also interesting from a broader phenomenological perspective, for example in the study of lepton-number-violating hadron decays, see *e.g.* Ref. [225]. The procedure we use for identifying these operators draws from the earlier $\Delta L = 2$ catalogues, Hilbert series techniques [108–112] as well as more recent automated approaches [222, 226–230].

Although operators related by field redefinitions through the classical EOM lead to identical S-matrix elements, we do not account for these redundancies in our catalogue of operators containing derivatives. This is done for two reasons: (1) we are ultimately interested in comparing Green's functions in the effective theory to those in various compatible UV theories; and (2) we are only interested in tree-level completions of effective operators, and EOM redundancies may relate operators generated from tree graphs to those generated by loops [231, 232]. Redundancies arising from integration by parts (IBP) are also not accounted for, and it should be understood that derivatives act on the operators listed in Table B.1 in all possible ways. In our listing, we prefer to act them in whichever way maximises the number of non-vanishing $\mathrm{SU}(2)_L$ structures, so that they can all be labelled. Often this means that derivatives will be carried by Higgs fields.

2.3 Tree-level matching forwards and backwards

In this section we outline the procedure we use for opening up operators of the sort introduced in Sec. 2.2.1 and Sec. 2.2.2 for the purpose of exploratory model building. We refer back to the prefatory comments made in Sec. 1.3.1 on tree-level matching for scalars and fermions, and include a discussion of the tree-level completions of operators containing derivatives and field-strength tensors. We highlight that the results of this section are not specific to $\Delta L = 2$ physics, and the model-building prescription can be applied (high-dimensional) operators in other EFTs. To illustrate the point, we apply the methods to an EFT unrelated to neutrino masses: the SMEFT at dimension-six.

The model-building framework introduced and used in Ref. [233] assumes that the new heavy fields introduced in the UV completions are only scalars, vector-like Dirac fermions or Majorana fermions. This particle content ensures the models are genuinely UV complete in the sense that their predictions can be extrapolated to arbitrarily high energies. Chiral fermions will in general introduce gauge anomalies, and the generation of their masses may introduce unnecessary complications. This treatment of exotic fermion fields is also used in Ref. [23], where a tree-level dictionary of the dimension-six SMEFT is written down. Exotic Proca fields will still need to be interpreted in the context of some larger UV framework (*e.g.* an extended gauge group), and so these are not introduced in our approach. Thus for the remainder of the paper we limit the discussion of building UV-complete models to those containing only scalars and non-chiral fermions.

In Sec. 1.3.1 we introduced the process of of matching a UV Lagrangian onto an effective theory. In this case, we are interested in the case where the UV theory is unknown. Here, the EFT is a useful way to encapsulate the effects of the entire class of possible UV theories in a model-agnostic way. We advocate that it is also a practical model-building tool, since the operators provide information about the types of UV models from which the EFT may arise. Subject to a number of assumptions, the possible UV models implied by an effective operator can be enumerated by building all possible tree graphs with an external-leg structure reflecting that of the operator. The quantum numbers of the heavy propagators can then be read off by imposing Lorentz- and gauge-invariance at every vertex, starting with vertices with two or three (for scalars) external edges. This is equivalent to exploring all of the possible ways the light fields may have been grouped into terms in $\mathscr{L}[\pi, \Pi]$ and distributed in the products of Eqs. (1.32) and (1.39). In the following we develop this picture into a precise algorithm.

Exploding operators

As an introductory example we use the Weinberg operator $\mathcal{O}_1 = (L^i L^j) H^k H^l \epsilon_{ik} \epsilon_{jl}$, whose minimal tree-level completions are the canonical seesaw models: $N \sim (\mathbf{1}, \mathbf{1}, 0)_{(2,1)}$, $\Xi_1 \sim$

$(\mathbf{1}, \mathbf{3}, 1)_S$ and $\Sigma \sim (\mathbf{1}, \mathbf{3}, 0)_{(2,1)}$. These can be derived by considering the allowed ways of decorating the two tree-level two-scalar–two-fermion topologies with the field content of the operator. These topologies are shown in Fig. 2.1 along with the possible ways of furnishing the topologies into Feynman diagrams, each corresponding to a seesaw model. As discussed above, this is equivalent to grouping fields together as they may have arisen in the partial derivatives of Eqs. (1.32) and (1.39). For the Weinberg operator, these groupings are:

$$L^i L^j H^k H^l \epsilon_{ik}\epsilon_{jl} \quad \Rightarrow \quad \frac{\partial \mathscr{L}^{lh}}{\partial N_\alpha} \supseteq x_r L_r^{\alpha i} H^k \epsilon_{ik} \sim N, \tag{2.7a}$$

$$L^i L^j H^k H^l \epsilon_{ik}\epsilon_{jl} \quad \Rightarrow \quad \frac{\partial \mathscr{L}^{lh}}{\partial \Xi_{1\alpha}^{kl}} \supseteq [y_{rs}(L_r^{\{i} L_s^{j\}}) + \kappa \tilde{H}^i \tilde{H}^j]\epsilon_{ik}\epsilon_{jl} \sim \Xi_1^\dagger, \tag{2.7b}$$

$$L^i L^j H^k H^l \epsilon_{ik}\epsilon_{jl} \quad \Rightarrow \quad \frac{\partial \mathscr{L}^{lh}}{\partial \Sigma_\alpha^{kj}} \supseteq z_r L_r^{\alpha\{i} H^{l\}} \epsilon_{ik}\epsilon_{jl} \sim \Sigma, \tag{2.7c}$$

where we use $\sim$ to mean 'transforms as' under $\mathrm{SU}(2)_+ \otimes \mathrm{SU}(2)_- \otimes G_{\mathrm{SM}}$. Each pattern of contractions corresponds to a topology, with each individual grouping of the fields corresponding to a vertex, or equivalently, a term in the $\Delta L = 2$ UV Lagrangian. The explicit form of these terms can be written down by keeping track of the isospin indices as in Eq. (2.7), and expanding implicit index structures in all possible ways (*i.e.* decomposing products of fields into irreducible representations), consistent with our model building assumptions. (In our case this means keeping only scalar and fermion Lorentz irreps.) In Eq. (2.7c), the indices i, l are symmetrised since this is the only way the component $L^i H^l$ (with i, l not antisymmetric under exchange) can appear in the Yukawa interaction $L\Sigma H$. Note that we adopt the convention that the conjugate exotic field couples to the contracted fields in the operator. This means that $\Xi_1^\dagger$ transforms like $L^{\{i} L^{j\}}$, as implied in Eq. (2.7b), but the renormalisable term in the UV theory which corresponds to the vertex is $L\Xi_1 L$. For Majorana fermions there is only one state which can couple in both cases, while for a Dirac fermion $\psi + \bar{\psi}^\dagger$ we arbitrarily choose $\bar{\psi}$ to couple to the contracted fields.

This process of grouping fields into renormalisable interaction terms can be conveniently expressed with the following replacement rules:

$$\psi_1^\alpha \psi_{2\alpha} \to \Phi^\dagger, \quad \phi_1 \phi_2 \to \Phi^\dagger, \quad \phi_1 \phi_2 \phi_3 \to \Phi^\dagger, \quad \phi \psi^\alpha \to \bar{\Psi}^\alpha, \quad \psi_1^\alpha \psi_2^{\dagger\dot{\alpha}} \to ✗, \tag{2.8}$$

with free raised or lowered gauge-indices (suppressed above) of the same type always symmetrised on the right-hand side. We are using Φ and $\bar{\Psi}$ to represent a heavy scalar and fermion; while the lowercase ϕ_i and ψ_i represent scalar and fermion fields that may be light or heavy. Note that $\bar{\Psi} = \Psi$ for a Majorana fermion. The mark ✗ signals that the completion should be discarded, in this case because it represents a model involving a

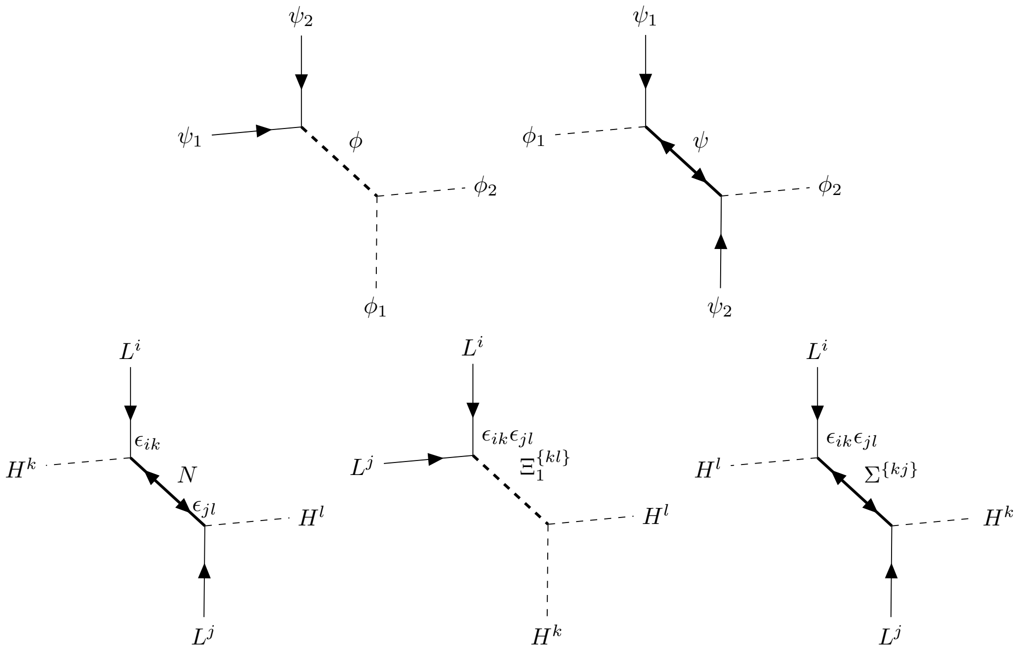

Figure 2.1: *Above:* Scalar-only and fermion-only topologies which complete dimension-five two-scalar–two-fermion operators, like the Weinberg operator $\mathcal{O}_1$. *Below:* The three minimal tree-level completions of $\mathcal{O}_1$, each corresponding to a different permutation of the fields on the external lines of the topologies. These are traditionally called (read from left to right) the type-I, type-II and type-III seesaw models. The $\mathrm{SU}(2)_L$ indices are included explicitly to distinguish type-I and type-III, while making a more clear connection to Eq. (2.7). The exotic propagators are shown in bold.

heavy vector field. The repeated application of these rules allows us to build explicit computational representations of the $\Delta L = 2$ Lagrangian and diagram topology for a completion.

We move on with a more involved example that also involves colour structure: a completion of $\mathcal{O}_{12} = LLQ^\dagger Q^\dagger \bar{u}^\dagger \bar{u}^\dagger$. According to Table B.1 there are two SU(2) structures. Both of these structures need to be opened up to enumerate all of the completions, and models will in general generate sums of these with a specific Lorentz structure, as per the discussion in Sec. 2.2.1. We choose to look at

$$\underset{rstuvw}{\mathcal{O}_{12a}} = \underset{r}{L^i}\underset{s}{L^j}\underset{t}{\tilde{Q}^k}\underset{u}{\tilde{Q}^l}\underset{v}{\bar{u}^\dagger}\underset{w}{\bar{u}^\dagger}\epsilon_{ik}\epsilon_{jl} \tag{2.9}$$

and begin with some preliminary comments. There are only two topologies that accommodate tree-level completions for six-fermion operators. A scalar-only topology (shown in Fig. 2.2a), where pairs of fermions are contracted into scalars which meet at a trilinear vertex, and a scalar-plus-fermion topology (shown in Fig. 2.2b) in which two exotic scalars come about by fermion contractions and each meets another SM fermion. Since we are not interested in introducing exotic vector fields, contractions between fermions must come about by grouping only fields with dotted or undotted indices, *i.e.* from $(\mathbf{2},\mathbf{1}) \otimes (\mathbf{2},\mathbf{1})$ or $(\mathbf{1},\mathbf{2}) \otimes (\mathbf{1},\mathbf{2})$ contracted into a $\mathrm{SU}(2)_{\pm}$-scalar representation with an epsilon tensor. These contractions fix the Lorentz-structure of the generated type-2 operator. For $\mathcal{O}_{12a}$ it is clear that all scalar-only completions will contain the triplet scalar Ξ_1, since the two L fields in the operator are the only fermions carrying undotted indices, making the contraction

$$\overbrace{L^i L^j}^{\Xi_1^\dagger \sim (\mathbf{1},\mathbf{3},-1)} \tilde{Q}^k \tilde{Q}^l \bar{u}^\dagger \bar{u}^\dagger \epsilon_{ik}\epsilon_{jl} \tag{2.10}$$

unique. For the quark fields there are a number of choices to be made. First, the choice of grouping. There are only two choices for how to group the quark fields: as $(\tilde{Q}\tilde{Q})(\bar{u}^\dagger \bar{u}^\dagger)$ or $(\tilde{Q}\bar{u}^\dagger)^2$. The second choice is of the colour representations. These can be explored recursively, or all invariants can be constructed and each opened up separately, following the conventions of Sec. 2.2.1. We opt for the latter case, and enumerate the colour contractions

$$\mathcal{O}_{12a\epsilon} = L^i L^j \tilde{Q}^k_a \tilde{Q}^l_b \bar{u}^{\dagger c} \bar{u}^{\dagger d} \epsilon_{ik}\epsilon_{jl}\epsilon^{abe}\epsilon_{cde}, \tag{2.11a}$$
$$\mathcal{O}_{12a\delta} = L^i L^j \tilde{Q}^k_a \tilde{Q}^l_b \bar{u}^{\dagger c} \bar{u}^{\dagger d} \epsilon_{ik}\epsilon_{jl}\delta^a_c \delta^b_d. \tag{2.11b}$$

The colour sextet combinations $Q^\dagger_{\{a}Q^\dagger_{b\}}\bar{u}^{\dagger a}\bar{u}^{\dagger b}$ come about as a sum of flavour permutations of the left-handed quark doublets in $\mathcal{O}_{12a\delta}$, and the octet combinations $(Q^\dagger \lambda^A \bar{u}^\dagger)^2$ as a linear combination of $\mathcal{O}_{12a\delta}$ and $\mathcal{O}_{12a\epsilon}$. Thus, we understand contractions like $Q^\dagger_a Q^\dagger_b \delta^a_c \delta^b_d$ as coming about from colour-sextet scalars, and $Q^\dagger_a \bar{u}^{\dagger b}\delta^a_c \delta^d_b$ or $Q^\dagger_a \bar{u}^{\dagger b}\epsilon_{bce}\epsilon^{ade}$ as coming about from octets.

Finding all of the completions of $\mathcal{O}_{12a}$ involves contracting all fields in all possible ways for each colour contraction. We work through the example of a particular scalar-only completion of $\mathcal{O}_{12a\delta}$ in Fig. 2.3. Each step follows the grouping of fields into a vertex, the Lagrangian term this grouping corresponds to, and the evolving topology of the completion under the replacement rules of Eq. (2.8). At intermediate stages in the explosion of the operator, the theory described is still effective because some vertices still correspond to irrelevant operators[5]. The procedure stops once all vertices have mass-dimension $d \leq 4$. We replace the contracted fields in the operator with the irreducible representation that, following the restrictions described in Sec. 2.2.1, could give

[5] We note that one can make a connection here to the framework of Ref. [234], where neutrino-mass models are classified and studied in the context of single-field extensions of the SM, corresponding to the first intermediate step in our completions procedure. Similar approaches to SMEFT extensions have also been considered elsewhere in the literature, *e.g.* [235].

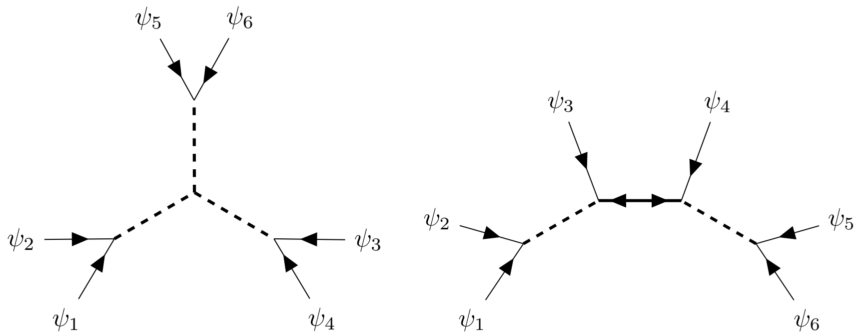

(a) **(b)**

Figure 2.2: The two tree-level topologies relevant to six-fermion operators. For some operators, some fermion arrows may be reversed. The exotic propagators are shown in bold. (a) The scalar-only topology. (b) The scalar-plus-fermion or central-fermion topology.

rise to the contraction. This will in general require the addition of other structures[6], although this is not the case here. The operator generated by the model highlighted in Fig. 2.3 is

$$(\underset{r}{L}^{\{i}\underset{s}{L}^{j\}})(\underset{t}{Q}^{\dagger}_{ia}\underset{u}{Q}^{\dagger}_{jb})(\underset{v}{\bar{u}}^{\dagger\{a}\underset{w}{\bar{u}}^{\dagger b\}}) = \underset{rstuvw}{\mathcal{O}_{12a\delta}} + \underset{srtuvw}{\mathcal{O}_{12a\delta}} + \underset{rsutvw}{\mathcal{O}_{12a\delta}} + \underset{srutvw}{\mathcal{O}_{12a\delta}}, \tag{2.12}$$

with the same Lorentz structure carried through $\mathcal{O}_{12a\delta}$. The relevant part of the $\Delta L = 2$ Lagrangian of the model can be read directly off each contraction

$$\begin{aligned} -\mathscr{L}_{\Delta L=2} \supseteq\ & x_{\{rs\}}(\underset{r}{L}^{i}\underset{s}{L}^{j})\Xi_{1\{ij\}} + y_{\{tu\}}(\underset{t}{\tilde{Q}}^{k}_{a}\underset{u}{\tilde{Q}}^{l}_{b})\Upsilon^{\{ab\}}_{\{kl\}} + z_{[vw]}(\underset{v}{\bar{u}}^{\dagger a}\underset{w}{\bar{u}}^{\dagger b})\Omega_{4\{ab\}} \\ & + \kappa\Xi_{1\{ij\}}\Upsilon^{\{ab\}}_{\{kl\}}\Omega_{4\{ab\}}\epsilon_{ik}\epsilon_{jl} + \text{h.c.}, \end{aligned} \tag{2.13}$$

although the generation of the entire Lagrangian implied by the field content requires a program implementing group-theory methods, spin-statistics and tensor algebra (see Sec. 2.3.2). This particular model inherits the high level of symmetry in the effective operator. This introduces symmetries in the Yukawa couplings of the model, reducing the total number of free parameters.

Given an effective operator, we have established a simple rule for reducing it to a renormalisable interaction through a processes of contracting fields into each other, corresponding diagrammatically to pairing the fields off into Yukawa or scalar interaction vertices according to a system of rewrite rules. Applying these groupings in all

[6]The organic operator of the model can be written as a linear combination of these other operators and the operator being opened up, and all of these share the model as a completion in our sense.

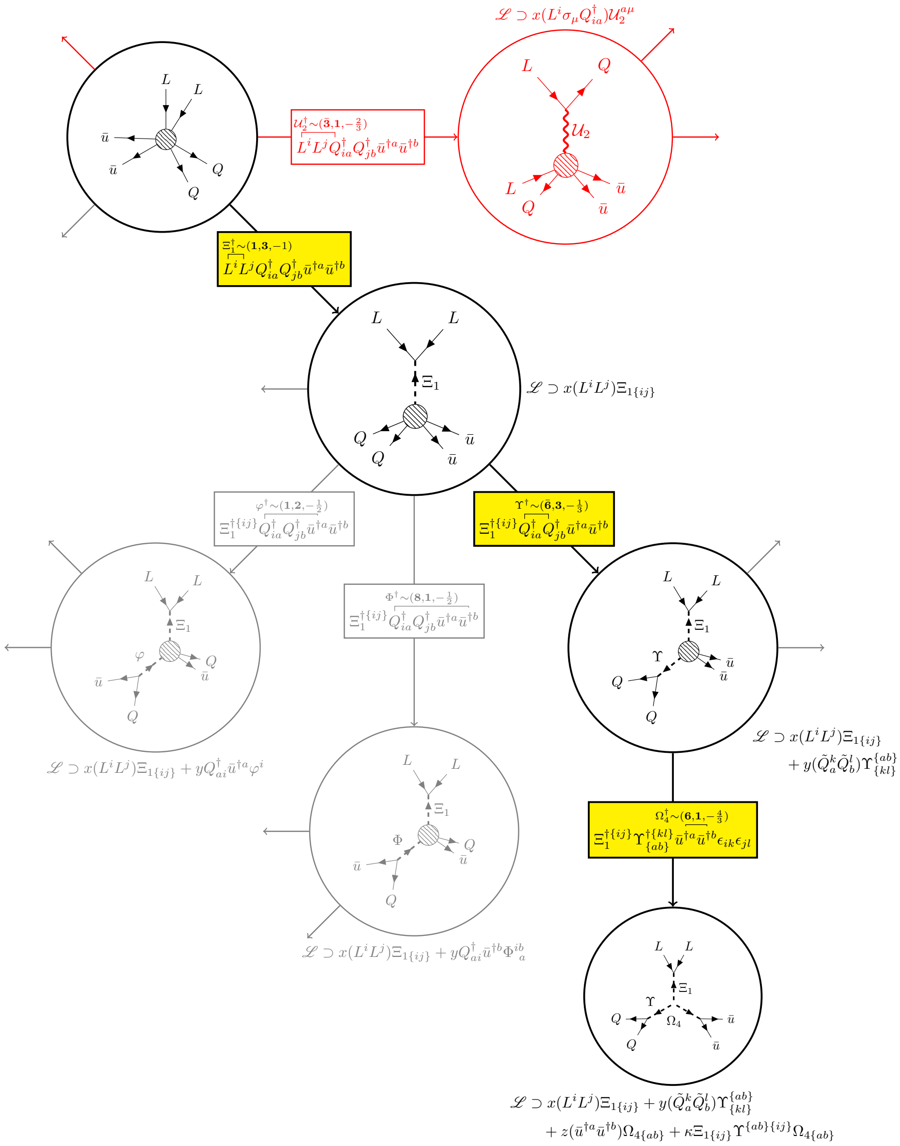

Figure 2.3: The graph visualises our completion procedure by showing some of the possible ways to explode the operator $\mathcal{O}_{12a\delta} = L^i L^j Q^{\dagger}_{ia} Q^{\dagger}_{jb} \bar{u}^{\dagger a} \bar{u}^{\dagger b}$. The options are only followed to a fully UV-complete model on one branch, shown in bold with yellow edge labels. In each step groups of fields are contracted at a vertex, fixing the properties of the exotic field as well as the structure of the term describing the interaction, shown alongside each diagram. The effective operator is gradually opened up until each vertex in the diagram corresponds to a term with mass-dimension $d \leq 4$. Opening up the operator fully requires repeating this procedure for all possible contractions. In this case this includes other scalar-only completions and scalar-plus-fermion models. We also show steps that we choose to forbid in our approach in red, like the vector contraction giving rise to the vector leptoquark $\mathcal{U}_2$ in the figure. Flavour indices have been suppressed.

possible ways and following quantum numbers through index structure allows one to efficiently write down not only the particle content generating the operator at tree-level, but also the pertinent interaction terms in the Lagrangian. In the next section, we discuss how to expand this rule to reducing operators containing derivatives.

2.3.1 Tree-level completions of derivative operators

In the following we broaden the discussion to exploratory model building through effective operators containing (covariant) derivatives and field-strength tensors. We begin by summarising the main results of this section. We argue that (if only scalars and fermions are introduced) a large class of such operators do not contribute new completions to the pool of models. That is, models derived from these operators could be found by opening up operators without derivatives and field strengths. With notable exceptions, it is usually sufficient to study only single-derivative operators. Some of the derivative operators also admit fermion-only completions, which are otherwise only found for the Weinberg-like operators [103]. The completion of operators containing derivatives has been studied before in the context of $\Delta L = 2$ physics [236–238], and our work expands on this.

Exploding derivative operators

In our setup, derivatives in effective operators arise at tree-level by the expansions given in Eqs. (1.39) and (1.32). It is clear that derivatives occur in one of two ways: (1) in pairs as D^2 or X from next-to-leading order terms in the EFT expansion, or (2) as single derivatives contracted with fermions ($\not{D}$ in traditional notation) coming about from arrow-preserving fermion propagators. The job of finding the completions of operators containing derivatives is therefore equivalent to enumerating all possible tree graphs with the appropriate external-leg structure including arrow-preserving propagators proportional to momentum for heavy fermion fields and taking powers of momentum from past the leading order in the expansion of all propagators. As in the non-derivative case, the quantum numbers of the heavy fields can then be deduced by imposing Lorentz and gauge invariance at each vertex.

It is not always guaranteed that a tree-level topology with internal fermion and scalar lines exists for an effective operator containing derivatives. This is in contrast to the non-derivative case, where this is guaranteed for all operators of mass dimension larger than four. For example, at dimension seven there are $\Delta L = 2$ effective operators like $\bar{d}_\alpha \bar{u}^\dagger_{\dot{\alpha}} L^{i\beta} D^{\alpha\dot{\alpha}} L^i_\beta \epsilon_{ij}$ containing four fermions: three with undotted indices and one with a dotted index. In this case there is no tree-level topology that allows a arrow-preserving fermion propagator to give rise to the derivative, and so the operator can only be generated with loops. We call such operators *non-explosive*. This distinction between tree and loop operators has been discussed in the literature in the context of the dimension-six operators of the SMEFT, see *e.g.* [23, 231, 232], and more recently for the dimension-eight operators [239].

The derivatives originating from arrow-preserving fermion propagators in the UV theory enter the effective Lagrangian through the first term in Eq. (1.39). Here, the derivative acts on an object with which it shares a contracted index, *i.e.* it is contracted as $(\mathbf{2},\mathbf{2})\otimes(\mathbf{1},\mathbf{2}) = (\mathbf{2},\mathbf{1})$ with the object carrying the index $\dot\beta$. This object must be a $(\mathbf{1},\mathbf{2})$-fermion if it comes from a renormalisable interaction, which in our case is uniquely a Yukawa interaction. Thus,

$$\frac{\partial \mathscr{L}^{lh}}{\partial \Pi^{\dagger}_{\dot\beta}} = \sum_i \psi_i^{\dagger\dot\beta}\phi_i, \tag{2.14}$$

with ψ_i and ϕ_i defined as in Eq. (2.8). For example, a structure like $D^{\alpha\dot\alpha}\psi_1^{\dagger\dot\beta}\phi_1\epsilon_{\dot\alpha\dot\beta}$ could enter an effective operator by integrating out a heavy fermion Π that couples through $\mathscr{L} \supset \Pi^\dagger\psi_1^\dagger\phi_1$. For clarity, the effective Lagrangian looks like

$$\mathscr{L}_{\text{eff}}[\pi] \supset \frac{\partial \mathscr{L}^{lh}}{\partial \Pi_\beta}\frac{1}{m_\Pi^2}D^{\alpha\dot\alpha}\frac{\partial \mathscr{L}^{lh}}{\partial \Pi^{\dagger}_{\dot\beta}}\epsilon_{\alpha\beta}\epsilon_{\dot\alpha\dot\beta} + \cdots \tag{2.15}$$

$$= \frac{\partial \mathscr{L}^{lh}}{\partial \Pi_\beta}\frac{1}{m_\Pi^2}D^{\alpha\dot\alpha}\left(\psi_1^{\dagger\dot\beta}\phi_1 + \cdots\right)\epsilon_{\alpha\beta}\epsilon_{\dot\alpha\dot\beta} \tag{2.16}$$

in this case. The fields ϕ_i and ψ_i need not be light, and could have arisen from the contraction of fields in a complicated way. For example, ϕ_1 may have come from the contraction of two light fermions $\phi_1 \sim \xi_1\xi_2$. This situation is visualised diagrammatically in Fig. 2.4a. The figure shows the ξ_i fermions coupling to the heavy ϕ propagator, which in turn couples to $\psi_1^\dagger$ leading to the arrow-preserving fermion propagator for the heavy Π carrying momentum $k^{\alpha\dot\alpha}$. It is clear from Eq. (2.16) that the derivative acts on both the fermion and the scalar, reflecting the fact that in the diagram k is the sum of the ψ and ϕ momenta. So, derivatives acting on fermions or scalars can be grouped off into a Yukawa interaction in this way, leaving a arrow-preserving fermion propagator in their wake. This corresponds to the replacement rules

$$D^{\alpha\dot\alpha}(\psi^\dagger_{\dot\alpha})\phi \to \Pi^\alpha, \qquad D^{\alpha\dot\alpha}(\psi^\dagger_{\dot\alpha}\phi) \to \Pi^\alpha, \qquad D^{\alpha\dot\alpha}(\phi)\psi^\dagger_{\dot\alpha} \to \Pi^\alpha. \tag{2.17}$$

We highlight that the arrow-preserving propagator implies that only one chirality of the Dirac fermion Π is necessary for LNV in these models. However, we still only work with vector-like fermions in our completions to guarantee anomaly cancellation and straightforwardly give them large masses.

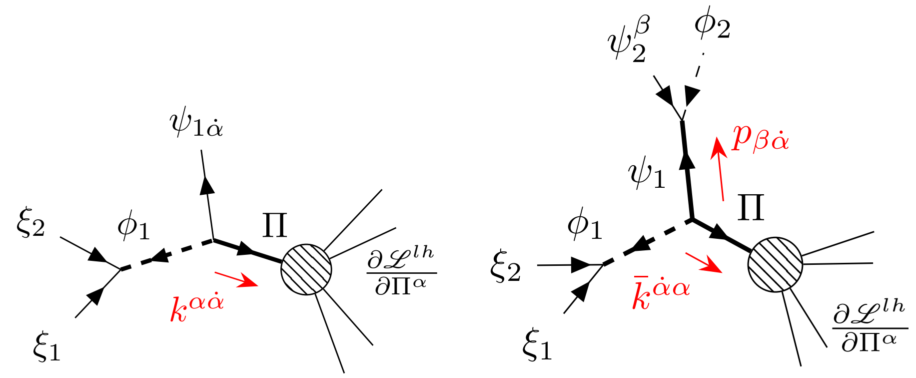

(a) **(b)**

Figure 2.4: (a) The diagram shows an example opening of an operator containing at least one derivative. The derivative can be understood as arising from the leading-order term in the expansion of the arrow-preserving fermion propagator, emphasised in the diagram. As shown, the fields ξ_i and ψ_1 are external and therefore light, but in general they could themselves be heavy propagators. (b) The case where the fermion ψ_1 is heavy, coupling to the light fields ψ_2 and ϕ_2. The σ-matrix structure of the propagators is in accordance with the conventions of Ref. [22]. Here, the Lorentz structure is such that the momenta are contracted, which arises from contractions of derivatives which share one contracted index.

In an effective operator the derivative may act on a fermion with which it does not share a contracted index. For example, in the model shown in Fig. 2.4a, the effective operator at the low scale looks something like

$$D^{\beta\dot\beta}(\xi_1^\alpha \xi_{2\alpha}\psi^\dagger_{1\dot\beta})\frac{\partial\mathscr{L}^{lh}}{\partial\Pi^\beta} = D^{\beta\dot\beta}(\xi_1^\alpha)\xi_{2\alpha}\psi^\dagger_{1\dot\beta}\frac{\partial\mathscr{L}^{lh}}{\partial\Pi^\beta} + \cdots \tag{2.18}$$

although as long as the operator is generated at tree-level, the term with the derivative acting on $\psi^\dagger$ will always also be present as long as it is not removed by a field redefinition involving its classical EOM. Our approach is the following: act the derivative in all possible ways on the fields constituting the effective operator and discard the topologies in which a contraction like $(D^{\alpha\dot\alpha}\psi_1^\beta)\phi$ is made. After a UV-complete model is derived, the operator it implies will still have the form of the one on the left-hand side of Eq. (2.18), so no information is lost. This implies the rules

$$(D^{\alpha\dot\alpha}\psi^\beta)\phi \to \text{✗}, \qquad (D^{\alpha\dot\alpha}\psi^\beta\phi) \to \text{✗}, \qquad (D^{\alpha\dot\alpha}\phi)\psi^\beta \to \text{✗}, \qquad (D^{\alpha\dot\alpha}\phi_1)\phi_2 \to \text{✗}. \tag{2.19}$$

The first parentheses of Eqs. (1.39) and (1.32) contribute powers of D^2 or X to operators in the effective Lagrangian. They contribute the rules

$$\begin{aligned} &(D^{\alpha\dot{\alpha}}\psi_1^{\beta})(D_{\alpha\dot{\alpha}}\psi_{2\beta}) \to \Phi^{\dagger}, \quad (D^{\alpha\dot{\alpha}}\phi_1)(D_{\alpha\dot{\alpha}}\phi_2) \to \Phi^{\dagger} \\ &(D^{\alpha\dot{\alpha}}\psi^{\beta})(D_{\alpha\dot{\alpha}}\phi) \to \bar{\Psi}^{\beta}, \quad (D^{\alpha\dot{\alpha}}\phi_1)(D_{\alpha\dot{\alpha}}\phi_2)\phi_3 \to \Phi^{\dagger} \end{aligned} \tag{2.20}$$

to those discussed previously. We intend these to stand in for similar rules like *e.g.* $\phi_1 \Box \phi_2$ as well. For the field-strength contractions, there is the additional requirement that one or both of the fields in the contraction be charged under the corresponding gauge interaction, but these cannot be contracted into a gauge singlet, since the field-strength tensor comes about from the anticommutator of the covariant derivatives acting on the exotic fermion. These rules are

$$\psi_{\mathrm{i}}^{\alpha} X_{\alpha \mathrm{j}}^{\mathrm{i}\beta} \phi \to \bar{\Psi}_{\mathrm{j}}^{\beta}, \quad \phi X_{\alpha}^{\beta} \phi \to \text{✗}, \quad \psi_{\mathrm{i}}^{\alpha} X_{\alpha \mathrm{j}}^{\mathrm{i}\beta} \phi^{\mathrm{j}} \to \text{✗}, \tag{2.21}$$

where i and j stand in for fundamental indices of $SU(2)_L$, $SU(3)_c$, or no indices at all for the field-strength tensor of $U(1)_Y$.

Operators with derivatives coming about as this way, *i.e.* as D^2 or X, are often redundant from the perspective of model discovery, since they imply the existence of the leading-order operator in which these derivatives do not appear. Thus, the tree-level completions of these operators can be found by studying the lower-dimensional operators without those derivatives or field-strength tensors. It may however be the case that the leading-order operator is absent, in which case these operators may be important. For the $n_f = 3$ SMEFT with one Higgs doublet, we conjecture this can only come about from operators with a structure like

$$\mathcal{O}^{\mu} H^i \partial_{\mu} H^j \epsilon_{ij}, \tag{2.22}$$

which vanishes when the derivative is removed. (Similar structures like $L_r^i L_s^j \epsilon_{ij}$ are non-vanishing since there is an additional space of flavour indices to carry the antisymmetry.) This exception does not apply to the case of field-strength tensors, since $[X^{\mu\nu}, H] = 0$ for all field strengths X. This is the justification for our earlier comments that operators containing field-strength tensors are not interesting from the perspective of model discovery.

The replacement rules given in Eq. (2.20) do not exhaust the possible Lorentz-structures for two derivatives, scalars and fermions. The additional structures involve single indices contracted between the derivatives, and others contracted into fermions. Diagrammatically, we find that these combinations come about from fermion lines containing two arrow-preserving propagators, each contributing a factor of momentum. This would be the case, for example, if ψ in Fig. 2.4 were a heavy arrow-preserving propagator, as shown in Fig. 2.4b. Here the rules are

$$(D^{\alpha\dot{\alpha}}\psi_{1\alpha})(D^{\beta\dot{\beta}}\psi_{2\beta})\epsilon_{\dot{\alpha}\dot{\beta}} \to \Phi^{\dagger}, \quad (D^{\alpha\dot{\alpha}}\psi)(D^{\beta\dot{\beta}}\phi)\epsilon_{\dot{\alpha}\dot{\beta}} \to \bar{\Psi}^{\beta}, \quad \text{other combinations} \to \text{✗}.$$

(2.23)

In summary, exploding derivative operators can lead to novel models that would not be found by exploding non-derivative operators. We have already seen that this happens when a structure such as Eq. (2.22) is present in the operator. It can also happen when the presence of an odd number of derivatives allows new topologies with novel chirality structures. The presence of an even number of derivatives implies either that the derivatives arose as D^2 or X, which usually do not contribute new models, or else from the contractions of structures like those in Eq. (2.23). It is clear from Fig. 2.4b that in such cases, the two arrow-preserving fermion propagators can be replaced with arrow-violating propagators, and indeed these will generically be present since we work with vector-like fermions. So, with the exception of operators with structures like Eq. (2.22), studying single derivative operators is sufficient for model discovery.

Derivative operator examples

Among the simplest derivative operators in the $\Delta L = 2$ SMEFT is the dimension seven operator

$$\mathcal{O}_{D3} = L^i_\alpha \bar{e}^\dagger_{\dot\beta} H^j (DH)^{\alpha\dot\beta k} H^l \epsilon_{ij}\epsilon_{kl} \tag{2.24}$$

which we use as a paradigm for showing how single-derivative operators can be opened up. We note that the operator's tree-level completions have also been discussed in Ref. [237]. The placement of the derivative on the Higgs field is enforced by the unique $\mathrm{SU}(2)_L$ contraction. This is not generally true, and the derivative should be acted in all possible ways if it can be. The contraction of (DH) into another Higgs is forbidden by Eq. (2.19). Thus, the (DH) must be contracted into a fermion. The options are

$$L^i_\alpha (DH)^{\alpha\dot\beta k}\epsilon_{ij}\epsilon_{kl} \sim \Sigma^{\dagger\dot\beta}_{jl} \quad \text{and} \quad \bar{e}^\dagger_{\dot\beta}(DH)^{\alpha\dot\beta k} \sim \bar{\Delta}^{\alpha k}_1 \tag{2.25}$$

with the Dirac fermion $\Delta_1 + \bar{\Delta}^\dagger_1 \sim (\mathbf{1}, \mathbf{2}, -\frac{1}{2})$ transforming like L under G_{SM}. The field Σ is the protagonist in the type-III seesaw model, and further contractions on the resulting operator $\Sigma^\dagger_{jl}\bar{e}^\dagger H^j H^l$ lead to the models $\{\Sigma, \Delta_1 + \bar{\Delta}^\dagger_1\}$ (from $\bar{e}^\dagger H$) and $\{\Sigma, \Xi_1\}$ (from HH) in that case. The second option in Eq. (2.25) leads to the operator $L^i \Delta^k_1 H^j H^l \epsilon_{ij}\epsilon_{jl}$, which is the Weinberg operator with the second L replaced with the exotic vector-like lepton. This contraction is illustrated diagrammatically in Fig. 2.5a. It thus implies the same completions[7] as $\mathcal{O}_1$, each along with $\Delta_1 + \bar{\Delta}^\dagger_1$. This is expected since $\bar{e}^\dagger(DH)$ transforms like L. There are then a total of five completions, but four models, since two have

[7] This phenomenon is discussed in more detail in Sec. 2.4.2.

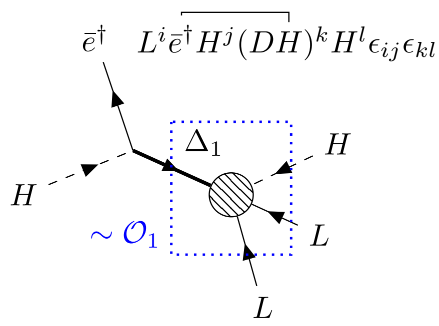

(a)

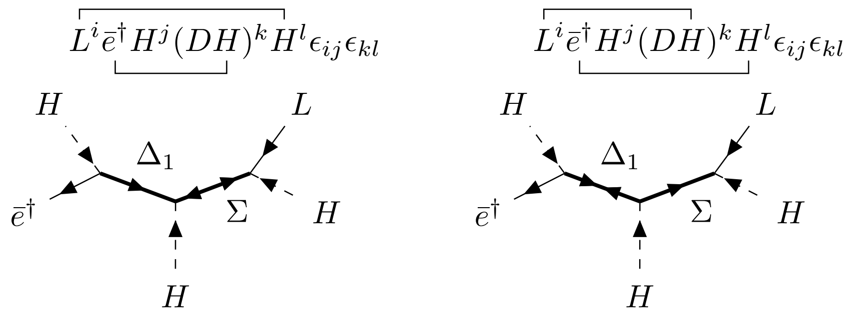

(b)

Figure 2.5: (a) An intermediate topology representing the operator $\mathcal{O}_{D3}$ with all heavy fields except Δ_1 integrated out. The contraction $\bar{e}^\dagger H \sim \Delta_1^\dagger$ gives rise to an effective operator similar to the Weinberg operator $\mathcal{O}_1$, shown in blue. This branch of the completion tree therefore involves models featuring Δ_1 along with one of the seesaw fields. (b) The model with field content $\{\Sigma, \Delta_1 + \bar{\Delta}^\dagger\}$ arises from two similar diagrams, shown here. These correspond to the two ways the arrow-preserving and arrow-violating fermion propagators can be placed in the graphs for this furnishing of the topology.

the same particle content: $\{\Sigma, \Delta_1 + \bar{\Delta}_1^\dagger\}$. In Fig. 2.5b we show how this can be seen as coming about from the fact that the chirality structure of the diagram allows two positions for the arrow-preserving fermion propagator. Note that this is not the case for the completion with the singlet fermion N. Interestingly, there are two fermion-only models found: $\{N, \Delta_1 + \bar{\Delta}_1^\dagger\}$ and $\{\Sigma, \Delta_1 + \bar{\Delta}_1^\dagger\}$. Both of them contain seesaw fields, which is consistent with the proof of Ref. [104] that models containing two exotic fermion fields must contain one of N or Σ if they violate lepton-number by two units. Since the structure of the operator $\mathcal{O}_{D3}$ is unique, there is no work to be done in writing down the organic operator generated by these models at the low scale.

We move on to a two-derivative operator example by studying a completion of

$$\mathcal{O}_{18d} = L^i L^j H^k H^l (D^\mu H)^m (D_\mu \tilde{H})^n \epsilon_{ij} \epsilon_{km} \epsilon_{ln}, \tag{2.26}$$

which has the property that it vanishes when the derivatives are removed. (Note that, comparing to the operator in Table B.1, the first derivative has been moved onto a Higgs field.) Applying the only allowed replacement rule on the derivatives first implies the presence of the real triplet scalar[8] $\Xi \sim (\mathbf{1}, \mathbf{3}, 0)_S$ in the theory

$$L^i L^j H^k H^l (D^\mu H)^m (D_\mu \tilde{H})^n \epsilon_{ij} \epsilon_{km} \epsilon_{ln} \to L^i L^j H^k H^l \Xi^{mn} \epsilon_{ij} \epsilon_{km} \epsilon_{ln}. \tag{2.27}$$

From here there are a number of choices. We choose to look at a particular scalar-only completion involving the unit-hypercharge isosinglet scalar present in the Zee model $\mathcal{S}_1 \sim (\mathbf{1}, \mathbf{1}, 1)$:

$$L^i L^j H^k H^l \Xi^{mn} \epsilon_{ij} \epsilon_{km} \epsilon_{ln} \to \mathcal{S}_1^\dagger H^k H^l \Xi^\dagger_{kl}, \tag{2.28}$$

implying the interaction Lagrangian

$$\mathcal{L}_{\text{int}} \supset x_{[rs]} L_r L_s \mathcal{S}_1 + \kappa H^i \tilde{H}^j \Xi_{\{ij\}} + \lambda \mathcal{S}_1 \Xi^{ij} H_i^\dagger H_j^\dagger + \text{h.c.} \tag{2.29}$$

This model was studied in Ref. [240] and identified as the simplest neutrino mass model according to their assumptions. It has remarkably few free parameters since the scalar Ξ does not have Yukawa couplings to SM fermions, and the couplings of $\mathcal{S}_1$ to leptons are antisymmetric in flavour. As in the minimal Zee–Wolfenstein scenario [93], this model implies a neutrino-mass matrix with zeros down the diagonal and is therefore incompatible with neutrino oscillation data [241]. It is, however, a good example of how interesting models can be missed when overlooking operators with derivatives in this model-building framework. The model generates the following combination of basis operators at the low scale

$$\mathcal{O}^{[rs]}_{\mathcal{S}_1+\Xi} = (L^i_r L^j_s) H^k H^l \Box (H^m \tilde{H}^n) \epsilon_{ij} \epsilon_{km} \epsilon_{ln}. \tag{2.30}$$

Note that the operator is already symmetric under the interchange $m \leftrightarrow n$, so another structure need not be added.

2.3.2 An algorithm for model building

With our basic completion recipe established, in the following we outline the procedures we use to build the UV models that generate the operators listed in Table B.1,

[8] We remind the reader that this is not the seesaw field present in the type-II scenario, which has unit hypercharge.

along with relevant metadata: the tree-level diagrams and the models' Lagrangians. The methods are presented as they are implemented in our example code [220].

We use a computational representation for tensors representing fields transforming as irreducible representations of $\mathrm{SU}(2)_+ \otimes \mathrm{SU}(2)_- \otimes G_{\mathrm{SM}}$ built on top of the SymPy package [242] for symbolic computation in Python, as well as BasisGen [227] for group-theory functionality. The code implements the Butler–Portugal algorithm [243, 244] for obtaining the canonical form of tensorial expressions, which we use to simplify operators and compare them for equality. Strings of fields and their derivatives representing gauge- and Lorentz-invariant effective operators are dressed with ϵ and δ tensors to form all possible invariants. In our specific case, the content of these operators is constructed directly by taking the product of all field combinations and keeping only those that contain a singlet part in the decomposition. We checked this against results from the Hilbert series, projecting out the $\Delta L = 2$ component for the pertinent operators, and removing the spurions accounting for redundancies from field redefinitions involving the classical EOM and IBP. For our study of the $\Delta L = 2$ operators, since we are interested in model discovery, we excluded derivative operators that are non-explosive along with those that contain field-strength tensors and contracted pairs of derivatives that do not lead to a vanishing structure upon removal.

In practice we start with a template pattern of contractions corresponding to the topologies that can accommodate the field content of the operators at tree-level. These are generated using FeynArts [245] through Mathematica, and filtered for isomorphism with graph-theory tools [246–249]. These templates provide the order and pattern of contractions for classes of operators based on the number of scalars and fermions they contain. Since no distinction is made at this level between $(\mathbf{2}, \mathbf{1})$- and $(\mathbf{1}, \mathbf{2})$-fermions, for some operators only a subset of these templates will be relevant for our purposes, since some contractions may always imply Proca fields. These templates are used to open up the operator with the assumptions and methods presented in Sec. 2.3. Every time a replacement rule is applied, the Feynman graph information is updated and a Lagrangian term is generated as described in Sec. 2.3. After the procedure is finished, the full Lagrangian of the model can be generated in the same way as the input effective operators, described above.

We keep track of the quantum numbers of the heavy fields so as to be economic with exotic degrees of freedom, while still providing some flexibility in the model database. Concretely, if a field arises from a contraction whose corresponding term has already appeared in the Lagrangian, the two associated exotic fields are identified. If two fields come about from different contractions but share the same quantum numbers they are distinguished, since it may be possible that some symmetry would forbid one term but not the other. The choice to identify fields not only reduces the number of fields in each model, but may also reduce the total number of completions for a given operator. This is due to couplings between exotic fields that vanish in the absence of some exotic generational structure. For example, $\phi^i \phi^j \epsilon_{ij} = 0$ for some exotic isodoublet ϕ, or

$\eta^a \eta^b \eta^c \epsilon_{abc} = 0$ for a colour-triplet η.

We have attempted to validate our example code against many results in the literature. We have been able to reproduce the results of Refs. [23, 101, 224, 237, 238], which give systematic listings of models that generate effective operators at tree-level. Ref. [23] provides a UV dictionary for the dimension-six SMEFT. Validation of these results first required the adaptation of the dimension-six operators to something analogous to the overcomplete spanning set of type-3 operators used here. The entire process in this case—including generating the set of operators, finding the completions and matching examples back onto the Warsaw basis—is provided as an interactive notebook accompanying our example code. We note that such matching calculations can also be automated with the help of automated tools [250, 251]. For the other studies mentioned, we provide our validation of their results along with our example code.

2.4 Neutrino mass model building

Up until now we have tried to keep the discussion of exploding operators general, but in this and following sections we specialise to the case of opening up operators to build radiative models of Majorana neutrino mass. We discuss the process of turning $\Delta L = 2$ operators into neutrino self-energy graphs, the tree-level topologies of the operators, and the methods we use to ensure a given model's contribution to the neutrino mass is the dominant one.

2.4.1 Operator closures and neutrino-mass estimates

For operators other than the Weinberg-like ones, neutrino masses are necessarily generated at loop level. The fields of the $\Delta L = 2$ operator need to be looped off using SM interactions in such a way that a Weinberg-like operator is generated after the SM fields are integrated out. We call this the operator *closure* and it represents the mixing between the $\Delta L = 2$ operator and the Weinberg-like ones. Examples of $\Delta L = 2$ operator closures are given in Table 2.1, and these are referred to throughout this section. The closure provides enough information to know the number of loops in the neutrino self-energy graph (since the $\Delta L = 2$ operator is generated at tree level) and to estimate the scale of the new physics underlying the operator. We automate the operator-closure process by applying the methods discussed below through a pattern-matching algorithm [252, 253]. The program is a part of our public example-code repository.

Current neutrino oscillation data provide a lower bound on the mass of the heaviest neutrino, coming from the measured atmospheric mass-squared difference $\Delta m^2_{\text{atm}} \approx (0.05 \text{ eV})^2$ [7, 254]. We take the neutrino-mass scale $m_\nu \approx 0.05$ eV, so that the new-physics scale is bounded above by the implied scale we estimate for each operator.

This is derived by estimating the loop-level operator closure diagrams. In our case we are interested in estimating the scale of the neutrino mass in the UV models generating the operator, rather than the calculable loop-level contributions to the neutrino mass in the EFT. We associate a factor of $(16\pi^2)^{-1} \approx 6.3 \cdot 10^{-3}$ with each loop and assume unit operator coefficients for the non-renormalisable $\Delta L = 2$ vertices. We take the SM Yukawa couplings to be diagonal and include factors of $g \approx 0.63$ appropriately for interaction vertices involving W bosons. Neutrino-mass matrices proportional to Yukawa couplings will be dominated by the contributions from the third generation of SM fermions in the absence of any special flavour hierarchy in the new-physics couplings. For this reason, we consider only the effects of third-generation SM fermions in our estimates, but mention that our program can be straightforwardly extended to accommodate the general case where light-fermion Yukawas and off-diagonal CKM matrix elements appear in the neutrino-mass matrix. For derivative-operator closures, we can include the W boson from the covariant derivative if it is present and necessary to correctly close off the diagram. Otherwise, the vertex should come with an additional factor of momentum. We work in the Feynman gauge to avoid spurious factors of Λ in the neutrino-mass estimates [237]. The overall scale-suppression of the neutrino mass is determined by the Weinberg-like operator generated at the low scale. In most cases, this is the dimension-five operator $\mathcal{O}_1$, which implies $m_\nu^{\mathcal{O}_1} \sim v^2/\Lambda$. Closures leading to the loop-level generation of $\mathcal{O}_1'$ and $\mathcal{O}_1''$ can also be found, and these naively imply a significant suppression of the neutrino mass compared to the $\mathcal{O}_1$ case: $m_\nu^{\mathcal{O}_1'} \sim v^4/\Lambda^3$ and $m_\nu^{\mathcal{O}_1''} \sim v^6/\Lambda^5$. However, a diagram with additional Higgs loops can always be drawn to recover the Weinberg operator at the low scale. Despite the additional loop suppression, these diagrams will dominate over those generating $\mathcal{O}_1'$ and $\mathcal{O}_1''$ as long as $\Lambda \gtrsim 4\pi v \approx 2.2\,\text{TeV}$ [86, 99].

It is still true that higher-dimensional operators typically imply smaller neutrino masses. There are two main reasons for this. First, the number of loops required for the closure of the operator generally increases with increasing mass dimension. Second, operators containing more fields imply neutrino self-energy diagrams containing more couplings. Many of these are SM Yukawas which (with the exception of y_t) are small and tend to suppress the neutrino mass, despite the contributions being dominated by the third generation. Non-minimal choices such as small exotic Yukawa couplings or hierarchical flavour structures in the operator coefficients can also lead to additional suppression of the neutrino mass, and in turn of the implied scale of the new physics.

In Fig. 2.6 we show the new-physics scales Λ associated with neutrino-mass generation from the $\Delta L = 2$ operators in the SMEFT up to dimension 13, assuming unit operator coefficients and the dominance of third-generation couplings. We separate single-derivative operators from those that contain no derivatives, and choose not to include operators containing more than one derivative in the figure. This is because these operators most often arise at next-to-leading order in the EFT expansion, and therefore usually imply a neutrino-mass scale identical to that of lower-dimensional operators. The dimension-eleven operators with derivatives as well as the dimension-13 operators are constructed only as products of lower-dimensional ones, making the set of operators incomplete. We highlight that similar kinds of product operators at dimensions eleven and nine do not imply special values for the estimated neutrino-mass scale or Λ, and therefore we expect the results to be representative of the situation up to dimension 13. From the figure, it is clear that there is a trend towards smaller values of Λ with increasing mass dimension. By dimension 13, the implied new-physics scale is between 1 and 100 TeV for most operators. It seems to be the case that the most constrained closures are generally those of non-derivative operators.

Table 2.1: The table shows an assortment of $\Delta L = 2$ operator closures, displaying a number of paradigmatic motifs. We represent flavour indices in a sans-serif typeface here to avoid confusion with subscripts labelling the Yukawa couplings. The expressions given for m_ν^{rs} needs to be symmetrised in rs, something we do not explicitly indicate in the table. These expressions carry flavour indices in alphabetical order on the fields as they appear in Table B.1. Here κ represents the operator coefficient, V is the CKM matrix and $y_{e,u,d}^{\mathsf{r}}$ are the diagonal electron, up-type and down-type Yukawa couplings in the SM. A number of operators require an external electron to be converted into a neutrino. This often necessitates the introduction of a W boson or an unphysical charged Higgs H^+. Operator $\mathcal{O}_8$ generates the dimension-seven analogue of the Weinberg operator with the two-loop diagram shown. (There is a lower order diagram with an H^+ in place of the W that happens to vanish [29].) A three-loop diagram in which two of the external Higgs lines are looped off leads to mixing with the Weinberg operator. Operator $\mathcal{O}_{76}$ generates the dimension-nine operator $LLHH(H^\dagger H)^2$, and hence five- and six-loop diagrams are also implied. There is usually more than one choice about where to attach the W boson if one is present in a diagram, and the additional diagrams with the W connecting in other possible ways are left implicit.

Operator	Diagram	m_ν^{rs}
$4b$	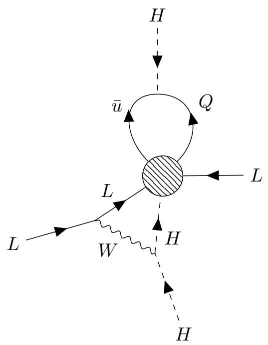	$\kappa_{[\mathsf{rs}]\mathsf{tt}} \dfrac{g^2 y_u^{\mathsf{t}}}{(16\pi^2)^2} \dfrac{v^2}{\Lambda}$

Operator	Diagram	m_ν^{rs}
8	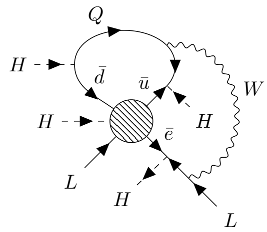	$\kappa_{\mathrm{rstu}} V_{\mathrm{tu}} \frac{g^2 y_e^{\mathrm{s}} y_u^{\mathrm{t}} y_d^{\mathrm{u}}}{(16\pi^2)^2} \frac{v^2}{\Lambda} \left(\frac{v^2}{\Lambda^2} + \frac{1}{16\pi^2} \right)$
$D3$	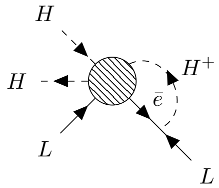	$\kappa_{\mathrm{rs}} \frac{y_e^{\mathrm{s}}}{16\pi^2} \frac{v^2}{\Lambda}$
$11b$	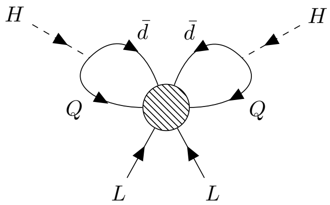	$\kappa_{\mathrm{rstutu}} \frac{y_d^{\mathrm{t}} y_d^{\mathrm{u}}}{(16\pi^2)^2} \frac{v^2}{\Lambda}$
76	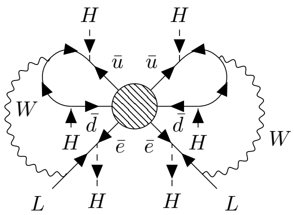	$\kappa_{\mathrm{rstuvw}} V_{\mathrm{tv}} V_{\mathrm{uw}} \frac{g^4 y_e^{\mathrm{r}} y_e^{\mathrm{s}} y_u^{\mathrm{t}} y_u^{\mathrm{u}} y_d^{\mathrm{v}} y_d^{\mathrm{w}}}{(16\pi^2)^4} \frac{v^2}{\Lambda} \left(\frac{v^2}{\Lambda^2} + \frac{1}{16\pi^2} \right)^2$
$47a$	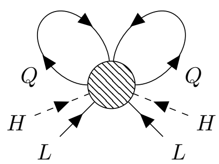	$\kappa_{\mathrm{rstuvw}} \frac{1}{(16\pi^2)^2} \frac{v^2}{\Lambda}$
56	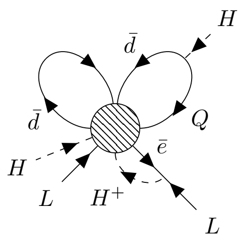	$\kappa_{\mathrm{rsttvv}} \frac{y_e^{\mathrm{s}} y_d^{\mathrm{t}}}{(16\pi^2)^3} \frac{v^2}{\Lambda}$

We note that at dimension eleven it begins to become clear that the neutrino-mass estimates associated with a category of operators remain large. These operators include $\mathcal{O}_{47a}$, whose closure is shown in Table 2.1, and 44 others like it which have loops that contain no connecting Higgs, and therefore no additional suppression from SM Yukawa couplings[9]. These operators have the form

$$\mathcal{O}_1 \cdot \prod_{i=1}^{n} \psi_i^\dagger \psi_i, \tag{2.31}$$

where ψ_i are SM fermion fields, and imply

$$m_\nu \sim \kappa \frac{1}{(16\pi^2)^n} \frac{v^2}{\Lambda}, \tag{2.32}$$

with κ the operator coefficient. The loop suppression becomes too great to meet the atmospheric bound at $n = 6$. Although five loops are viable in the absence of any other suppression, the operators $\mathcal{O}_1 \cdot \prod_{i=1}^{5}(\psi_i^\dagger \psi_i)$ cannot form a Lorentz-singlet without a derivative. This suggests that dimension-21 operators of the form

$$LLH(\partial^\mu H) \cdot (\psi_0 \sigma_\mu \psi_0^\dagger) \prod_{i=1}^{4} \psi_i^\dagger \psi_i \tag{2.33}$$

are the highest-dimensional operators leading to phenomenologically viable neutrino masses. They require new physics below $\sim$ 6 TeV. All of the tree-level topologies associated with the structure in Eq. (2.33) imply that the neutrino mass depends on the product of nine or more dimensionless couplings. It is clear from Fig. 2.6 that these operators are outliers, and the associated new-physics scale is already heavily constrained by dimension 13 for most.

Estimates for the neutrino mass for the majority of the $\Delta L = 2$ operators without derivatives have been given previously in Ref. [86]. Those that we present here differ in two ways:

1. We aim to estimate the contribution to the neutrino mass implied by the completions of the operator, not the operator alone. This means, for example, that we do not need more loops of gauge bosons to provide additional factors of momentum on fermion loops with no mass insertions, since it is implicit that the appropriate factors of momentum will arise at higher orders in the EFT expansion. Such arrow-preserving loops, as shown in the closures of $\mathcal{O}_{47a}$ and $\mathcal{O}_{56}$ in Table 2.1, vanish by even–odd parity arguments absent these higher-order contributions [86]. Indeed, in UV models built from these operators the additional gauge-boson loops are not necessary [4, 233]. This means that for operators such as $\mathcal{O}_{47a}$ and $\mathcal{O}_{56}$, our neutrino-mass estimates are enhanced with respect to those presented in Ref. [86] by $16\pi^2/g^2$.

[9] A UV example of such a model was presented and studied in Ref. [4] for $\mathcal{O}_{47j}$. A number of other examples were also mentioned in Ref. [255], including a two-loop model generating a dimension-13 operator at tree level.

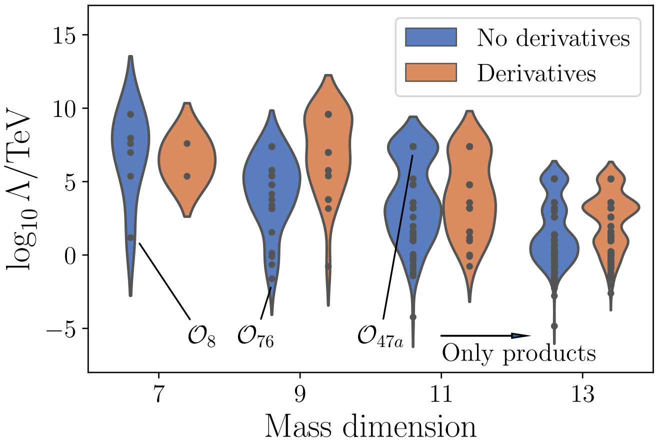

Figure 2.6: The figure shows smoothed histograms of the number of operators that have an estimated upper bound of Λ on the new-physics scale. Black dots generally represent more than one operator. The strips are broken up by mass dimension and whether the operators contain derivatives or not. We assume unit operator coefficients and the dominance of third-generation SM-fermion contributions in the closure diagrams. Operators containing no derivatives (blue) are separated from those containing one derivative (orange). Those containing more than one derivative are not included in the figure, since in most cases these come about at next-to-leading order in the EFT expansion, and therefore imply the same Λ values as the lower-dimensional operator with two fewer derivatives. The dimension-eleven operators containing one derivative and all of the dimension-13 operators shown are constructed from the lower-dimensional operators in our listing only as products. This means that the set of operators plotted above that do not feature in Table B.1 are incomplete. However, we do not find that similar product-type operators at dimensions nine and eleven give special estimates for the neutrino mass or Λ, and so we expect these results to be representative of the true situation up to mass-dimension 13. The general decrease in Λ with increasing operator mass dimension is evident in the figure. The most suppressed closures tend to be of non-derivative operators. By mass-dimension eleven it becomes clear that a class of operators, those with the structure shown in Eq. (2.31), are less suppressed than the rest.

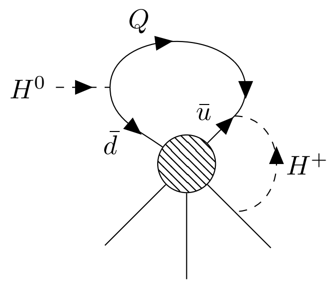

Figure 2.7: For some operators containing $\bar{d}\bar{u}^\dagger$ the operator closure involves a motif like that shown in the figure. There is always an additional diagram with the roles of the unphysical Higgs and H^0 interchanged. Both diagrams are proportional to $y_u y_d$ but related by a negative sign coming from the couplings of H^+ to up- and down-type quarks as shown in Eq. (2.34), and therefore their sum vanishes.

2. In some cases, operators containing a factor of $\bar{u}^\dagger \bar{d}$ require a closure with W bosons rather than H^+, since the sum of the diagrams with the unphysical Higgs fields vanishes [29]. The situation is shown in Fig. 2.7 for a general one-loop case of this phenomenon. Ultimately this comes from the relative negative sign in the Lagrangian between the up- and down-type Yukawa interactions:

$$\mathscr{L}_{\text{Yuk}} \supset y_u^r V_{rt} d_t \bar{u}_r H^+ - y_d^r V_{tr} \bar{d}_r^\dagger u_t^\dagger H^+ \,. \tag{2.34}$$

As shown in the Fig. 2.7, the fermion loop requires a mass insertion on the quark line to which the H^+ does not connect, making both loops proportional to $y_u y_d$ but with differing signs. Care must be taken to ensure that the loop functions are also necessarily the same in cases where this property is used.

It might be possible that, in a similar way to (2) above, the sum of diagrams with different W placements or of the neutrino-flavour-symmetrised diagrams might also lead to additional cancellations which further decrease the upper bound on the new-physics scale. This not a possibility we explore in detail here, but note that similar cancellations have been noted in the literature [4].

Our estimates for the neutrino mass are provided as symbolic mathematical expressions in our model database. Where possible these been checked against more detailed calculations and UV models in the literature generating the operators to ensure acceptable agreement [4, 29, 84, 85, 101, 237, 256–258]. The predictions for the new-physics scale associated with each operator are provided in Table B.1, along with the number of loops in the closure. Operators for which a range is given for the number of loops are those that generate the dimension-seven or dimension-nine analogues of the Weinberg operator. As touched on above, the additional Higgs fields in these closures can always be closed off, adding more loops to the neutrino self-energy diagram while reducing the overall scale suppression. The contribution with the highest number of loops will dominate for scales $\Lambda \gtrsim 4\pi v$.

We note that in some cases, more insights can be made about the structure of the neutrino-mass matrix from the nature of the operator, even in the general form with which they appear in our classification. For example, there is only one independent Lorentz-structure associated with $\mathcal{O}_{4b}$: $\kappa^{\mathcal{O}_{4b}}_{rstt}(L^i_r L^j_s \epsilon_{ij})(Q^\dagger_{tk} \bar{u}^\dagger_t)H^k$, from which it can be seen that the operator coefficient must be antisymmetric in rs from Fermi–Dirac statistics. It is clear from the diagram associated with the operator in Table 2.1 that the loop integral will depend on an external lepton flavour, and this dependence can only come from charged-lepton masses, *i.e.* $I(m_e^r)$. Then the complete expression for the estimated neutrino mass will be something like

$$m_\nu^{\{rs\}} \sim \sum_t \frac{g_2^2 y_u^t}{(16\pi^2)^2} \frac{v^2}{\Lambda} [\kappa_{[rs]tt} I(m_e^r) + \kappa_{[sr]tt} I(m_e^s)] \tag{2.35}$$

$$= \sum_t \frac{g_2^2 y_u^t}{(16\pi^2)^2} \frac{v^2}{\Lambda} \kappa_{[rs]tt} [I(m_e^r) - I(m_e^s)], \tag{2.36}$$

which implies a neutrino-mass matrix with zeros down the diagonal, similar to that following from the Lagrangian in Eq. (2.29). Such a texture is disfavoured by neutrino oscillation data. Studying the structure of the neutrino-mass matrices implied by a complete basis of $\Delta L = 2$ operators would allow more, similar conclusions to be drawn in a model-independent way. Recently, a complete basis of operators in the SMEFT at dimension nine has been written down [144], and this could facilitate such an effort.

2.4.2 UV considerations

We now turn to the UV structure of the operators: their completion topologies, the associated neutrino self-energy graphs, and the nature of the exotic fields that feature therein. Central to our study of neutrino mass is the requirement that a model represent the leading contribution to the neutrino mass, a condition we impose through a process of model filtering, also discussed in the present section.

Tree-level completion topologies

The tree-level UV topologies depend on the number of fermions and scalars in the operator, and this is how we choose to label them. Thus, a dimension-eleven operator with two scalars and six fermions has topologies labelled $2s6f_i$. We do not distinguish between $(\mathbf{2}, \mathbf{1})$- and $(\mathbf{1}, \mathbf{2})$-fermions in this classification, and some of these topologies will therefore always imply the existence of heavy vector particles in the completions.

In our analysis these models are not considered, but the topologies are still presented here in general. Each topology corresponds to a pattern of contractions in the language of Sec. 2.3, and sometimes we use this perspective.

We present the different topology types in Table 2.2 along with peripheral information relating to these. The number of propagators in the diagrams represents an inclusive upper bound on the number of exotic fields allowed in the completions of the associated operators, counting Dirac fermions as one exotic field. In many cases, repetition in the operator's field content can lead to fewer fields furnishing the internal lines of the diagram, since we identify fields with the same quantum numbers. To avoid clutter we keep the complete gallery of tree-level diagrams in our online example-code repository, and instead only show some of the graphs here. For some topology types the relevant diagrams have already appeared in earlier parts of the paper, and these figures are referenced in the table. We make more specific comments about the topology types by operator mass dimension below.

Dimension seven At dimension seven there are three broad classes of $\Delta L = 2$ operators by field-content: $0s4f$, $1s4f$ and $4s2f$ in our classification scheme. Operator $\mathcal{O}_{D1}$ is one of only two $0s4f$ operators in the entire listing, both of which are non-explosive[10]. The Weinberg-like $\mathcal{O}'_1$ is the only $4s2f$ operator at dimension seven, while there are six $4s2f$ operators: $\mathcal{O}_2$, $\mathcal{O}_{3a,b}$, $\mathcal{O}_{4a,b}$ and $\mathcal{O}_8$. The UV topologies relevant for the dimension-seven operators are presented in Fig. 2.8. There are only two tree-level topologies associated with the $1s4f$ operators. One involves two exotic scalars, the other an exotic scalar and a heavy fermion with an arrow-violating propagator line. There are ten topologies associated with the $4s2f$ class, for which the only pertinent operator is $\mathcal{O}'_1$. Only topology $4s2f_3$ is associated with a model that does not contain seesaw fields. Topology $4s2f_6$ accommodates up to three exotic scalars and $4s2f_8$ allows up to three exotic fermions. Such fermion-only models are expected only for the Weinberg-like operators, in the absence of derivatives. The remaining topologies allow all other combinations up to three fields for the number of exotic scalars and fermions introduced. Radiative neutrino mass from the dimension-seven operators without derivatives was also studied in Ref. [101].

Dimension nine At dimension nine there are 79 operators in our catalogue. There are 16 operators containing six fermions, these are $\mathcal{O}_9$ through to $\mathcal{O}_{20}$ as well as $\mathcal{O}_{76}$. The relevant tree-level topologies are presented in Fig. 2.2. There are 15 $3s4f$ operators, most of which have the form $\mathcal{O}_1 \cdot \mathcal{O}_{\text{SM Yukawa}}$ or $H^\dagger H$ times a $1s4f$ dimension-seven operator. These are operators $\mathcal{O}_5$ through to $\mathcal{O}_7$ as well as $\mathcal{O}_{61}$, $\mathcal{O}_{71}$, $\mathcal{O}_{77}$, $\mathcal{O}_{78}$ and $\mathcal{O}'_8$. These topologies are shown in Fig. 2.9a. There is a single $6s2f$ operator: the Weinberg-

[10] We note that although $\mathcal{O}_{D1}$ is non-explosive, one-loop completions exist that lead to three-loop neutrino mass models.

Topology type	Operators	Topologies	Propagators	Figure
$0s4f$	2	1	1	$\hookrightarrow$
$0s6f$	16	2	3	2.2
$1s4f$	16	2	2	2.8b
$2s2f$	7	1	1	2.1
$2s4f$	29	8	2,3	2.9b
$2s6f$	137	35	4,5	2.11
$3s2f$	3	4	1,2	2.10b
$3s4f$	15	23	3,4	2.9a
$4s2f$	8	10	2,3	2.8a
$5s2f$	1	24	2,3,4	2.10a
$5s4f$	15	264	4,5,6	$\hookrightarrow$
$6s2f$	1	66	3,4,5	$\hookrightarrow$

Table 2.2: The table shows the topology classes encountered in our operator listing along with related information: the number of pertinent operators, the number of tree-level topologies associated with each topology type, the number of internal lines featuring in the diagrams (given as a range), and the appropriate figure reference in the text. Although there is one $0s4f$ topology, all of the pertinent operators in our listing are non-explosive because they contain derivatives. The symbol $\hookrightarrow$ indicates that we do not present these topologies in this paper; instead, we point the interested reader to our online database and example code for the relevant diagrams. We highlight that although the topologies are labelled only by their field content, the pertinent operators may include one or more derivatives. We point the reader to the main text for a detailed breakdown by mass-dimension of the topologies that are relevant to each operator.

like $\mathcal{O}_1''$. The remaining 47 operators contain derivatives. Those that contain an even number share topologies with dimension-five or dimension-seven operators. These include $\mathcal{O}_{D19}$, a $2s2f$ operator, $\mathcal{O}_{D18}$ and $\mathcal{O}_{D22}$ which are $4s2f$ operators with associated topologies shown in Fig. 2.8a, as well as $\mathcal{O}_{D4}$, $\mathcal{O}_{D7}$, $\mathcal{O}_{D13}$ and $\mathcal{O}_{D15}$ for which the $1s4f$ topologies of Fig. 2.8b are relevant. The remaining operators contain an odd number of derivatives. The operators $\mathcal{O}_{D5}$, $\mathcal{O}_{D6}$, $\mathcal{O}_{D8}-\mathcal{O}_{D10}$, $\mathcal{O}_{D12}$, $\mathcal{O}_{D14}$, $\mathcal{O}_{D16}$ and $\mathcal{O}_{D17}$ are of type $2s4f$, implying entirely new topologies, shown in Fig. 2.9b. To these we add the $5s2f$ operator $\mathcal{O}_{D20}$ and the $3s2f$ operator $\mathcal{O}_{D21}$, which also have novel structure. Fig. 2.10a and Fig. 2.10b are relevant in this case. For the operators that contain an odd number of derivatives, only the topologies allowing at least one arrow-preserving fermion propagator do not contain exotic Proca fields. Some $3s4f$ and $5s2f$ topologies have the interesting property that they involve exotic fields that couple only to other exotic fields in the diagram. These are the lowest-dimensional operators in our listing

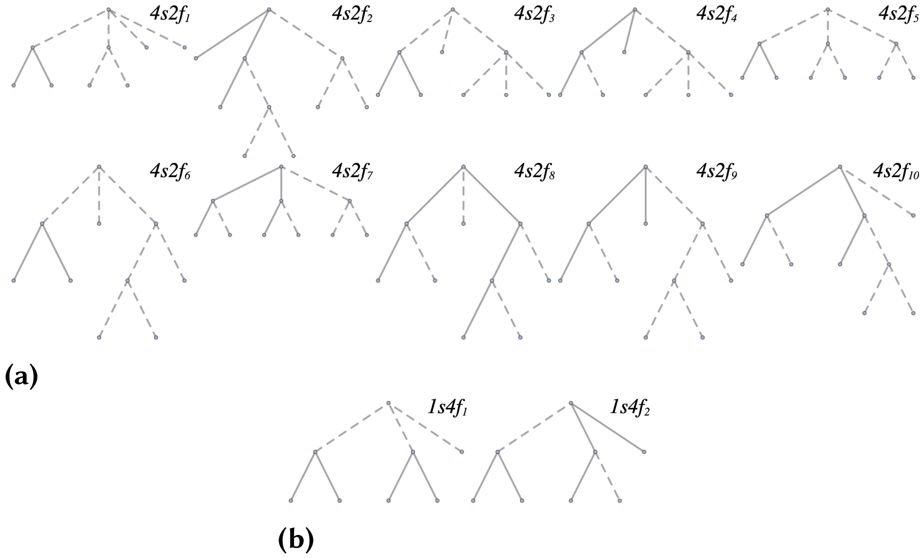

Figure 2.8: (a) The tree-level topologies relevant for the completions of the four-scalar–two-fermion operator $\mathcal{O}_1'$. Only topology $4s2f_3$ leads to a novel completion that does not feature a seesaw field. We point out that topology $4s2f_8$ permits fermion-only completions, which are expected only for the Weinberg-like operators in the absence of derivatives. (b) The two tree-level topologies relevant for the completions of the one-scalar–four-fermion dimension-seven operators in Table B.1. The internal fermion line on $1s4f_2$ must be arrow-violating for all of the operators we consider.

having this feature, although this becomes more common at dimension eleven.

We note that the tree-level topologies can also be important in telling which derivative operators might provide novel completions. As discussed in Sec. 2.3.1, many operators containing more than one derivative have no model-discovery utility. These are operators generated past the leading order in the expansion of the heavy propagators in the UV theory, and their completions are always found by exploding the lower-dimensional operators with an even number of fewer derivatives. One way to diagnose such a situation is to check how many arrow-preserving fermion lines are present in the tree-level topologies associated with an operator. If all of the graphs contain fewer such propagators than the number of derivatives in the operator, then any model generating this operator will also generate the corresponding lower-dimensional one. At dimension nine there are seven operator classes that fall into this category. The four operator families $\mathcal{O}_{D4}$, $\mathcal{O}_{D7}$, $\mathcal{O}_{D13}$ and $\mathcal{O}_{D15}$ each contain two derivatives. These operators are identified above as fitting into the $1s4f$ topology class. It is clear from Fig. 2.8b that no two-fermion completions are relevant to this class, and the Lorentz structure of these operators is such that the internal fermion can only by arrow-violating. This suggests that models generating these operators at tree-level will always also generate the derivative-free dimension-seven operators $\mathcal{O}_2$, $\mathcal{O}_3$, $\mathcal{O}_4$ and $\mathcal{O}_8$, respectively. There are two three-derivative operators: $\mathcal{O}_{D21}$, of topology class $3s2f$, and $\mathcal{O}_{D11}$, a $0s4f$ operator. The latter is non-explosive and therefore not relevant to a discussion of tree-level model building. The $3s2f$ class admits completions that contain one and two fermions: those associated with topologies $3s2f_4$ and $3s2f_2$, respectively. In both both cases we find that the operator's structure allows for only a single arrow-preserving propagator in each diagram. As before, this suggests that $\mathcal{O}_{D21}$ is not interesting for model discovery, and its completions will be found by studying $\mathcal{O}_{D3}$. Finally, there is also one four-derivative operator at dimension nine: the $2s2f$ operator $\mathcal{O}_{D19}$ whose completions coincide with those of the Weinberg operator $\mathcal{O}_1$. This means that the only two-derivative operators in our listing that could contribute new completions to the pool of neutrino-mass models are $\mathcal{O}_{D18}$ and $\mathcal{O}_{D22}$. Operator $\mathcal{O}_{D22}$ has the feature that the removal of the derivatives causes the operator to vanish, while this is not true for all of the $\mathrm{SU}(2)_L$ structures associated with $\mathcal{O}_{D18}$.

Dimension eleven By far the largest class of operators at dimension eleven is the $2s6f$ topology type, for which the topologies are presented in Fig. 2.11. These operators are mostly formed as products of $0s6f$ dimension-nine operators with $H^\dagger H$, or $1s4f$ dimension-seven operators with SM Yukawa couplings. They are operators $\mathcal{O}_{21}$ through to $\mathcal{O}_{65}$, excluding the structures associated with $\mathcal{O}_{61}$, as well as $\mathcal{O}_{75}$, $\mathcal{O}'_{76}$ and $\mathcal{O}_{82}$. The only other major class relevant to the derivative-free dimension-eleven operators is $5s4f$ for which there are 264 tree-level topologies. These are presented with our example code, along with the topologies relevant to the single $6s2f$ operator $\mathcal{O}_1'''$. This dimension-eleven generalisation of the Weinberg operator has already received some attention in the literature [103].

Model filtering

The completions constructed by exploding the $\Delta L = 2$ operators are not all automatically guaranteed to provide the leading-order contribution to the neutrino mass. The same $\Delta L = 2$ Lagrangian may, for example, inevitably imply another, larger contribution. Alternatively, the dominant contribution may come from other LNV combinations of couplings in the model's full Lagrangian. The relative importance of different mechanisms may also depend on the assumptions of the model builder. Some neutrino-mass diagrams will dominate over others only in certain regions of parameter space. Are these regions accessible without large hierarchies in exotic couplings? Are such hierarchies acceptable, if necessary to render a mechanism dominant? What about exotic flavours or additional symmetries? Model filtering is the process of removing those models that, under some set of assumptions, do not provide the leading-order

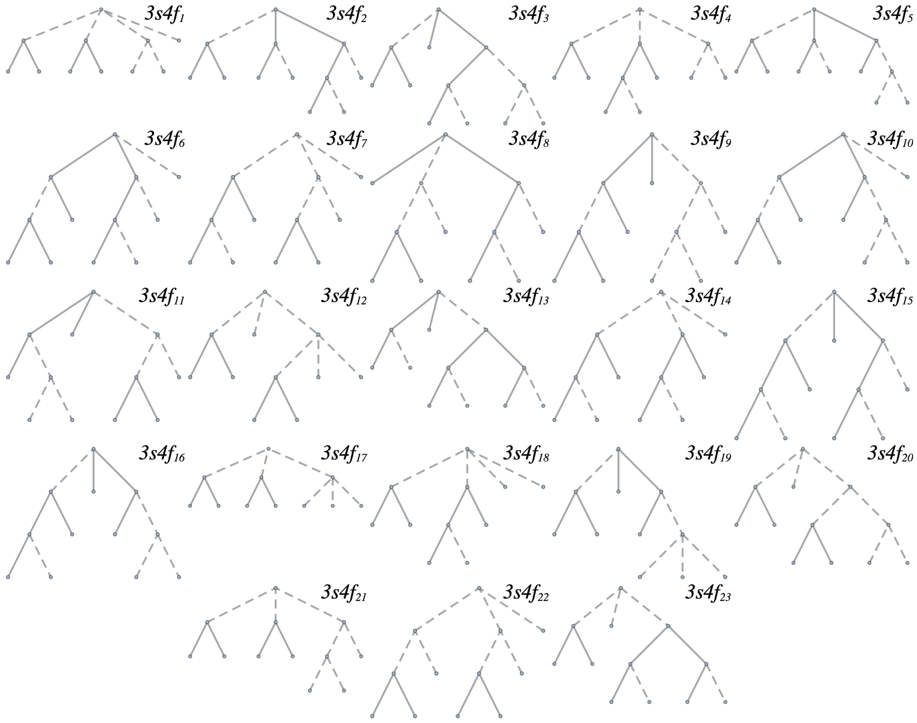

(a)

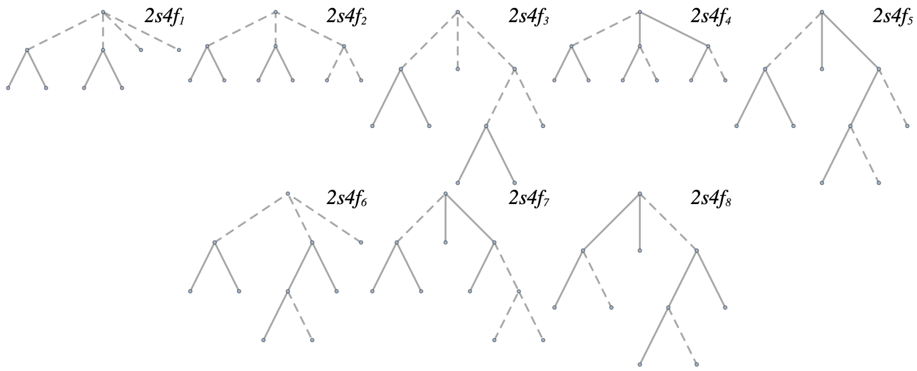

(b)

Figure 2.9: (a) The figure shows the tree-level topologies relevant to $3s4f$ operators. Topologies $3s4f_3$, $3s4f_{13}$, $3s4f_{20}$ and $3s4f_{23}$ imply one exotic field that couples only to other exotics in the diagram. This topology class is relevant to a large number of dimension-nine operators, and these are the lowest-dimensional examples of operators containing this property in our listing. (b) The two-scalar–four-fermion topologies associated with dimension-nine single-derivative operators in our catalogue. Since only single-derivative operators furnish these graphs, only those topologies containing at least one arrow-preserving internal fermion line are relevant. These are topologies $2s4f_4$ – $2s4f_8$; the other fermion propagator in $2s4f_4$ and $2s4f_5$ must be arrow violating. Topologies $2s4f_1$ – $2s4f_3$ each give rise to completions involving exotic Proca fields.

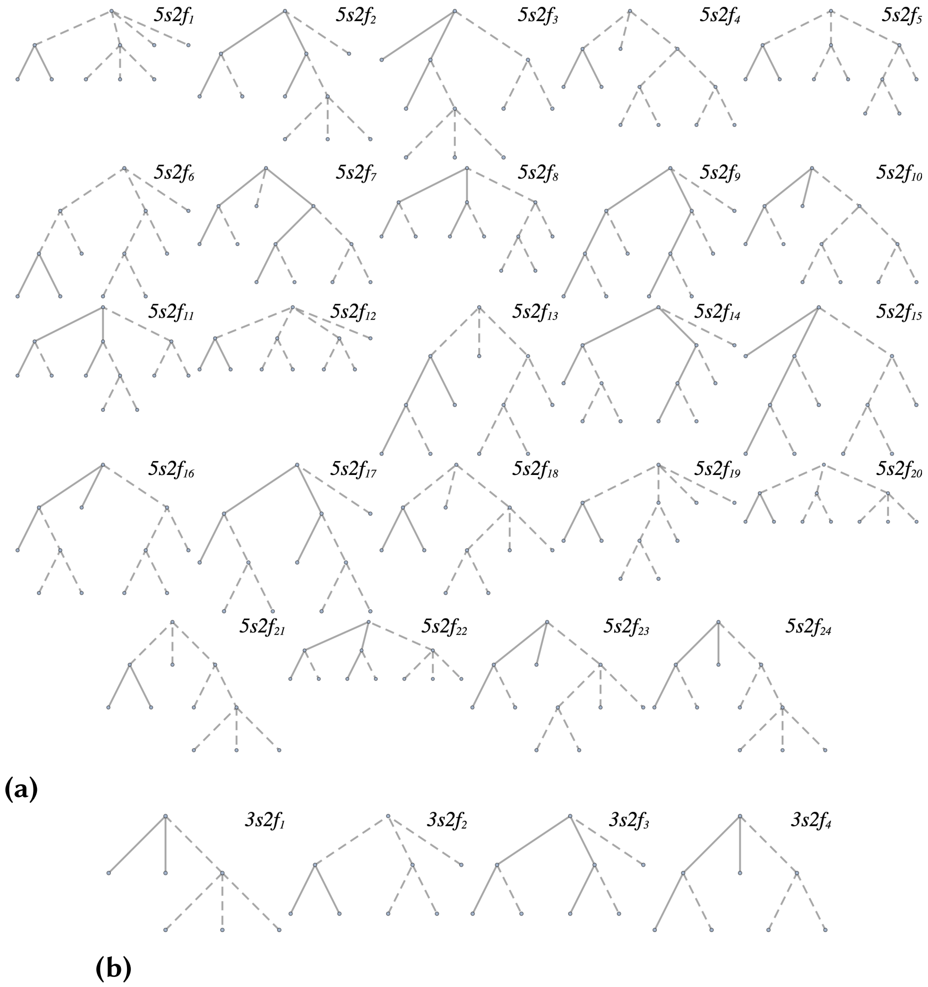

Figure 2.10: (a) The $5s2f$ topologies relevant only to the single-derivative operator $\mathcal{O}_{D20}$. Only those topologies allowing one arrow-preserving internal fermion line give completions allowed in our framework. Topologies $5s2f_4$, $5s2f_7$ and $5s2f_{10}$ contain heavy fields that couple only to other exotics in the diagram. (b) The UV diagrams associated with the $3s2f$ operator $\mathcal{O}_{D21}$. Only the last two diagrams can generate the operator under our model-building assumptions.

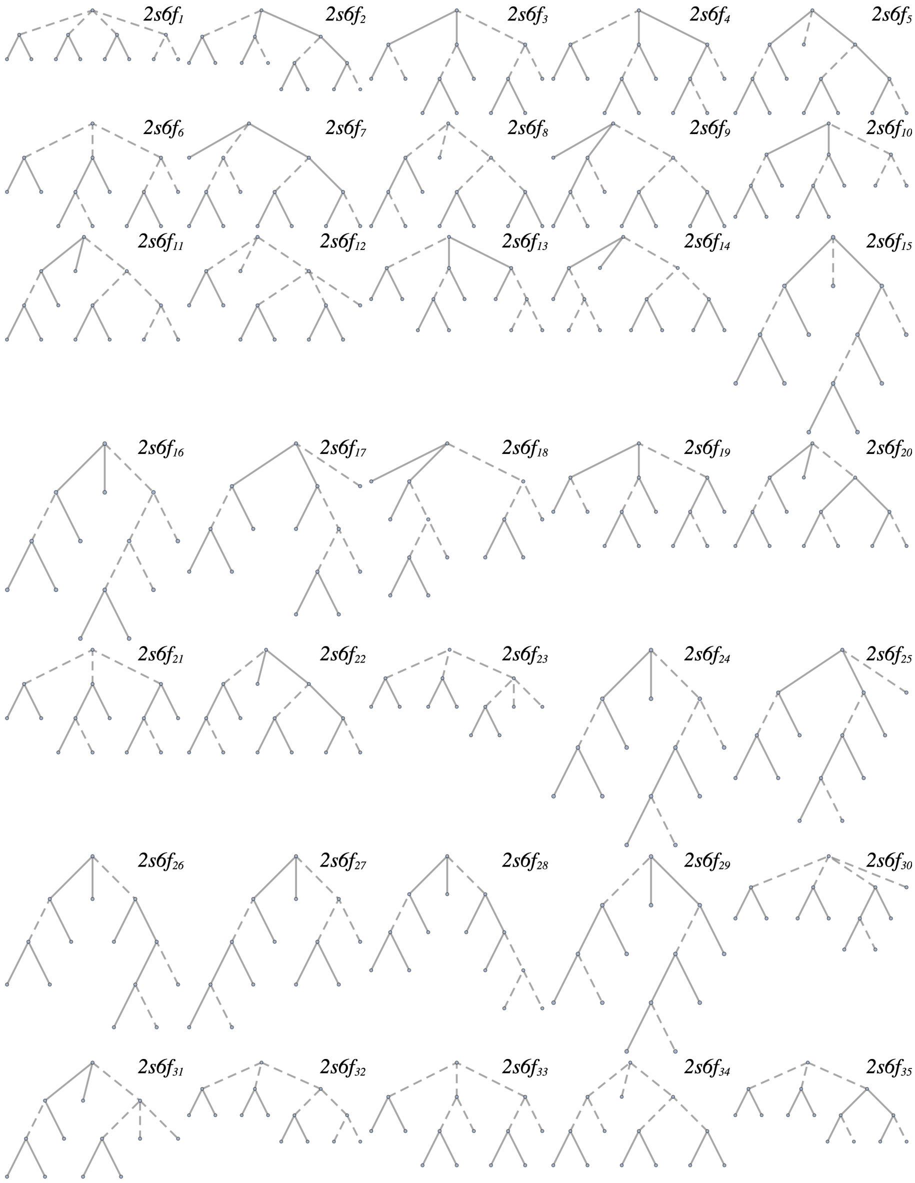

Figure 2.11: The tree-level topologies associated with the large class of $2s6f$ dimension-eleven operators in our listing. A number of graphs display the feature — less common at dimension nine — that an exotic field in the diagram couples only to other internal lines.

contribution to the neutrino mass. Our approach to filtering neutrino mass models is contrasted against other possible approaches below, and we also make more general comments about model filtering in other contexts. We mention that the following discussion of filtering is similar in intent to that of ‘genuineness’ in the loop-level matching paradigm [24, 26, 96, 97]. We sometimes adopt this notation as well, and call models ‘genuine’ if they represent the dominant contribution to the neutrino mass.

Filtering criterion We begin by noting that model filtering is ubiquitous when considering tree-level effects. Here, the filtering criterion is unambiguously the operator dimension, since higher-dimensional operators are inevitably suppressed compared to lower-dimensional ones. With regard to the $\Delta L = 2$ EFT, such a dimension-focused criterion is useful for thinking about LNV scattering events, for example. As discussed in Sec. 2.4.1, the operator dimension is also a rough indication of the predicted neutrino-mass scale, and therefore has some utility in anticipating which models will dominate the neutrino mass.

We point out that this approach to model filtering allows for the immediate rejection of some models, already during the process of opening up the operator. This can happen, for example, when a contraction introduces an exotic particle transforming like a SM field. Taking $\mathcal{O}_2$ as an example, contractions like

$$L^i \overbrace{L^j L^k \bar{e}}^{\varphi^\dagger \sim (\mathbf{1},\mathbf{2},\frac{1}{2})} H^l \epsilon_{ij}\epsilon_{kl} \to L^i L^k \tilde{\varphi}^j H^l \epsilon_{ij}\epsilon_{kl}, \tag{2.37}$$

with $\tilde{\varphi}$ a second Higgs doublet, always imply that further contractions will produce seesaw fields, since the RHS of Eq. (2.37) has the same structure as the Weinberg operator. We note that for fermions the situation is more subtle because of the Lorentz structure. Specifically, although $H\bar{u}$ transforms like $Q^\dagger$ under G_{SM}, the Lorentz transformation properties are different. The derivative contraction $(D^{\alpha\dot{\alpha}}H)\bar{u}_\alpha$ does transform like Q under $\mathrm{SU}(2)_+ \otimes \mathrm{SU}(2)_- \otimes G_{\mathrm{SM}}$ and that makes a number of such contractions forbidden if one is interested in only dominant contributions according to the mass-dimension criterion. This is the same phenomenon as that seen in the paradigmatic opening of the derivative operator $\mathcal{O}_{D3}$ given in Sec. 2.3.1, where an exotic field transforming like L [see Eq. (2.25)] lead to a similar Weinberg-like operator at an intermediate stage in the completion procedure. We note that this does not completely rule out exotic copies of SM fields featuring in radiative neutrino mass models. Using $\mathcal{O}_2$ again as an example:

$$L^i L^j \overbrace{L^k \bar{e}}^{\varphi^\dagger \sim (\mathbf{1},\mathbf{2},\frac{1}{2})} H^l \epsilon_{ij}\epsilon_{kl} \to L^i L^j \tilde{\varphi}^k H^l \epsilon_{ij}\epsilon_{kl} \tag{2.38}$$

is allowed, since the $\mathrm{SU}(2)_L$ structure of this operator differs to that of the Weinberg operator. Similarly, vector-like quarks and leptons are extensively found in completions of both derivative and non-derivative operators after the filtering procedure, but their SM and Lorentz quantum numbers are interchanged with respect to their SM counterparts. For example, a particular completion of $\mathcal{O}_{3a}$ is

$$L^i L^j \overbrace{Q^k \bar{d}}^{U\sim(\mathbf{3},\mathbf{1},\frac{2}{3})} H^l \epsilon_{ij}\epsilon_{kl} \to \overbrace{L^i}^{\mathcal{S}_1^\dagger\sim(\mathbf{1},\mathbf{1},-1)} L^j U \bar{d} \epsilon_{ij}\epsilon_{kl} \to \mathcal{S}_1^\dagger U \bar{d} \ , \tag{2.39}$$

which contains the vector-like quark $U + \bar{U}^\dagger$. Note however that U transforms like $\bar{u}^\dagger$ under G_{SM}, but oppositely under the Lorentz group. It is true that $\bar{U}$, the vector-like partner of U, does transform like $\bar{u}$, but this plays no role in the operator.

Since we are most interested in radiative neutrino mass, a more direct and relevant filtering criterion in our case is the neutrino-mass estimate from the closure graph of the operator. This is the metric we use to compare and filter models in the results we present in Sec. 2.5. Whichever filtering criterion is chosen, the conditions for generating the lower-dimensional operator or the dominant neutrino self-energy graph still depend on the filtering philosophy.

Filtering philosophy The filtering criterion defines a hierarchy among the effective operators. If one is interested in tree-level effects, then operators of low dimension have a high priority in the sense that their effects are dominant over those of high-dimensional operators, whose influence is suppressed by additional powers of Λ. Similarly, the operators whose closure graphs imply large contributions to the neutrino mass have a higher priority than those implying small contributions.

One could take the view that it is sufficient for a subset of the field content associated with a completion of a high-priority operator to be present in that of a lower-priority one for it to be filtered out, even if the relevant diagrams depend on entirely different couplings and interactions. We call this perspective *democratic*, in the sense that it treats all allowed couplings and interactions fairly and ignores possible hierarchies in free parameters. A democratic approach would then filter out all completions of $\Delta L = 2$ operators of mass dimension larger than five containing one of the seesaw fields, for example, since these always imply a dominant contribution from the dimension-five Weinberg operator. Even if the same couplings are not present in both diagrams, there is no reason, on this view, for one coupling to be very much larger than another, making the tree-level contribution dominant.

An alternative approach might be to filter out only those completions that necessarily lead to subdominant contributions to the neutrino mass in all regions of parameter space. Naively it seems that neutrino-mass mechanisms involving different couplings would all survive the filtering process in this case, since the relative ordering of the contributions from each diagram depends on the chosen values of the coupling constants. This is in general only guaranteed if a symmetry is recovered in the Lagrangian when one coupling is turned off, so that the forbidden coupling is not generated at some higher order in perturbation theory. We call this approach *stringent* filtering, since the conditions for removing a model are more difficult to satisfy.

For our results in Sec. 2.5 we take an intermediate view, leaning more towards the democratic side. We filter on the basis of particle content, but always keep track of the baryon-number assignment of the field. We then keep models with identical SM quantum numbers if the baryon-number assignments of the fields differ. With a concrete example, we treat $\zeta^{(\prime)} \sim (\bar{\mathbf{3}}, \mathbf{1}, \frac{1}{3})$ in $x(L^i Q^j)\zeta^{\{kl\}}\epsilon_{ik}\epsilon_{jl}$ and $y(Q^i Q^j)\zeta'^{\{kl\}}\epsilon_{ik}\epsilon_{jl}$ as different fields.

In practice, we enumerate the completions of the operators in order of their estimated contribution to the neutrino mass. We associate a prime number with each exotic field encountered, including baryon-number as a distinguishing property. Models then correspond to products of prime numbers. As we explode each operator in order, we remove models from the list of completions if their characteristic number is divisible by that of any models already seen. In this way, we remove those mechanisms that are subdominant contributions to the neutrino mass in the democratic sense.

We emphasise that this procedure is not sufficient to fully ensure that the remaining models are genuinely dominant contributions to the neutrino mass. For example, it may be the case that the Weinberg operator is generated by loops of a subset of the exotic particles in one of our models. We are not sensitive to these models since we are concerned only with tree-level completions of the operators. One-loop contributions to the neutrino mass from heavy loops can be diagnosed easily on topological grounds. For example, topology T-3 of Ref. [102] will come about whenever the neutrinos in the diagram are connected by a single exotic fermion [233]. At two-loops, one could check the full gauge- and Lorentz-invariant Lagrangian for each model against Table 1 of Ref. [24], for example. We do not include this in our default filtering procedure, since it would require generating the full Lagrangian of each model. This is a computationally prohibitive task, especially since Table 2.2 suggests that the completions of some operators can contain up to six exotic fields. Should any model from our database be chosen for further study, the full Lagrangian can be generated with the functions in our example code and studied for the presence such heavy loops. We note that sometimes the presence of a heavy loop can be diagnosed from the neutrino self-energy graph, or even the tree-level topology, and we give a detailed example of such a case in Sec. 2.5.2. An additional filter on the models that goes beyond our initial tree-level filtering analysis is the possibility of exotic fields gaining vacuum expectation values. In this case, diagrams may exist that imply larger contributions to the neutrino mass than that suggested by our approach, and we are not sensitive to these since they generate exotic operators other than the Weinberg operator at the low scale. Examples are presented in Refs. [259, 260], where in both cases a two-loop completion of the Weinberg operator also generates the exotic operator $LLH^\dagger\Theta_3$, where $\Theta_3 \sim (\mathbf{1}, \mathbf{4}, \frac{3}{2})_S$.

We note that our model database [221] contains both the unfiltered completions of the operators in Table B.1, as well as the models filtered according to the above method. Our example code also includes functions for filtering on interactions rather than fields, and finding U(1) symmetries present in models' Lagrangians. Thus, the results presented in Sec. 2.5 and Table B.1 can be readily reproduced with alternative filtering criteria, philosophies or approaches.

2.5 Models

In this section we present the radiative models derived by exploding the $\Delta L = 2$ operators catalogued in Table B.1. We give an overview of the models, and explore their particle content and the effects of the partial model-filtering method we present in Sec. 2.4.2. We do not provide the entire listing of models here because there are very many, but instead give some examples. We point the interested reader to our database for the full searchable listing.

We distinguish the terms 'model' and 'neutrino-mass mechanism' or '$\Delta L = 2$ Lagrangian' in this section. By model we mean a collection of particle content. Those same multiplets may have many combinations of couplings that violate lepton-number by two units, leading to meany neutrino-mass mechanisms, or $\Delta L = 2$ Lagrangians. We use the word 'completion' here to mean a neutrino-mass mechanism derived from a particular effective operator. Used in this way, the same $\Delta L = 2$ Lagrangian may be shared by two completions, but they correspond to the same model. We also remind the reader that we use the words 'field' and 'multiplet' interchangeably.

We note here that the following analysis does not include the dimension-eleven generalisation of the Weinberg operator $\mathcal{O}_1'''$, since the operator has an unwieldy number of topologies and the relevant tree-level completions have already been studied in the literature [103].

2.5.1 Overview

The models are generated by running the algorithm summarised in Sec. 2.3.2, as found in our example code, on our catalogue of the $\Delta L = 2$ operators. The results for the number of completions before and after filtering are presented in Table B.1. In the language of Sec. 2.4.2, we use the democratic filtering procedure with the neutrino-mass scale as the filtering criterion for these data. We note again that this leaves us with an overestimate of the actual number of genuine neutrino-mass models. Even so, one can see that 54 operators end up with no completions after filtering, ruling them out as possibly playing a dominant role in generating the neutrino masses, at least according to our model-building assumptions. The complete list of unfiltered $\Delta L = 2$ Lagrangians and tree-level completion diagrams is compiled in our database, and the documentation provides information for how to perform different kinds of filtering on the models.

The database contains 430,810 inequivalent $\Delta L = 2$ Lagrangians before filtering. Counted democratically (*i.e.* by particle content) these correspond to 141,989 unfiltered models. Of the distinct Lagrangians, only around 3% (11,483) survive democratic filtering with the neutrino-mass criterion. This corresponds to 11,216 distinct models. In our filtering analysis we also incorporate information from the one-loop study of the Weinberg operator[11] done in Ref. [97]. We generate a listing of the models from Tables 2 and 3 of Ref. [97] with hypercharges that are multiples of $1/6$ in the range $[-3, 3]$ and ranges for the $\mathrm{SU}(3)_c$ and $\mathrm{SU}(2)_L$ representations that cover those of the exotic fields featuring in our models. We remove the completions in our listing that contain a subset of these fields and imply neutrino masses suppressed by more than one loop factor, since the models presented in Ref. [97] generate the Weinberg operator at one loop.

We visualise the number of models with democratic and no filtering in Fig. 2.12 broken down by mass dimension. After filtering there are three models at dimension five, 16 models at dimension seven, 244 models at dimension nine and 10,969 models at dimension eleven[12]. It is clear that the number of filtered neutrino-mass models grows with operator dimension, which is perhaps unintuitive. For any high dimensional operator, there are competing effects influencing the number of viable completions. First, the large number of models derived already from lower-dimensional operators means that the chances some model will be filtered out are larger. Second, high dimensional operators involve more fields, meaning that there are more combinations of contractions that can be made, and therefore more completions expected. Despite the increased filtering odds, evidently the combinatorial explosion of different models wins.

In Fig. 2.13 we present data relevant to the number of fields present in the models. Fig. 2.13a shows the number of exotic scalars and fermions present in the completions. Despite the fact that the UV topologies associated with some derivative operators allow completions containing no scalars, we find that only the Weinberg-like operators keep their fermion-only models after the democratic filtering procedure. By far the most common kinds of models contain five heavy fields, especially three fermions and two scalars, or two fermions and three scalars. This is due to the fact that, as is clear from Fig. 2.12, most of the models generate dimension-eleven operators. In Fig. 2.13b we show the estimated new-physics scale Λ against the number of fields featuring in the models. With the exception of one model with two fields, those required to lie at collider-accessible energies contain three or more fields. Models with few fields that imply suppressed neutrino masses, or equivalently a low new-physics scale, have a kind of selection pressure acting against them: since there are few fields, it is likely they will arise in the completion of other operators, that generally will filter out the former

[11] We anticipate the number of models in our database generating the Weinberg operator with exotic loops at higher-loop order to be small. Such models would need to contain upwards of four exotic fields, and it becomes increasingly less likely that a model will contain a subset of these fields to be filtered out.

[12] We note that the sum of these numbers is not 11,216 since one model can generate multiple operators of different mass dimension in a way consistent with our neutrino-mass filtering criterion.

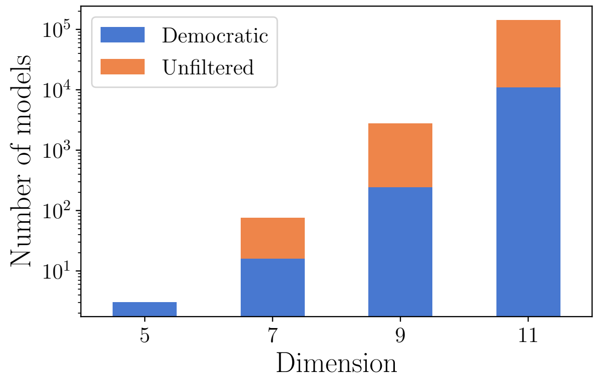

Figure 2.12: The bar chart shows the number of distinct Lagrangians derived from operators of different mass dimension. The orange bars show the number of distinct unfiltered models. The blue bars show the number after democratic filtering. The number of filtered completions grows with mass dimension.

and imply a larger value of Λ. At dimension-seven, for example, $\mathcal{O}_8$ is generated by models featuring two fields and predicts that these should not be heavier than about 15 TeV. However, of its four tree-level completions, only one survives the filtering procedure. This is the outlier two-field model evident in the figure. It was first derived[13] in Ref. [101] and later in Ref. [104]. The model contains the fields $\Pi_1 \sim (\mathbf{3}, \mathbf{1}, \frac{1}{6})_S$ and $\mathcal{Q}_7 \sim (\mathbf{3}, \mathbf{2}, \frac{7}{6})_F$. We list the models containing three exotic fields that are required to lie below 100 TeV in Sec. 2.5.2.

Of the unfiltered 430,810 models, close to 67% (290,492) contain at least one of the seesaw fields: $N \sim (\mathbf{1}, \mathbf{1}, 0)_F$, $\Xi_1 \sim (\mathbf{1}, \mathbf{3}, 1)_S$ or $\Sigma \sim (\mathbf{1}, \mathbf{3}, 0)_F$. We present the exact breakdown by the interactions involved in the models in Table 2.3. These are by far the most common fields appearing in the list of unfiltered models. Since our default filtering philosophy in this analysis is democratic, all of these are absent from the filtered list of models, and they only appear in completions of the Weinberg operator and $\mathcal{O}_{D2}$.

The distinct exotic fields appearing in the completions number 171, although five fields are completely removed following filtering. These are $(\bar{\mathbf{6}}, \mathbf{1}, \frac{7}{6})_S^{1/3}$, $(\bar{\mathbf{6}}, \mathbf{3}, \frac{5}{3})_S^{1/3}$, $(\mathbf{1}, \mathbf{3}, 3)_S^0$, $(\mathbf{1}, \mathbf{5}, 2)_F^0$ and $(\bar{\mathbf{6}}, \mathbf{1}, \frac{5}{3})_S^{1/3}$, where the superscript represents the B assignment of the field. There are 83 different scalar fields and 83 different fermion species. We distinguish three broad classes of scalars on the basis of their interaction with the SM fermions: leptoquarks, diquarks and dileptons. For exotic fermions we differentiate between those arising from contractions between the Higgs and a SM quark (vectorlike quarks), and the Higgs and a SM lepton (vectorlike leptons). The relative frequencies

[13]We note that the other completion of $\mathcal{O}_8$ listed in Ref. [101] also generates $\mathcal{O}_{50a}$ through a diagram which dominates the neutrino mass.

(a)

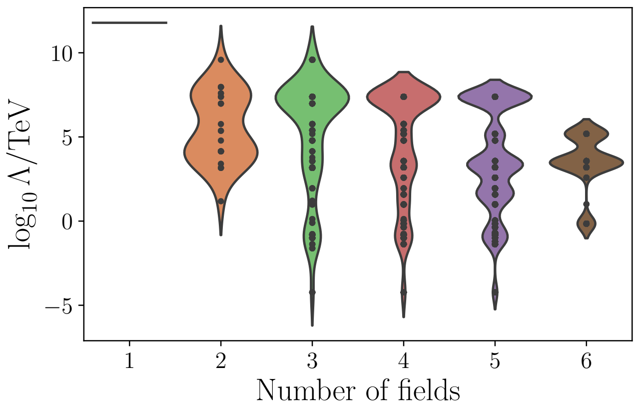

(b)

Figure 2.13: (a) The number of filtered models containing different numbers of exotic scalar and fermion fields. Most models contain five fields, with the most common combination being three fermions and two scalars. The fermion-only models are associated only with Weinberg-like operators. (b) The rough upper bound on the new-physics scale Λ shown against the number of exotic fields introduced in the models. The black dots show the upper bound on the scale of the new physics for each model. A given black dot generally denotes more than one model. Each strip is a smoothed histogram of the number of models having a given Λ as the new-physics upper bound for the specified number of fields. A sizeable class of models are testable at current or future collider experiments.

Field	Interactions	$\Delta L = 2$ Lagrangians	Models
$N \sim (\mathbf{1}, \mathbf{1}, 0)_F$	LHN	51,245 (11.9%)	17,139 (17.1%)
	Other	12,433 (2.9%)	
$\Sigma \sim (\mathbf{1}, \mathbf{3}, 0)_F$	$LH\Sigma$	87,535 (20.3%)	31,629 (31.5%)
	Other	28,157 (6.5%)	
$\Xi_1 \sim (\mathbf{1}, \mathbf{3}, 1)_S$	$LL\Xi_1$	59,791 (13.0%)	51,576 (51.4%)
	$HH\Xi_1^\dagger$	95,410 (22.1%)	
	Both	10,323 (2.4%)	
	Other	30,761 (7.1%)	

Table 2.3: The table shows the number of unfiltered models in which the seesaw fields appear. The category 'other' includes interactions such as $L\varphi N$, where one of the SM fields in the interaction has been replaced with an exotic copy, as well as couplings involving other exotic fields whose quantum numbers are unrelated to those of SM fields.

with which these field classes appear in the filtered completions are shown in Fig. 2.14 as pie charts. The wedges represent the number of Lagrangians in which the field couples as a leptoquark, diquark, dilepton, vectorlike quark or vectorlike lepton. We label fields coupling in all other ways as 'other' in the figure. The most represented family of scalars are leptoquarks, with the most common field being $\Pi_7 \sim (\mathbf{3}, \mathbf{2}, \frac{7}{6})_S$, commonly called R_2 in the literature [261]. This leptoquark appears in simplified models of $R_{D^{(*)}}$ and the neutral-current flavour anomalies like $R_{K^{(*)}}$, see *e.g.* Refs. [214, 216, 259, 262, 263]. It was recently shown to be able to reconcile the discrepant measurements in the anomalous magnetic moments of both the muon and the electron [264, 265]. The second most common scalar appearing in our neutrino-mass models is $\zeta \sim (\bar{\mathbf{3}}, \mathbf{3}, \frac{1}{3})_S$, frequently referred to as S_3. This leptoquark is a popular explanation of the neutral-current $b \to s$ anomalies such as $R_{K^{(*)}}$, see *e.g.* [216, 266–269]. The most frequently encountered fermions are vectorlike quarks, with the most common being $T_2 \sim (\mathbf{3}, \mathbf{3}, \frac{2}{3})_F$. It contains components that mix with both the up- and down-type SM quarks. We emphasise that the plots and numbers presented here are directly related to our filtering and model-counting conventions. In Fig. 2.14 for example, we do not count fields just by their quantum numbers, but also include coupling information as discussed above. Additionally, we count independent Lagrangians as different models rather than just counting distinct sets of fields, which is perhaps more in line with our 'democratic' approach to filtering. We note that the qualitative features discussed here are all relatively robust against these different conventions. We encourage the interested reader to explore our model database to see how different approaches to filtering and counting can answer specific questions they may have of the data.

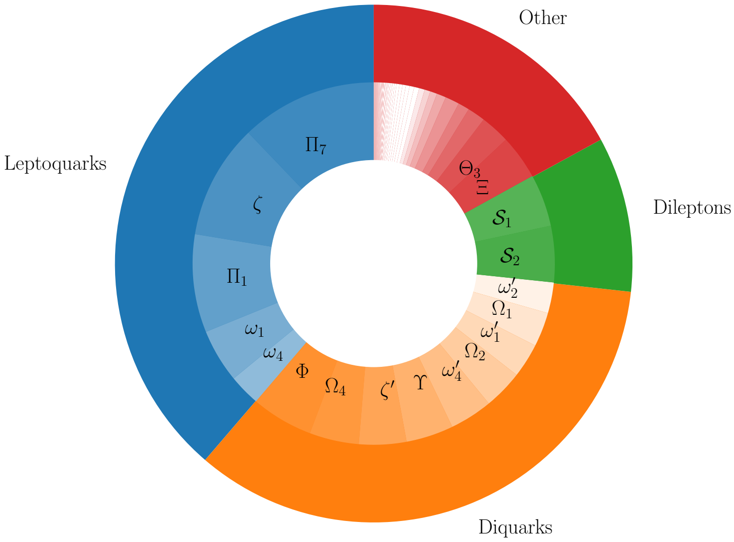

(a)

(b)

Figure 2.14: The number of models in which each field appears in the completions shown as a pie chart for scalars and fermions separately. The exotics are distinguished by their couplings to SM fields. (a) The pie chart of scalar fields appearing in the completions. Primed fields represent leptoquarks whose baryon-number assignment allows only the diquark couplings. (b) The pie chart of fermion fields appearing in the completions. See Table A.2 or Ref. [23] for the convention used for the field names.

We are also interested in the connectivity between fields as they feature in the models. To explore this we study a graph in which each vertex represents one of the 163 exotic fields introduced in the completions that contain at least two fields, and an edge is drawn between fields featuring together in a model. The graph is shown shown Fig. 2.15. The exterior sectors at each node represent the number of degree of the node. The edges in the graph are weighted by the number of times the corresponding pair of fields appears in the models; this is shown with a linear colour scaling in the figure. There are 3036 edges in the graph, and the average node degree is approximately 37. About a fifth of all possible connections in the graph are realised. The ten most heavily weighted edges, representing the ten most common pairs of fields appearing in the models, are shown in Table 2.4. Many of these correlations can be understood on the basis of common contractions in the derivation of the models, especially those involving H or L. There is a propensity for scalars and fermions with the same gauge quantum numbers to appear in models together. This seems to come about from the fact that $H \otimes L$ is a gauge singlet but transforms like $(\mathbf{2}, \mathbf{1})$ under $\mathrm{SU}(2)_+ \otimes \mathrm{SU}(2)_-$. We note that all of the fields in the table have $|B| = \frac{1}{3}$, and so this edge cannot come about from $(\bar{\mathbf{3}}, \mathbf{2}, \frac{5}{6})_F \otimes \bar{d} \sim (\mathbf{3}, \mathbf{2}, \frac{7}{6})_S$.

2.5.2 Example models

In this section we present some example neutrino-mass models, illustrating use cases of the model database, aspects to be careful of in its use, and representative features of the novel models derived from dimension-eleven and dimension-nine operators.

Simple models at the TeV scale

We are particularly interested in models that are simple, in the sense that they involve few exotic fields, and testable, in that they predict new physics at currently or nearly accessible energy ranges. We query our model database to return models featuring three fields or fewer with the estimated upper bound on the new-physics scale required to be between 700 GeV and 100 TeV. The results of the query are presented in Table 2.5. There are twelve[14] models listed, only one of which has explicitly appeared before in the literature to our knowledge: the completion of $\mathcal{O}_8$ discussed in Sec. 2.5.1. It is interesting to note that the scalar leptoquark[15] $\Pi_1 \sim (\mathbf{3}, \mathbf{2}, \frac{1}{6})_S$ appears in almost every model listed

[14] We note that there are technically more models: those for which the colour-sextet fields in Table 2.5 are replaced with colour triplets, with a corresponding baryon-number assignment such that the same interactions as the sextet are picked out.

[15] We mention parenthetically that although this leptoquark does not possess diquark couplings, baryon-number violation does occur through a term in the scalar potential. The leading-order contribu-

Rank	Edge
1	$(3, 3, \frac{2}{3})_F, (3, 4, \frac{1}{6})_S$
2	$(3, 2, \frac{1}{6})_S, (3, 2, \frac{1}{6})_F$
3	$(3, 3, \frac{2}{3})_S, (3, 2, \frac{7}{6})_S$
4	$(3, 2, \frac{7}{6})_F, (3, 2, \frac{1}{6})_S$
5	$(3, 3, \frac{2}{3})_F, (3, 4, \frac{7}{6})_F$
6	$(\bar{3}, 3, \frac{1}{3})_S, (3, 4, \frac{1}{6})_S$
7	$(3, 2, \frac{1}{6})_F, (3, 3, \frac{2}{3})_S$
8	$(\bar{3}, 3, \frac{4}{3})_F, (\bar{3}, 2, \frac{5}{6})_F$
9	$(3, 2, \frac{1}{6})_S, (3, 3, \frac{2}{3})_S$
10	$(3, 2, \frac{7}{6})_S, (\bar{3}, 2, \frac{5}{6})_F$

Table 2.4: The table shows the pairs of fields that most often appear together in the filtered completions of the $\Delta L = 2$ operators we consider. In the context of the graph of field connections introduced in the main text, these are the top ten edges by edge weight. Many of the connections can be understood on the basis of common couplings to SM fields, especially L and H. For example, $(3, 3, \frac{2}{3})_F \otimes L \sim (3, 4, \frac{1}{6})_S$ and $(3, 3, \frac{2}{3})_S \otimes H \sim (3, 2, \frac{7}{6})_S$. All of the fields in the table have $|B| = \frac{1}{3}$.

in the table. This suggests that our general analysis of the frequency of fields appearing in the completions in Sec. 2.5.1 may look different if specific selection criteria are placed on the data. We have checked the full Lagrangians implied by the field content of each model and found that seven of the models listed in the table imply the generation of the Weinberg operator through heavy loops. We emphasise that these non-genuine completions are potentially interesting and new radiative models, although the neutrino self-energy diagram will look different to that implied by the closure of the tree-level graph from which the model was derived. This means that the bound on the implied new-physics scale is in general higher than that suggested by the closure of the original operator. In this class are all of the models for which the upper bound on the new-physics scale is larger than 15 TeV. This means that there are only five models in our database with fewer than four fields for which the upper bound on Λ is between 700 GeV and 100 TeV, and they all predict new physics below 15 TeV. In the following we present two example models from the table:

1. We look at one of the models—the one derived from $\mathcal{O}_{62b}$—that generates the

tion is through a dimension-ten operator mediating $p \to \pi^+\pi^+e^-\nu\nu$ [270].

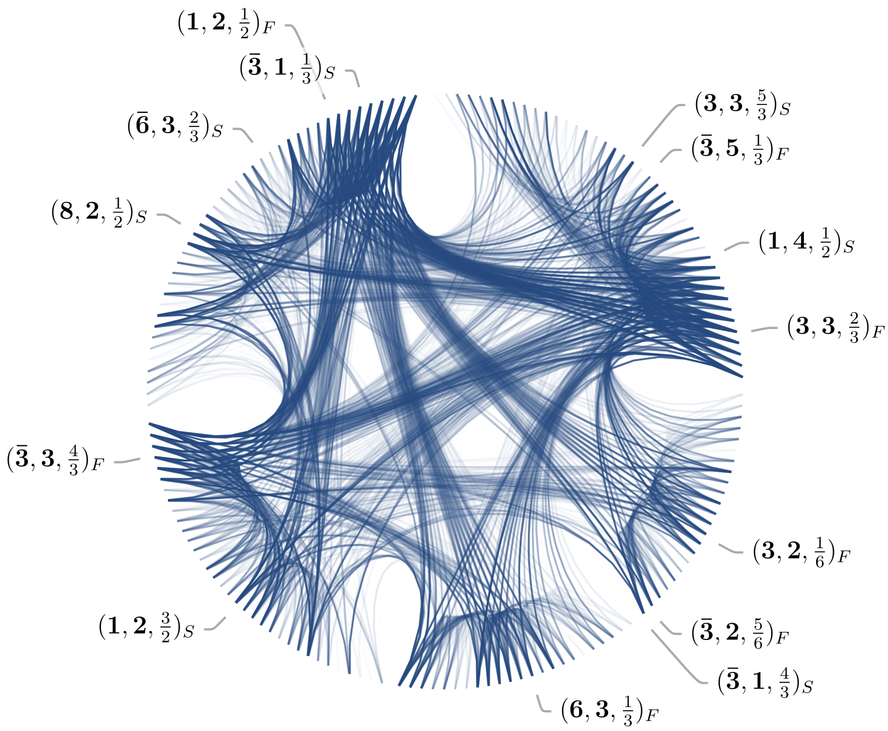

Figure 2.15: The graph is a representation of the connectivity between exotic fields in the neutrino-mass models. Each node represents an exotic field and edges connect fields featuring together in a neutrino-mass model. The colour is an indication of the weight of the edge, *i.e.* the number of times the two nodes appear in models together. The graph is clustered into roughly five communities within which there are many mutual connections. Only a handful of node labels are shown.

Weinberg operator through a heavy loop. We intend this to be an example of how this phenomenon can appear and how it is easy to diagnose in some cases.

2. We present a brief study of the implications for neutrino mass implied by the model given in the last row.

Model derived from $\mathcal{O}_{62b}$ The model derived from $\mathcal{O}_{62b}$ is especially simple since it does not require the imposition of $\mathrm{U}(1)_B$. The exotic fields introduced are $\Delta_1 \sim (\mathbf{1},\mathbf{2},\frac{1}{2})_F$, $\mathcal{S}_1 \sim (\mathbf{1},\mathbf{1},1)_S$ and $\chi \sim (\mathbf{1},\mathbf{2},\frac{3}{2})_S$. The additional interaction Lagrangian necessary to generate $\mathcal{O}_{62b}$ at tree level is $\Delta\mathcal{L} = \mathcal{L}_Y - \mathcal{V}$, with

$$-\mathcal{L}_Y = m_{\Delta_1}\bar{\Delta}_1\Delta_1 + x_{[rs]}L_r^i L_s^j \mathcal{S}_1\epsilon_{ij} + y_r\bar{e}_r\bar{\Delta}_1^i\tilde{H}^j\epsilon_{ij} + z_r\bar{e}_r\tilde{\chi}^i\Delta_1^j\epsilon_{ij}\,, \tag{2.40}$$

$$\mathcal{V} = m_{\mathcal{S}_1}^2\mathcal{S}_1^\dagger\mathcal{S}_1 + m_\chi^2\chi^\dagger\chi + wH^i\chi^j\mathcal{S}_1^\dagger\mathcal{S}_1^\dagger\epsilon_{ij}\,. \tag{2.41}$$

Field content	Operators	Λ [TeV]	Dominant?
$(\mathbf{3}, \mathbf{2}, \frac{1}{6})_S, (\mathbf{3}, \mathbf{2}, \frac{7}{6})_F$	$8, D15$	15	Y
$(\mathbf{1}, \mathbf{2}, \frac{1}{2})_F, (\mathbf{1}, \mathbf{1}, 1)_S, (\mathbf{1}, \mathbf{2}, \frac{3}{2})_S$	$62b$	16	N
$(\bar{\mathbf{3}}, \mathbf{2}, \frac{5}{6})_S, (\mathbf{3}, \mathbf{2}, \frac{1}{6})_F, (\mathbf{3}, \mathbf{2}, \frac{1}{6})_S$	$8'$	1	N
$(\bar{\mathbf{3}}, \mathbf{1}, \frac{1}{3})_S, (\bar{\mathbf{6}}, \mathbf{2}, \frac{1}{6})_S, (\mathbf{3}, \mathbf{2}, \frac{1}{6})_F$	$24f$	89	N
$(\bar{\mathbf{3}}, \mathbf{3}, \frac{1}{3})_F, (\bar{\mathbf{6}}, \mathbf{2}, \frac{1}{6})_S, (\mathbf{3}, \mathbf{2}, \frac{1}{6})_S$	$24d$	89	N
$(\bar{\mathbf{3}}, \mathbf{2}, \frac{5}{6})_S, (\mathbf{1}, \mathbf{2}, \frac{3}{2})_F, (\mathbf{3}, \mathbf{2}, \frac{1}{6})_S$	$8'$	1	N
$(\bar{\mathbf{3}}, \mathbf{3}, \frac{1}{3})_F, (\bar{\mathbf{6}}, \mathbf{4}, \frac{1}{6})_S, (\mathbf{3}, \mathbf{2}, \frac{1}{6})_S$	$24f$	89	N
$(\bar{\mathbf{3}}, \mathbf{1}, \frac{1}{3})_F, (\bar{\mathbf{6}}, \mathbf{2}, \frac{1}{6})_S, (\mathbf{3}, \mathbf{2}, \frac{1}{6})_S$	$24d$	89	N
$(\bar{\mathbf{6}}, \mathbf{2}, \frac{7}{6})_F, (\mathbf{8}, \mathbf{2}, \frac{1}{2})_S, (\mathbf{3}, \mathbf{2}, \frac{1}{6})_S$	20	0.8	Y
$(\mathbf{6}, \mathbf{1}, \frac{4}{3})_S, (\mathbf{6}, \mathbf{1}, \frac{1}{3})_F, (\mathbf{3}, \mathbf{2}, \frac{1}{6})_S$	20	0.8	Y
$(\mathbf{6}, \mathbf{2}, \frac{5}{6})_S, (\mathbf{3}, \mathbf{2}, \frac{1}{6})_F, (\mathbf{3}, \mathbf{2}, \frac{1}{6})_S$	$50a, b$	10	Y
$(\bar{\mathbf{6}}, \mathbf{2}, \frac{1}{6})_S, (\bar{\mathbf{3}}, \mathbf{2}, \frac{5}{6})_F, (\mathbf{3}, \mathbf{2}, \frac{1}{6})_S$	$50a, b$	10	Y

Table 2.5: The table shows the models in our filtered list that contain fewer than four fields with the estimate of the upper-bound on the new-physics scale Λ in the range $700\,\mathrm{GeV} < \Lambda < 100\,\mathrm{TeV}$. Models containing colour sextet fields can be replaced with the corresponding colour-triplet fields with a different baryon-number assignment. The fields and models are listed in no special order. The scalar leptoquark $\Pi_1 \sim (\mathbf{3}, \mathbf{2}, \frac{1}{6})$ appears in almost all of the models listed. Completions marked as non-dominant may be viable and interesting neutrino-mass models, but the main contribution to the neutrino mass does not come from the closure of the tree-level diagram from which the particle content was derived. This means, among other things, that the upper bound on the scale of the new physics associated with the model will differ to that presented here.

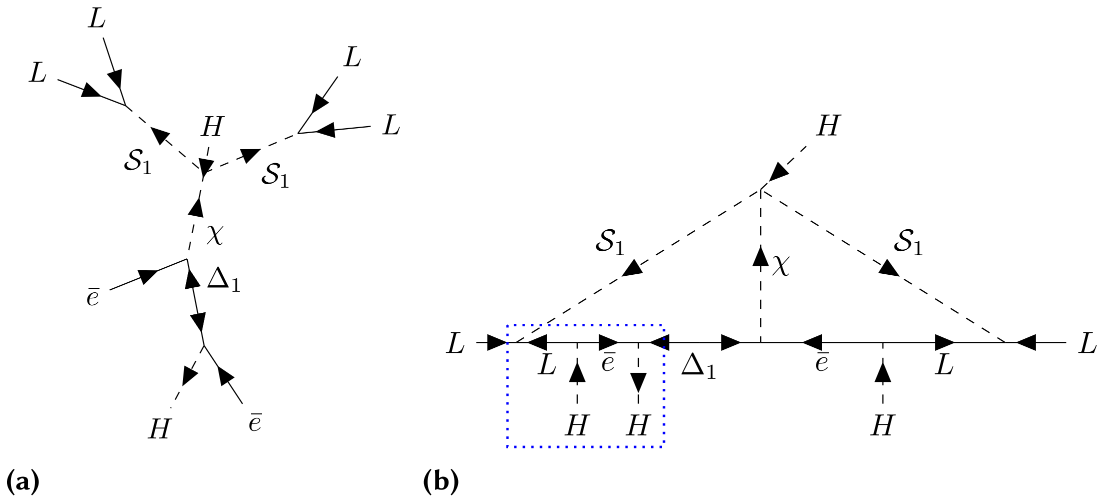

Figure 2.16: (a) The furnishing of the tree-level topology, labelled $2s6f_4$ in our scheme, that generates $\mathcal{O}_{62b}$ at tree level. The interactions allowed in the theory are such that the Δ_1 line can be connected straight into one of the $LL\mathcal{S}_1$ vertices in place of an L, leading to a loop-level completion of $\mathcal{O}_2$. (b) The neutrino self-energy diagram relevant to the non-genuine completion of $\mathcal{O}_{62b}$. It is clear that this diagram does not represent the dominant contribution to the neutrino mass, since the the highlighted collection of fields can be replaced with the interaction $\bar{\Delta}_1 L \mathcal{S}_1$. This leads to a diagram with heavy loop involving Δ_1, χ and $\mathcal{S}_1$, which dominates the neutrino masses. In both cases, the relevant topology is CLBZ-7 in the classification of Ref. [24].

This implies that the neutrino-mass mechanism depends on 13 new parameters: nine Yukawa couplings, w and the three masses; although there are a much larger number of terms present in the full Lagrangian of the model. Importantly, one of these is $x_r' L_r^i \bar{\Delta}_1^j \mathcal{S}_1 \epsilon_{ij}$, which we now show is sufficient to generate the Weinberg operator through a two-loop diagram containing one heavy loop.

The tree-level completion diagram and the neutrino-mass diagram relevant to the model are shown in Fig. 2.16. There are two- and three-loop neutrino self-energies, where the three-loop models arise by connecting the H and $H^\dagger$ lines in Fig. 2.16b in all possible ways. In this case, the first part of the fermion line (highlighted in Fig. 2.16b) can be replaced with the aforementioned $L\bar{\Delta}_1\mathcal{S}_1$ vertex so that the left loop contains only $\mathcal{S}_1$, χ and the Dirac fermion $\Delta_1 + \bar{\Delta}_1^\dagger$. (It can also be noticed from the tree-level opening in Fig. 2.16a that the Δ_1 line can be connected directly to one of the $LL\mathcal{S}_1$ vertices, giving rise to a loop-level completion of $\mathcal{O}_2$.) This heavy-loop neutrino-mass diagram, although interesting in its own right, predicts a different mass-scale for the exotic fields (roughly 10^6 TeV), and a different structure for the neutrino-mass matrix.

A genuine low-scale model Below we present a brief exploration of the model derived from $\mathcal{O}_{50}$ that contains the exotic fields $\phi \sim (\mathbf{6}, \mathbf{2}, -\frac{1}{6})_F$, $\Pi_1 \sim (\mathbf{3}, \mathbf{2}, \frac{1}{6})_S$ and $Q_5 \sim (\mathbf{3}, \mathbf{2}, -\frac{5}{6})_F$. The estimate for the neutrino mass derived from the operator closure suggests this model's exotic particle content should live roughly below 10 TeV. The corresponding $\Delta L = 2$ Lagrangian we write again as $\Delta\mathscr{L} = \mathscr{L}_Y - \mathscr{V}$, with

$$-\mathscr{L}_Y = x_{rs} L_r^i \bar{d}_{sa} \Pi_1^{aj} \epsilon_{ij} + y_r \phi^{\{ab\}i} \bar{u}_{ra} \bar{Q}_{5b}^j \epsilon_{ij} + z_r \bar{d}_{ra} H^i Q_5^{aj} \epsilon_{ij} + \text{h.c.} \tag{2.42}$$

$$\mathscr{V} = \lambda \tilde{\Pi}_{1a}^i \tilde{\Pi}_{1b}^j \phi^{\{ab\}k} H^l (\epsilon_{ik}\epsilon_{jl} + \epsilon_{il}\epsilon_{jk}) . \tag{2.43}$$

We note that $\mathrm{U}(1)_B$ must be imposed on the Lagrangian to prevent terms like $\Pi_1^3 H^\dagger$, $|\phi|^2 \phi^\dagger \Pi_1$ and $|\Pi_1|^2 \Pi_1 \phi$ that destabilise the proton in the presence of the Yukawa interactions of Eq. (2.42). The field ϕ only couples to SM fermions together with Q_5 in this model, and so it generates no dimension-six operators at tree level. The completion graph and one of the neutrino self-energy diagrams are shown in Fig. 2.17. The tree-level topology is again $2s6f_4$, and the neutrino masses are realised at three and four loops, with the additional loop arising from the connection of an H and $H^\dagger$. One of the loops involves a W boson, and so the diagram does not fit into existing topological classifications. The three-loop diagram is similar to the topology D_9^M of Ref. [26], with one of the scalar lines replaced with a vector boson. The W boson line must connect to Q in the diagram, but could end on any field with non-trivial $\mathrm{SU}(2)_L$ charge. The connection to the L line is shown, since the loop integral then depends on leptonic flavour indices, which can change the structure of the neutrino-mass matrix. There are also several ways of connecting the Higgs lines and only one combination is shown in the figure. The four-loop diagrams will be the dominant contribution to the neutrino masses for exotic fields above $4\pi v \approx 2$ TeV.

The neutrino-mass matrix in this model can be estimated as

$$[\mathbf{m}_\nu]_{rs} = \frac{\lambda g^2}{(16\pi^2)^3} \left(\frac{v^2}{\Lambda^2} + \frac{1}{16\pi^2} \right) \frac{1}{\Lambda} \sum_{t,u,v} x_{rt} z_t^* y_u^* [\mathbf{m}_u]_u V_{uv} [\mathbf{m}_d]_v x_{sv} I_{rstuv} + (r \leftrightarrow s) , \tag{2.44}$$

where the V_{rs} are CKM matrix elements, Λ is the generic UV scale, and I_{rstuv} is the loop function. The dependence on the masses of the up- and down-type quarks implies that the largest contributions to the neutrino masses will come from loops containing top and bottom quarks. If the parameters $y_{1,2}$, x_{r1} and x_{r2} play no significant role in the physics of neutrino mass, then the matrix will have rank 1 if the loop function carries no leptonic flavour indices. It may be the case that an additional generation of Q_5, ϕ or Π_7 is therefore required for the model to successfully reproduce the measured pattern of neutrino masses and mixings.

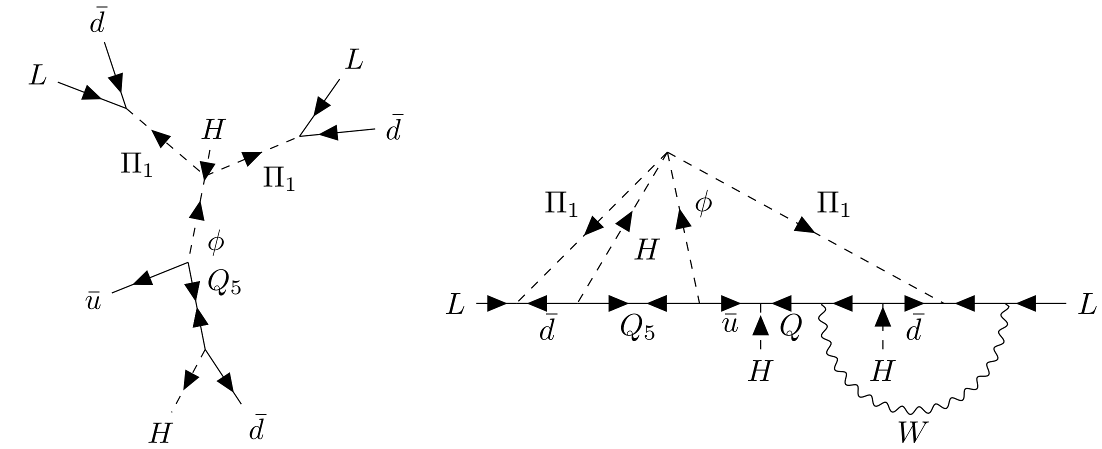

(a) **(b)**

Figure 2.17: (a) The tree-level completion diagram for the model derived from exploding $\mathcal{O}_{50}$ and discussed in the main text. The topology is $2s6f_4$ in our classification scheme. The closure involves an arrow-preserving loop connecting the $\bar{d}^\dagger$ to one of the $\bar{d}$ lines, and the W-boson closure motif discussed in Sec. 2.4.1. (b) One of the neutrino-mass diagrams relevant to the model derived from $\mathcal{O}_{50}$. There is a three-loop diagram with the H line broken into an $H^\dagger, H$ pair that generates the dimension-seven generalised Weinberg operator. The four-loop diagrams all involve connecting the $H^\dagger$ to each of the three H legs in the diagram. There are also multiple places the W could end in the diagram, although it must couple to the Q line. The four-loop diagrams will give larger contributions to the neutrino mass than the three-loop diagrams for $\Lambda \gtrsim 2\,\text{TeV}$.

A model derived from a derivative operator

We move on to discuss a model generating the single-derivative dimension-nine operators $\mathcal{O}_{D10a,b,c}$. The estimated upper-bound on the exotic scale is close to 1.5×10^3 TeV in this case. The model contains the fields $\rho \sim (\mathbf{1}, \mathbf{2}, \frac{3}{2})_S$, $Q_5 \sim (\mathbf{3}, \mathbf{2}, \frac{5}{6})_F$ and $\Sigma_1 \sim (\mathbf{1}, \mathbf{3}, 1)_F$. Such two-fermion–one-scalar models are unique to completions of single-derivative operators at dimension nine.

The part of the Lagrangian relevant to lepton-number violation is

$$-\Delta\mathscr{L} = x_r L^i_r \Sigma_1^{\{jk\}} H^\dagger_k \epsilon_{ij} + y_r L^i_r \rho^j \bar{\Sigma}_1^{\{kl\}} \epsilon_{ik}\epsilon_{jl} + z_r \bar{d}_{ra} H^i Q_5^{aj} \epsilon_{ij} + w_r \bar{u}_{ra} \rho^i Q_5^{aj} \epsilon_{ij} + \text{h.c.} \tag{2.45}$$

The only additions to the scalar potential are the expected $|\rho|^2|H|^2$ and $|\rho|^4$ terms, and these play no role in the lepton-number violation. Notably, there are no Yukawa couplings involving $\bar{Q}_5$, and the field ρ generates no dimension-six operators at tree-level, since the naively expected coupling $H^i H^j H^k \rho_k \epsilon_{ij}$ vanishes. The model also has the nice feature that no baryon-number violating interactions are present.

The tree-level completion diagram and one of the neutrino-mass diagrams are shown in Fig. 2.18. The completion diagram has topology $2s4f_8$, which requires one of the heavy fermions to have an arrow-preserving propagator. The neutrino-mass diagram shown is cocktail-like [25], although there are also two-loop diagrams generating $\mathcal{O}_1'$ at the low scale, as well as other diagrams with the W and H lines in different places. The topology of the neutrino self-energy diagram is similar to D_{15}^M in Ref. [26].

The flavour structure of the neutrino-mass matrix has the approximate form

$$[\mathbf{m}_\nu]_{rs} = \frac{g^2}{(16\pi^2)^3}\frac{1}{\Lambda}\sum_{t,u} y_r x_s w_t^* z_t [\mathbf{m}_d]_t V_{ut}[\mathbf{m}_u]_u I_{rstu} + (r \leftrightarrow s)\,. \tag{2.46}$$

The dependence on the up- and down-type mass matrices, as in the example presented in Sec. 2.5.2, means that the couplings $w_{1,2}$ and $z_{1,2}$ will not play an important role in generating the observed pattern of neutrino masses and mixings. In this case the matrix has at least rank 2, even if the leptonic-flavour structure of the loop integrals I_{rstu} is flat. Thus, the structure of the neutrino masses and mixing parameters emerges mostly from the six parameters x_r and y_r.

A model of neutrino mass and the flavour anomalies

Here we present a model designed specifically to generate a particular set of dimension-six operators. The example is motivated by the recent flavour anomalies, discussed in detail in Sec. 1.4. In the following we adhere to the conventions[16] of Ref. [114] relevant to the Warsaw basis for the SMEFT and the flavio basis [271] for the Weak Effective Theory (WET). The leptoquarks $\omega_1 \sim (\bar{\mathbf{3}}, \mathbf{1}, \frac{1}{3})_S$ and $\Pi_7 \sim (\mathbf{3}, \mathbf{2}, \frac{7}{6})_S$ can provide an explanation of the anomalies in $R_{D^{(*)}}$ with contributions to the SMEFT operators

$$[C_{lequ}^{(1)}]_{3332} = \begin{cases} -4[C_{lequ}^{(3)}]_{3332} & \text{for } \omega_1 \\ 4[C_{lequ}^{(3)}]_{3332} & \text{for } \Pi_7 \end{cases}, \tag{2.47}$$

since they have Yukawa couplings to left- and right-handed SM fields. [We note that Eq. (2.47) holds at the high scale, and the relation between the operators is altered by running.] The Yukawa terms are

$$-\mathscr{L}_{\omega_1} = f_{rs} L_r Q_s \omega_1 + g_{rs} \bar{e}_r^\dagger \bar{u}_s^\dagger \omega_1 + \text{h.c.} \tag{2.48}$$

$$-\mathscr{L}_{\Pi_7} = x_{rs} L_r \bar{u}_s \Pi_7 + y_{rs} \bar{e}_r^\dagger Q_s^\dagger \Pi_7 + \text{h.c.} \tag{2.49}$$

[16] These can be accessed easily at https://flav-io.github.io/docs/operators.html.

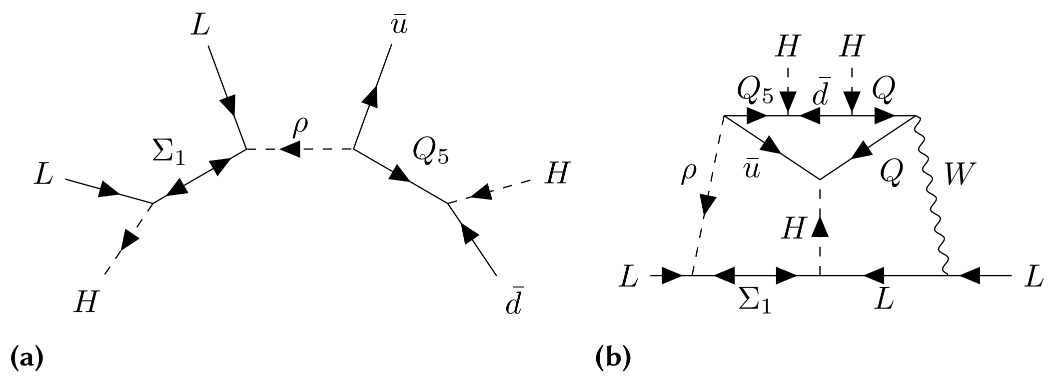

Figure 2.18: (a) The tree-level completion diagram for the model that generates the single-derivative operators $\mathcal{O}_{D10,a,b,c}$ and discussed in the main text. The topology is $2s4f_8$ in our classification scheme. This class of topologies is only relevant to single-derivative operators, and contains an arrow-preserving fermion propagator, that of Q_5 in the diagram. The closure of the diagram involves a W-boson loop, similar to that required in Fig. 2.17. (b) One of the neutrino-mass diagrams relevant to the model generating $\mathcal{O}_{D10a,b,c}$. The diagram generates the Weinberg operator as drawn, but additional diagrams exist with the central H line cut into an $H, H^\dagger$ pair that generate $\mathcal{O}_1'$ instead. These diagrams will only be relevant for exotic masses less than about 2 TeV. Additional three-loop diagrams exist in which the Higgs coming from the $\Sigma_1 LH^\dagger$ interaction loops into any of the other external H fields. The W boson must connect to the Q line, but could end on any other field with non-trivial $\mathrm{SU}(2)_L$ charge. The topology is cocktail-like [25], and resembles D_{15}^M in Ref. [26].

and these imply

$$[C_{lequ}^{(1)}]_{3332} = \begin{cases} \dfrac{f_{33}g_{32}^*}{2m_{\omega_1}^2} & \text{for } \omega_1 \\ \dfrac{x_{32}^* y_{33}}{2m_{\Pi_7}^2} & \text{for } \Pi_7 \end{cases} \tag{2.50}$$

at tree level. A satisfactory explanation of $R_{D^{(*)}}$ requires $\mathcal{O}(1)$ couplings, *e.g.* [2, 259], and for Π_7 fits are consistent with the operator coefficient being purely imaginary, *e.g.* [216].

The $b \to s$ data can be explained by the tree-level exchange of the leptoquark $\zeta \sim (\bar{\mathbf{3}}, \mathbf{3}, \frac{1}{3})_S$, which generates

$$[C_{lq}^{(1)}]_{2223} = 3[C_{lq}^{(3)}]_{2223} \,, \tag{2.51}$$

relevant for the neutral-current anomalies. Fits are usually performed to four-fermion operators in the WET, defined below the electroweak scale. For the $b \to s\ell\ell$ data, a good fit is given for [14]

$$C_9^{bs\mu\mu} = -C_{10}^{bs\mu\mu} = \frac{1}{2}\left(V_{tb}V_{ts}^* \frac{e^2}{16\pi^2}\frac{4G_F}{\sqrt{2}}\right)^{-1}\left[C_{lq}^{(1)} + C_{lq}^{(3)}\right]_{2232} \approx -0.5\,, \tag{2.52}$$

where $C_{9,10}^{bs\mu\mu}$ are referred to simply as $C_{9,10}$ in Sec. 1.4.

It was pointed out in Ref. [14] that there exists a mild tension between the fit to $R_{K^{(*)}}$ and the other anomalous $b \to s$ data, which can be reconciled with an additional LFU contribution to $C_9^{bs\ell\ell}$ such that

$$C_9^{bs\mu\mu} \approx -0.44 \quad \text{and} \quad C_9^{bs\ell\ell} \approx -0.5\,, \tag{2.53}$$

for $\ell \in \{e, \mu, \tau\}$. A potential source of this universal contribution to C_9 is new physics in four-quark operators like [14]

$$[\mathcal{O}_{qu}^{(1)}]_{2322} = (\bar{Q}_2\gamma_\mu Q_3)(\bar{u}_2\gamma^\mu \bar{u}_2)\,, \tag{2.54}$$

which can be generated, for example, by $\Phi \sim (\mathbf{8}, \mathbf{2}, \frac{1}{2})_S$. The relevant Yukawa terms are

$$-\mathscr{L}_\Phi = w_{rs} Q_r^{ai}\bar{u}_{sb}\Phi^{bj}_{a}\epsilon_{ij} + \text{h.c.} \tag{2.55}$$

and a contribution of about the right size to $C_9^{bs\ell\ell}$ can be generated while avoiding dijet exclusion bounds from the LHC for $m_\Phi \sim 2\,\text{TeV}$ and $|w_{22}|, |w_{32}| \sim 1$ [14].

We construct a UV model that contains ζ and Φ as well as one of ω_1 or Π_7 in an attempt to incorporate this explanation into a model of neutrino mass. We emphasise that our goal here is not to present the most elegant or motivated model of neutrino mass and the flavour anomalies, but rather to show that our database can be used to motivate complex models with a specific structure.

We query the filtered model database for neutrino-mass models that contain the interactions $Q\bar{u}\Phi$, needed to generate $\mathcal{O}_{qu}^{(1)}$; $LQ\zeta$, needed to generate $C_9^{bs\mu\mu} = -C_{10}^{bs\mu\mu}$; and one of ω_1 or Π_7, required to explain $R_{D^{(*)}}$. Our query returns a number of models, and we choose one to study briefly below. We note that none of the models involve the leptoquark ω_1, and none feature the interaction $\bar{e}^\dagger Q^\dagger \Pi_7$, implying some freedom in the explanation of $R_{D^{(*)}}$ since the couplings y_{rs} of Eqs. (2.49) and (2.50) will be unrelated[17] to the neutrino mass.

[17]Expanding our search criteria, we find no viable models in the database in which both sets of couplings presented in Eqs. (2.48) and (2.49) feature. This can be understood in the following way. Any neutrino self-energy diagram containing both couplings will also imply another where $\bar{e}^\dagger\bar{u}^\dagger\omega_1$ or $\bar{e}^\dagger Q^\dagger \Pi_7$ is replaced with the corresponding coupling to L, which contains a neutrino field. This generally gives a larger contribution to the neutrino mass, since the closure of the diagram containing the $\bar{e}$ will involve an additional loop with a W boson. Thus, diagrams with both sets of Yukawa interactions to SM fermions relevant to ω_1 and Π_7 are likely to be removed by our filtering procedure. We note that, after studying the unfiltered list of models, we find that some models can be engineered so that a sizeable (but not dominant) contribution to the neutrino masses does come from such diagrams involving both sets of leptoquark–fermion Yukawa couplings.

The model contains the additional fields Φ, ζ, Π_7 and $\eta \sim (\mathbf{8}, \mathbf{1}, 1)_S$, necessary for lepton-number violation. It generates $\mathcal{O}_{29b}$, which implies an upper bound on the new-physics scale of roughly 10^7 TeV. The additional piece of the Lagrangian is $\Delta\mathscr{L} = \mathscr{L}_Y - \mathscr{V}$, with

$$-\mathscr{L}_Y = x_{rs} L_r^i \bar{u}_{sa} \Pi_7^{ja} \epsilon_{ij} + y_{rs} \bar{e}_r^\dagger Q_{sai}^\dagger \Pi_7^{ai} + z_{rs} L_r^i Q_s^{ja} \zeta_a^{\{kl\}} \epsilon_{ik}\epsilon_{jl} + w_{rs} Q_r^{ai} \bar{u}_{sb} \Phi^{bj}_{\ a} \epsilon_{ij} + \text{h.c.} \tag{2.56}$$

$$\mathscr{V} = \kappa H^i \Phi^{aj}_{\ b} \eta^{\dagger b}_{\ \ a} \epsilon_{ij} + \lambda H^i \eta^a_{\ b} \tilde{\Pi}^j_{7a} \tilde{\zeta}^{b\{kl\}} \epsilon_{ik}\epsilon_{jl} + \text{h.c.} + \cdots \,, \tag{2.57}$$

where we have only shown the part of the scalar potential relevant to lepton-number violation in this model, since the full expression contains a large number of terms. The leptoquark ζ has a diquark coupling which we forbid by imposing $\mathrm{U}(1)_B$ on the Lagrangian, assigning baryon numbers of $-\frac{1}{3}$ and $\frac{1}{3}$ to ζ and Π_7, respectively. (All other exotic fields have $B = 0$.) The model contains 33 free parameters, although not all of them are necessary to address the flavour anomalies and generate viable neutrino masses.

The tree-level completion diagram and the neutrino self-energy diagram are shown in Fig. 2.19. The neutrino mass arises at two loops, and the topology has the feature that no fermion propagators are arrow-violating. This implies that the neutrino masses are not proportional to any SM-fermion masses. This feature has been studied before in the context of a specific UV model in Ref. [4]. The phenomenon is particular to models derived from operators whose closures feature arrow-preserving loops, as discussed in Sec. 2.4.1. From a model-building perspective, one consequence is that the neutrino masses need not be dominated by Yukawa couplings to SM fermions of the third generation. Indeed, motivated by the pattern of operators required to explain the flavour anomalies, we adopt textures for the Yukawa couplings of Eq. (2.56) that imply dominance of the bottom-quark couplings for ζ, but the charm-quark couplings for Π_7:

$$\mathbf{x} = \begin{pmatrix} 0 & x_{12} & 0 \\ 0 & x_{22} & 0 \\ 0 & x_{32} & 0 \end{pmatrix}, \quad \mathbf{z} = \begin{pmatrix} 0 & 0 & z_{13} \\ 0 & z_{22} & z_{23} \\ 0 & 0 & z_{33} \end{pmatrix}, \tag{2.58}$$

where the additional coupling z_{22} is required to generate the relevant dimension-six operators $[\mathcal{O}_{lq}^{(1,3)}]_{2232}$. Interestingly, the minimal set of couplings w_{rs} that gives viable neutrino masses while incorporating the key ingredients required to generate both $[\mathcal{O}_{lq}^{(1,3)}]_{2232}$ and $[\mathcal{O}_{lequ}^{(1,3)}]_{3332}$ is

$$\mathbf{w} = \begin{pmatrix} 0 & 0 & 0 \\ 0 & w_{22} & 0 \\ 0 & w_{32} & 0 \end{pmatrix}, \tag{2.59}$$

which is exactly the correct set required to also generate the operator given in Eq. (2.54). Thus, there is a natural connection in this model between the explanation of the charged- and neutral-current anomalies through the neutrino masses. With the exception of y_{33}, all of the couplings featuring in the explanation of the flavour anomalies also play a role in the generation of the neutrino masses. The structure of the neutrino-mass matrix is

$$\begin{aligned}[\mathbf{m}_\nu]_{rs} &\simeq \frac{\lambda\kappa}{(16\pi^2)^2}\frac{v^2}{\Lambda^2}\sum_{t,u}[z_{rt}w_{tu}x_{su} + (r \leftrightarrow s)] \\ &= \frac{\lambda\kappa}{(16\pi^2)^2}\frac{v^2}{\Lambda^2}[z_{r2}w_{22}x_{s2} + z_{r3}w_{32}x_{s2} + (r \leftrightarrow s)] \,.\end{aligned} \tag{2.60}$$

The matrix is rank 2, and so implies an almost massless neutrino. Since there is no suppression of the neutrino-mass scale by SM Yukawa couplings, we distinguish the UV scales Λ and κ so that

$$\Lambda \simeq \max\left(m_\zeta, m_\Phi, m_\eta, m_{\Pi_7}\right) \tag{2.61}$$

and consider the region of parameter space in which $\lambda\kappa \ll \Lambda$.

An explanation of the flavour anomalies in this picture can be achieved with $\mathcal{O}(1)$ couplings for Π_7 and Φ at a few TeV, and ζ at tens of TeV. We take η slightly heavier at $\sim 50\,\mathrm{TeV}$ to decouple its phenomenology and aid in suppressing the neutrino mass. This implies $\lambda\kappa \sim 0.05\,\mathrm{GeV}$ for neutrino masses saturating the atmospheric bound. This choice is technically natural, since in the limit of vanishing λ or κ the Lagrangian regains $\mathrm{U}(1)_L$. We rewrite Eq. (2.60) as

$$[\mathbf{m}_\nu]_{rs} = m_0[x_{s2}(z_{r2}w_{22} + z_{r3}w_{32}) + (r \leftrightarrow s)] \,, \tag{2.62}$$

where $m_0 \approx \lambda\kappa v^2(16\pi^2)^{-2}m_\eta^{-2}$. This allows for the adoption of a Casas–Ibarra-like parametrisation of the vectors x_{s2} and

$$\mathbf{Z} = \begin{pmatrix} z_{13}w_{32} \\ z_{22}w_{22} + z_{23}w_{32} \\ z_{33}w_{32}\end{pmatrix} \,, \tag{2.63}$$

so that [101]

$$x_{r2} = \frac{\xi}{\sqrt{2m_0}}\left(\sqrt{m_2}u_2^* + i\sqrt{m_3}u_3^*\right) \,, \tag{2.64}$$

$$Z_r = \frac{1}{\xi\sqrt{2m_0}}\left(\sqrt{m_2}u_2^* - i\sqrt{m_3}u_3^*\right) \,, \tag{2.65}$$

where the u_i are the ith columns of the PMNS matrix; m_i are the neutrino masses, fixed by the measured squared mass differences and the choice of normal ordering; and ξ is

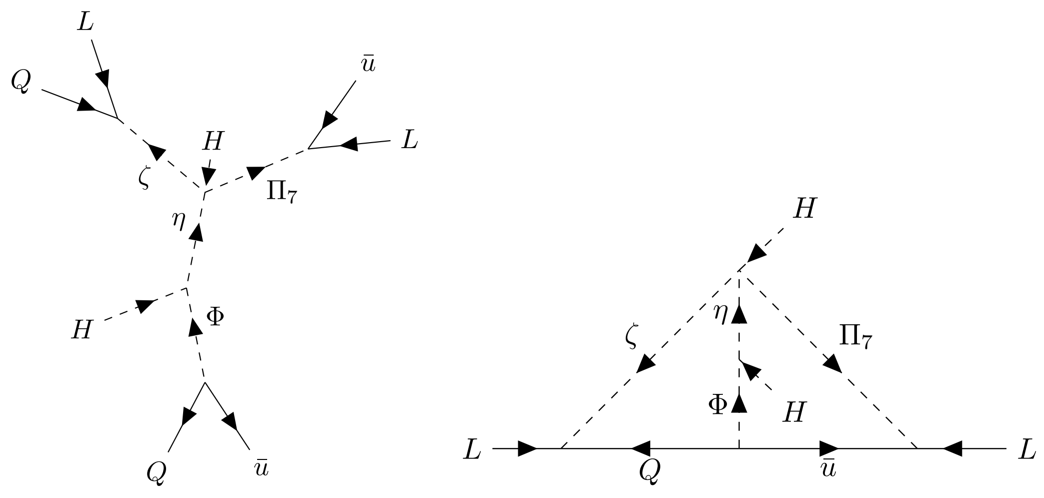

(a) **(b)**

Figure 2.19: (a) The figure shows the tree-level completion diagram for the model constructed to address the flavour anomalies and neutrino masses. The topology is labelled $2s6f_2$ in our scheme. The closure contains two arrow-preserving loops, which arise by looping the $\bar{u}$ into the $\bar{u}^\dagger$ and the Q into the $Q^\dagger$. (b) The self-energy diagram for the same model. The diagram has a CLBZ-10 topology in the language of Ref. [24]. The neutrino masses are not suppressed by SM-fermion masses on account of the arrow-preserving fermion lines. This feature raises the bound on the new-physics scale relevant to the model, but also allows couplings to the second generation of fermions to play a role in the physics of neutrino mass. This is beneficial in our case since many of these couplings are involved in generating the pattern of dimension-six operators that motivates this example, and so provides for a more intimate connection between the flavour anomalies and neutrino masses.

a free complex parameter. We find, for example, that the choices $m_\Phi = 2\,\text{TeV}$, $m_{\Pi_7} = 1\,\text{TeV}$, $m_\zeta = 15\,\text{TeV}$, $m_\eta = 50\,\text{TeV}$, $\lambda\kappa = 0.05\,\text{GeV}$, $\xi = e^{3i/2}$, $z_{23} = 1$, $w_{22} = -w_{32} = 1$ and $y_{33} = 2e^{2i}$ give approximately the right values to generate the pattern of dimension-six operators discussed and explain the flavour anomalies. This includes the additional lepton-flavour universal contribution to $C_9^{bs\ell\ell}$, discussed in Ref. [14]. Although a more detailed study of the phenomenological implications of the model is beyond the scope of this simple example, we have shown how a specific UV scenario can be embedded into a radiative model in a way consistent with the measured neutrino masses and mixing parameters.

2.6 Conclusions

We have described a procedure for building UV-complete models from effective operators in a way amenable to automation. We have applied the algorithm, as found in our publicly available example code [220], to the $\Delta L = 2$ operators in the SMEFT up to and including dimension eleven, producing just over 11,000 minimal and predictive models of radiative Majorana neutrino mass. We share our complete listing of models, as well as the set reduced by model filtering, in our searchable model database [221].

Our analysis includes new operators that have not appeared in previous catalogues, along with updated estimates for the upper bounds on the new-physics scales associated with these. We performed a preliminary study of the UV models, showing that the most represented exotic fields featuring in the completions are leptoquarks. We find that a number of simple models predict new physics that must live below 100 TeV. Adding the additional requirements that the models contain fewer than four exotic fields and that the new-physics scale should be larger than 700 GeV gives at most five models fitting this description, all of which predict new fields below 15 TeV. One of these models was studied briefly, along with a model derived from a derivative operator, and one that addresses the flavour anomalies.

Our model database is perhaps a good laboratory for experiments in automated phenomenological analysis. Now that the models have been written down and compiled into this computationally accessible format, our hope is that a large number of them can be ruled out in a systematic way through improved model filtering, neutrino oscillation data, or collider constraints. Our results also pave the way for more detailed studies of the models that are currently accessible to experiments. As each model is tested, we will either get very lucky and discover the origin of neutrino masses at low energies, or else falsify these scenarios and build a stronger circumstantial case for those that cannot be tested at collider experiments.

3

The S_1 leptoquark as an explanation of the flavour anomalies

This chapter is based on the publication 'Reconsidering the One Leptoquark scenario: flavour anomalies and neutrino mass,' written in collaboration with Yi Cai, Michael A. Schmidt, and Raymond R. Volkas [2]. We study the potential of the S_1 leptoquark to explain the flavour anomalies and the anomalous magnetic moment of the muon in a new region of parameter space.

3.1 Introduction

A common origin for $R_{D^{(*)}}$ and the anomalous $b \to s$ data is suggested naturally if the former is explained by the effects of the operator $(c^\dagger \bar{\sigma}_\mu b)(\tau^\dagger \bar{\sigma}^\mu \nu)$, related in its general structure by $\mathrm{SU}(2)_L$ invariance to the aforementioned four-fermion effective operator accounting for the $b \to s$ anomalies. A number of models exploring this idea have been suggested in the literature [272–286] (along with many others addressing one or the other anomaly, *e.g.* [191, 214, 263, 266, 267, 287–299]) and among these minimal explanations the Bauer–Neubert (BN) model [273] is one of notable simplicity and explanatory power: a TeV-scale scalar leptoquark protagonist mediating $B \to D^{(*)}\tau\nu$ at tree-level and the $b \to s$ decays through one-loop box diagrams. The leptoquark transforms under the SM gauge group like a right-handed down-type quark and its pattern of couplings to SM fermions can also reconcile the measured and predicted values of the anomalous magnetic moment of the muon.

Our aim in this chapter is to study the scalar-leptoquark model in the context of some previously unconsidered constraints and comment more definietely on its viability as an explanation of both the charged- and neutral-current anomalies.

4 Models of neutrino mass and the flavour anomalies

4.1 Introduction

Taken together, the anomalies studied in the previous chapter paint a picture of new physics interacting more strongly with the second and third generations of SM fermions, introducing lepton flavour non-universality and FCNC interactions at energies not significantly higher than the electroweak scale. Interestingly, many of these phenomenological motifs arise naturally in radiative models of neutrino mass, hinting towards the attractive possibility of a common explanation for both phenomena. Previous work has also considered radiative neutrino mass models whose particle content addresses R_K [286, 294, 300–302], $R_{D^{(*)}}$ [280, 286] and $(g-2)_\mu$ [29, 286, 300–302]. In Refs. [280, 294] the flavour anomalies are explained through two light scalar or vector leptoquarks whose couplings to the SM Higgs doublet and fermions prohibit a consistent assignment of lepton number to the leptoquarks such that the symmetry is respected. Thus $\mathrm{U}(1)_L$ is explicitly broken by two units and the neutrinos gain mass at the one-loop level [303], apart from the imposition of any additional symmetries[1]. A general feature of such models is that large amounts of fine-tuning are required to suppress the neutrino mass to the required scale with at least one set of leptoquark–fermion couplings

[1]Mass generation in Ref. [29] occurs at the two-loop level because the Yukawa couplings of one of the leptoquarks to the left-chiral fermions is turned off.

sizeable enough to explain the anomalies.

5

The two-photon decay of a scalar-quirk bound state

We use ϛ to represent the scalar diquark.

5.1 Introduction

An excess of events containing two photons with invariant mass near 750 GeV has been observed in 13 TeV proton–proton collisions by the ATLAS and CMS collaborations [304, 305]. The cross section $\sigma(pp \to \gamma\gamma)$ is estimated to be

$$\sigma(pp \to \gamma\gamma) = \begin{cases} (10 \pm 3)\ \mathrm{fb} & \text{ATLAS} \\ (6 \pm 3)\ \mathrm{fb} & \text{CMS} \end{cases} \tag{5.1}$$

and there is no evidence of any accompanying excess in the dilepton channel [306]. If we interpret this excess as the two photon decay of a single new particle of mass m then ATLAS data provide a hint of a large width: $\Gamma/m \sim 0.06$, while CMS data prefer a narrow width. Naturally, further data collected at the LHC should provide a clearer picture as to the nature of this excess.

There has been vast interest in the possibility that the diphoton excess results from physics beyond the SM. Most discussion has focused on models where the excess is due to a new scalar particle which subsequently decays into two photons *e.g.* Ref. [307]. The possibility that the new scalar particle is a bound state of exotic charged fermions has also been considered, *e.g.* Refs. [308–312]. Here we consider the case that the 750 GeV state is a non-relativistic bound state constituted by an exotic *scalar* particle χ and its antiparticle, charged under $\mathrm{SU}(3)_c$ as well as a new unbroken non-abelian gauge interaction. Having χ be a scalar rather than a fermion is not merely a matter of taste: In such a framework a fermionic χ would lead to the formation of bound states which (typically) decay to dileptons more often than to photons; a situation which is not favoured by the data.

The bound state, which we denote Π, can be produced through gluon–gluon fusion directly (*i.e.* at threshold $\sqrt{s_{gg}} \simeq M_\Pi$) or indirectly via $gg \to \chi^\dagger \chi \to \Pi + \textit{soft quanta}$ (*i.e.* above Π threshold: $\sqrt{s_{gg}} > M_\Pi$). The indirect production mechanism can dominate the production of the bound state, which is an interesting feature of this kind of theory.

5.2 The model

We take the new confining unbroken gauge interaction to be $\mathrm{SU}(N)$, and assume that, like $\mathrm{SU}(3)_c$, it is asymptotically free and confining at low energies. However, the new $\mathrm{SU}(N)$ dynamics is qualitatively different from QCD as all the matter particles [assumed to be in the fundamental representation of $\mathrm{SU}(N)$] are taken to be much heavier than the confinement scale, Λ_N. In fact we here consider only one such matter particle, χ, so that $M_\chi \gg \Lambda_N$ is assumed. In this circumstance a $\chi^\dagger\chi$ pair produced at the LHC above the threshold $2M_\chi$ but below $4M_\chi$ cannot fragment into two jets. The $\mathrm{SU}(N)$ string which connects them cannot break as there are no light $\mathrm{SU}(N)$-charged states available. This is in contrast to heavy quark production in QCD where light quarks can be produced out of the vacuum enabling the color string to break. The produced $\chi^\dagger\chi$ pair can be viewed as a highly excited bound state, which de-excites by $\mathrm{SU}(N)$-ball and soft glueball/pion emission [313].

With the new unbroken gauge interaction assumed to be $\mathrm{SU}(N)$ the gauge symmetry of the SM is extended to

$$\mathrm{SU}(3)_c \otimes \mathrm{SU}(2)_L \otimes \mathrm{U}(1)_Y \otimes \mathrm{SU}(N). \tag{5.2}$$

This kind of theory can arise naturally in models which feature large colour groups [314–316] and in models with leptonic colour [317–320] but was also considered earlier by Okun [321]. The notation *quirks* for heavy particles charged under an unbroken gauge symmetry (where $M_\chi \gg \Lambda_N$) was introduced in [313] where the relevant phenomenology was examined in some detail in a particular model[1]. For convenience we borrow their nomenclature and call the new quantum number *hue* and the massless gauge bosons *huons* ($\mathscr{H}$).

[1] Some other aspects of such models have been discussed over the years, including the possibility that the $\mathrm{SU}(N)$ confining scale is low ($\sim$ keV), a situation which leads to macroscopic strings [322].

The phenomenological signatures of the bound states (quirkonia) formed depend on whether the quirk is a fermion or boson. Here we assume that the quirk χ is a Lorentz scalar in light of previous work which indicated that bound states formed from a fermionic χ state would be expected to be observed at the LHC via decays of the spin-1 bound state into opposite-sign lepton pairs ($\ell^+\ell^-$) [313, 320]. In fact, this appears to be a serious difficulty in attempts to interpret the 750 GeV state as a bound state of fermionic quirk particles (such as those of Refs. [308–310]). The detailed consideration of a scalar χ appears to have been largely overlooked[2], perhaps due to the paucity of known elementary scalar particles. With the recent discovery of a Higgs-like scalar at 125 GeV [324, 325] it is perhaps worth examining signatures of scalar quirk particles. In fact, we point out here that the two photon decay is the most important experimental signature of bound states formed from electrically charged scalar quirks. Furthermore this explanation is only weakly constrained by current data and thus appears to be a simple and plausible option for the new physics suggested by the observed diphoton excess.

5.3 Explaining the excess

The scalar χ that we introduce transforms under the extended gauge group (Eq. 5.2) as

$$\chi \sim (\mathbf{3}, \mathbf{1}, Y; \mathbf{N}), \tag{5.3}$$

where we use the normalisation $Q = Y/2$. The possibility that χ also transforms non-trivially under $\mathrm{SU}(2)_L$ is interesting, however for the purposes of this letter we focus on the $\mathrm{SU}(2)_L$ singlet case for definiteness. Since two-photon decays of non-relativistic quirkonium will be assumed to be responsible for the diphoton excess observed at the LHC, the mass of χ will need to be around 375 GeV.

We have assumed that χ is charged under $\mathrm{SU}(3)_c$ so that it can be produced at tree-level through QCD-driven pair production. We present the production mechanisms in Fig. 5.1. To estimate the production cross section of the bound states, we first consider the indirect production mechanism which we expect to be dominant. Here, a $\chi^\dagger\chi$ pair is produced above threshold and de-excites emitting soft glueballs/pions and hueballs: $gg \to \chi^\dagger\chi \to \Pi + \textit{soft quanta}$. We first consider the case where the confinement scale of the new $\mathrm{SU}(N)$ interaction is similar to that of QCD. What happens in this case can be adapted from the discussion in [313], where a fermionic quirk charged under an unbroken SU(2) gauge interaction was considered. As already briefly discussed in the introduction, the $\chi^\dagger\chi$ pairs initially form a highly excited bound state, which subsequently de-excites in two stages. The first stage is the non-perturbative regime where the hue string is longer than Λ_N^{-1}. The second stage is characterised by a string scale

[2] The idea has been briefly mentioned in recent literature [311, 323].

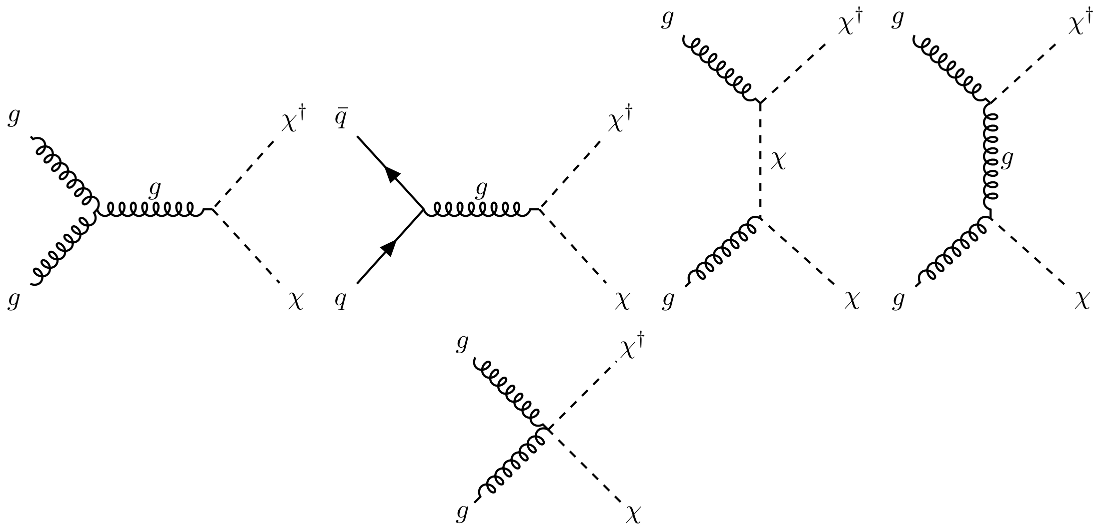

Figure 5.1: Tree-level pair production mechanisms for the scalar quirk χ.

significantly less than Λ_N^{-1}: the perturbative Coulomb region. Here the bound state can be characterised by the quantum numbers n and l. De-excitation continues until quirkonium is in a lowly excited state with $l \leq 1$ and n. Imagine first that de-excitation continued until the ground state ($n = 1$, $l = 0$) is reached. Given we are considering χ to be a scalar, the quirkonium ground state, Π, will have spin 0, and is thus expected to decay into SM gauge bosons and huons. The cross section $\sigma(pp \to \Pi \to \gamma\gamma)$ in this case is then

$$\sigma(pp \to \gamma\gamma) \approx \sigma(pp \to \chi^\dagger \chi) \times \mathrm{Br}(\Pi \to \gamma\gamma). \tag{5.4}$$

Since production is governed by QCD interactions, we can use the values of the pair production cross sections for stops/sbottoms in the limit of decoupled squarks and gluinos [326]. For a χ mass of 375 GeV

$$\sigma(pp \to \chi^\dagger \chi) \approx \begin{cases} 2.6N \text{ pb} & \text{at } 13 \text{ TeV} \\ 0.5N \text{ pb} & \text{at } 8 \text{ TeV} \end{cases} . \tag{5.5}$$

The branching fraction is to leading order

$$\mathrm{Br}(\Pi \to \gamma\gamma) \simeq \frac{3NQ^4\alpha^2}{\frac{2}{3}N\alpha_s^2 + \frac{3}{2}C_N\alpha_N^2 + 3NQ^4\alpha^2}, \tag{5.6}$$

where $C_N \equiv (N^2 - 1)/(2N)$, α_N is the new SU(N) interaction strength and we have neglected the small contribution of $\Pi \to Z\gamma/ZZ$ to the total width. Eq. (5.6) also neglects the decay to Higgs particles: $\Pi \to hh$, which arises from the Higgs potential portal term $\lambda_\chi \chi^\dagger \chi \phi^\dagger \phi$. Theoretically this rate is unconstrained given the dependence on the unknown parameter λ_χ, but could potentially be important. However, limits from resonant Higgs boson pair production derived from 13 TeV data: $\sigma(pp \to X \to hh \to bbbb) \lesssim 50$ fb at $M_X \approx 750$ GeV [327, 328] imply that the Higgs decay channel must indeed be subdominant (*c.f.* $\Pi \to gg, \mathcal{H}\mathcal{H}$).

The renormalised gauge coupling constants in Eq. (5.6) are evaluated at the renormalisation scale $\mu \sim M_\Pi/2$. Taking for instance the specific case of $N = 2$, $\alpha_N = \alpha_s \simeq 0.10$ (at $\mu \sim M_\Pi/2$) gives

$$\sigma(pp \to \gamma\gamma) \approx 5 \left(\frac{Q}{1/2}\right)^4 \text{ fb at } 13\,\text{TeV}\,. \tag{5.7}$$

At $\sqrt{s} = 8$ TeV the cross section is around five times smaller. We present the cross section $\sigma(pp \to \Pi \to \gamma\gamma)$ for a range of masses M_Π and different combinations of Q and N in Fig. 5.2. The parameter choice $\alpha_N = \alpha_s$ and $\Lambda_N = \Lambda_{\text{QCD}}$ has been assumed. (The cross section is not highly sensitive to Λ_N, α_N so long as we are in the perturbative regime: $\Lambda_N \lesssim \Lambda_{\text{QCD}}$.) Evidently, for $N = 2$, a χ with electric charge $Q \approx 1/2$ is produced at approximately the right rate to explain the diphoton excess.

In practice de-excitation of the produced quirkonium does not always continue until the ground state is reached. In this case annihilations of excited states can also contribute. However those with $l = 0$ will decay in the same way as the ground state. The only difference is that the excited states will have a slightly larger mass (which we will estimate in a moment) due to the change in the binding energy. This detail could be important as it can effectively enlarge the observed width. Annihilation of excited states with non-zero orbital angular momentum could in principle also be important, however these are suppressed as the radial wavefunction vanishes at the origin: $R(0) = 0$ for $l \geq 1$. They are expected to de-excite predominately to $l = 0$ states rather than annihilate [313]. Nevertheless, for sufficiently large α_N the $l = 1$ annihilations: $\Pi \to \mu^+\mu^-$ and $\Pi \to e^+e^-$ could potentially be observable.

The $l = 0$ excited states can be characterized by the quantum number n with binding energies:

$$\frac{E_n}{M_\Pi} = -\frac{1}{8n^2}\left[\frac{4}{3}\bar{\alpha}_s + C_N\bar{\alpha}_N + Q^2\bar{\alpha}\right]^2 . \tag{5.8}$$

The above formula was adapted from known results with quarkonium, *e.g.* [308] (and of course also the hydrogen atom). The coupling constants $\bar{\alpha}_s$, $\bar{\alpha}_N$ and $\bar{\alpha}$ are evaluated at a renomalisation scale corresponding to the mean distance between the particles which is of order the Bohr radius: $a_0 = 4/[(4\bar{\alpha}_s/3 + C_N\bar{\alpha}_N + Q^2\bar{\alpha})M_\Pi]$. The bound state, described by the radial quantum number n has mass given by $M_\Pi(n) = 2M_\chi + E_n$. Considering as an example $N = 2$ and $\bar{\alpha}_N = \bar{\alpha}_s = 0.15$, $\bar{\alpha} = 1/137$ we find the mass difference between the $n = 1$ and $n = 2$ states to be $\Delta M = (E_1 - E_2) \approx 0.01 M_\Pi$. Larger mass splittings

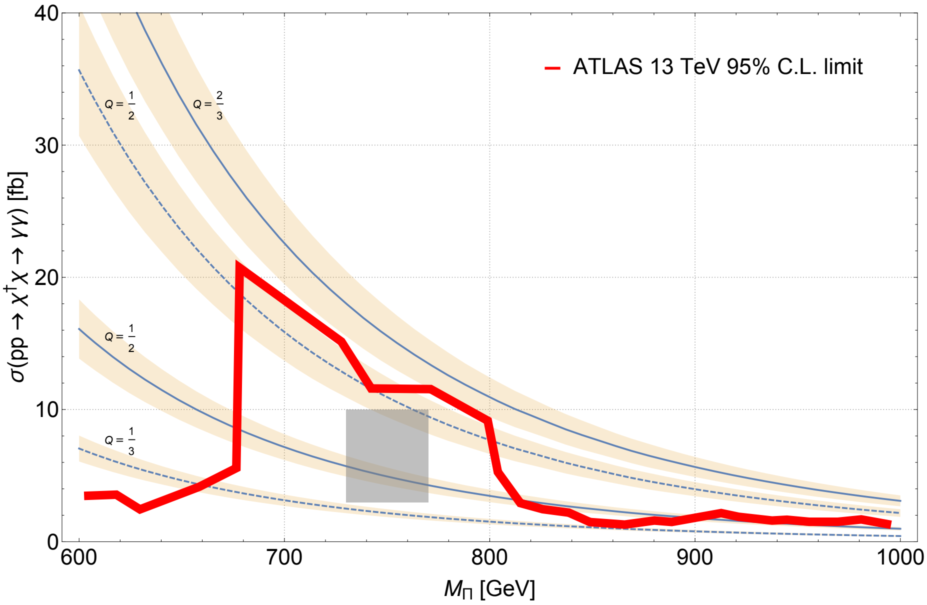

Figure 5.2: The cross section $\sigma(pp \to \Pi \to \gamma\gamma)$ at 13 TeV for a range of quirkonium masses M_Π and charge assignments. Solid lines denote choices of $N = 2$ and dashed lines choices of $N = 5$. The rectangle represents the $\sigma \in [3, 10]$ fb indicative region accommodated by the ATLAS and CMS data. The solid red line is the ATLAS 13 TeV exclusion limit. Uncertainties reflect error associated with the parton distribution functions.

will be possible[3] if $\bar{\alpha}_N > \bar{\alpha}_s$, although it has been shown in the context of fermionic quirk models that the phenomenology is substantially altered in this regime [309]. In particular, the hueballs can become so heavy that the decays of the bound state into hueballs is kinematically forbidden.

In the above calculation of the bound state production cross section, we considered only the *indirect* production following pair production of $\chi^\dagger\chi$ above threshold. The bound state can also be produced directly: $gg \to \Pi$, where $\sqrt{s_{gg}} \approx M_\Pi$. The cross section of the ground state direct resonance production is

$$\sigma(pp \to \Pi)_{\mathrm{DR}} \approx \frac{C_{gg} K_{gg} \Gamma(\Pi \to gg)}{s M_\Pi}, \tag{5.9}$$

[3] Additional possibilities arise if χ transforms non-trivially under $\mathrm{SU}(2)_L$, *i.e.* forming a representation $\mathbf{N}_L$. The mass degeneracy of the multiplet will be broken at tree-level by Higgs potential terms along with electroweak radiative corrections. The net effect is that the predicted width of the $pp \to \gamma\gamma$ bump can be effectively larger as there are N_L distinct bound states, Π^i, (of differing masses) which can each contribute to the decay width. Although each state is expected to have a narrow width, when smeared by the detector resolution the effect can potentially be a broad feature.

where C_{gg} is the appropriate parton luminosity coefficient and K_{gg} is the gluon NLO QCD K-factor. For $\sqrt{s} = 13\,\text{TeV}$ we take $C_{gg} \approx 2137$ [307] and $K_{gg} = 1.6$ [329]. The partial width $\Gamma(\Pi \to gg)$ of the $n = 1, l = 0$ ground state is given by

$$\Gamma(\Pi \to gg) = \frac{4}{3} M_\Pi N \alpha_s^2 \frac{|R(0)|^2}{M_\Pi^3}, \tag{5.10}$$

where the radial wavefunction at the origin for the ground state is:

$$\frac{|R(0)|^2}{M_\Pi^3} = \frac{1}{16}\left[\frac{4}{3}\bar{\alpha}_s + C_N \bar{\alpha}_N + Q^2 \bar{\alpha}\right]^3 . \tag{5.11}$$

Considering again the example of $N = 2$ and $\bar{\alpha}_N = \bar{\alpha}_s = 0.15$, $\bar{\alpha} = 1/137$ we find

$$\sigma(pp \to \Pi)_{DR} \approx 0.40\,\text{pb} \quad \text{at } 13\,\text{TeV} . \tag{5.12}$$

Evidently, the direct resonance production cross section is indeed expected to be sub-dominant, around 8% that of the indirect production cross section (Eq. 5.5)[4].

We now comment on the regime where Λ_N is smaller than Λ_{QCD}. In fact, if the SU(N) confining scale is only a little smaller than Λ_{QCD} then a light quark pair can form out of the vacuum, leading to a bound state of two QCD color singlet states: $\chi\bar{q}$ and $\chi^\dagger q$. These color singlet states would themselves be bound together by SU(N) gauge interactions to form the SU(N) singlet bound state. Since only SU(N) interactions bind the two composite states ($\chi\bar{q}$ and $\chi^\dagger q$), it follows that $\frac{4}{3}\bar{\alpha}_s + C_N\bar{\alpha}_N + Q^2\bar{\alpha} \to C_N\bar{\alpha}_N + (Q - Q_q)^2\bar{\alpha}$ in eqs. 5.8 and 5.11. Therefore if the confinement scale of SU(N) is smaller than that of QCD then the direct production rate becomes completely negligible relative to the indirect production mechanism. The rate of Π production is the same as that found earlier in Eq. 5.5, but the branching ratio to two photons is modified:

$$\text{Br}(\Pi \to \gamma\gamma) \simeq \frac{3NQ^4\alpha^2}{\frac{7}{3}N\alpha_s^2 + \frac{3}{2}C_N\alpha_N^2 + 3NQ^4\alpha^2}, \tag{5.13}$$

where, as before, we have neglected the small contribution of $\Pi \to Z\gamma/ZZ$ to the total width, and also the contribution from $\Pi \to hh$. In this regime somewhat larger values of Q can be accommodated, such as $Q = 5/6$ for $N = 2$ [5].

[4] If $\bar{\alpha}_N$ is sufficiently large, one can potentially have direct resonance production comparable or even dominating indirect production (such a scenario has been contemplated recently in [310, 311]). Naturally at such large $\bar{\alpha}_N$ the perturbative calculations become unreliable, and one would have to resort to non-perturbative techniques such as lattice computations.

[5] Although it is perhaps too early to speculate on the possible role of χ in a more elaborate framework, we nevertheless remark here that particles fitting its description are required for spontaneous symmetry breaking of extended Pati–Salam type unified theories [330].

Notice that in the $\Lambda_N < \Lambda_{\rm QCD}$ regime the size of the mass splittings between the excited states becomes small as $\frac{4}{3}\bar{\alpha}_s + C_N\bar{\alpha}_N + Q^2\bar{\alpha} \to C_N\bar{\alpha}_N + (Q-Q_q)^2\bar{\alpha}$ in Eq. 5.8. We therefore expect no effective width enhancement due to the excited state decays at the LHC in the small Λ_N regime. Of course a larger effective width is still possible if there are several nearly degenerate scalar quirk states, which, as briefly mentioned earlier, can arise if χ transforms nontrivially under $SU(2)_L$.

Other signatures

While the two photon decay channel of the bound state should be the most important signature, the dominant decay is expected to be via $\Pi \to gg$ and $\Pi \to \mathscr{H}\mathscr{H}$. The former process is expected to lead to dijet production while the latter will be an invisible decay. The dijet cross section is easily estimated:

$$\sigma(pp \to jj) \approx \begin{cases} 2.6N \times \mathrm{Br}(\Pi \to gg)\ \mathrm{pb} & \text{at 13 TeV} \\ 0.5N \times \mathrm{Br}(\Pi \to gg)\ \mathrm{pb} & \text{at 8 TeV} \end{cases} . \tag{5.14}$$

The limit from 8 TeV data is $\sigma(pp \to jj) \lesssim 2.5$ pb [331, 332]. If gluons dominate the Π decays (i.e. $\mathrm{Br}(\Pi \to gg) \approx 1$) then this experimental limit is satisfied for $N \leq 5$. For sufficiently large α_N the invisible decay can be enhanced, thereby reducing $\mathrm{Br}(\Pi \to gg)$. In this circumstance the bound on N from dijet searches would weaken.

The invisible decays $\Pi \to \mathscr{H}\mathscr{H}$ are not expected to lead to an observable signal at leading order for much of the parameter space of interest[6]. However, the bremsstrahlung of a hard gluon from the initial state: $pp \to \Pi g \to \mathscr{H}\mathscr{H} g$ can lead to a jet plus missing transverse energy signature. Current data are not expected to give stringent limits from such decay channels, however this signature could become important when a larger data sample is collected. Note though that the rate will become negligible in the limit that α_N becomes small. Also, in the small Λ_N regime, where the bound state is formed from $\chi\bar{q}$ and $\chi^\dagger q$, the two-body decay $\Pi \to g\gamma$ (jet+photon) will also arise as in this case the scalar quirk pair is not necessarily in the color singlet configuration. The decay rate at leading order is substantial:

$$\frac{\Gamma(\Pi \to j\gamma)}{\Gamma(\Pi \to \gamma\gamma)} = \frac{8\alpha_s}{3\alpha Q^2} . \tag{5.15}$$

Nevertheless, we estimate that this is still consistent with current data [335], but would be expected to become important when a larger data sample is collected.

[6]Scalar quirk loops can mediate hueball decays into gluons and other SM bosons [313, 333, 334]. The decay rate is uncertain, depending on the non-perturbative hueball dynamics. However, if the hueballs are able to decay within the detector then they can lead to observable signatures including displaced vertices. This represents another possible collider signature of the model.

Another important signature of the model will be the $pp \to \Pi \to Z\gamma$ and $pp \to \Pi \to ZZ$ processes. The rates of these decays, relative to $\Pi \to \gamma\gamma$, are estimated to be:

$$\begin{aligned}\frac{\Gamma(\Pi \to Z\gamma)}{\Gamma(\Pi \to \gamma\gamma)} &= 2\tan^2\theta_W, \\ \frac{\Gamma(\Pi \to ZZ)}{\Gamma(\Pi \to \gamma\gamma)} &= \tan^4\theta_W.\end{aligned} \tag{5.16}$$

If χ transforms nontrivially under $SU(2)_L$ then deviations from these predicted rates arize along with the tree-level decay $\Pi \to W^+W^-$.

Conclusions

We have considered a charged scalar particle χ of mass around 375GeV charged under both $\mathrm{SU}(3)_c$ and a new confining gauge interaction (assigned to be SU(N) for definiteness). These interactions confine $\chi^\dagger\chi$ into non-relativistic bound states whose decays into photons can explain the 750 GeV diphoton excess observed at the LHC. Taking the new confining group to be SU(2), we found that the diphoton excess required χ to have electric charge approximately $Q \sim [\frac{1}{2}, 1]$. An important feature of our model is that the exotic particle χ has a mass much greater than the SU(N)-confinement scale Λ_N. In the absence of light SU(N)-charged matter fields this makes the dynamics of this new interaction qualitatively different to that of QCD: pair production of the scalars and the subsequent formation of the bound state dominates over direct bound state resonance production (at least in the perturbative regime where $\Lambda_N \lesssim \Lambda_{\mathrm{QCD}}$). Since χ is a Lorentz scalar, decays of $\chi^\dagger\chi$ bound states to lepton pairs are naturally suppressed, and thus constraints from dilepton searches at the LHC can be ameliorated. This explanation is quite weakly constrained by current searches and data from the forthcoming run at the LHC will be able to probe our scenario more fully. In particular, dijet, mono-jet, di-Higgs and jet + photon searches may be the most promising discovery channels.

Acknowledgements

This work was supported by the Australian Research Council. Feynman diagrams were generated using the Ti*k*Z-Feynman package for LaTeX [336].

A
Mathematical notation

Throughout this thesis we choose to label representations by their dimension, which we typeset in bold. Fields are labelled by their transformation properties under the Lorentz group and the SM gauge group $\mathrm{SU}(3)_c \otimes \mathrm{SU}(2)_L \otimes \mathrm{U}(1)_Y$. All spinors are treated as two-component objects transforming as either $(\mathbf{2}, \mathbf{1})$ (left-handed) or $(\mathbf{1}, \mathbf{2})$ (right-handed) under the Lorentz group, written as $\mathrm{SU}(2)_+ \otimes \mathrm{SU}(2)_-$. The left-handed spinors carry undotted spinor indices $\alpha, \beta, \ldots \in \{1, 2\}$, while the right-handed spinors carry dotted indices $\dot{\alpha}, \dot{\beta}, \ldots \in \{\dot{1}, \dot{2}\}$. Wherever possible we attempt to conform to the conventions of Ref. [22] when working with spinor fields (see appendix G for the correspondence to four-component notation and appendix J for SM-fermion nomenclature). For objects carrying a single spacetime index V_μ we define

$$V_{\alpha\dot{\beta}} = \sigma^\mu_{\alpha\dot{\beta}} V_\mu \quad \text{and} \quad \bar{V}_{\dot{\alpha}\beta} = \bar{\sigma}^\mu_{\dot{\alpha}\beta} V_\mu. \tag{A.1}$$

Note that in this notation

$$\Box = \partial_\mu \partial^\mu = \tfrac{1}{2}\mathrm{Tr}[\partial\bar{\partial}] = \tfrac{1}{2}\mathrm{Tr}[\bar{\partial}\partial], \tag{A.2}$$

and we will often just use $\Box$ to represent the contraction of two covariant derivatives $D_\mu D^\mu$ where this is clear from context. For field-strength tensors, generically $X_{\mu\nu}$, we work with the irreducible representations (irreps) $X_{\alpha\beta}$ and $\bar{X}_{\dot{\alpha}\dot{\beta}}$, where

$$X_{\{\alpha\beta\}} = 2i[\sigma^{\mu\nu}]_\alpha^{\ \gamma} \epsilon_{\gamma\beta} X_{\mu\nu} \quad \text{and} \quad \bar{X}_{\{\dot{\alpha}\dot{\beta}\}} = 2i[\bar{\sigma}^{\mu\nu}]^{\dot{\gamma}}_{\ \dot{\beta}} \epsilon_{\dot{\alpha}\dot{\gamma}} X_{\mu\nu}, \tag{A.3}$$

or the alternate forms with one raised and one lowered index.

Indices for $SU(2)_L$ (isospin) are taken from the middle of the Latin alphabet. These are kept lowercase for the fundamental representation for which $i, j, k, \ldots \in \{1, 2\}$ and the indices of the adjoint are capitalised $I, J, K, \ldots \in \{1, 2, 3\}$. Colour indices are taken from the beginning of the Latin alphabet and the same distinction between lowercase and uppercase letters is made. For both SU(2) and SU(3), a distinction between raised and lowered indices is maintained such that, for example, $(\psi^i)^\dagger = (\psi^\dagger)_i$ for an isodoublet field ψ. However, we often specialise to the case of only raised, symmetrised indices for SU(2), and use a tilde to denote a conjugate field whose $SU(2)_L$ indices have been raised:

$$\tilde{\psi}^i \equiv \epsilon^{ij}\psi_j^\dagger . \tag{A.4}$$

We adopt this notation from the usual definition of $\tilde{H}$, and note that throughout the paper we freely interchange between $\tilde{\psi}^i$ and $\psi_i^\dagger$. For the sake of tidiness, we sometimes use parentheses $(\cdots)$ to indicate the contraction of suppressed indices. Curly braces are reserved to indicate symmetrised indices $\{\cdots\}$ and square brackets enclose antisymmetrised indices $[\cdots]$, but this notation is avoided when the permutation symmetry between indices is clear. We use τ^I and λ^A for the Pauli and Gell-Mann matrices, and normalise the non-abelian vector potentials of the SM such that

$$(W_{\alpha\dot{\beta}})^i{}_j = \frac{1}{2}(\tau^I)^i{}_j W^I_{\alpha\dot{\beta}} \quad \text{and} \quad (G_{\alpha\dot{\beta}})^a{}_b = \frac{1}{2}(\lambda^A)^a{}_b G^A_{\alpha\dot{\beta}}. \tag{A.5}$$

Flavour (or family) indices of the SM fermions are represented by the lowercase Latin letters $\{r, s, t, u, v, w\}$.

For the non-gauge degrees of freedom in the SM we capitalise isospin doublets (Q, L, H), while the left-handed isosinglets are written in lowercase with a bar featuring as a part of the name of the field ($\bar{u}$, $\bar{d}$, $\bar{e}$). The representations and hypercharges for the SM field content are summarised in Table A.1. Our definition of the SM gauge-covariant derivative is exemplified by

$$\bar{D}_{\dot{\alpha}\beta} Q_r^{\beta a i} = \left[\delta^a_b \delta^i_j (\bar{\partial}_{\dot{\alpha}\beta} + i g_1 Y_Q \bar{B}_{\dot{\alpha}\beta}) + i g_2 \delta^a_b (\bar{W}_{\dot{\alpha}\beta})^i{}_j + i g_3 \delta^i_j (\bar{G}_{\dot{\alpha}\beta})^a{}_b\right] Q_r^{\beta b j} . \tag{A.6}$$

Note that the derivative implicitly carries $SU(2)_L$ and $SU(3)_c$ indices [explicit on the right-hand side of Eq. (A.6)] which are suppressed on the left-hand side to reduce clutter. Where appropriate we show these indices explicitly.

We represent the SM quantum numbers of fields as a 3-tuple $(\mathbf{C}, \mathbf{I}, Y)_L$, with $\mathbf{C}$ and $\mathbf{I}$ the dimension of the colour and isospin representations, Y the hypercharge of the field, and L an (often omitted) label of the Lorentz representation: S (scalar), F (fermion) or V (vector), although sometimes we use the irrep, *e.g.* $(\mathbf{2}, \mathbf{1})$. We normalise the hypercharge such that $Q = I_3 + Y$. Finally, for exotic fields that contribute to dimension-six operators at tree-level, we try and adopt names consistent with Table 3 of Ref. [23], which we reproduce here in Table A.2.

Field	$SU(3)_c \otimes SU(2)_L \otimes U(1)_Y$	$SU(2)_+ \otimes SU(2)_-$
$Q^{\alpha a i}$	$(\mathbf{3}, \mathbf{2}, \frac{1}{6})$	$(\mathbf{2}, \mathbf{1})$
$L^{\alpha i}$	$(\mathbf{1}, \mathbf{2}, -\frac{1}{2})$	$(\mathbf{2}, \mathbf{1})$
$\bar{u}^{\alpha}_{a}$	$(\bar{\mathbf{3}}, \mathbf{1}, -\frac{2}{3})$	$(\mathbf{2}, \mathbf{1})$
$\bar{d}^{\alpha}_{a}$	$(\bar{\mathbf{3}}, \mathbf{1}, \frac{1}{3})$	$(\mathbf{2}, \mathbf{1})$
$\bar{e}^{\alpha}$	$(\mathbf{1}, \mathbf{1}, 1)$	$(\mathbf{2}, \mathbf{1})$
$(G_{\alpha\beta})^{a}{}_{b}$	$(\mathbf{8}, \mathbf{1}, 0)$	$(\mathbf{3}, \mathbf{1})$
$(W_{\alpha\beta})^{i}{}_{j}$	$(\mathbf{1}, \mathbf{3}, 0)$	$(\mathbf{3}, \mathbf{1})$
$B_{\alpha\beta}$	$(\mathbf{1}, \mathbf{1}, 0)$	$(\mathbf{3}, \mathbf{1})$
H^{i}	$(\mathbf{1}, \mathbf{2}, \frac{1}{2})$	$(\mathbf{1}, \mathbf{1})$

Table A.1: The SM fields and their transformation properties under the SM gauge group G_{SM} and the Lorentz group. The final unbolded number in the 3-tuples of the G_{SM} column represents the $U(1)_Y$ charge of the field, normalised such that $Q = I_3 + Y$. For the fermions a generational index has been suppressed.

Name	S	S_1	S_2	φ	Ξ	Ξ_1	Θ_1	Θ_3
Irrep	$(\mathbf{1},\mathbf{1},0)$	$(\mathbf{1},\mathbf{1},1)$	$(\mathbf{1},\mathbf{1},2)$	$(\mathbf{1},\mathbf{2},\frac{1}{2})$	$(\mathbf{1},\mathbf{3},0)$	$(\mathbf{1},\mathbf{3},1)$	$(\mathbf{1},\mathbf{4},\frac{1}{2})$	$(\mathbf{1},\mathbf{4},\frac{3}{2})$
Name	ω_1	ω_2	ω_4	Π_1	Π_7	ζ		
Irrep	$(\bar{\mathbf{3}},\mathbf{1},\frac{1}{3})$	$(\mathbf{3},\mathbf{1},\frac{2}{3})$	$(\bar{\mathbf{3}},\mathbf{1},\frac{4}{3})$	$(\mathbf{3},\mathbf{2},\frac{1}{6})$	$(\mathbf{3},\mathbf{2},\frac{7}{6})$	$(\bar{\mathbf{3}},\mathbf{3},\frac{1}{3})$		
Name	Ω_1	Ω_2	Ω_4	Υ	Φ			
Irrep	$(\mathbf{6},\mathbf{1},\frac{1}{3})$	$(\bar{\mathbf{6}},\mathbf{1},\frac{2}{3})$	$(\mathbf{6},\mathbf{1},\frac{4}{3})$	$(\mathbf{6},\mathbf{3},\frac{1}{3})$	$(\mathbf{8},\mathbf{2},\frac{1}{2})$			
Name	N	E	Δ_1	Δ_3	Σ	Σ_1		
Irrep	$(\mathbf{1},\mathbf{1},0)$	$(\mathbf{1},\mathbf{1},1)$	$(\mathbf{1},\mathbf{2},\frac{1}{2})$	$(\mathbf{1},\mathbf{2},\frac{3}{2})$	$(\mathbf{1},\mathbf{3},0)$	$(\mathbf{1},\mathbf{3},1)$		
Name	U	D	Q_1	Q_5	Q_7	T_1	T_2	
Irrep	$(\mathbf{3},\mathbf{1},\frac{2}{3})$,	$(\bar{\mathbf{3}},\mathbf{1},\frac{1}{3})$	$(\mathbf{3},\mathbf{2},\frac{1}{6})$	$(\mathbf{3},\mathbf{2},-\frac{5}{6})$	$(\mathbf{3},\mathbf{2},\frac{7}{6})$	$(\bar{\mathbf{3}},\mathbf{3},\frac{1}{3})$	$(\mathbf{3},\mathbf{3},\frac{2}{3})$	

Table A.2: The table shows the exotic scalars (top) and vectorlike or Majorana fermions (bottom) contributing to the dimension-six SMEFT at tree-level [23]. We sometimes use the label of a field as presented in the table to represent its conjugate, although we always define the transformation properties each time a field is mentioned to avoid confusion. For the leptoquarks (second row), we add a prime to the field name presented here if the baryon-number assignment is such that only the diquark couplings are allowed.

B

Table of lepton-number-violating operators

Below we present the catalogue of $\Delta L = 2$ operators we use in our study. The operators are listed and labelled in a way consistent with the previous catalogues [86, 99], although we enforce that operators with the same field content carry the same numerical labels. This means that our listing may contain more $\mathrm{SU}(2)_L$ structures for any numbered family of operators. Product operators as presented in the table must be read with care. This is just a convenient shorthand to represent the field-content of an operator and illustrate that isospin indices are internally contracted. For example, by writing $\mathcal{O}_{5b} = \mathcal{O}_1 Q^i \bar{d} \tilde{H}^j \epsilon_{ij}$, we do not mean to suggest that Lorentz indices must be contracted internally to $\mathcal{O}_1$ and the down-type Yukawa.

In each row we also provide information relevant to the number of completions. The number of unfiltered models (sets of field content) derived from the operator using our techniques is presented, along with the number that survive the democratic filtering procedure with the neutrino-mass filtering criterion. A sizeable number of operators end up with no completions that can play a dominant role in the physics of neutrino mass.

Other information relevant to the operators is also shown, including the number of loops required for the operator closure (the same as the number of loops appearing in the associated neutrino self-energy diagram) and the upper-bound on the scale of the new physics generating the operator at tree level, derived from the atmospheric lower bound on the mass of the heaviest neutrino. Operators for which a range is given for the number of loops are those that generate the dimension-seven or dimension-nine analogues of the Weinberg operator. The additional Higgs fields in these diagrams can always be closed off, adding more loops to the neutrino self-energy while reducing the overall scale suppression. The contribution with the highest number of loops will dominate for scales $\Lambda \gtrsim 4\pi v$.

We remind the reader that our analysis does not include the number of unfiltered completions of $\mathcal{O}_1'''$. In this case, the number of filtered models comes from Ref. [103]. Other operators featuring a '—' are non-explosive, *i.e.* they do not support tree-level topologies containing only scalars and fermions.

Table B.1: The table displays our listing of the $\Delta L = 2$ operators along with the number of completions before and after our model-filtering procedure, the number of loops in the neutrino self-energy diagram, and the upper bound on the new-physics scale associated with each operator. See the main text of the appendix for more information.

Labels	Operator	Models	Filtered	Loops	Λ [TeV]
1	$L^iL^jH^kH^l \cdot \epsilon_{ik}\epsilon_{jl}$	3	3	0	$6 \cdot 10^{11}$
2	$L^iL^jL^k\bar{e}H^l \cdot \epsilon_{ik}\epsilon_{jl}$	8	2	1	$4 \cdot 10^{7}$
3a	$L^iL^jQ^k\bar{d}H^l \cdot \epsilon_{ij}\epsilon_{kl}$	9	2	2	$2 \cdot 10^{5}$
3b	$L^iL^jQ^k\bar{d}H^l \cdot \epsilon_{ik}\epsilon_{jl}$	14	5	1	$9 \cdot 10^{7}$
4a	$L^iL^j\tilde{Q}^k\bar{u}^\dagger H^l \cdot \epsilon_{ik}\epsilon_{jl}$	5	0	1	$4 \cdot 10^{9}$
4b	$L^iL^j\tilde{Q}^k\bar{u}^\dagger H^l \cdot \epsilon_{ij}\epsilon_{kl}$	4	2	2	$10 \cdot 10^{6}$
5a	$L^iL^jQ^k\bar{d}H^lH^m\tilde{H}^n \cdot \epsilon_{il}\epsilon_{jn}\epsilon_{km}$	790	36	2	$6 \cdot 10^{5}$
5b	$\mathcal{O}_1 \cdot Q^i\bar{d}\tilde{H}^j \cdot \epsilon_{ij}$	492	14	1,2	$6 \cdot 10^{5}$
5c	$\mathcal{O}_{3a} \cdot H^i\tilde{H}^j \cdot \epsilon_{ij}$	509	0	2,3	$1 \cdot 10^{3}$
5d	$\mathcal{O}_{3b} \cdot H^i\tilde{H}^j \cdot \epsilon_{ij}$	799	16	1,2	$6 \cdot 10^{5}$
6a	$L^iL^j\tilde{Q}^k\bar{u}^\dagger H^lH^m\tilde{H}^n \cdot \epsilon_{il}\epsilon_{jn}\epsilon_{km}$	289	14	2	$2 \cdot 10^{7}$
6b	$\mathcal{O}_1 \cdot \tilde{Q}^i\bar{u}^\dagger\tilde{H}^j \cdot \epsilon_{ij}$	177	0	1,2	$2 \cdot 10^{7}$
6c	$\mathcal{O}_{4a} \cdot H^i\tilde{H}^j \cdot \epsilon_{ij}$	262	0	1,2	$2 \cdot 10^{7}$
6d	$\mathcal{O}_{4b} \cdot H^i\tilde{H}^j \cdot \epsilon_{ij}$	208	0	2,3	$6 \cdot 10^{4}$
7	$L^i\bar{e}^\dagger Q^j\tilde{Q}^kH^lH^mH^n \cdot \epsilon_{il}\epsilon_{jm}\epsilon_{kn}$	240	15	2	$2 \cdot 10^{5}$
8	$L^i\bar{e}^\dagger\bar{u}^\dagger\bar{d}H^j \cdot \epsilon_{ij}$	5	1	2,3	$2 \cdot 10^{1}$
9	$L^iL^jL^kL^l\bar{e}\bar{e} \cdot \epsilon_{ik}\epsilon_{jl}$	14	1	2	$3 \cdot 10^{3}$
10	$L^iL^jL^k\bar{e}Q^l\bar{d} \cdot \epsilon_{ik}\epsilon_{jl}$	50	1	2	$6 \cdot 10^{3}$
11a	$L^iL^jQ^kQ^l\bar{d}\bar{d} \cdot \epsilon_{ij}\epsilon_{kl}$	48	0	3	$4 \cdot 10^{1}$
11b	$L^iL^jQ^kQ^l\bar{d}\bar{d} \cdot \epsilon_{ik}\epsilon_{jl}$	72	16	2	$1 \cdot 10^{4}$
12a	$L^iL^j\tilde{Q}^k\tilde{Q}^l\bar{u}^\dagger\bar{u}^\dagger \cdot \epsilon_{ik}\epsilon_{jl}$	19	0	2	$2 \cdot 10^{7}$
12b	$L^iL^j\tilde{Q}^k\tilde{Q}^l\bar{u}^\dagger\bar{u}^\dagger \cdot \epsilon_{ij}\epsilon_{kl}$	17	4	3	$6 \cdot 10^{4}$
13	$L^iL^jL^k\bar{e}\tilde{Q}^l\bar{u}^\dagger \cdot \epsilon_{ik}\epsilon_{jl}$	12	0	2	$2 \cdot 10^{5}$
14a	$L^iL^jQ^k\tilde{Q}^l\bar{u}^\dagger\bar{d} \cdot \epsilon_{ij}\epsilon_{kl}$	29	1	3	$1 \cdot 10^{3}$

Labels	Operator	Models	Filtered	Loops	Λ [TeV]
14b	$L^iL^jQ^k\tilde{Q}^l\bar{u}^\dagger\bar{d}\cdot\epsilon_{ik}\epsilon_{jl}$	43	1	2	$6\cdot10^5$
15	$L^iL^jL^k\tilde{L}^l\bar{u}^\dagger\bar{d}\cdot\epsilon_{ik}\epsilon_{jl}$	12	1	3	$1\cdot10^3$
16	$L^iL^j\bar{e}\bar{e}^\dagger\bar{u}^\dagger\bar{d}\cdot\epsilon_{ij}$	13	1	3	$1\cdot10^3$
17	$L^iL^j\bar{u}^\dagger\bar{d}\bar{d}\bar{d}^\dagger\cdot\epsilon_{ij}$	18	12	3	$1\cdot10^3$
18	$L^iL^j\bar{u}\bar{u}^\dagger\bar{u}^\dagger\bar{d}\cdot\epsilon_{ij}$	22	8	3	$1\cdot10^3$
19	$L^i\bar{e}^\dagger Q^j\bar{u}^\dagger\bar{d}\bar{d}\cdot\epsilon_{ij}$	27	0	3,4	$2\cdot10^{-1}$
20	$L^i\bar{e}^\dagger\tilde{Q}^j\bar{u}^\dagger\bar{u}^\dagger\bar{d}\cdot\epsilon_{ij}$	27	3	3,4	$8\cdot10^{-1}$
21a	$L^iL^jL^k\bar{e}Q^l\bar{u}H^mH^n\cdot\epsilon_{il}\epsilon_{jm}\epsilon_{kn}$	3943	1	2,3	$2\cdot10^3$
21b	$L^iL^jL^k\bar{e}Q^l\bar{u}H^mH^n\cdot\epsilon_{ik}\epsilon_{jm}\epsilon_{ln}$	4080	4	3	$2\cdot10^3$
22a	$L^iL^jL^k\tilde{L}^l\bar{e}\bar{e}^\dagger H^mH^n\cdot\epsilon_{il}\epsilon_{jm}\epsilon_{kn}$	726	0	2	$2\cdot10^7$
22b	$\mathcal{O}_2\cdot\tilde{L}^i\bar{e}^\dagger H^j\epsilon_{ij}$	931	0	2	$2\cdot10^7$
23a	$L^iL^jL^k\bar{e}\tilde{Q}^l\bar{d}^\dagger H^mH^n\cdot\epsilon_{il}\epsilon_{jm}\epsilon_{kn}$	780	0	2,3	$4\cdot10^1$
23b	$\mathcal{O}_2\cdot\tilde{Q}^i\bar{d}^\dagger H^j\cdot\epsilon_{ij}$	969	0	2,3	$4\cdot10^1$
24a	$L^iL^jQ^kQ^l\bar{d}\bar{d}H^m\tilde{H}^n\cdot\epsilon_{il}\epsilon_{jn}\epsilon_{km}$	9613	193	3	$9\cdot10^1$
24b	$L^iL^jQ^kQ^l\bar{d}\bar{d}H^m\tilde{H}^n\cdot\epsilon_{im}\epsilon_{jn}\epsilon_{kl}$	6058	110	3	$9\cdot10^1$
24c	$\mathcal{O}_{3a}\cdot Q^i\bar{d}\tilde{H}^j\cdot\epsilon_{ij}$	6022	34	3,4	1
24d	$\mathcal{O}_{3b}\cdot Q^i\bar{d}\tilde{H}^j\cdot\epsilon_{ij}$	9616	211	2,3	$9\cdot10^1$
24e	$\mathcal{O}_{11a}\cdot H^i\tilde{H}^j\cdot\epsilon_{ij}$	3834	18	3,4	1
24f	$\mathcal{O}_{11b}\cdot H^i\tilde{H}^j\cdot\epsilon_{ij}$	5915	131	2,3	$9\cdot10^1$
25a	$L^iL^jQ^kQ^l\bar{u}\bar{d}H^mH^n\cdot\epsilon_{im}\epsilon_{jn}\epsilon_{kl}$	5960	151	2,3	$4\cdot10^3$
25b	$\mathcal{O}_{3a}\cdot Q^i\bar{u}H^j\cdot\epsilon_{ij}$	5913	9	3,4	10
25c	$\mathcal{O}_{3b}\cdot Q^i\bar{u}H^j\cdot\epsilon_{ij}$	14036	470	2,3	$4\cdot10^3$
26a	$L^iL^j\tilde{L}^k\bar{e}^\dagger Q^l\bar{d}H^mH^n\cdot\epsilon_{ik}\epsilon_{jm}\epsilon_{ln}$	1600	0	3	$4\cdot10^1$
26b	$L^iL^j\tilde{L}^k\bar{e}^\dagger Q^l\bar{d}H^mH^n\cdot\epsilon_{im}\epsilon_{jn}\epsilon_{kl}$	1040	0	2,3	$4\cdot10^1$
26c	$\mathcal{O}_{3a}\cdot\tilde{L}^i\bar{e}^\dagger H^j\cdot\epsilon_{ij}$	1149	0	3	$4\cdot10^1$
26d	$\mathcal{O}_{3b}\cdot\tilde{L}^i\bar{e}^\dagger H^j\cdot\epsilon_{ij}$	1797	0	2,3	$4\cdot10^1$
27a	$L^iL^jQ^k\tilde{Q}^l\bar{d}\bar{d}^\dagger H^mH^n\cdot\epsilon_{ik}\epsilon_{jm}\epsilon_{ln}$	3851	164	2	$2\cdot10^7$
27b	$L^iL^jQ^k\tilde{Q}^l\bar{d}\bar{d}^\dagger H^mH^n\cdot\epsilon_{im}\epsilon_{jn}\epsilon_{kl}$	2226	74	2	$2\cdot10^7$
27c	$\mathcal{O}_{3a}\cdot\tilde{Q}^i\bar{d}^\dagger H^j\cdot\epsilon_{ij}$	2469	33	3	$6\cdot10^4$
27d	$\mathcal{O}_{3b}\cdot\tilde{Q}^i\bar{d}^\dagger H^j\cdot\epsilon_{ij}$	3443	165	2	$2\cdot10^7$
28a	$L^iL^jQ^k\tilde{Q}^l\bar{u}^\dagger\bar{d}H^m\tilde{H}^n\cdot\epsilon_{il}\epsilon_{jn}\epsilon_{km}$	4038	64	3	$4\cdot10^3$
28b	$L^iL^jQ^k\tilde{Q}^l\bar{u}^\dagger\bar{d}H^m\tilde{H}^n\cdot\epsilon_{im}\epsilon_{jn}\epsilon_{kl}$	4103	0	3,4	10
28c	$L^iL^jQ^k\tilde{Q}^l\bar{u}^\dagger\bar{d}H^m\tilde{H}^n\cdot\epsilon_{ik}\epsilon_{jn}\epsilon_{lm}$	4305	123	3	$4\cdot10^3$
28d	$\mathcal{O}_{3a}\cdot\tilde{Q}^i\bar{u}^\dagger\tilde{H}^j\cdot\epsilon_{ij}$	2749	7	3,4	10
28e	$\mathcal{O}_{3b}\cdot\tilde{Q}^i\bar{u}^\dagger\tilde{H}^j\cdot\epsilon_{ij}$	4304	90	2,3	$4\cdot10^3$
28f	$\mathcal{O}_{4a}\cdot Q^i\bar{d}\tilde{H}^j\cdot\epsilon_{ij}$	4039	74	2,3	$4\cdot10^3$
28g	$\mathcal{O}_{4b}\cdot Q^i\bar{d}\tilde{H}^j\cdot\epsilon_{ij}$	2748	14	3,4	10

Labels	Operator	Models	Filtered	Loops	Λ [TeV]
$28h$	$\mathcal{O}_{14a} \cdot H^i \tilde{H}^j \cdot \epsilon_{ij}$	2701	10	3,4	10
$28i$	$\mathcal{O}_{14b} \cdot H^i \tilde{H}^j \cdot \epsilon_{ij}$	4177	90	3	$4 \cdot 10^3$
$29a$	$L^i L^j Q^k \tilde{Q}^l \bar{u} \bar{u}^\dagger H^m H^n \cdot \epsilon_{im}\epsilon_{jn}\epsilon_{kl}$	2226	267	2	$2 \cdot 10^7$
$29b$	$L^i L^j Q^k \tilde{Q}^l \bar{u} \bar{u}^\dagger H^m H^n \cdot \epsilon_{ik}\epsilon_{jm}\epsilon_{ln}$	3846	498	2	$2 \cdot 10^7$
$29c$	$\mathcal{O}_{4a} \cdot Q^i \bar{u} H^j \cdot \epsilon_{ij}$	3444	422	2	$2 \cdot 10^7$
$29d$	$\mathcal{O}_{4b} \cdot Q^i \bar{u} H^j \cdot \epsilon_{ij}$	2468	64	3	$6 \cdot 10^4$
$30a$	$L^i L^j \tilde{L}^k \bar{e}^\dagger \tilde{Q}^l \bar{u}^\dagger H^m H^n \cdot \epsilon_{ik}\epsilon_{jm}\epsilon_{ln}$	1772	0	3	$2 \cdot 10^3$
$30b$	$L^i L^j \tilde{L}^k \bar{e}^\dagger \tilde{Q}^l \bar{u}^\dagger H^m H^n \cdot \epsilon_{im}\epsilon_{jn}\epsilon_{kl}$	1140	2	3	$2 \cdot 10^3$
$30c$	$\mathcal{O}_{4a} \cdot \tilde{L}^i \bar{e}^\dagger H^j \cdot \epsilon_{ij}$	1776	2	2,3	$2 \cdot 10^3$
$30d$	$\mathcal{O}_{4b} \cdot \tilde{L}^i \bar{e}^\dagger H^j \cdot \epsilon_{ij}$	1398	11	3	$2 \cdot 10^3$
$31a$	$\mathcal{O}_{4a} \cdot \tilde{Q}^i \bar{d}^\dagger H^j \cdot \epsilon_{ij}$	3107	10	2,3	$4 \cdot 10^3$
$31b$	$L^i L^j \tilde{Q}^k \tilde{Q}^l \bar{u}^\dagger \bar{d}^\dagger H^m H^n \cdot \epsilon_{im}\epsilon_{jn}\epsilon_{kl}$	1404	4	2,3	$4 \cdot 10^3$
$31c$	$\mathcal{O}_{4b} \cdot \tilde{Q}^i \bar{d}^\dagger H^j \cdot \epsilon_{ij}$	1654	8	3,4	10
$32a$	$L^i L^j \tilde{Q}^k \tilde{Q}^l \bar{u}^\dagger \bar{u}^\dagger H^m \tilde{H}^n \cdot \epsilon_{il}\epsilon_{jn}\epsilon_{km}$	2103	157	3	$2 \cdot 10^5$
$32b$	$L^i L^j \tilde{Q}^k \tilde{Q}^l \bar{u}^\dagger \bar{u}^\dagger H^m \tilde{H}^n \cdot \epsilon_{im}\epsilon_{jn}\epsilon_{kl}$	1493	151	3	$2 \cdot 10^5$
$32c$	$\mathcal{O}_{4a} \cdot \tilde{Q}^i \bar{u}^\dagger \tilde{H}^j \cdot \epsilon_{ij}$	2100	56	3	$2 \cdot 10^5$
$32d$	$\mathcal{O}_{4b} \cdot \tilde{Q}^i \bar{u}^\dagger \tilde{H}^j \cdot \epsilon_{ij}$	1747	26	3,4	$4 \cdot 10^2$
$32e$	$\mathcal{O}_{12a} \cdot H^i \tilde{H}^j$	1250	36	3	$2 \cdot 10^5$
$32f$	$\mathcal{O}_{12b} \cdot H^i \tilde{H}^j$	1143	24	3,4	$4 \cdot 10^2$
33	$\mathcal{O}_1 \cdot \bar{e}\bar{e}\bar{e}^\dagger \bar{e}^\dagger$	451	5	2	$2 \cdot 10^7$
34	$L^i \bar{e}\bar{e}^\dagger \bar{e}^\dagger Q^j \bar{d} H^k H^l \cdot \epsilon_{ik}\epsilon_{jl}$	1377	231	3	$4 \cdot 10^1$
35	$L^i \bar{e}\bar{e}^\dagger \bar{e}^\dagger \tilde{Q}^j \bar{u}^\dagger H^k H^l \cdot \epsilon_{ik}\epsilon_{jl}$	1126	15	3	$2 \cdot 10^3$
36	$\bar{e}^\dagger \bar{e}^\dagger Q^i Q^j \bar{d}\bar{d} H^k H^l \cdot \epsilon_{ik}\epsilon_{jl}$	970	208	4	$6 \cdot 10^{-5}$
37	$\bar{e}^\dagger \bar{e}^\dagger Q^i \tilde{Q}^j \bar{u}^\dagger \bar{d} H^k H^l \cdot \epsilon_{ik}\epsilon_{jl}$	2470	58	4,5,6,7	$4 \cdot 10^{-2}$
38	$\bar{e}^\dagger \bar{e}^\dagger \tilde{Q}^i \tilde{Q}^j \bar{u}^\dagger \bar{u}^\dagger H^k H^l \cdot \epsilon_{ik}\epsilon_{jl}$	3358	451	4	$1 \cdot 10^{-1}$
$39a$	$\mathcal{O}_1 \cdot L^i L^j \tilde{L}^k \tilde{L}^l \cdot \epsilon_{ik}\epsilon_{jl}$	296	0	2	$2 \cdot 10^7$
$39b$	$L^i L^j L^k L^l \tilde{L}^m \tilde{L}^n H^p H^q \cdot \epsilon_{ik}\epsilon_{jl}\epsilon_{mp}\epsilon_{nq}$	220	6	2	$2 \cdot 10^7$
$39c$	$L^i L^j L^k L^l \tilde{L}^m \tilde{L}^n H^p H^q \cdot \epsilon_{il}\epsilon_{jn}\epsilon_{kp}\epsilon_{mq}$	588	0	2	$2 \cdot 10^7$
$39d$	$\mathcal{O}_1 \cdot L^i L^j \tilde{L}^k \tilde{L}^l \cdot \epsilon_{ij}\epsilon_{kl}$	324	0	2	$2 \cdot 10^7$
$40a$	$L^i L^j L^k \tilde{L}^l Q^m \tilde{Q}^n H^p H^q \cdot \epsilon_{il}\epsilon_{jn}\epsilon_{kp}\epsilon_{mq}$	963	22	2	$2 \cdot 10^7$
$40b$	$L^i L^j L^k \tilde{L}^l Q^m \tilde{Q}^n H^p H^q \cdot \epsilon_{il}\epsilon_{jp}\epsilon_{kq}\epsilon_{mn}$	729	25	2	$2 \cdot 10^7$
$40c$	$L^i L^j L^k \tilde{L}^l Q^m \tilde{Q}^n H^p H^q \cdot \epsilon_{in}\epsilon_{jp}\epsilon_{kq}\epsilon_{lm}$	759	25	2	$2 \cdot 10^7$
$40d$	$L^i L^j L^k \tilde{L}^l Q^m \tilde{Q}^n H^p H^q \cdot \epsilon_{ik}\epsilon_{jl}\epsilon_{mp}\epsilon_{nq}$	953	0	3	$6 \cdot 10^4$
$40e$	$L^i L^j L^k \tilde{L}^l Q^m \tilde{Q}^n H^p H^q \cdot \epsilon_{il}\epsilon_{jm}\epsilon_{kp}\epsilon_{nq}$	1321	31	2	$2 \cdot 10^7$
$40f$	$L^i L^j L^k \tilde{L}^l Q^m \tilde{Q}^n H^p H^q \cdot \epsilon_{ik}\epsilon_{jn}\epsilon_{lp}\epsilon_{mq}$	963	100	2	$2 \cdot 10^7$
$40g$	$L^i L^j L^k \tilde{L}^l Q^m \tilde{Q}^n H^p H^q \cdot \epsilon_{im}\epsilon_{jn}\epsilon_{kp}\epsilon_{lq}$	1339	30	2	$2 \cdot 10^7$
$40h$	$L^i L^j L^k \tilde{L}^l Q^m \tilde{Q}^n H^p H^q \cdot \epsilon_{ik}\epsilon_{jm}\epsilon_{lp}\epsilon_{nq}$	820	56	2	$2 \cdot 10^7$

Labels	Operator	Models	Filtered	Loops	Λ [TeV]
40*i*	$L^iL^jL^k\tilde{L}^lQ^m\tilde{Q}^nH^pH^q \cdot \epsilon_{im}\epsilon_{jp}\epsilon_{kq}\epsilon_{ln}$	844	9	2	$2 \cdot 10^7$
40*j*	$L^iL^jL^k\tilde{L}^lQ^m\tilde{Q}^nH^pH^q \cdot \epsilon_{ik}\epsilon_{jp}\epsilon_{ln}\epsilon_{mq}$	908	60	2	$2 \cdot 10^7$
40*k*	$L^iL^jL^k\tilde{L}^lQ^m\tilde{Q}^nH^pH^q \cdot \epsilon_{ik}\epsilon_{jp}\epsilon_{lm}\epsilon_{nq}$	970	98	2	$2 \cdot 10^7$
40*l*	$L^iL^jL^k\tilde{L}^lQ^m\tilde{Q}^nH^pH^q \cdot \epsilon_{ik}\epsilon_{jp}\epsilon_{lq}\epsilon_{mn}$	933	87	2	$2 \cdot 10^7$
41*a*	$L^iL^jL^k\tilde{L}^l\bar{d}\bar{d}^\dagger H^mH^n \cdot \epsilon_{il}\epsilon_{jm}\epsilon_{kn}$	729	6	2	$2 \cdot 10^7$
41*b*	$L^iL^jL^k\tilde{L}^l\bar{d}\bar{d}^\dagger H^mH^n \cdot \epsilon_{ik}\epsilon_{jm}\epsilon_{ln}$	933	71	2	$2 \cdot 10^7$
42*a*	$L^iL^jL^k\tilde{L}^l\bar{u}\bar{u}^\dagger H^mH^n \cdot \epsilon_{il}\epsilon_{jm}\epsilon_{kn}$	729	21	2	$2 \cdot 10^7$
42*b*	$L^iL^jL^k\tilde{L}^l\bar{u}\bar{u}^\dagger H^mH^n \cdot \epsilon_{ik}\epsilon_{jm}\epsilon_{ln}$	933	120	2	$2 \cdot 10^7$
43*a*	$L^iL^jL^k\tilde{L}^l\bar{u}^\dagger\bar{d}H^m\tilde{H}^n \cdot \epsilon_{ik}\epsilon_{jn}\epsilon_{lm}$	1068	7	3,4	10
43*b*	$L^iL^jL^k\tilde{L}^l\bar{u}^\dagger\bar{d}H^m\tilde{H}^n \cdot \epsilon_{il}\epsilon_{jm}\epsilon_{kn}$	1438	7	3,4	10
43*c*	$L^iL^jL^k\tilde{L}^l\bar{u}^\dagger\bar{d}H^m\tilde{H}^n \cdot \epsilon_{ik}\epsilon_{jm}\epsilon_{ln}$	1068	8	3,4	10
43*d*	$L^iL^jL^k\tilde{L}^l\bar{u}^\dagger\bar{d}H^m\tilde{H}^n \cdot \epsilon_{ik}\epsilon_{jl}\epsilon_{mn}$	1068	8	3,4	10
44*a*	$L^iL^j\bar{e}\bar{e}^\dagger Q^k\tilde{Q}^lH^mH^n \cdot \epsilon_{il}\epsilon_{jm}\epsilon_{kn}$	1571	155	2	$2 \cdot 10^7$
44*b*	$L^iL^j\bar{e}\bar{e}^\dagger Q^k\tilde{Q}^lH^mH^n \cdot \epsilon_{im}\epsilon_{jn}\epsilon_{kl}$	1016	91	2	$2 \cdot 10^7$
44*c*	$L^iL^j\bar{e}\bar{e}^\dagger Q^k\tilde{Q}^lH^mH^n \cdot \epsilon_{ij}\epsilon_{km}\epsilon_{ln}$	1137	2	3	$6 \cdot 10^4$
44*d*	$L^iL^j\bar{e}\bar{e}^\dagger Q^k\tilde{Q}^lH^mH^n \cdot \epsilon_{ik}\epsilon_{jm}\epsilon_{ln}$	1765	133	2	$2 \cdot 10^7$
45	$L^iL^j\bar{e}\bar{e}^\dagger\bar{d}\bar{d}^\dagger H^kH^l \cdot \epsilon_{ik}\epsilon_{jl}$	1016	81	2	$2 \cdot 10^7$
46	$L^iL^j\bar{e}\bar{e}^\dagger\bar{u}\bar{u}^\dagger H^kH^l \cdot \epsilon_{ik}\epsilon_{jl}$	1016	49	2	$2 \cdot 10^7$
47*a*	$L^iL^jQ^kQ^l\tilde{Q}^m\tilde{Q}^nH^pH^q \cdot \epsilon_{im}\epsilon_{jn}\epsilon_{kp}\epsilon_{lq}$	1013	236	2	$2 \cdot 10^7$
47*b*	$L^iL^jQ^kQ^l\tilde{Q}^m\tilde{Q}^nH^pH^q \cdot \epsilon_{im}\epsilon_{jp}\epsilon_{kn}\epsilon_{lq}$	2253	423	2	$2 \cdot 10^7$
47*c*	$L^iL^jQ^kQ^l\tilde{Q}^m\tilde{Q}^nH^pH^q \cdot \epsilon_{ip}\epsilon_{jq}\epsilon_{km}\epsilon_{ln}$	1007	200	2	$2 \cdot 10^7$
47*d*	$L^iL^jQ^kQ^l\tilde{Q}^m\tilde{Q}^nH^pH^q \cdot \epsilon_{il}\epsilon_{jn}\epsilon_{kp}\epsilon_{mq}$	2838	690	2	$2 \cdot 10^7$
47*e*	$L^iL^jQ^kQ^l\tilde{Q}^m\tilde{Q}^nH^pH^q \cdot \epsilon_{in}\epsilon_{jp}\epsilon_{kl}\epsilon_{mq}$	1730	387	2	$2 \cdot 10^7$
47*f*	$L^iL^jQ^kQ^l\tilde{Q}^m\tilde{Q}^nH^pH^q \cdot \epsilon_{ij}\epsilon_{kn}\epsilon_{lp}\epsilon_{mq}$	1702	60	3	$6 \cdot 10^4$
47*g*	$L^iL^jQ^kQ^l\tilde{Q}^m\tilde{Q}^nH^pH^q \cdot \epsilon_{il}\epsilon_{jp}\epsilon_{kn}\epsilon_{mq}$	2796	530	2	$2 \cdot 10^7$
47*h*	$L^iL^jQ^kQ^l\tilde{Q}^m\tilde{Q}^nH^pH^q \cdot \epsilon_{ij}\epsilon_{kp}\epsilon_{lq}\epsilon_{mn}$	924	46	3	$6 \cdot 10^4$
47*i*	$L^iL^jQ^kQ^l\tilde{Q}^m\tilde{Q}^nH^pH^q \cdot \epsilon_{il}\epsilon_{jp}\epsilon_{kq}\epsilon_{mn}$	2078	369	2	$2 \cdot 10^7$
47*j*	$L^iL^jQ^kQ^l\tilde{Q}^m\tilde{Q}^nH^pH^q \cdot \epsilon_{ip}\epsilon_{jq}\epsilon_{kl}\epsilon_{mn}$	902	183	2	$2 \cdot 10^7$
47*k*	$L^iL^jQ^kQ^l\tilde{Q}^m\tilde{Q}^nH^pH^q \cdot \epsilon_{ik}\epsilon_{jl}\epsilon_{mp}\epsilon_{nq}$	1203	258	2	$2 \cdot 10^7$
47*l*	$L^iL^jQ^kQ^l\tilde{Q}^m\tilde{Q}^nH^pH^q \cdot \epsilon_{ij}\epsilon_{kl}\epsilon_{mp}\epsilon_{nq}$	814	46	3	$6 \cdot 10^4$
48	$L^iL^j\bar{d}\bar{d}\bar{d}^\dagger\bar{d}^\dagger H^kH^l \cdot \epsilon_{ik}\epsilon_{jl}$	921	125	2	$2 \cdot 10^7$
49	$L^iL^j\bar{u}\bar{u}^\dagger\bar{d}\bar{d}^\dagger H^kH^l \cdot \epsilon_{ik}\epsilon_{jl}$	2086	384	2	$2 \cdot 10^7$
50*a*	$L^iL^j\bar{u}^\dagger\bar{d}\bar{d}\bar{d}^\dagger H^k\tilde{H}^l \cdot \epsilon_{ik}\epsilon_{jl}$	2285	68	3,4	10
50*b*	$\mathcal{O}_{17} \cdot H^i\tilde{H}^j \cdot \epsilon_{ij}$	1523	52	3,4	10
51	$L^iL^j\bar{u}\bar{u}\bar{u}^\dagger\bar{u}^\dagger H^kH^l \cdot \epsilon_{ik}\epsilon_{jl}$	921	225	2	$2 \cdot 10^7$
52*a*	$L^iL^j\bar{u}\bar{u}^\dagger\bar{u}^\dagger\bar{d}H^k\tilde{H}^l \cdot \epsilon_{ik}\epsilon_{jl}$	2896	170	3,4	10
52*b*	$\mathcal{O}_{18} \cdot H^i\tilde{H}^j \cdot \epsilon_{ij}$	1872	94	3,4	10

Labels	Operator	Models	Filtered	Loops	Λ [TeV]
53	$L^i L^j \bar{u}^\dagger \bar{u}^\dagger \bar{d}\bar{d} \tilde{H}^k \tilde{H}^l \cdot \epsilon_{ik}\epsilon_{jl}$	939	162	4,5,6	$2 \cdot 10^{-1}$
54a	$L^i \bar{e}^\dagger Q^j Q^k \tilde{Q}^l \bar{d} H^m H^n \cdot \epsilon_{il}\epsilon_{jm}\epsilon_{kn}$	2203	92	3	$4 \cdot 10^1$
54b	$L^i \bar{e}^\dagger Q^j Q^k \tilde{Q}^l \bar{d} H^m H^n \cdot \epsilon_{im}\epsilon_{jl}\epsilon_{kn}$	3393	89	3	$4 \cdot 10^1$
54c	$L^i \bar{e}^\dagger Q^j Q^k \tilde{Q}^l \bar{d} H^m H^n \cdot \epsilon_{im}\epsilon_{jk}\epsilon_{ln}$	2456	30	3	$4 \cdot 10^1$
54d	$L^i \bar{e}^\dagger Q^j Q^k \tilde{Q}^l \bar{d} H^m H^n \cdot \epsilon_{ik}\epsilon_{jm}\epsilon_{ln}$	3835	100	3	$4 \cdot 10^1$
55a	$L^i \bar{e}^\dagger Q^j \tilde{Q}^k \tilde{Q}^l \bar{u}^\dagger H^m H^n \cdot \epsilon_{il}\epsilon_{jm}\epsilon_{kn}$	3478	143	3	$2 \cdot 10^3$
55b	$L^i \bar{e}^\dagger Q^j \tilde{Q}^k \tilde{Q}^l \bar{u}^\dagger H^m H^n \cdot \epsilon_{im}\epsilon_{jl}\epsilon_{kn}$	3493	144	3	$2 \cdot 10^3$
55c	$L^i \bar{e}^\dagger Q^j \tilde{Q}^k \tilde{Q}^l \bar{u}^\dagger H^m H^n \cdot \epsilon_{im}\epsilon_{jn}\epsilon_{kl}$	2049	86	3	$2 \cdot 10^3$
55d	$L^i \bar{e}^\dagger Q^j \tilde{Q}^k \tilde{Q}^l \bar{u}^\dagger H^m H^n \cdot \epsilon_{ij}\epsilon_{km}\epsilon_{ln}$	2156	106	3	$2 \cdot 10^3$
56	$L^i \bar{e}^\dagger Q^j \bar{d}\bar{d}\bar{d}^\dagger H^k H^l \cdot \epsilon_{ik}\epsilon_{jl}$	2273	252	3	$4 \cdot 10^1$
57	$L^i \bar{e}^\dagger \tilde{Q}^j \bar{u}^\dagger \bar{d}\bar{d}^\dagger H^k H^l \cdot \epsilon_{ik}\epsilon_{jl}$	4251	481	3	$2 \cdot 10^3$
58	$L^i \bar{e}^\dagger \tilde{Q}^j \bar{u}\bar{u}^\dagger \bar{u}^\dagger H^k H^l \cdot \epsilon_{ik}\epsilon_{jl}$	2408	183	3	$2 \cdot 10^3$
59a	$L^i \bar{e}^\dagger Q^j \bar{u}^\dagger \bar{d}\bar{d} H^k \tilde{H}^l \cdot \epsilon_{ik}\epsilon_{jl}$	2638	65	3,4,5	$2 \cdot 10^{-1}$
59b	$\mathcal{O}_{19} \cdot H^i \tilde{H}^j \cdot \epsilon_{ij}$	2583	65	3,4,5	$2 \cdot 10^{-1}$
59c	$\mathcal{O}_8 \cdot Q^i \bar{d} \tilde{H}^j \cdot \epsilon_{ij}$	2639	42	4,5,6	$6 \cdot 10^{-2}$
60a	$L^i \bar{e}^\dagger \tilde{Q}^j \bar{u}^\dagger \bar{u}^\dagger \bar{d} H^k \tilde{H}^l \cdot \epsilon_{il}\epsilon_{jk}$	2687	35	4,5	$1 \cdot 10^{-1}$
60b	$\mathcal{O}_8 \cdot \tilde{Q}^i \bar{u}^\dagger \tilde{H}^j \cdot \epsilon_{ij}$	2687	121	3,4,5	$4 \cdot 10^{-1}$
60c	$\mathcal{O}_{20} \cdot H^i \tilde{H}^j \cdot \epsilon_{ij}$	2687	104	3,4,5	$4 \cdot 10^{-1}$
61a	$\mathcal{O}_1 \cdot L^i \bar{e} \tilde{H}^j \cdot \epsilon_{ij}$	382	0	1,2	$2 \cdot 10^5$
61b	$\mathcal{O}_2 \cdot H^i \tilde{H}^j \cdot \epsilon_{ij}$	408	0	1,2	$2 \cdot 10^5$
62a	$L^i L^j L^k L^l \bar{e}\bar{e} H^m \tilde{H}^n \cdot \epsilon_{il}\epsilon_{jm}\epsilon_{kn}$	1820	0	2,3	$2 \cdot 10^1$
62b	$\mathcal{O}_9 \cdot H^i \tilde{H}^j \cdot \epsilon_{ij}$	830	1	2,3	$2 \cdot 10^1$
63a	$L^i L^j L^k \bar{e} Q^l \bar{d} H^m \tilde{H}^n \cdot \epsilon_{ik}\epsilon_{jn}\epsilon_{lm}$	4619	12	3	$4 \cdot 10^1$
63b	$L^i L^j L^k \bar{e} Q^l \bar{d} H^m \tilde{H}^n \cdot \epsilon_{il}\epsilon_{jm}\epsilon_{kn}$	7216	77	2,3	$4 \cdot 10^1$
63c	$\mathcal{O}_2 \cdot Q^i \bar{d} \tilde{H}^j \cdot \epsilon_{ij}$	4621	49	2,3	$4 \cdot 10^1$
63d	$\mathcal{O}_{10} \cdot H^i \tilde{H}^j \cdot \epsilon_{ij}$	4590	45	2,3	$4 \cdot 10^1$
64a	$L^i L^j L^k \bar{e} \tilde{Q}^l \bar{u}^\dagger H^m \tilde{H}^n \cdot \epsilon_{il}\epsilon_{jm}\epsilon_{kn}$	1370	0	3	$2 \cdot 10^3$
64b	$L^i L^j L^k \bar{e} \tilde{Q}^l \bar{u}^\dagger H^m \tilde{H}^n \cdot \epsilon_{ik}\epsilon_{jn}\epsilon_{lm}$	1050	0	3	$2 \cdot 10^3$
64c	$\mathcal{O}_2 \cdot \tilde{Q}^i \bar{u}^\dagger \tilde{H}^j \cdot \epsilon_{ij}$	1049	0	2,3	$2 \cdot 10^3$
64d	$\mathcal{O}_{13} \cdot H^i \tilde{H}^j \cdot \epsilon_{ij}$	1008	0	3	$2 \cdot 10^3$
65a	$L^i L^j \bar{e}\bar{e}^\dagger \bar{u}^\dagger \bar{d} H^k \tilde{H}^l \cdot \epsilon_{ik}\epsilon_{jl}$	1925	17	3,4	10
65b	$\mathcal{O}_{16} \cdot H^i \tilde{H}^j \cdot \epsilon_{ij}$	1259	11	3,4	10
71	$\mathcal{O}_1 \cdot Q^i \bar{u} H^j \cdot \epsilon_{ij}$	396	9	2	$2 \cdot 10^7$
75	$\mathcal{O}_8 \cdot Q^i \bar{u} H^j \cdot \epsilon_{ij}$	3951	84	3	$4 \cdot 10^1$
76	$\bar{e}^\dagger \bar{e}^\dagger \bar{u}^\dagger \bar{u}^\dagger \bar{d}\bar{d}$	16	4	4,5,6	$2 \cdot 10^{-2}$
77	$\mathcal{O}_1 \cdot \tilde{L}^i \bar{e}^\dagger H^j \cdot \epsilon_{ij}$	156	0	2	$2 \cdot 10^5$
78	$\mathcal{O}_1 \cdot \tilde{Q}^i \bar{d}^\dagger H^j \cdot \epsilon_{ij}$	156	0	2	$6 \cdot 10^5$
1′	$\mathcal{O}_1 \cdot \tilde{H}^i H^j \cdot \epsilon_{ij}$	53	1	0,1	$4 \cdot 10^9$

Labels	Operator	Models	Filtered	Loops	Λ [TeV]
$8'$	$\mathcal{O}_8 \cdot \tilde{H}^i H^j \cdot \epsilon_{ij}$	301	4	2,3,4	1
$1''$	$\mathcal{O}_1 \cdot \tilde{H}^i H^j \tilde{H}^k H^l \cdot \epsilon_{ij}\epsilon_{kl}$	1893	6	0,1,2	$2 \cdot 10^7$
$1'''$	$\mathcal{O}_1 \cdot \tilde{H}^i H^j \tilde{H}^k H^l \tilde{H}^m H^n \cdot \epsilon_{ij}\epsilon_{kl}\epsilon_{mn}$	—	2	0,1,2	$2 \cdot 10^7$
$7'$	$\mathcal{O}_7 \cdot \tilde{H}^i H^j \cdot \epsilon_{ij}$	24951	374	2,3	$2 \cdot 10^3$
$8''$	$\mathcal{O}_8 \cdot \tilde{H}^i H^j \tilde{H}^k H^l \cdot \epsilon_{ij}\epsilon_{kl}$	19229	197	2,3,4,5	$7 \cdot 10^{-1}$
$71'$	$\mathcal{O}_{71} \cdot \tilde{H}^i H^j \cdot \epsilon_{ij}$	39331	446	2,3	$2 \cdot 10^5$
$76'$	$\mathcal{O}_{76} \cdot \tilde{H}^i H^j \cdot \epsilon_{ij}$	679	209	4,5,6,7	$4 \cdot 10^{-2}$
$77'$	$\mathcal{O}_{77} \cdot \tilde{H}^i H^j \cdot \epsilon_{ij}$	14598	0	1,2,3	$2 \cdot 10^3$
$78'$	$\mathcal{O}_{78} \cdot \tilde{H}^i H^j \cdot \epsilon_{ij}$	14644	1	2,3	$4 \cdot 10^3$
$79a$	$\mathcal{O}_{61a} \cdot \tilde{H}^i H^j \cdot \epsilon_{ij}$	31791	14	1,2,3	$2 \cdot 10^3$
$79b$	$\mathcal{O}_2 \cdot \tilde{H}^i H^j \tilde{H}^k H^l \cdot \epsilon_{ij}\epsilon_{kl}$	23931	14	1,2,3	$2 \cdot 10^3$
$80a$	$\mathcal{O}_{5a} \cdot \tilde{H}^i H^j \cdot \epsilon_{ij}$	72694	154	2,3	$4 \cdot 10^3$
$80b$	$\mathcal{O}_{5b} \cdot \tilde{H}^i H^j \cdot \epsilon_{ij}$	49108	371	1,2,3	$4 \cdot 10^3$
$80c$	$\mathcal{O}_{3a} \cdot \tilde{H}^i H^j \tilde{H}^k H^l \cdot \epsilon_{ij}\epsilon_{kl}$	31569	16	2,3,4	$1 \cdot 10^1$
$80d$	$\mathcal{O}_{3b} \cdot \tilde{H}^i H^j \tilde{H}^k H^l \cdot \epsilon_{ij}\epsilon_{kl}$	49505	367	1,2,3	$4 \cdot 10^3$
$81a$	$\mathcal{O}_{6a} \cdot \tilde{H}^i H^j \cdot \epsilon_{ij}$	26174	95	2,3	$2 \cdot 10^5$
$81b$	$\mathcal{O}_{6b} \cdot \tilde{H}^i H^j \cdot \epsilon_{ij}$	17298	18	1,2,3	$2 \cdot 10^5$
$81c$	$\mathcal{O}_{4a} \cdot \tilde{H}^i H^j \tilde{H}^k H^l \cdot \epsilon_{ij}\epsilon_{kl}$	15575	18	1,2,3	$2 \cdot 10^5$
$81d$	$\mathcal{O}_{4b} \cdot \tilde{H}^i H^j \tilde{H}^k H^l \cdot \epsilon_{ij}\epsilon_{kl}$	12400	41	2,3,4	$4 \cdot 10^2$
82	$L^i \tilde{L}^j \bar{e}^\dagger \bar{e}^\dagger \bar{u}^\dagger \bar{d} H^k H^l \cdot \epsilon_{ik}\epsilon_{jl}$	1151	56	3,4,5	$2 \cdot 10^{-1}$
$D1$	$(DL)^i L^j \bar{u}^\dagger \bar{d} \cdot \epsilon_{ij}$	—	—	3,4,5	$2 \cdot 10^{-1}$
$D2a$	$(DL)^i L^j (DH)^k H^l \cdot \epsilon_{ij}\epsilon_{kl}$	1	0	1	$2 \cdot 10^9$
$D2b$	$(DL)^i L^j (DH)^k H^l \cdot \epsilon_{il}\epsilon_{jk}$	3	3	0	$6 \cdot 10^{11}$
$D2c$	$(DL)^i L^j (DH)^k H^l \cdot \epsilon_{ik}\epsilon_{jl}$	3	3	0	$6 \cdot 10^{11}$
$D3$	$L^i \bar{e}^\dagger H^j H^k (DH)^l \cdot \epsilon_{ik}\epsilon_{jl}$	4	0	1	$4 \cdot 10^7$
$D4a$	$L^i L^j (DL)^k (D\bar{e}) H^l \cdot \epsilon_{ik}\epsilon_{jl}$	8	2	1	$4 \cdot 10^7$
$D4b$	$L^i L^j (DL)^k (D\bar{e}) H^l \cdot \epsilon_{ij}\epsilon_{kl}$	8	2	1	$4 \cdot 10^7$
$D5a$	$L^i L^j (DL)^k \tilde{L}^l H^m H^n \cdot \epsilon_{il}\epsilon_{jm}\epsilon_{kn}$	21	0	1	$4 \cdot 10^9$
$D5b$	$L^i L^j (DL)^k \tilde{L}^l H^m H^n \cdot \epsilon_{ik}\epsilon_{jm}\epsilon_{ln}$	30	4	1	$4 \cdot 10^9$
$D5c$	$L^i L^j (DL)^k \tilde{L}^l H^m H^n \cdot \epsilon_{ij}\epsilon_{km}\epsilon_{ln}$	30	4	1	$4 \cdot 10^9$
$D5d$	$L^i L^j (DL)^k \tilde{L}^l H^m H^n \cdot \epsilon_{im}\epsilon_{jn}\epsilon_{kl}$	21	0	1	$4 \cdot 10^9$
$D6a$	$L^i L^j \bar{e}\bar{e}^\dagger (DH)^k H^l \cdot \epsilon_{ik}\epsilon_{jl}$	30	2	1	$4 \cdot 10^9$
$D6b$	$L^i L^j \bar{e}\bar{e}^\dagger (DH)^k H^l \cdot \epsilon_{ij}\epsilon_{kl}$	16	0	2	$10 \cdot 10^6$
$D7a$	$(DL)^i L^j Q^k (D\bar{d}) H^l \cdot \epsilon_{ij}\epsilon_{kl}$	9	2	2	$2 \cdot 10^5$
$D7b$	$(DL)^i L^j Q^k (D\bar{d}) H^l \cdot \epsilon_{ik}\epsilon_{jl}$	14	5	1	$9 \cdot 10^7$
$D7c$	$(DL)^i L^j Q^k (D\bar{d}) H^l \cdot \epsilon_{il}\epsilon_{jk}$	14	5	1	$9 \cdot 10^7$
$D8a$	$L^i L^j Q^k \tilde{Q}^l (DH)^m H^n \cdot \epsilon_{in}\epsilon_{jk}\epsilon_{lm}$	53	11	1	$4 \cdot 10^9$
$D8b$	$L^i L^j Q^k \tilde{Q}^l (DH)^m H^n \cdot \epsilon_{in}\epsilon_{jl}\epsilon_{km}$	44	6	1	$4 \cdot 10^9$

Labels	Operator	Models	Filtered	Loops	Λ [TeV]
$D8c$	$L^iL^jQ^k\tilde{Q}^l(DH)^mH^n \cdot \epsilon_{ik}\epsilon_{jl}\epsilon_{mn}$	25	0	2	$10 \cdot 10^6$
$D8d$	$L^iL^jQ^k\tilde{Q}^l(DH)^mH^n \cdot \epsilon_{im}\epsilon_{jk}\epsilon_{ln}$	53	11	1	$4 \cdot 10^9$
$D8e$	$L^iL^jQ^k\tilde{Q}^l(DH)^mH^n \cdot \epsilon_{im}\epsilon_{jl}\epsilon_{kn}$	44	6	1	$4 \cdot 10^9$
$D8f$	$L^iL^jQ^k\tilde{Q}^l(DH)^mH^n \cdot \epsilon_{im}\epsilon_{jn}\epsilon_{kl}$	30	5	1	$4 \cdot 10^9$
$D8g$	$L^iL^jQ^k\tilde{Q}^l(DH)^mH^n \cdot \epsilon_{ij}\epsilon_{km}\epsilon_{ln}$	35	7	2	$10 \cdot 10^6$
$D8h$	$L^iL^jQ^k\tilde{Q}^l(DH)^mH^n \cdot \epsilon_{ij}\epsilon_{kn}\epsilon_{lm}$	35	7	2	$10 \cdot 10^6$
$D8i$	$L^iL^jQ^k\tilde{Q}^l(DH)^mH^n \cdot \epsilon_{ij}\epsilon_{kl}\epsilon_{mn}$	16	3	2	$10 \cdot 10^6$
$D9a$	$L^iL^j\bar{d}\bar{d}^\dagger(DH)^kH^l \cdot \epsilon_{ik}\epsilon_{jl}$	30	5	1	$4 \cdot 10^9$
$D9b$	$L^iL^j\bar{d}\bar{d}^\dagger(DH)^kH^l \cdot \epsilon_{ij}\epsilon_{kl}$	16	4	2	$10 \cdot 10^6$
$D10a$	$(DL)^iL^j\bar{u}^\dagger\bar{d}H^k\tilde{H}^l \cdot \epsilon_{il}\epsilon_{jk}$	56	13	2,3	$1 \cdot 10^3$
$D10b$	$(DL)^iL^j\bar{u}^\dagger\bar{d}H^k\tilde{H}^l \cdot \epsilon_{ij}\epsilon_{kl}$	36	7	2,3	$1 \cdot 10^3$
$D10c$	$(DL)^iL^j\bar{u}^\dagger\bar{d}H^k\tilde{H}^l \cdot \epsilon_{ik}\epsilon_{jl}$	56	13	2,3	$1 \cdot 10^3$
$D11$	$(DL)^iL^j(D\bar{u}^\dagger)(D\bar{d}) \cdot \epsilon_{ij}$	—	—	2,3	$1 \cdot 10^3$
$D12a$	$L^iL^j\bar{u}\bar{u}^\dagger(DH)^kH^l \cdot \epsilon_{ik}\epsilon_{jl}$	30	5	1	$4 \cdot 10^9$
$D12b$	$L^iL^j\bar{u}\bar{u}^\dagger(DH)^kH^l \cdot \epsilon_{ij}\epsilon_{kl}$	16	4	2	$10 \cdot 10^6$
$D13a$	$(DL)^iL^j\tilde{Q}^k(D\bar{u}^\dagger)H^l \cdot \epsilon_{ij}\epsilon_{kl}$	4	2	2	$10 \cdot 10^6$
$D13b$	$(DL)^iL^j\tilde{Q}^k(D\bar{u}^\dagger)H^l \cdot \epsilon_{ik}\epsilon_{jl}$	5	0	1	$4 \cdot 10^9$
$D14a$	$L^i\bar{e}^\dagger Q^j\bar{d}(DH)^kH^l \cdot \epsilon_{ik}\epsilon_{jl}$	53	0	2	$6 \cdot 10^3$
$D14b$	$L^i\bar{e}^\dagger Q^j\bar{d}(DH)^kH^l \cdot \epsilon_{il}\epsilon_{jk}$	53	0	2	$6 \cdot 10^3$
$D14c$	$L^i\bar{e}^\dagger Q^j\bar{d}(DH)^kH^l \cdot \epsilon_{ij}\epsilon_{kl}$	27	0	2	$6 \cdot 10^3$
$D15$	$(DL)^i\bar{e}^\dagger(D\bar{u}^\dagger)\bar{d}H^j \cdot \epsilon_{ij}$	5	1	2,3	$2 \cdot 10^1$
$D16a$	$L^i\bar{e}^\dagger\tilde{Q}^j\bar{u}^\dagger(DH)^kH^l \cdot \epsilon_{ik}\epsilon_{jl}$	58	8	2	$2 \cdot 10^5$
$D16b$	$L^i\bar{e}^\dagger\tilde{Q}^j\bar{u}^\dagger(DH)^kH^l \cdot \epsilon_{il}\epsilon_{jk}$	58	8	2	$2 \cdot 10^5$
$D16c$	$L^i\bar{e}^\dagger\tilde{Q}^j\bar{u}^\dagger(DH)^kH^l \cdot \epsilon_{ij}\epsilon_{kl}$	27	4	2	$2 \cdot 10^5$
$D17$	$\bar{e}^\dagger\bar{e}^\dagger\bar{u}^\dagger\bar{d}(DH)^iH^j \cdot \epsilon_{ij}$	16	7	3,4	$2 \cdot 10^{-1}$
$D18a$	$(DL)^iL^jH^kH^l(DH)^m\tilde{H}^n \cdot \epsilon_{ik}\epsilon_{jm}\epsilon_{ln}$	53	1	0,1	$4 \cdot 10^9$
$D18b$	$(DL)^iL^jH^kH^l(DH)^m\tilde{H}^n \cdot \epsilon_{ik}\epsilon_{jl}\epsilon_{mn}$	53	1	0,1	$4 \cdot 10^9$
$D18c$	$(DL)^iL^jH^kH^l(DH)^m\tilde{H}^n \cdot \epsilon_{im}\epsilon_{jl}\epsilon_{kn}$	53	1	0,1	$4 \cdot 10^9$
$D18d$	$(DL)^iL^jH^kH^l(DH)^m\tilde{H}^n \cdot \epsilon_{ij}\epsilon_{km}\epsilon_{ln}$	24	1	1,2	$10 \cdot 10^6$
$D18e$	$(DL)^iL^jH^kH^l(DH)^m\tilde{H}^n \cdot \epsilon_{in}\epsilon_{jl}\epsilon_{km}$	34	0	1	$4 \cdot 10^9$
$D18f$	$(DL)^iL^jH^kH^l(DH)^m\tilde{H}^n \cdot \epsilon_{il}\epsilon_{jn}\epsilon_{km}$	34	0	1	$4 \cdot 10^9$
$D19a$	$(D^2L)^iL^j(D^2H)^kH^l \cdot \epsilon_{ij}\epsilon_{kl}$	1	0	1	$2 \cdot 10^9$
$D19b$	$(D^2L)^iL^j(D^2H)^kH^l \cdot \epsilon_{il}\epsilon_{jk}$	3	3	0	$6 \cdot 10^{11}$
$D19c$	$(D^2L)^iL^j(D^2H)^kH^l \cdot \epsilon_{ik}\epsilon_{jl}$	3	3	0	$6 \cdot 10^{11}$
$D20$	$L^i\bar{e}^\dagger H^jH^kH^l(DH)^m\tilde{H}^n \cdot \epsilon_{il}\epsilon_{jm}\epsilon_{kn}$	129	0	1,2	$2 \cdot 10^5$
$D21$	$(DL)^i(D\bar{e}^\dagger)H^jH^k(DH)^l \cdot \epsilon_{ik}\epsilon_{jl}$	2	0	1	$4 \cdot 10^7$
$D22$	$\bar{e}^\dagger\bar{e}^\dagger(DH)^i(DH)^jH^kH^l \cdot \epsilon_{ik}\epsilon_{jl}$	9	0	2	$3 \cdot 10^3$

Definition of Symbols and Acronyms

D

DFT density functional theory

L

lipsum Lorem Ipsum, a special type of fudge
  dolor No idea why
  ibit Sounds right, doesn't it?

P

π (π) Greek letter pi, Π does this work?

R

radial distribution function ($g(r)$)
RDF radial distribution function

Index

Bibliography

[1] R. Foot and J. Gargalionis, *Explaining the 750 GeV diphoton excess with a colored scalar charged under a new confining gauge interaction*, *Phys. Rev. D* **94** (2016), no. 1 011703, [arXiv:1604.06180].

[2] Y. Cai, J. Gargalionis, M. A. Schmidt, and R. R. Volkas, *Reconsidering the One Leptoquark solution: flavor anomalies and neutrino mass*, *JHEP* **10** (2017) 047, [arXiv:1704.05849].

[3] I. Bigaran, J. Gargalionis, and R. R. Volkas, *A near-minimal leptoquark model for reconciling flavour anomalies and generating radiative neutrino masses*, *JHEP* **10** (2019) 106, [arXiv:1906.01870].

[4] J. Gargalionis, I. Popa-Mateiu, and R. R. Volkas, *Radiative neutrino mass model from a mass dimension-11 $\Delta L = 2$ effective operator*, *JHEP* **03** (2020) 150, [arXiv:1912.12386].

[5] J. Gargalionis and R. R. Volkas, *Exploding operators for Majorana neutrino masses and beyond*, arXiv:2009.13537.

[6] I. Esteban, M. Gonzalez-Garcia, M. Maltoni, T. Schwetz, and A. Zhou, *The fate of hints: updated global analysis of three-flavor neutrino oscillations*, arXiv:2007.14792.

[7] "Nufit 5.0 (2020)." www.nu-fit.org. Accessed: 2020-09-03.

[8] **GERDA** Collaboration, M. Agostini et al., *Probing Majorana neutrinos with double-β decay*, *Science* **365** (2019) 1445, [arXiv:1909.02726].

[9] **DARWIN** Collaboration, F. Agostini et al., *Sensitivity of the DARWIN observatory to the neutrinoless double beta decay of ^{136}Xe*, arXiv:2003.13407.

[10] A. Bharucha, D. M. Straub, and R. Zwicky, *$B \to V\ell^+\ell^-$ in the Standard Model from light-cone sum rules*, *JHEP* **08** (2016) 098, [arXiv:1503.05534].

[11] W. Altmannshofer and D. M. Straub, *New physics in $b \to s$ transitions after LHC run 1*, *Eur. Phys. J. C* **75** (2015), no. 8 382, [arXiv:1411.3161].

[12] R. R. Horgan, Z. Liu, S. Meinel, and M. Wingate, *Calculation of $B^0 \to K^{*0}\mu^+\mu^-$ and $B_s^0 \to \phi\mu^+\mu^-$ observables using form factors from lattice QCD*, *Phys. Rev. Lett.* **112** (2014) 212003, [arXiv:1310.3887].

[13] T. Blake, M. Gersabeck, L. Hofer, S. Jäger, Z. Liu, and R. Zwicky, *Round table: Flavour anomalies in b ⟶ sl+l– processes*, *EPJ Web Conf.* **137** (2017) 01001, [arXiv:1703.10005].

[14] J. Aebischer, W. Altmannshofer, D. Guadagnoli, M. Reboud, P. Stangl, and D. M. Straub, *B-decay discrepancies after Moriond 2019*, *Eur. Phys. J. C* **80** (2020), no. 3 252, [arXiv:1903.10434].

[15] **LHCb** Collaboration, R. Aaij et al., *Search for lepton-universality violation in $B^+ \to K^+\ell^+\ell^-$ decays*, *Phys. Rev. Lett.* **122** (2019), no. 19 191801, [arXiv:1903.09252].

[16] **Belle** Collaboration, A. Abdesselam et al., *Test of lepton flavor universality in $B \to K\ell^+\ell^-$ decays*, arXiv:1908.01848.

[17] **BaBar** Collaboration, J. Lees et al., *Measurement of Branching Fractions and Rate Asymmetries in the Rare Decays $B \to K^{(*)}l^+l^-$*, *Phys. Rev. D* **86** (2012) 032012, [arXiv:1204.3933].

[18] **Belle** Collaboration, A. Abdesselam et al., *Test of lepton flavor universality in $B \to K^*\ell^+\ell^-$ decays at Belle*, arXiv:1904.02440.

[19] **LHCb** Collaboration, R. Aaij et al., *Test of lepton universality with $B^0 \to K^{*0}\ell^+\ell^-$ decays*, *JHEP* **08** (2017) 055, [arXiv:1705.05802].

[20] P. Koppenburg, Z. Dolezal, and M. Smizanska, *Rare decays of b hadrons*, *Scholarpedia* **11** (2016) 32643, [arXiv:1606.00999].

[21] **HFLAV** Collaboration, Y. S. Amhis et al., *Averages of b-hadron, c-hadron, and τ-lepton properties as of 2018*, arXiv:1909.12524. updated results and plots available at https://hflav.web.cern.ch/.

[22] H. K. Dreiner, H. E. Haber, and S. P. Martin, *Two-component spinor techniques and Feynman rules for quantum field theory and supersymmetry*, *Phys. Rept.* **494** (2010) 1–196, [arXiv:0812.1594].

[23] J. de Blas, J. C. Criado, M. Perez-Victoria, and J. Santiago, *Effective description of general extensions of the Standard Model: the complete tree-level dictionary*, *JHEP* **03** (2018) 109, [arXiv:1711.10391].

[24] D. Aristizabal Sierra, A. Degee, L. Dorame, and M. Hirsch, *Systematic classification of two-loop realizations of the Weinberg operator*, *JHEP* **03** (2015) 040, [arXiv:1411.7038].

[25] M. Gustafsson, J. M. No, and M. A. Rivera, *Predictive Model for Radiatively Induced Neutrino Masses and Mixings with Dark Matter*, *Phys. Rev. Lett.* **110** (2013), no. 21 211802, [arXiv:1212.4806]. [Erratum: Phys.Rev.Lett. 112, 259902 (2014)].

[26] R. Cepedello, R. M. Fonseca, and M. Hirsch, *Systematic classification of three-loop realizations of the Weinberg operator*, *JHEP* **10** (2018) 197, [arXiv:1807.00629].

[27] W. Buchmuller and D. Wyler, *Effective Lagrangian Analysis of New Interactions and Flavor Conservation*, *Nucl. Phys. B* **268** (1986) 621–653.

[28] B. Grzadkowski, M. Iskrzynski, M. Misiak, and J. Rosiek, *Dimension-Six Terms in the Standard Model Lagrangian*, *JHEP* **10** (2010) 085, [arXiv:1008.4884].

[29] K. S. Babu and J. Julio, *Two-Loop Neutrino Mass Generation through Leptoquarks*, *Nucl. Phys.* **B841** (2010) 130–156, [arXiv:1006.1092].

[30] S. Glashow, *Partial Symmetries of Weak Interactions*, *Nucl. Phys.* **22** (1961) 579–588.

[31] S. Weinberg, *A Model of Leptons*, *Phys. Rev. Lett.* **19** (1967) 1264–1266.

[32] A. Salam, *Weak and Electromagnetic Interactions*, *Conf. Proc. C* **680519** (1968) 367–377.

[33] G. 't Hooft, *Renormalization of Massless Yang-Mills Fields*, *Nucl. Phys. B* **33** (1971) 173–199.

[34] S. Glashow, J. Iliopoulos, and L. Maiani, *Weak Interactions with Lepton-Hadron Symmetry*, *Phys. Rev. D* **2** (1970) 1285–1292.

[35] D. J. Gross and F. Wilczek, *Ultraviolet Behavior of Nonabelian Gauge Theories*, *Phys. Rev. Lett.* **30** (1973) 1343–1346.

[36] B. Pontecorvo, *Mesonium and anti-mesonium*, *Sov. Phys. JETP* **6** (1957) 429.

[37] Z. Maki, M. Nakagawa, and S. Sakata, *Remarks on the unified model of elementary particles*, *Prog. Theor. Phys.* **28** (1962) 870–880.

[38] J. N. Bahcall and R. K. Ulrich, *Solar models, neutrino experiments, and helioseismology*, *Rev. Mod. Phys.* **60** (Apr, 1988) 297–372.

[39] S. Turck-Chieze, S. Cahen, M. Casse, and C. Doom, *Revisiting the Standard Solar Model*, *APJ* **335** (Dec., 1988) 415.

[40] J. N. Bahcall and M. H. Pinsonneault, *Standard solar models, with and without helium diffusion, and the solar neutrino problem*, *Rev. Mod. Phys.* **64** (Oct, 1992) 885–926.

[41] J. N. Bahcall, M. H. Pinsonneault, and G. J. Wasserburg, *Solar models with helium and heavy-element diffusion*, *Rev. Mod. Phys.* **67** (Oct, 1995) 781–808.

[42] D. R. Morrison, *Review of solar models and solar neutrino experiments*, *Part. World* **3** (1992), no. 1 30–39.

[43] R. Davis, *Solar neutrinos. ii. experimental*, *Phys. Rev. Lett.* **12** (Mar, 1964) 303–305.

[44] **Kamiokande-II** Collaboration, K. Hirata et al., *Observation of B-8 Solar Neutrinos in the Kamiokande-II Detector*, *Phys. Rev. Lett.* **63** (1989) 16.

[45] **Kamiokande-II** Collaboration, K. Hirata et al., *Results from one thousand days of real time directional solar neutrino data*, *Phys. Rev. Lett.* **65** (1990) 1297–1300.

[46] **GALLEX** Collaboration, W. Hampel et al., *GALLEX solar neutrino observations: Results for GALLEX IV*, *Phys. Lett. B* **447** (1999) 127–133.

[47] **SAGE** Collaboration, J. Abdurashitov et al., *Measurement of the solar neutrino capture rate with gallium metal*, *Phys. Rev. C* **60** (1999) 055801, [astro-ph/9907113].

[48] **SNO** Collaboration, Q. Ahmad et al., *Measurement of the rate of $\nu_e + d \to p + p + e^-$ interactions produced by ^8B solar neutrinos at the Sudbury Neutrino Observatory*, *Phys. Rev. Lett.* **87** (2001) 071301, [nucl-ex/0106015].

[49] **SNO** Collaboration, Q. Ahmad et al., *Direct evidence for neutrino flavor transformation from neutral current interactions in the Sudbury Neutrino Observatory*, *Phys. Rev. Lett.* **89** (2002) 011301, [nucl-ex/0204008].

[50] **Kamiokande-II** Collaboration, K. Hirata et al., *Observation of a small atmospheric muon-neutrino / electron-neutrino ratio in Kamiokande*, *Phys. Lett. B* **280** (1992) 146–152.

[51] R. Becker-Szendy et al., *Neutrino measurements with the IMB detector*, *Nucl. Phys. B Proc. Suppl.* **38** (1995) 331–336.

[52] **Super-Kamiokande** Collaboration, Y. Fukuda et al., *Evidence for oscillation of atmospheric neutrinos*, *Phys. Rev. Lett.* **81** (1998) 1562–1567, [hep-ex/9807003].

[53] F. von Feilitzsch and N. Schmitz, eds., *Neutrino physics and astrophysics. Proceedings, 20th International Conference, Neutrino 2002, Munich, Germany, May 25-30, 2002*, vol. 118, 2003.

[54] M. Shiozawa, "Experimental results on atmospheric neutrinos in Super-Kamiokande-I." Neutrino 2002, 2002.

[55] **Super-Kamiokande** Collaboration, M. Smy, *Solar neutrino precision measurements using all 1496 days of Super-Kamiokande I data*, *Nucl. Phys. B Proc. Suppl.* **118** (2003) 25–32, [hep-ex/0208004].

[56] C. Giganti, S. Lavignac, and M. Zito, *Neutrino oscillations: The rise of the PMNS paradigm*, *Prog. Part. Nucl. Phys.* **98** (2018) 1–54, [arXiv:1710.00715].

[57] F. Capozzi, E. Di Valentino, E. Lisi, A. Marrone, A. Melchiorri, and A. Palazzo, *Global constraints on absolute neutrino masses and their ordering*, *Phys. Rev. D* **95** (2017), no. 9 096014, [arXiv:2003.08511]. [Addendum: Phys.Rev.D 101, 116013 (2020)].

[58] **KamLAND** Collaboration, K. Eguchi et al., *First results from KamLAND: Evidence for reactor anti-neutrino disappearance*, *Phys. Rev. Lett.* **90** (2003) 021802, [hep-ex/0212021].

[59] **T2K** Collaboration, K. Abe et al., *Measurements of neutrino oscillation in appearance and disappearance channels by the T2K experiment with 6.6×10^{20} protons on target*, *Phys. Rev. D* **91** (2015), no. 7 072010, [arXiv:1502.01550].

[60] **NOvA** Collaboration, P. Adamson et al., *Measurement of the neutrino mixing angle θ_{23} in NOvA*, *Phys. Rev. Lett.* **118** (2017), no. 15 151802, [arXiv:1701.05891].

[61] **Double Chooz** Collaboration, F. Ardellier et al., *Double Chooz: A Search for the neutrino mixing angle theta(13)*, hep-ex/0606025.

[62] **RENO** Collaboration, J. Ahn et al., *RENO: An Experiment for Neutrino Oscillation Parameter θ_{13} Using Reactor Neutrinos at Yonggwang*, arXiv:1003.1391.

[63] **Daya Bay** Collaboration, F. An et al., *The Detector System of The Daya Bay Reactor Neutrino Experiment*, *Nucl. Instrum. Meth. A* **811** (2016) 133–161, [arXiv:1508.03943].

[64] R. Shrock, *New Tests For, and Bounds On, Neutrino Masses and Lepton Mixing*, *Phys. Lett. B* **96** (1980) 159–164.

[65] **KATRIN** Collaboration, M. Aker et al., *Improved Upper Limit on the Neutrino Mass from a Direct Kinematic Method by KATRIN*, *Phys. Rev. Lett.* **123** (2019), no. 22 221802, [arXiv:1909.06048].

[66] **KATRIN** Collaboration, M. Aker et al., *First operation of the KATRIN experiment with tritium*, *Eur. Phys. J. C* **80** (2020), no. 3 264, [arXiv:1909.06069].

[67] J. Schechter and J. Valle, *Neutrinoless Double beta Decay in SU(2) x U(1) Theories*, *Phys. Rev. D* **25** (1982) 2951.

[68] E. Takasugi, *Can the Neutrinoless Double Beta Decay Take Place in the Case of Dirac Neutrinos?*, *Phys. Lett. B* **149** (1984) 372–376.

[69] M. Hirsch, S. Kovalenko, and I. Schmidt, *Extended black box theorem for lepton number and flavor violating processes*, *Phys. Lett. B* **642** (2006) 106–110, [hep-ph/0608207].

[70] M. J. Dolinski, A. W. Poon, and W. Rodejohann, *Neutrinoless Double-Beta Decay: Status and Prospects*, *Ann. Rev. Nucl. Part. Sci.* **69** (2019) 219–251, [arXiv:1902.04097].

[71] **Planck** Collaboration, N. Aghanim et al., *Planck 2018 results. VI. Cosmological parameters*, arXiv:1807.06209.

[72] P. Minkowski, *$\mu \to e\gamma$ at a rate of one out of 10^9 muon decays?*, *Physics Letters B* **67** (1977), no. 4 421 – 428.

[73] T. Yanagida, *Horizontal gauge symmetry and masses of neutrinos*, *Conf. Proc.* **C7902131** (1979) 95–99.

[74] M. Gell-Mann, P. Ramond, and R. Slansky, *Complex Spinors and Unified Theories*, *Conf. Proc.* **C790927** (1979) 315–321, [arXiv:1306.4669].

[75] R. N. Mohapatra and G. Senjanović, *Neutrino mass and spontaneous parity nonconservation*, *Phys. Rev. Lett.* **44** (Apr, 1980) 912–915.

[76] S. L. Glashow, *The Future of Elementary Particle Physics*, *NATO Sci. Ser. B* **61** (1980) 687.

[77] M. Magg and C. Wetterich, *Neutrino Mass Problem and Gauge Hierarchy*, *Phys. Lett.* **94B** (1980) 61–64.

[78] J. Schechter and J. W. F. Valle, *Neutrino masses in su(2) $\bigotimes$ u(1) theories*, *Phys. Rev. D* **22** (Nov, 1980) 2227–2235.

[79] G. Lazarides, Q. Shafi, and C. Wetterich, *Proton lifetime and fermion masses in an so(10) model*, *Nuclear Physics B* **181** (1981), no. 2 287 – 300.

[80] C. Wetterich, *Neutrino Masses and the Scale of B-L Violation*, *Nucl. Phys.* **B187** (1981) 343–375.

[81] R. N. Mohapatra and G. Senjanović, *Neutrino masses and mixings in gauge models with spontaneous parity violation*, *Phys. Rev. D* **23** (Jan, 1981) 165–180.

[82] R. Foot, H. Lew, X. G. He, and G. C. Joshi, *Seesaw Neutrino Masses Induced by a Triplet of Leptons*, *Z. Phys.* **C44** (1989) 441.

[83] A. Zee, *A Theory of Lepton Number Violation, Neutrino Majorana Mass, and Oscillation*, *Phys. Lett.* **93B** (1980) 389. [Erratum: Phys. Lett.95B,461(1980)].

[84] A. Zee, *Quantum Numbers of Majorana Neutrino Masses*, *Nucl. Phys.* **B264** (1986) 99–110.

[85] K. S. Babu, *Model of 'Calculable' Majorana Neutrino Masses*, *Phys. Lett.* **B203** (1988) 132–136.

[86] A. de Gouvea and J. Jenkins, *A Survey of Lepton Number Violation Via Effective Operators*, *Phys. Rev.* **D77** (2008) 013008, [arXiv:0708.1344].

[87] **ATLAS** Collaboration, G. Aad et al., *Search for doubly-charged Higgs bosons in like-sign dilepton final states at $\sqrt{s} = 7$ TeV with the ATLAS detector*, *Eur. Phys. J. C* **72** (2012) 2244, [arXiv:1210.5070].

[88] **ATLAS** Collaboration, G. Aad et al., *Search for anomalous production of prompt same-sign lepton pairs and pair-produced doubly charged Higgs bosons with $\sqrt{s} = 8$ TeV pp collisions using the ATLAS detector*, *JHEP* **03** (2015) 041, [arXiv:1412.0237].

[89] **ATLAS** Collaboration, M. Aaboud et al., *Search for doubly charged Higgs boson production in multi-lepton final states with the ATLAS detector using proton–proton collisions at $\sqrt{s} = 13$ TeV*, *Eur. Phys. J. C* **78** (2018), no. 3 199, [arXiv:1710.09748].

[90] **CMS** Collaboration, S. Chatrchyan et al., *A Search for a Doubly-Charged Higgs Boson in pp Collisions at $\sqrt{s} = 7$ TeV*, *Eur. Phys. J. C* **72** (2012) 2189, [arXiv:1207.2666].

[91] **CMS** Collaboration, *Search for a doubly-charged Higgs boson with $\sqrt{s} = 8$ TeV pp collisions at the CMS experiment*, .

[92] **CMS** Collaboration, *A search for doubly-charged Higgs boson production in three and four lepton final states at* $\sqrt{s} = 13$ TeV, .

[93] L. Wolfenstein, *A Theoretical Pattern for Neutrino Oscillations*, *Nucl. Phys. B* **175** (1980) 93–96.

[94] S. M. Boucenna, S. Morisi, and J. W. F. Valle, *The low-scale approach to neutrino masses*, *Adv. High Energy Phys.* **2014** (2014) 831598, [arXiv:1404.3751].

[95] Y. Cai, J. Herrero-García, M. A. Schmidt, A. Vicente, and R. R. Volkas, *From the trees to the forest: a review of radiative neutrino mass models*, *Front.in Phys.* **5** (2017) 63, [arXiv:1706.08524].

[96] Y. Farzan, S. Pascoli, and M. A. Schmidt, *Recipes and Ingredients for Neutrino Mass at Loop Level*, *JHEP* **03** (2013) 107, [arXiv:1208.2732].

[97] F. Bonnet, M. Hirsch, T. Ota, and W. Winter, *Systematic study of the d=5 Weinberg operator at one-loop order*, *JHEP* **07** (2012) 153, [arXiv:1204.5862].

[98] R. Cepedello, M. Hirsch, and J. Helo, *Loop neutrino masses from* $d = 7$ *operator*, *JHEP* **07** (2017) 079, [arXiv:1705.01489].

[99] K. S. Babu and C. N. Leung, *Classification of effective neutrino mass operators*, *Nucl. Phys.* **B619** (2001) 667–689, [hep-ph/0106054].

[100] P. W. Angel, N. L. Rodd, and R. R. Volkas, *Origin of neutrino masses at the lhc:* $\Delta l = 2$ *effective operators and their ultraviolet completions*, *Phys. Rev. D* **87** (Apr, 2013) 073007.

[101] Y. Cai, J. D. Clarke, M. A. Schmidt, and R. R. Volkas, *Testing Radiative Neutrino Mass Models at the LHC*, *JHEP* **02** (2015) 161, [arXiv:1410.0689].

[102] F. Bonnet, D. Hernandez, T. Ota, and W. Winter, *Neutrino masses from higher than d=5 effective operators*, *JHEP* **10** (2009) 076, [arXiv:0907.3143].

[103] G. Anamiati, O. Castillo-Felisola, R. M. Fonseca, J. C. Helo, and M. Hirsch, *High-dimensional neutrino masses*, *JHEP* **12** (2018) 066, [arXiv:1806.07264].

[104] C. Klein, M. Lindner, and S. Ohmer, *Minimal Radiative Neutrino Masses*, *JHEP* **03** (2019) 018, [arXiv:1901.03225].

[105] C. Klein, M. Lindner, and S. Vogl, *Radiative neutrino masses and successful* $SU(5)$ *unification*, *Phys. Rev. D* **100** (2019), no. 7 075024, [arXiv:1907.05328].

[106] B. Henning, X. Lu, and H. Murayama, *How to use the Standard Model effective field theory*, *JHEP* **01** (2016) 023, [arXiv:1412.1837].

[107] I. Brivio and M. Trott, *The Standard Model as an Effective Field Theory*, *Phys. Rept.* **793** (2019) 1–98, [arXiv:1706.08945].

[108] L. Lehman and A. Martin, *Hilbert Series for Constructing Lagrangians: expanding the phenomenologist's toolbox*, *Phys. Rev.* **D91** (2015) 105014, [arXiv:1503.07537].

[109] B. Henning, X. Lu, T. Melia, and H. Murayama, *Hilbert series and operator bases with derivatives in effective field theories*, *Commun. Math. Phys.* **347** (2016), no. 2 363–388, [arXiv:1507.07240].

[110] L. Lehman and A. Martin, *Low-derivative operators of the Standard Model effective field theory via Hilbert series methods*, *JHEP* **02** (2016) 081, [arXiv:1510.00372].

[111] B. Henning, X. Lu, T. Melia, and H. Murayama, *2, 84, 30, 993, 560, 15456, 11962, 261485, ...: Higher dimension operators in the SM EFT*, *JHEP* **08** (2017) 016, [arXiv:1512.03433]. [Erratum: JHEP09,019(2019)].

[112] B. Henning, X. Lu, T. Melia, and H. Murayama, *Operator bases, S-matrices, and their partition functions*, *JHEP* **10** (2017) 199, [arXiv:1706.08520].

[113] A. Kobach, *Baryon Number, Lepton Number, and Operator Dimension in the Standard Model*, *Phys. Lett. B* **758** (2016) 455–457, [arXiv:1604.05726].

[114] J. Aebischer et al., *WCxf: an exchange format for Wilson coefficients beyond the Standard Model*, *Comput. Phys. Commun.* **232** (2018) 71–83, [arXiv:1712.05298].

[115] E. E. Jenkins, A. V. Manohar, and P. Stoffer, *Low-Energy Effective Field Theory below the Electroweak Scale: Operators and Matching*, *JHEP* **03** (2018) 016, [arXiv:1709.04486].

[116] J. Aebischer, M. Fael, C. Greub, and J. Virto, *B physics Beyond the Standard Model at One Loop: Complete Renormalization Group Evolution below the Electroweak Scale*, *JHEP* **09** (2017) 158, [arXiv:1704.06639].

[117] E. E. Jenkins, A. V. Manohar, and P. Stoffer, *Low-Energy Effective Field Theory below the Electroweak Scale: Anomalous Dimensions*, *JHEP* **01** (2018) 084, [arXiv:1711.05270].

[118] J. Aebischer, A. Crivellin, M. Fael, and C. Greub, *Matching of gauge invariant dimension-six operators for $b \to s$ and $b \to c$ transitions*, *JHEP* **05** (2016) 037, [arXiv:1512.02830].

[119] G. Buchalla, A. J. Buras, and M. E. Lautenbacher, *Weak decays beyond leading logarithms*, *Rev. Mod. Phys.* **68** (1996) 1125–1144, [hep-ph/9512380].

[120] C. Arzt, *Reduced effective Lagrangians*, *Phys. Lett. B* **342** (1995) 189–195, [hep-ph/9304230].

[121] H. Georgi, *On-shell effective field theory*, *Nucl. Phys. B* **361** (1991) 339–350.

[122] J. Gasser and H. Leutwyler, *Chiral Perturbation Theory to One Loop*, *Annals Phys.* **158** (1984) 142.

[123] J. Gasser and H. Leutwyler, *Chiral Perturbation Theory: Expansions in the Mass of the Strange Quark*, *Nucl. Phys. B* **250** (1985) 465–516.

[124] A. De Rujula, M. Gavela, P. Hernandez, and E. Masso, *The Selfcouplings of vector bosons: Does LEP-1 obviate LEP-2?*, *Nucl. Phys. B* **384** (1992) 3–58.

[125] J. Chisholm, *Change of variables in quantum field theories*, *Nuclear Physics* **26** (1961), no. 3 469 – 479.

[126] S. Kamefuchi, L. O'Raifeartaigh, and A. Salam, *Change of variables and equivalence theorems in quantum field theories*, *Nucl. Phys.* **28** (1961) 529–549.

[127] P. Divakaran, *Equivalence theorems and point transformations in field theory*, *Nuclear Physics* **42** (1963) 235–246.

[128] M. Bergere and Y.-M. P. Lam, *Equivalence Theorem and Faddeev-Popov Ghosts*, *Phys. Rev. D* **13** (1976) 3247–3255.

[129] H. Sharatchandra, *The equivalence theorem is subtle*, *Annals of Physics* **116** (1978), no. 2 408 – 418.

[130] A. Salam and J. Strathdee, *Equivalent formulations of massive vector field theories*, *Phys. Rev. D* **2** (Dec, 1970) 2869–2876.

[131] R. Kallosh and I. Tyutin, *The Equivalence theorem and gauge invariance in renormalizable theories*, *Yad. Fiz.* **17** (1973) 190–209.

[132] H. Lehmann, K. Symanzik, and W. Zimmermann, *On the formulation of quantized field theories*, *Nuovo Cim.* **1** (1955) 205–225.

[133] P. Pouliot, *Molien function for duality*, *JHEP* **01** (1999) 021, [hep-th/9812015].

[134] S. Benvenuti, B. Feng, A. Hanany, and Y.-H. He, *Counting BPS Operators in Gauge Theories: Quivers, Syzygies and Plethystics*, *JHEP* **11** (2007) 050, [hep-th/0608050].

[135] F. Dolan, *Counting BPS operators in N=4 SYM*, *Nucl. Phys. B* **790** (2008) 432–464, [arXiv:0704.1038].

[136] A. Hanany, E. E. Jenkins, A. V. Manohar, and G. Torri, *Hilbert Series for Flavor Invariants of the Standard Model*, *JHEP* **03** (2011) 096, [arXiv:1010.3161].

[137] E. E. Jenkins and A. V. Manohar, *Algebraic Structure of Lepton and Quark Flavor Invariants and CP Violation*, *JHEP* **10** (2009) 094, [arXiv:0907.4763].

[138] A. Hanany and R. Kalveks, *Highest Weight Generating Functions for Hilbert Series*, *JHEP* **10** (2014) 152, [arXiv:1408.4690].

[139] A. Hanany, N. Mekareeya, and G. Torri, *The Hilbert Series of Adjoint SQCD*, *Nucl. Phys. B* **825** (2010) 52–97, [arXiv:0812.2315].

[140] R. Feger and T. W. Kephart, *LieART—A Mathematica application for Lie algebras and representation theory*, *Comput. Phys. Commun.* **192** (2015) 166–195, [arXiv:1206.6379].

[141] T. Ma, J. Shu, and M.-L. Xiao, *Standard Model Effective Field Theory from On-shell Amplitudes*, arXiv:1902.06752.

[142] B. Henning and T. Melia, *Constructing effective field theories via their harmonics*, *Phys. Rev. D* **100** (2019), no. 1 016015, [arXiv:1902.06754].

[143] H.-L. Li, Z. Ren, J. Shu, M.-L. Xiao, J.-H. Yu, and Y.-H. Zheng, *Complete Set of Dimension-8 Operators in the Standard Model Effective Field Theory*, arXiv:2005.00008.

[144] H.-L. Li, Z. Ren, M.-L. Xiao, J.-H. Yu, and Y.-H. Zheng, *Complete Set of Dimension-9 Operators in the Standard Model Effective Field Theory*, arXiv:2007.07899.

[145] **Muon g-2** Collaboration, G. Bennett et al., *Final Report of the Muon E821 Anomalous Magnetic Moment Measurement at BNL*, *Phys. Rev. D* **73** (2006) 072003, [hep-ex/0602035].

[146] T. Blum, A. Denig, I. Logashenko, E. de Rafael, B. L. Roberts, T. Teubner, and G. Venanzoni, *The Muon (g-2) Theory Value: Present and Future*, arXiv:1311.2198.

[147] R. H. Parker, C. Yu, W. Zhong, B. Estey, and H. Müller, *Measurement of the fine-structure constant as a test of the standard model*, *Science* **360** (Apr, 2018) 191–195.

[148] **LHCb** Collaboration, R. Aaij et al., *Differential branching fractions and isospin asymmetries of $B \to K^{(*)}\mu^+\mu^-$ decays*, *JHEP* **06** (2014) 133, [arXiv:1403.8044].

[149] **LHCb** Collaboration, R. Aaij et al., *Angular analysis and differential branching fraction of the decay $B_s^0 \to \phi\mu^+\mu^-$*, *JHEP* **09** (2015) 179, [arXiv:1506.08777].

[150] **CMS Collaboration** Collaboration, *Measurement of properties of Bs0 to mu+mu- decays and search for B0 to mu+mu- with the CMS experiment*, Tech. Rep. CMS-PAS-BPH-16-004, CERN, Geneva, 2019.

[151] **LHCb** Collaboration, R. Aaij et al., *First Evidence for the Decay $B_s^0 \to \mu^+\mu^-$*, *Phys. Rev. Lett.* **110** (2013), no. 2 021801, [arXiv:1211.2674].

[152] **LHCb** Collaboration, R. Aaij et al., *Measurement of the $B_s^0 \to \mu^+\mu^-$ branching fraction and effective lifetime and search for $B^0 \to \mu^+\mu^-$ decays*, *Phys. Rev. Lett.* **118** (2017), no. 19 191801, [arXiv:1703.05747].

[153] **ATLAS** Collaboration, M. Aaboud et al., *Study of the rare decays of B_s^0 and B^0 mesons into muon pairs using data collected during 2015 and 2016 with the ATLAS detector*, *JHEP* **04** (2019) 098, [arXiv:1812.03017].

[154] **LHCb** Collaboration, R. Aaij et al., *Differential branching fraction and angular analysis of $\Lambda_b^0 \to \Lambda\mu^+\mu^-$ decays*, *JHEP* **06** (2015) 115, [arXiv:1503.07138]. [Erratum: JHEP 09, 145 (2018)].

[155] F. Kruger, L. M. Sehgal, N. Sinha, and R. Sinha, *Angular distribution and CP asymmetries in the decays $\bar{B} \to K^-\pi^+e^-e^+$ and $\bar{B} \to \pi^-\pi^+e^-e^+$*, *Phys. Rev. D* **61** (2000) 114028, [hep-ph/9907386]. [Erratum: Phys.Rev.D 63, 019901 (2001)].

[156] U. Egede and J. Serrano, *Rare b-hadron decays*, *Comptes Rendus Physique* **21** (2020), no. 1 93–106.

[157] C. Bobeth, M. Gorbahn, T. Hermann, M. Misiak, E. Stamou, and M. Steinhauser, *$B_{s,d} \to l^+l^-$ in the Standard Model with Reduced Theoretical Uncertainty*, *Phys. Rev. Lett.* **112** (2014) 101801, [arXiv:1311.0903].

[158] G. Hiller and F. Krüger, *More model-independent analysis of $b \to s$ processes*, *Phys. Rev.* **D69** (2004) 074020, [hep-ph/0310219].

[159] B. Capdevila, A. Crivellin, S. Descotes-Genon, J. Matias, and J. Virto, *Patterns of New Physics in $b \to s\ell^+\ell^-$ transitions in the light of recent data*, arXiv:1704.05340.

[160] B. Capdevila, S. Descotes-Genon, J. Matias, and J. Virto, *Assessing lepton-flavour non-universality from $B \to K^*\ell\ell$ angular analyses*, *JHEP* **10** (2016) 075, [arXiv:1605.03156].

[161] C. Bobeth, G. Hiller, and G. Piranishvili, *Angular distributions of $\bar{B} \to \bar{K}\ell^+\ell^-$ decays*, *JHEP* **12** (2007) 040, [arXiv:0709.4174].

[162] A. Ali, T. Mannel, and T. Morozumi, *Forward backward asymmetry of dilepton angular distribution in the decay b —> s l+ l-*, *Phys. Lett. B* **273** (1991) 505–512.

[163] U. Egede, T. Hurth, J. Matias, M. Ramon, and W. Reece, *New observables in the decay mode $\bar{B}_d \to \bar{K}^{*0}l^+l^-$*, *JHEP* **11** (2008) 032, [arXiv:0807.2589].

[164] S. Descotes-Genon, T. Hurth, J. Matias, and J. Virto, *Optimizing the basis of $B \to K^*ll$ observables in the full kinematic range*, *JHEP* **05** (2013) 137, [arXiv:1303.5794].

[165] **LHCb** Collaboration, R. Aaij et al., *Measurement of Form-Factor-Independent Observables in the Decay $B^0 \to K^{*0}\mu^+\mu^-$*, *Phys. Rev. Lett.* **111** (2013) 191801, [arXiv:1308.1707].

[166] **LHCb** Collaboration, R. Aaij et al., *Measurement of CP-Averaged Observables in the $B^0 \to K^{*0}\mu^+\mu^-$ Decay*, *Phys. Rev. Lett.* **125** (2020), no. 1 011802, [arXiv:2003.04831].

[167] **Belle** Collaboration, S. Wehle et al., *Lepton-Flavor-Dependent Angular Analysis of $B \to K^*\ell^+\ell^-$*, *Phys. Rev. Lett.* **118** (2017), no. 11 111801, [arXiv:1612.05014].

[168] **ATLAS** Collaboration, M. Aaboud et al., *Angular analysis of $B^0_d \to K^*\mu^+\mu^-$ decays in pp collisions at $\sqrt{s} = 8$ TeV with the ATLAS detector*, *JHEP* **10** (2018) 047, [arXiv:1805.04000].

[169] **CMS** Collaboration, A. M. Sirunyan et al., *Measurement of angular parameters from the decay $\mathrm{B}^0 \to \mathrm{K}^{*0}\mu^+\mu^-$ in proton-proton collisions at $\sqrt{s} = 8$ TeV*, *Phys. Lett. B* **781** (2018) 517–541, [arXiv:1710.02846].

[170] S. Descotes-Genon, L. Hofer, J. Matias, and J. Virto, *On the impact of power corrections in the prediction of $B \to K^*\mu^+\mu^-$ observables*, *JHEP* **12** (2014) 125, [arXiv:1407.8526].

[171] A. Khodjamirian, T. Mannel, A. Pivovarov, and Y.-M. Wang, *Charm-loop effect in $B \to K^{(*)}\ell^+\ell^-$ and $B \to K^*\gamma$*, *JHEP* **09** (2010) 089, [arXiv:1006.4945].

[172] M. Algueró, B. Capdevila, A. Crivellin, S. Descotes-Genon, P. Masjuan, J. Matias, M. Novoa Brunet, and J. Virto, *Emerging patterns of New Physics with and without Lepton Flavour Universal contributions*, *Eur. Phys. J. C* **79** (2019), no. 8 714, [arXiv:1903.09578]. [Addendum: Eur.Phys.J.C 80, 511 (2020)].

[173] A. Arbey, T. Hurth, F. Mahmoudi, D. M. Santos, and S. Neshatpour, *Update on the $b \to s$ anomalies*, *Phys. Rev. D* **100** (2019), no. 1 015045, [arXiv:1904.08399].

[174] M. Ciuchini, A. M. Coutinho, M. Fedele, E. Franco, A. Paul, L. Silvestrini, and M. Valli, *New Physics in $b \to s\ell^+\ell^-$ confronts new data on Lepton Universality*, *Eur. Phys. J. C* **79** (2019), no. 8 719, [arXiv:1903.09632].

[175] S. Descotes-Genon, J. Matias, and J. Virto, *Understanding the $B \to K^*\mu^+\mu^-$ Anomaly*, *Phys. Rev. D* **88** (2013) 074002, [arXiv:1307.5683].

[176] W. Altmannshofer and D. M. Straub, *Implications of $b \to s$ measurements*, in *50th Rencontres de Moriond on EW Interactions and Unified Theories*, pp. 333–338, 3, 2015. arXiv:1503.06199.

[177] S. Descotes-Genon, L. Hofer, J. Matias, and J. Virto, *Global analysis of $b \to s\ell\ell$ anomalies*, *JHEP* **06** (2016) 092, [arXiv:1510.04239].

[178] **BaBar** Collaboration, J. Lees et al., *Evidence for an excess of $\bar{B} \to D^{(*)}\tau^-\bar{\nu}_\tau$ decays*, *Phys. Rev. Lett.* **109** (2012) 101802, [arXiv:1205.5442].

[179] **BaBar** Collaboration, J. Lees et al., *Measurement of an Excess of $\bar{B} \to D^{(*)}\tau^-\bar{\nu}_\tau$ Decays and Implications for Charged Higgs Bosons*, *Phys. Rev. D* **88** (2013), no. 7 072012, [arXiv:1303.0571].

[180] **Belle** Collaboration, M. Huschle et al., *Measurement of the branching ratio of $\bar{B} \to D^{(*)}\tau^-\bar{\nu}_\tau$ relative to $\bar{B} \to D^{(*)}\ell^-\bar{\nu}_\ell$ decays with hadronic tagging at Belle*, *Phys. Rev. D* **92** (2015), no. 7 072014, [arXiv:1507.03233].

[181] **Belle** Collaboration, S. Hirose et al., *Measurement of the τ lepton polarization and $R(D^*)$ in the decay $\bar{B} \to D^*\tau^-\bar{\nu}_\tau$*, *Phys. Rev. Lett.* **118** (2017), no. 21 211801, [arXiv:1612.00529].

[182] **Belle** Collaboration, S. Hirose et al., *Measurement of the τ lepton polarization and $R(D^*)$ in the decay $\bar{B} \to D^*\tau^-\bar{\nu}_\tau$ with one-prong hadronic τ decays at Belle*, *Phys. Rev. D* **97** (2018), no. 1 012004, [arXiv:1709.00129].

[183] **Belle** Collaboration, A. Abdesselam et al., *Measurement of $\mathcal{R}(D)$ and $\mathcal{R}(D^*)$ with a semileptonic tagging method*, arXiv:1904.08794.

[184] **LHCb** Collaboration, R. Aaij et al., *Measurement of the ratio of branching fractions $\mathcal{B}(\bar{B}^0 \to D^{*+}\tau^-\bar{\nu}_\tau)/\mathcal{B}(\bar{B}^0 \to D^{*+}\mu^-\bar{\nu}_\mu)$*, *Phys. Rev. Lett.* **115** (2015), no. 11 111803, [arXiv:1506.08614]. [Erratum: Phys.Rev.Lett. 115, 159901 (2015)].

[185] **LHCb** Collaboration, R. Aaij et al., *Measurement of the ratio of the $B^0 \to D^{*-}\tau^+\nu_\tau$ and $B^0 \to D^{*-}\mu^+\nu_\mu$ branching fractions using three-prong τ-lepton decays*, *Phys. Rev. Lett.* **120** (2018), no. 17 171802, [arXiv:1708.08856].

[186] **LHCb** Collaboration, R. Aaij et al., *Test of Lepton Flavor Universality by the measurement of the $B^0 \to D^{*-}\tau^+\nu_\tau$ branching fraction using three-prong τ decays*, *Phys. Rev. D* **97** (2018), no. 7 072013, [arXiv:1711.02505].

[187] D. Bigi and P. Gambino, *Revisiting $B \to D\ell\nu$*, *Phys. Rev. D* **94** (2016), no. 9 094008, [arXiv:1606.08030].

[188] F. U. Bernlochner, Z. Ligeti, M. Papucci, and D. J. Robinson, *Combined analysis of semileptonic B decays to D and D^*: $R(D^{(*)})$, $|V_{cb}|$, and new physics*, *Phys. Rev. D* **95** (2017), no. 11 115008, [arXiv:1703.05330]. [Erratum: Phys.Rev.D 97, 059902 (2018)].

[189] D. Bigi, P. Gambino, and S. Schacht, *$R(D^*)$, $|V_{cb}|$, and the Heavy Quark Symmetry relations between form factors*, *JHEP* **11** (2017) 061, [arXiv:1707.09509].

[190] S. Jaiswal, S. Nandi, and S. K. Patra, *Extraction of $|V_{cb}|$ from $B \to D^{(*)}\ell\nu_\ell$ and the Standard Model predictions of $R(D^{(*)})$*, *JHEP* **12** (2017) 060, [arXiv:1707.09977].

[191] M. Freytsis, Z. Ligeti, and J. T. Ruderman, *Flavor models for $\bar{B} \to D^{(*)}\tau\bar{\nu}$*, *Phys. Rev. D* **92** (2015), no. 5 054018, [arXiv:1506.08896].

[192] **LHCb** Collaboration, R. Aaij et al., *Measurement of the ratio of branching fractions $\mathcal{B}(B_c^+ \to J/\psi\tau^+\nu_\tau)/\mathcal{B}(B_c^+ \to J/\psi\mu^+\nu_\mu)$*, *Phys. Rev. Lett.* **120** (2018), no. 12 121801, [arXiv:1711.05623].

[193] A. Yu. Anisimov, I. M. Narodetsky, C. Semay, and B. Silvestre-Brac, *The B_c meson lifetime in the light front constituent quark model*, *Phys. Lett.* **B452** (1999) 129–136, [hep-ph/9812514].

[194] V. V. Kiselev, *Exclusive decays and lifetime of B_c meson in QCD sum rules*, hep-ph/0211021.

[195] M. A. Ivanov, J. G. Korner, and P. Santorelli, *Exclusive semileptonic and nonleptonic decays of the B_c meson*, *Phys. Rev.* **D73** (2006) 054024, [hep-ph/0602050].

[196] E. Hernandez, J. Nieves, and J. M. Verde-Velasco, *Study of exclusive semileptonic and non-leptonic decays of B_c in a nonrelativistic quark model*, *Phys. Rev.* **D74** (2006) 074008, [hep-ph/0607150].

[197] T. Huang and F. Zuo, *Semileptonic B_c decays and charmonium distribution amplitude*, *Eur. Phys. J.* **C51** (2007) 833–839, [hep-ph/0702147].

[198] W. Wang, Y.-L. Shen, and C.-D. Lu, *Covariant Light-Front Approach for B(c) transition form factors*, *Phys. Rev.* **D79** (2009) 054012, [arXiv:0811.3748].

[199] A. Issadykov and M. A. Ivanov, *The decays $B_c \to J/\psi + \bar{\ell}\nu_\ell$ and $B_c \to J/\psi + \pi(K)$ in covariant confined quark model*, *Phys. Lett.* **B783** (2018) 178–182, [arXiv:1804.00472].

[200] W.-F. Wang, Y.-Y. Fan, and Z.-J. Xiao, *Semileptonic decays $B_c \to (\eta_c, J/\Psi)l\nu$ in the perturbative QCD approach*, *Chin. Phys.* **C37** (2013) 093102, [arXiv:1212.5903].

[201] A. K. Alok, D. Kumar, J. Kumar, S. Kumbhakar, and S. U. Sankar, *New physics solutions for R_D and R_{D^*}*, *JHEP* **09** (2018) 152, [arXiv:1710.04127].

[202] A. Azatov, D. Bardhan, D. Ghosh, F. Sgarlata, and E. Venturini, *Anatomy of $b \to c\tau\nu$ anomalies*, *JHEP* **11** (2018) 187, [arXiv:1805.03209].

[203] D. Leljak, B. Melic, and M. Patra, *On lepton flavour universality in semileptonic $B_c \to \eta_c, J/\psi$ decays*, arXiv:1901.08368.

[204] K. Azizi, Y. Sarac, and H. Sundu, *Lepton flavour universality violation in semileptonic tree level weak transitions*, arXiv:1904.08267.

[205] C. Murgui, A. Peñuelas, M. Jung, and A. Pich, *Global fit to $b \to c\tau\nu$ transitions*, arXiv:1904.09311.

[206] **Belle** Collaboration, A. Abdesselam et al., *Measurement of the D^{*-} polarization in the decay $B^0 \to D^{*-}\tau^+\nu_\tau$*, in *10th International Workshop on the CKM Unitarity Triangle (CKM 2018) Heidelberg, Germany, September 17-21, 2018*, 2019. arXiv:1903.03102.

[207] P. Asadi, M. R. Buckley, and D. Shih, *Asymmetry Observables and the Origin of $R_{D^{(*)}}$ Anomalies*, *Phys. Rev.* **D99** (2019), no. 3 035015, [arXiv:1810.06597].

[208] R. Alonso, J. Martin Camalich, and S. Westhoff, *Tau properties in $B \to D\tau\nu$ from visible final-state kinematics*, *Phys. Rev.* **D95** (2017), no. 9 093006, [arXiv:1702.02773].

[209] X.-Q. Li, Y.-D. Yang, and X. Zhang, *Revisiting the one leptoquark solution to the R($D^{(*)}$) anomalies and its phenomenological implications*, *JHEP* **08** (2016) 054, [arXiv:1605.09308].

[210] A. Akeroyd and C.-H. Chen, *Constraint on the branching ratio of $B_c \to \tau\bar{\nu}$ from LEP1 and consequences for $R(D^{(*)})$ anomaly*, *Phys. Rev. D* **96** (2017), no. 7 075011, [arXiv:1708.04072].

[211] R. Alonso, B. Grinstein, and J. Martin Camalich, *Lifetime of B_c^- Constrains Explanations for Anomalies in $B \to D^{(*)}\tau\nu$*, *Phys. Rev. Lett.* **118** (2017), no. 8 081802, [arXiv:1611.06676].

[212] M. Blanke, A. Crivellin, S. de Boer, T. Kitahara, M. Moscati, U. Nierste, and I. Nišandžić, *Impact of polarization observables and $B_c \to \tau\nu$ on new physics explanations of the $b \to c\tau\nu$ anomaly*, *Phys. Rev. D* **99** (2019), no. 7 075006, [arXiv:1811.09603].

[213] D. Bardhan and D. Ghosh, *B -meson charged current anomalies: The post-Moriond 2019 status*, *Phys. Rev. D* **100** (2019), no. 1 011701, [arXiv:1904.10432].

[214] Y. Sakaki, M. Tanaka, A. Tayduganov, and R. Watanabe, *Testing leptoquark models in $\bar{B} \to D^{(*)}\tau\bar{\nu}$*, *Phys. Rev. D* **88** (2013), no. 9 094012, [arXiv:1309.0301].

[215] M. Jung and D. M. Straub, *Constraining new physics in $b \to c\ell\nu$ transitions*, *JHEP* **01** (2019) 009, [arXiv:1801.01112].

[216] A. Angelescu, D. Bečirević, D. Faroughy, and O. Sumensari, *Closing the window on single leptoquark solutions to the B-physics anomalies*, *JHEP* **10** (2018) 183, [arXiv:1808.08179].

[217] Z.-R. Huang, Y. Li, C.-D. Lu, M. A. Paracha, and C. Wang, *Footprints of New Physics in $b \to c\tau\nu$ Transitions*, *Phys. Rev. D* **98** (2018), no. 9 095018, [arXiv:1808.03565].

[218] **Muon g-2** Collaboration, A. Chapelain, *The Muon g-2 experiment at Fermilab*, *EPJ Web Conf.* **137** (2017) 08001, [arXiv:1701.02807].

[219] R. Parker, C. Yu, W. Zhong, B. Estey, and H. Mãeller, *Measurement of the fine-structure constant as a test of the standard model*, *Science* **360** (04, 2018) 191–195.

[220] J. Gargalionis, "neutrinomass." https://github.com/johngarg/neutrinomass, 2020.

[221] J. Gargalionis and R. R. Volkas, *Database of tree-level completions of lepton-number-violating effective operators*, Sept., 2020. The database of filtered models is packaged into our example code at https://github.com/johngarg/neutrinomass.

[222] R. M. Fonseca, *Enumerating the operators of an effective field theory*, arXiv:1907.12584.

[223] L. Lehman, *Extending the Standard Model Effective Field Theory with the Complete Set of Dimension-7 Operators*, *Phys. Rev.* **D90** (2014), no. 12 125023, [arXiv:1410.4193].

[224] A. De Gouvêa, W.-C. Huang, J. König, and M. Sen, *Accessible Lepton-Number-Violating Models and Negligible Neutrino Masses*, *Phys. Rev. D* **100** (2019), no. 7 075033, [arXiv:1907.02541].

[225] O. Catà and T. Mannel, *Linking lepton number violation with B anomalies*, arXiv:1903.01799.

[226] B. Gripaios and D. Sutherland, *DEFT: A program for operators in EFT*, *JHEP* **01** (2019) 128, [arXiv:1807.07546].

[227] J. C. Criado, *BasisGen: automatic generation of operator bases*, *Eur. Phys. J.* **C79** (2019), no. 3 256, [arXiv:1901.03501].

[228] R. M. Fonseca, *Calculating the renormalisation group equations of a SUSY model with Susyno*, *Comput. Phys. Commun.* **183** (2012) 2298–2306, [arXiv:1106.5016].

[229] R. M. Fonseca, *The Sym2Int program: going from symmetries to interactions*, *J. Phys. Conf. Ser.* **873** (2017), no. 1 012045, [arXiv:1703.05221].

[230] U. Banerjee, J. Chakrabortty, S. Prakash, and S. U. Rahaman, *Characters and Group Invariant Polynomials of (Super)fields: Road to "Lagrangian"*, arXiv:2004.12830.

[231] C. Arzt, M. B. Einhorn, and J. Wudka, *Patterns of deviation from the standard model*, *Nucl. Phys.* **B433** (1995) 41–66, [hep-ph/9405214].

[232] M. B. Einhorn and J. Wudka, *The Bases of Effective Field Theories*, *Nucl. Phys.* **B876** (2013) 556–574, [arXiv:1307.0478].

[233] P. W. Angel, N. L. Rodd, and R. R. Volkas, *Origin of neutrino masses at the LHC: $\Delta L = 2$ effective operators and their ultraviolet completions*, *Phys. Rev.* **D87** (2013), no. 7 073007, [arXiv:1212.6111].

[234] J. Herrero-García and M. A. Schmidt, *Neutrino mass models: New classification and model-independent upper limits on their scale*, *Eur. Phys. J. C* **79** (2019), no. 11 938, [arXiv:1903.10552].

[235] U. Banerjee, J. Chakrabortty, S. Prakash, S. U. Rahaman, and M. Spannowsky, *Effective Operator Bases for Beyond Standard Model Scenarios: An EFT compendium for discoveries*, arXiv:2008.11512.

[236] F. del Aguila, A. Aparici, S. Bhattacharya, A. Santamaria, and J. Wudka, *A realistic model of neutrino masses with a large neutrinoless double beta decay rate*, *JHEP* **05** (2012) 133, [arXiv:1111.6960].

[237] F. del Aguila, A. Aparici, S. Bhattacharya, A. Santamaria, and J. Wudka, *Effective Lagrangian approach to neutrinoless double beta decay and neutrino masses*, *JHEP* **06** (2012) 146, [arXiv:1204.5986].

[238] J. Herrero-Garcia, N. Rius, and A. Santamaria, *Higgs lepton flavour violation: UV completions and connection to neutrino masses*, *JHEP* **11** (2016) 084, [arXiv:1605.06091].

[239] N. Craig, M. Jiang, Y.-Y. Li, and D. Sutherland, *Loops and Trees in Generic EFTs*, arXiv:2001.00017.

[240] S. S. Law and K. L. McDonald, *The simplest models of radiative neutrino mass*, *Int. J. Mod. Phys. A* **29** (2014) 1450064, [arXiv:1303.6384].

[241] X.-G. He, *Is the Zee model neutrino mass matrix ruled out?*, *Eur. Phys. J. C* **34** (2004) 371–376, [hep-ph/0307172].

[242] A. Meurer, C. P. Smith, M. Paprocki, O. Čertík, S. B. Kirpichev, M. Rocklin, A. Kumar, S. Ivanov, J. K. Moore, S. Singh, T. Rathnayake, S. Vig, B. E. Granger, R. P. Muller, F. Bonazzi, H. Gupta, S. Vats, F. Johansson, F. Pedregosa, M. J. Curry, A. R. Terrel, v. Roučka, A. Saboo, I. Fernando, S. Kulal, R. Cimrman, and A. Scopatz, *Sympy: symbolic computing in python*, *PeerJ Computer Science* **3** (Jan., 2017) e103.

[243] G. Butler, ed., *Fundamental Algorithms for Permutation Groups.* Springer Berlin Heidelberg, 1991.

[244] L. R. U. Manssur, R. Portugal, and B. F. Svaiter, *Group-theoretic approach for symbolic tensor manipulation*, *International Journal of Modern Physics C* **13** (Sep, 2002) 859–879.

[245] T. Hahn, *Generating Feynman diagrams and amplitudes with FeynArts 3*, *Comput. Phys. Commun.* **140** (2001) 418–431, [hep-ph/0012260].

[246] G. Csardi and T. Nepusz, *The igraph software package for complex network research*, *InterJournal* **Complex Systems** (2006) 1695.

[247] T. igraph Core Team, *igraph*, Apr., 2020.

[248] S. Horvát, *Igraph/m*, Apr., 2020. Please go to the GitHub repository to download an immediately usable version of this software.

[249] A. A. Hagberg, D. A. Schult, and P. J. Swart, *Exploring network structure, dynamics, and function using networkx*, in *Proceedings of the 7th Python in Science Conference* (G. Varoquaux, T. Vaught, and J. Millman, eds.), (Pasadena, CA USA), pp. 11 – 15, 2008.

[250] J. C. Criado, *MatchingTools: a Python library for symbolic effective field theory calculations*, *Comput. Phys. Commun.* **227** (2018) 42–50, [arXiv:1710.06445].

[251] S. Das Bakshi, J. Chakrabortty, and S. K. Patra, *CoDEx: Wilson coefficient calculator connecting SMEFT to UV theory*, *Eur. Phys. J.* **C79** (2019), no. 1 21, [arXiv:1808.04403].

[252] M. Krebber and H. Barthels, *MatchPy: Pattern Matching in Python*, *Journal of Open Source Software* **3** (June, 2018) 2.

[253] M. Krebber, *Non-linear associative-commutative many-to-one pattern matching with sequence variables*, 2017.

[254] I. Esteban, M. Gonzalez-Garcia, A. Hernandez-Cabezudo, M. Maltoni, and T. Schwetz, *Global analysis of three-flavour neutrino oscillations: synergies and tensions in the determination of θ_{23}, δ_{CP}, and the mass ordering*, *JHEP* **01** (2019) 106, [arXiv:1811.05487].

[255] K. Babu, P. B. Dev, S. Jana, and A. Thapa, *Non-Standard Interactions in Radiative Neutrino Mass Models*, *JHEP* **03** (2020) 006, [arXiv:1907.09498].

[256] M. Duerr, M. Lindner, and A. Merle, *On the Quantitative Impact of the Schechter-Valle Theorem*, *JHEP* **06** (2011) 091, [arXiv:1105.0901].

[257] K. Babu, S. Nandi, and Z. Tavartkiladze, *New Mechanism for Neutrino Mass Generation and Triply Charged Higgs Bosons at the LHC*, *Phys. Rev. D* **80** (2009) 071702, [arXiv:0905.2710].

[258] P. W. Angel, Y. Cai, N. L. Rodd, M. A. Schmidt, and R. R. Volkas, *Testable two-loop radiative neutrino mass model based on an $LLQd^cQd^c$ effective operator*, *JHEP* **10** (2013) 118, [arXiv:1308.0463]. [Erratum: JHEP11,092(2014)].

[259] O. Popov, M. A. Schmidt, and G. White, *R_2 as a single leptoquark solution to $R_{D^{(*)}}$ and $R_{K^{(*)}}$*, *Phys. Rev. D* **100** (2019), no. 3 035028, [arXiv:1905.06339].

[260] K. Babu, P. B. Dev, S. Jana, and A. Thapa, *Unified Framework for B-Anomalies, Muon $g-2$, and Neutrino Masses*, arXiv:2009.01771.

[261] I. Doršner, S. Fajfer, A. Greljo, J. F. Kamenik, and N. Košnik, *Physics of leptoquarks in precision experiments and at particle colliders*, *Phys. Rept.* **641** (2016) 1–68, [arXiv:1603.04993].

[262] D. Bečirević, B. Panes, O. Sumensari, and R. Zukanovich Funchal, *Seeking leptoquarks in IceCube*, *JHEP* **06** (2018) 032, [arXiv:1803.10112].

[263] D. Bečirević and O. Sumensari, *A leptoquark model to accommodate $R_K^{\rm exp} < R_K^{\rm SM}$ and $R_{K^*}^{\rm exp} < R_{K^*}^{\rm SM}$*, arXiv:1704.05835.

[264] I. Bigaran and R. R. Volkas, *Getting chirality right: single scalar leptoquark solution/s to the $(g-2)_{e,\mu}$ puzzle*, arXiv:2002.12544.

[265] I. Doršner, S. Fajfer, and S. Saad, *$\mu \to e\gamma$ selecting scalar leptoquark solutions for the $(g-2)_{e,\mu}$ puzzles*, arXiv:2006.11624.

[266] G. Hiller and M. Schmaltz, *R_K and future $b \to s\ell\ell$ physics beyond the standard model opportunities*, *Phys. Rev.* **D90** (2014) 054014, [arXiv:1408.1627].

[267] B. Gripaios, M. Nardecchia, and S. A. Renner, *Composite leptoquarks and anomalies in B-meson decays*, *JHEP* **05** (2015) 006, [arXiv:1412.1791].

[268] G. Hiller and I. Nisandzic, *R_K and R_{K^*} beyond the standard model*, *Phys. Rev. D* **96** (2017), no. 3 035003, [arXiv:1704.05444].

[269] I. Doršner, S. Fajfer, D. A. Faroughy, and N. Košnik, *Saga of the two GUT leptoquarks in flavor universality and collider searches*, arXiv:1706.07779.

[270] J. M. Arnold, B. Fornal, and M. B. Wise, *Simplified models with baryon number violation but no proton decay*, *Phys. Rev. D* **87** (2013) 075004, [arXiv:1212.4556].

[271] D. M. Straub, *flavio: a Python package for flavour and precision phenomenology in the Standard Model and beyond*, arXiv:1810.08132.

[272] R. Alonso, B. Grinstein, and J. Martin Camalich, *Lepton universality violation and lepton flavor conservation in B-meson decays*, *JHEP* **10** (2015) 184, [arXiv:1505.05164].

[273] M. Bauer and M. Neubert, *Minimal Leptoquark Explanation for the $R_{D^{(*)}}$, R_K, and $(g-2)_\mu$ Anomalies*, *Phys. Rev. Lett.* **116** (2016), no. 14 141802, [arXiv:1511.01900].

[274] D. Bečirević, N. Košnik, O. Sumensari, and R. Zukanovich Funchal, *Palatable Leptoquark Scenarios for Lepton Flavor Violation in Exclusive $b \to s\ell_1\ell_2$ modes*, *JHEP* **11** (2016) 035, [arXiv:1608.07583].

[275] D. Bečirević, S. Fajfer, N. Košnik, and O. Sumensari, *Leptoquark model to explain the B-physics anomalies, R_K and R_D*, *Phys. Rev.* **D94** (2016), no. 11 115021, [arXiv:1608.08501].

[276] S. M. Boucenna, A. Celis, J. Fuentes-Martin, A. Vicente, and J. Virto, *Non-abelian gauge extensions for B-decay anomalies*, *Phys. Lett.* **B760** (2016) 214–219, [arXiv:1604.03088].

[277] S. M. Boucenna, A. Celis, J. Fuentes-Martin, A. Vicente, and J. Virto, *Phenomenology of an $SU(2) \times SU(2) \times U(1)$ model with lepton-flavour non-universality*, *JHEP* **12** (2016) 059, [arXiv:1608.01349].

[278] L. Calibbi, A. Crivellin, and T. Ota, *Effective Field Theory Approach to $b \to s\ell\ell^{(\prime)}$, $B \to K(*)\nu\bar{\nu}$ and $B \to D(*)\tau\nu$ with Third Generation Couplings*, *Phys. Rev. Lett.* **115** (2015) 181801, [arXiv:1506.02661].

[279] A. Crivellin, D. Müller, and T. Ota, *Simultaneous Explanation of $R(D^{(*)})$ and $b \to s\mu^+\mu^-$: The Last Scalar Leptoquarks Standing*, arXiv:1703.09226.

[280] F. F. Deppisch, S. Kulkarni, H. Päs, and E. Schumacher, *Leptoquark patterns unifying neutrino masses, flavor anomalies, and the diphoton excess*, *Phys. Rev.* **D94** (2016), no. 1 013003, [arXiv:1603.07672].

[281] N. G. Deshpande and X.-G. He, *Consequences of R-parity violating interactions for anomalies in $\bar{B} \to D^{(*)}\tau\bar{\nu}$ and $b \to s\mu^+\mu^-$*, *Eur. Phys. J.* **C77** (2017), no. 2 134, [arXiv:1608.04817].

[282] S. Fajfer and N. Košnik, *Vector leptoquark resolution of R_K and $R_{D^{(*)}}$ puzzles*, *Phys. Lett.* **B755** (2016) 270–274, [arXiv:1511.06024].

[283] F. Feruglio, P. Paradisi, and A. Pattori, *Revisiting Lepton Flavor Universality in B Decays*, *Phys. Rev. Lett.* **118** (2017), no. 1 011801, [arXiv:1606.00524].

[284] F. Feruglio, P. Paradisi, and A. Pattori, *On the Importance of Electroweak Corrections for B Anomalies*, arXiv:1705.00929.

[285] E. Megias, M. Quiros, and L. Salas, *Lepton-flavor universality violation in $R_{D^{(*)}}$ and R_K from warped space*, arXiv:1703.06019.

[286] O. Popov and G. A. White, *One Leptoquark to unify them? Neutrino masses and unification in the light of $(g-2)_\mu$, $R_{D^{(*)}}$ and R_K anomalies*, arXiv:1611.04566.

[287] D. Bečirević, S. Fajfer, and N. Košnik, *Lepton flavor nonuniversality in $b \to s\ell^+\ell^-$ processes*, *Phys. Rev.* **D92** (2015), no. 1 014016, [arXiv:1503.09024].

[288] A. J. Buras and J. Girrbach, *Left-handed Z' and Z FCNC quark couplings facing new $b \to s\mu^+\mu^-$ data*, *JHEP* **12** (2013) 009, [arXiv:1309.2466].

[289] R. Gauld, F. Goertz, and U. Haisch, *On minimal Z' explanations of the $B \to K^*\mu^+\mu^-$ anomaly*, *Phys. Rev.* **D89** (2014) 015005, [arXiv:1308.1959].

[290] S. L. Glashow, D. Guadagnoli, and K. Lane, *Lepton Flavor Violation in B Decays?*, *Phys. Rev. Lett.* **114** (2015) 091801, [arXiv:1411.0565].

[291] G. Hiller and M. Schmaltz, *Diagnosing lepton-nonuniversality in $b \to s\ell\ell$*, *JHEP* **02** (2015) 055, [arXiv:1411.4773].

[292] F. Mahmoudi, S. Neshatpour, and J. Virto, *$B \to K^*\mu^+\mu^-$ optimised observables in the MSSM*, *Eur. Phys. J.* **C74** (2014), no. 6 2927, [arXiv:1401.2145].

[293] E. Megias, G. Panico, O. Pujolas, and M. Quiros, *A Natural origin for the LHCb anomalies*, *JHEP* **09** (2016) 118, [arXiv:1608.02362].

[294] H. Päs and E. Schumacher, *Common origin of R_K and neutrino masses*, *Phys. Rev.* **D92** (2015), no. 11 114025, [arXiv:1510.08757].

[295] S. Sahoo and R. Mohanta, *Leptoquark effects on $b \to s\nu\bar{\nu}$ and $B \to K\ell^+\ell^-$ decay processes*, *New J. Phys.* **18** (2016), no. 1 013032, [arXiv:1509.06248].

[296] S. Sahoo and R. Mohanta, *Study of the rare semileptonic decays $B_d^0 \to K^*\ell^+\ell^-$ in scalar leptoquark model*, *Phys. Rev.* **D93** (2016), no. 3 034018, [arXiv:1507.02070].

[297] D. Aristizabal Sierra, F. Staub, and A. Vicente, *Shedding light on the $b \to s$ anomalies with a dark sector*, *Phys. Rev.* **D92** (2015), no. 1 015001, [arXiv:1503.06077].

[298] I. de Medeiros Varzielas and G. Hiller, *Clues for flavor from rare lepton and quark decays*, *JHEP* **06** (2015) 072, [arXiv:1503.01084].

[299] S. de Boer and G. Hiller, *Flavor and new physics opportunities with rare charm decays into leptons*, *Phys. Rev.* **D93** (2016), no. 7 074001, [arXiv:1510.00311].

[300] K. Cheung, T. Nomura, and H. Okada, *Testable radiative neutrino mass model without additional symmetries and explanation for the $b \to s\ell^+\ell^-$ anomaly*, *Phys. Rev.* **D94** (2016), no. 11 115024, [arXiv:1610.02322].

[301] K. Cheung, T. Nomura, and H. Okada, *A Three-loop Neutrino Model with Leptoquark Triplet Scalars*, *Phys. Lett.* **B768** (2017) 359–364, [arXiv:1701.01080].

[302] K. Cheung, T. Nomura, and H. Okada, *Three-loop neutrino mass model with a colored triplet scalar*, *Phys. Rev.* **D95** (2017), no. 1 015026, [arXiv:1610.04986].

[303] D. Aristizabal Sierra, M. Hirsch, and S. G. Kovalenko, *Leptoquarks: Neutrino masses and accelerator phenomenology*, *Phys. Rev.* **D77** (2008) 055011, [arXiv:0710.5699].

[304] *Search for resonances decaying to photon pairs in 3.2 fb^{-1} of pp collisions at* $\sqrt{s} = 13$ TeV *with the ATLAS detector*, Tech. Rep. ATLAS-CONF-2015-081, CERN, Geneva, Dec, 2015.

[305] **CMS** Collaboration, *Search for new physics in high mass diphoton events in proton-proton collisions at 13TeV*, .

[306] *Search for new phenomena in the dilepton final state using proton-proton collisions at* $\sqrt{s} = 13$ TeV *with the ATLAS detector*, Tech. Rep. ATLAS-CONF-2015-070, CERN, Geneva, Dec, 2015.

[307] R. Franceschini, G. F. Giudice, J. F. Kamenik, M. McCullough, A. Pomarol, R. Rattazzi, M. Redi, F. Riva, A. Strumia, and R. Torre, *What is the $\gamma\gamma$ resonance at 750 GeV?*, *JHEP* **03** (2016) 144, [arXiv:1512.04933].

[308] Y. Kats and M. J. Strassler, *Resonances from QCD bound states and the 750 GeV diphoton excess*, *JHEP* **05** (2016) 092, [arXiv:1602.08819]. [Erratum: JHEP 07, 044 (2016)].

[309] D. Curtin and C. B. Verhaaren, *Quirky Explanations for the Diphoton Excess*, *Phys. Rev. D* **93** (2016), no. 5 055011, [arXiv:1512.05753].

[310] J. F. Kamenik and M. Redi, *Back to 1974: The $\mathcal{Q}$-onium*, *Phys. Lett. B* **760** (2016) 158–163, [arXiv:1603.07719].

[311] P. Ko, C. Yu, and T.-C. Yuan, *Probing a new strongly interacting sector via composite diboson resonances*, *Phys. Rev. D* **95** (2017), no. 11 115034, [arXiv:1603.08802].

[312] N. D. Barrie, A. Kobakhidze, S. Liang, M. Talia, and L. Wu, *Heavy Leptonium as the Origin of the 750 GeV Diphoton Excess*, arXiv:1604.02803.

[313] E. D. Carlson, L. J. Hall, U. Sarid, and J. W. Burton, *Cornering color SU(5)*, *Phys. Rev. D* **44** (1991) 1555–1568.

[314] R. Foot, O. F. Hernandez, and T. G. Rizzo, *SU(5)-c COLOR MODEL SIGNATURES AT HADRON COLLIDERS*, *Phys. Lett. B* **246** (1990) 183–187.

[315] R. Foot, *Top quark forward-backward asymmetry from SU(N_c) color*, *Phys. Rev. D* **83** (2011) 114013, [arXiv:1103.1940].

[316] T. Gherghetta, N. Nagata, and M. Shifman, *A Visible QCD Axion from an Enlarged Color Group*, *Phys. Rev. D* **93** (2016), no. 11 115010, [arXiv:1604.01127].

[317] R. Foot and H. Lew, *QUARK - LEPTON SYMMETRIC MODEL*, *Phys. Rev. D* **41** (1990) 3502.

[318] R. Foot, H. Lew, and R. Volkas, *Phenomenology of quark - lepton symmetric models*, *Phys. Rev. D* **44** (1991) 1531–1546.

[319] R. Foot and R. Volkas, *Generalised leptonic colour*, *Phys. Lett. B* **645** (2007) 345–350, [hep-ph/0607047].

[320] J. D. Clarke, R. Foot, and R. R. Volkas, *Quark-lepton symmetric model at the LHC*, *Phys. Rev. D* **85** (2012) 074012, [arXiv:1112.3405].

[321] L. Okun, *THETA PARTICLES*, *Nucl. Phys. B* **173** (1980) 1–12.

[322] J. Kang and M. A. Luty, *Macroscopic Strings and 'Quirks' at Colliders*, *JHEP* **11** (2009) 065, [arXiv:0805.4642].

[323] P. Agrawal, J. Fan, B. Heidenreich, M. Reece, and M. Strassler, *Experimental Considerations Motivated by the Diphoton Excess at the LHC*, *JHEP* **06** (2016) 082, [arXiv:1512.05775].

[324] **ATLAS** Collaboration, G. Aad et al., *Observation of a new particle in the search for the Standard Model Higgs boson with the ATLAS detector at the LHC*, *Phys. Lett. B* **716** (2012) 1–29, [arXiv:1207.7214].

[325] **CMS** Collaboration, S. Chatrchyan et al., *Observation of a New Boson at a Mass of 125 GeV with the CMS Experiment at the LHC*, *Phys. Lett. B* **716** (2012) 30–61, [arXiv:1207.7235].

[326] C. Borschensky, M. Krämer, A. Kulesza, M. Mangano, S. Padhi, T. Plehn, and X. Portell, *Squark and gluino production cross sections in pp collisions at $\sqrt{s}$ = 13, 14, 33 and 100 TeV*, *Eur. Phys. J. C* **74** (2014), no. 12 3174, [arXiv:1407.5066].

[327] *Search for pair production of Higgs bosons in the $b\bar{b}b\bar{b}$ final state using proton-proton collisions at $\sqrt{s} = 13$ TeV with the ATLAS detector*, Tech. Rep. ATLAS-CONF-2016-017, CERN, Geneva, Mar, 2016.

[328] **CMS Collaboration** Collaboration, *Search for resonant pair production of Higgs bosons decaying to two bottom quark-antiquark pairs in proton-proton collisions at 13 TeV*, Tech. Rep. CMS-PAS-HIG-16-002, CERN, Geneva, 2016.

[329] R. Harlander and P. Kant, *Higgs production and decay: Analytic results at next-to-leading order QCD*, *JHEP* **12** (2005) 015, [hep-ph/0509189].

[330] R. Foot, H. Lew, and R. Volkas, *Models of extended Pati-Salam gauge symmetry*, *Phys. Rev. D* **44** (1991) 859. [Erratum: Phys.Rev.D 47, 1272 (1993)].

[331] **ATLAS** Collaboration, G. Aad et al., *Search for new phenomena in the dijet mass distribution using $p-p$ collision data at $\sqrt{s}=8$ TeV with the ATLAS detector*, *Phys. Rev. D* **91** (2015), no. 5 052007, [arXiv:1407.1376].

[332] **CMS** Collaboration, V. Khachatryan et al., *Search for narrow resonances decaying to dijets in proton-proton collisions at $\sqrt{(s)}=13$ TeV*, *Phys. Rev. Lett.* **116** (2016), no. 7 071801, [arXiv:1512.01224].

[333] J. E. Juknevich, D. Melnikov, and M. J. Strassler, *A Pure-Glue Hidden Valley I. States and Decays*, *JHEP* **07** (2009) 055, [arXiv:0903.0883].

[334] J. E. Juknevich, *Pure-glue hidden valleys through the Higgs portal*, *JHEP* **08** (2010) 121, [arXiv:0911.5616].

[335] **ATLAS** Collaboration, G. Aad et al., *Search for new phenomena with photon+jet events in proton-proton collisions at $\sqrt{s}=13$ TeV with the ATLAS detector*, *JHEP* **03** (2016) 041, [arXiv:1512.05910].

[336] J. Ellis, *TikZ-Feynman: Feynman diagrams with TikZ*, *Comput. Phys. Commun.* **210** (2017) 103–123, [arXiv:1601.05437].